UNIVERSITÀ DEGLI STUDI DI CATANIA

Dipartimento di Agricoltura, Alimentazione e Ambiente – Di3A

Agricultural, Food and Environmental Science

XXXV Cycle

ADVANCING IN REMOTE SENSING-BASED MODELS AND METEOROLOGICAL DATA SOURCES FOR IMPROVING THE SUSTAINABILITY OF THE IRRIGATED AGRICULTURE

Giuseppe Longo Minnolo

Advisor:
Prof. Simona Consoli

Co-advisors:
Dr. Daniela Vanella
Dr. Juan Miguel Ramirez-Cuesta

Coordinators:
Prof. Alessandro Priolo
Prof. Antonio Biondi

Ph.D. attended during 2019/2022

Acknowledgements

Words cannot express my gratitude to my advisor, Prof. Simona Consoli, and co-advisors, Dr. Daniela Vanella and Dr. Juan Miguel Ramirez-Cuesta for their precious teachings and for having strongly believed in me.

A special thanks also to the Ph.D. coordinators, Prof. Alessandro Priolo and Prof. Antonio Biondi, for their tireless work and dedication to the Ph.D. students, and to Dr. Francesco Vuolo and all the colleagues of the Institute of Geomatics (BOKU) for their loving hospitality, there I spent one of the best experience ever.

A great thanks to the supervision committee, Dr. Oscar Belfiore and Dr. Isabel Pôças, who provided me suggestions and comments on my research activity advancements, and to the Thesis referees, Dr. Ignacio Lorite and Dr. Samuel Ortega-Farìas, who generously accepted to revise this Thesis, bringing their knowledge and expertise.

I would thank all the Hydraulic section, for permitting me to be part of the best research group of the Department of Agriculture, Food and Environment (Di3A). A very special mention to the young "Aula Aquatec" group: Alessandro, Angela, Emanuela, Fabiano, Luca, Liviana, Salvo Barresi, Salvo Pappalardo, Serena, Vincenzo. I found in them not simple colleagues, but friends and brothers. This amazing journey would not have been the same without our aperitifs, lunches, birthdays (reals and not), child behaviours, cinema acts and the other millions of foolish things we only can do.

Lastly, I would be remiss in not mentioning my family for their incessant stand.

This Thesis was supported by the Research Project of National Relevance (PRIN 2017) titled "INtegrated Computer modeling and monitoring for Irrigation Planning in Italy – INCIPIT". Additionally, I acknowledge the doctoral financial support received from Regione Sicilia within the Programma Operativo Fondo Sociale Europeo (PO F.S.E.) Sicilia 2020 – Avviso 2/2019.

Index

1 Introduction 1

1.1 Preface 1

1.2 State of the art 4

1.2.1 Remote Sensing of irrigated agriculture 4

1.2.2 Meteorological data sources 13

1.3 Aim of the Thesis 17

1.4 Thesis outline 18

2 Integrating forecast meteorological data into the ArcDualK_c model for estimating spatially distributed evapotranspiration rates of a citrus orchard 30

2.1 Introduction 31

2.2 Materials and methods 33

2.2.1 Site description 33

2.2.2 ArcDualK_c model description 34

2.2.3 Remote sensing data 37

2.2.4 Measured and forecast meteorological data 39

2.2.5 Statistical performance 40

2.3 Results 42

2.3.1 Comparison of K_{cb} obtained from ArcDualK_c and FAO-56 models 42

2.3.2 ET_c and crop coefficients comparison 45

2.4 Discussion 56

2.5 Conclusion 60

3 A stand-alone remote sensing approach based on the use of the optical trapezoid model for detecting the irrigated areas.....67

3.1 Introduction.....68

3.2 Materials and methods.....73
3.2.1 Study area.....73
3.2.2 Detection of the irrigated areas.....74
3.2.3 Statistical assessment.....81

3.3 Results.....84
3.3.1 Marchfeld Cropland.....84
3.3.2 Irrigation district Quota 102,50.....90

3.4 Discussion.....98

3.5 Conclusion.....103

4 Comparing the use of ERA5 reanalysis dataset and ground-based agrometeorological data under different climates and topography in Italy.....111

4.1 Introduction.....112

4.2 Materials and methods.....116
4.2.1 Ground-based agrometeorological variables at the study sites.....116
4.2.2 Reanalysis datasets description.....120
4.2.3 Calculating daily ET_0 estimates.....122
4.2.4 Statistical indicators.....123

4.3 Results.....125
4.3.1 Agrometeorological variable-by-variable comparisons.....125

4.4 Discussion.....145

4.5 Conclusion.....149

5 Assessing the use of ERA5-Land reanalysis and spatial interpolation methods for retrieving precipitation estimates at basin scale 157

5.1 Introduction 158

5.2 Materials and methods 162

5.2.1 Study area 162

5.2.2 Estimation of spatially distributed precipitation data 164

5.2.3 Statistical performance 172

5.3 Results 174

5.3.1 Evaluation of the interpolated precipitation data 174

5.3.2 Estimation of spatially distributed precipitation data by combining interpolated and ERA5-Land dataset 182

5.4 Discussion 190

5.5 Conclusion 193

6 General conclusions 204

7 Other research and academic activities 208

7.1 Scientific contributions 208

7.1.1 Published articles 208

7.1.2 Conference proceedings 209

7.1.3 Books 211

7.2 Visiting research stays 212

7.3 Participation at research projects 213

7.4 Scientific collaborations 213

7.5 Institutional activities 215

7.5.1 Scientific committee 215

7.5.2 Peer review of scientific articles 215

7.5.3 Given seminars 215
7.5.4 Educational activities 216
7.5.5 Thesis tutoring 216
7.6 Attendance to courses 217
Supplementary material 218

Abbreviation and acronyms

Abbreviation	Meaning
a	Intercept
α	Albedo
ACC	Accuracy
ALADIN	Aire Limitée Adaptation dynamique Développement InterNational
AMSR-E	Advanced Microwave Scanning Radiometer – Earth Observing System
ANN	Artificial Neural Networks
ASCAT	Advanced SCATterometer
b	Regression slope
BIAS	Mean bias error
BSk	Arid, steppe, cold climate
C3S	Copernicus Climate Change Service
CDS	Climate Data Store
Cfa	Hot summer temperate climate
CoOK	CoKriging
COSMO	European Consortium for Small-scale Modelling
Csa	Hot-summer Mediterranean climate
CV	Coefficient of Variation
CWR	Crop Water Requirements
DEM	Digital Elevation Model
Dfb	Warm-summer humid continental climate
DI	Deficit Irrigated
DISO	Distance between Indices of Simulation and Observation
DUK	Detrended Universal Kriging
E	Evaporation
e_a	Actual vapour pressure
EAP	Environment Action Programme
ECMWF	European Centre for Medium-Range Weather Forecasts
$e_o(T)$	Saturation vapour pressure
ERA5	ERA5 single levels
ERA5-L	ERA5 Land
ESA	European Space Agency
ESA CCI SM	European Space Agency Climate Change Initiative Soil Moisture
ET	Evapotranspiration
ET_0	Reference evapotranspiration
ET_c	Crop evapotranspiration

F1	F1 score
FC	Field Capacity
F_c	Ground cover fraction
FGGE	First Global Atmospheric Research Program Global Experiment
GEE	Google Earth Engine
GIS	Geographic Information System
GPM	Global Precipitation Measurement
GSMaP	Global Satellite Mapping of Precipitation
HIRLAM	HIgh Resolution Limited Area Model
I	Irrigation
IDW	Inverse Distance Weighting
INCIPIT	INtegrated Computer modeling and monitoring for Irrigation Planning in Italy
INEA	National Institute of Agricultural Economics
IWR	Irrigation Water Requirements
JPA	Japanese Meteorological Agency
JRA-55	Japanese 55-year Reanalysis
K_c	Crop coefficient
K_{cb}	Basal crop coefficient
K_e	Evaporation coefficient
LAI	Leaf Area Index
MAD	Mean Absolute Difference
MAE	Mean Absolute Error
MERRA	Modern-Era Retrospective analysis for Research and Applications
METRIC	Mapping Evapotranspiration with high Resolution and Internalized Calibration
MiPAAF	Ministry of Agricultural, Food and Forestry Policies
MReg	Multiple linear Regression
MRegIDW	Residual interpolation using IDW
MRegOK	Residual interpolation using OK
MSWEP	Multi-Source Weighted-Ensemble Precipitation
NASA	National Aeronautics and Space Administration
NCEP/NCAR	National Centers for Environment Prediction/National Center for Atmospheric Research
NDVI	Normalized Difference Vegetation Index
NeN	Nearest Neighbour
NIR	Near-infrared
NN	Natural Neighbour
NRMSE	Normalized Root-Mean-Square Error

NWP	Numerical Weather Prediction
OA	Autorità di Bacino del distretto idrografico della Sicilia, ex Osservatorio Acque
O-B	Object-Based
OK	Ordinary Kriging
OPTRAM	OPtical TRApezoid Model
P	Precipitaion
P-B	Pixel-Based
PBIAS	Percent bias
PDIFERENCE	Percentage Difference
PERSIANN	Precipitation Estimation from Remotely Sensed Information using Artificial Neural Networks
$P_{int,bias}$	Interpolated precipitation estimates corrected
$P_{int,nc}$	Interpolated precipitation estimates non-corrected
P-M	Penman-Monteith
POD	Probability Of Detection
PPV	Precision
r	Pearson correlation coefficient
R^2	Coefficient of determination
RB	Normalized Absolute Error
RBF	Radial Basis Functions
REW	Readily Evaporable Water
RF	Random Forest
RH	Relative Humidity
RMSD	Root Mean Square Difference
RMSE	Root Mean Square Error
RS	Remote Sensing
R_s	Solar radiation
SAR	Synthetic Aperture Radar
SAVI	Soil Adjusted Vegetation Index
SDGs	Sustainable Development Goals
SEB	Surface Energy Balance
SEBAL	Surface Energy Balance Algorithm for Land
SIAS	Sicilian Agro-meteorological Information Service
SIGRIAN	National Information System for Water Management in Agriculture
SMAP	Soil Moisture Active Passive
SMOS	Soil Moisture and Ocean Salinity
STR	Shortwave infrared transformed reflectance
SVM	Support Vector Machine
SWB	Soil Water Balance

SWC	Soil Water Content
SWIR	Short-Wave Infrared
T	Transpiration
T1	Full irrigation
T2	Sustained deficit irrigation
T3	Regulated deficit irrigation
T4	Partial root-zone drying
T_{air}	Air temperature
T_{dew}	Dew point temperature
TEW	Total Evaporable Water
TIR	Thermal-Infrared
TMPA	Multi-satellite Precipitation Analysis products
TPR	Recall
TPS	Thin Plate Spline
TRMM	Tropical Rainfall Measuring Mission
u	Wind speed
u_{10}	Wind speed at 10 m
u_2	Wind speed at 2 m
UK	Universal Kriging
VH	Vertical-Horizontal
VIS	Visible
VV	Vertical-Vertical
W	Water content
WFD	Water Framework Directive
WP	Wilting Point
ZAMG	Central Institute for Meteorology and Geodynamics
σ	Standard deviation

Research highlights

- RS modelling has allowed deriving spatially distributed crop evapotranspiration.
- High resolution irrigation maps have been derived by using optical RS.
- Climate reanalysis has provided reliable reference evapotranspiration estimates.
- Topography heterogeneity affects the reanalysis precipitation estimates accuracy.

Abstract

Under the current water scarcity scenario, the promotion of water saving strategies is essential for improving the irrigated agriculture sustainability. The general aim of this Thesis was to implement a methodological approach, based on the use of satellite RS and alternative agrometeorological data sources (including reanalysis and forecast data) for supporting farmers and water management authorities into the better management of the irrigation volumes and for the detection of the irrigated areas.

In particular, a RS-based model (i.e., ArcDualK_c, Ramírez-Cuesta et al., 2019b) was tested at farm scale in a DI orange orchard for deriving spatially distributed estimates of K_c and ET_c using both observed and forecast agrometeorological data provided by COSMO model. Overestimations on K_c and ET_c resulted when forecast agrometeorological data was used. Differences in terms of K_c and ET_c were identified among the irrigation strategies, mainly due to variations of the K_{cb}.

The unsupervised classification on NDVI was coupled with OPTRAM for detecting actual irrigated areas under different climate conditions. The proposed methodology was validated at the Marchfeld Cropland (Austria), showing a good overall accuracy. Then, it was applied at the irrigation district Quota 102,50 (Italy), where the results were compared with the information provided by the Reclamation Consortium, finding an overestimation of irrigated areas.

The reliability and consistency of the reanalysis dataset (global ERA5 and ERA5-Land) for predicting the main agrometeorological variables, including the ET_0, was explored at the irrigation district level under different climates and topography conditions in Italy. A general good agreement was obtained between observed and reanalysis agrometeorological data, at both daily and seasonal scales, confirming the potential of using reanalysis dataset as an alternative data source and overcoming the unavailability of observed agrometeorological data.

Additionally, the use of ERA5-Land and the interpolation methods was combined for enhancing the spatially distributed precipitation estimates at the basin scale. Underestimations on the ERA5-Land precipitation estimates were observed at monthly and seasonal scale. The performance was significantly improved when the interpolation estimates were corrected with local observations. The spatial distribution of the estimation errors associated to the climate reanalysis revealed a significant positive correlation with the altitude variation.

***Keywords*:** Sentinel-2; Vegetation indexes, Precision irrigation; Weather ground-based observation; Missing data; Climate reanalysis; Unsupervised classification; Soil moisture; Irrigated areas; Water management.

Riassunto

Nell'attuale scenario globale di scarsità d'acqua, l'impiego di strategie di risparmio idrico è essenziale al fine di migliorare la sostenibilità dell'agricoltura irrigua. Lo scopo generale della Tesi è stato di implementare un approccio metodologico, basato sull'utilizzo del telerilevamento da satellite e di fonti alternative di dati meteorologici (i.e., dati agrometeorologici previsionali e di rianalisi) a supporto degli agricoltori e delle autorità preposte alla gestione delle risorse idriche per migliorare la programmazione irrigua e il monitoraggio delle aree irrigate.

In particolare, un modello basato su dati telerilevati e agrometeorologici (ArcDualK_c, Ramírez-Cuesta et al., 2019b) è stato testato alla scala di campo in un agrumeto in condizioni di deficit idrico controllatoper determinare stime spazialmente distribuite del K_c e dell'ET_c. Il modello è stato implementato sia utilizzando dati agrometeorologici misurati a terra sia con dati previsionali forniti dal modello COSMO. Sovrastime di K_c e ET_c sono state ottenute utilizzando i dati previsionali rispetto ai dati meteorologici osservati a terra. Differenze in termini di K_c e ET_c sono state, inoltre, osservate tra le strategie irrigue applicate, principalmente legate a seguito delle variazioni del K_{cb}.

La classificazione non supervisionata sul NDVI è stata combinata con OPTRAM per rilevare le aree irrigue effettive, in differenti condizioni climatiche. La metodologia proposta è stata validata in Marchfeld Cropland (Austria), mostrando una buona accuratezza generale. Successivamente è stata applicata al distretto irriguo Quota 102,50 (Italia), dove i risultati sono stati confrontati con i dati dichiarati dal Consorzio di Bonifica, individuando una sovrastima di aree irrigate.

L'affidabilità e la consistenza dei dataset di rianalisi ERA5 ed ERA5-Land nel predire le principali variabili agrometeorologiche, così come l'ET_0, è stata analizzata a scala di distretto irriguo in differenti condizioni climatiche e topografiche nel territorio italiano.

Un buon accordo generale è stato osservato, tra i dati agrometeorologici osservati e di rianalisi, alle scale giornaliera e stagionale, confermando il potenziale nell'utilizzo dei dataset di rianalisi come fonte alternativa di dati, superando il limite dell'indisponibilità dei dati agrometeorologici osservati.

Inoltre, l'utilizzo di ERA5-Land e dei metodi di interpolazione spaziale è stato combinato per migliorare le stime spazialmente distribuite di precipitazione alla scala di bacino idrografico. Sottostime nei dati di precipitazione di ERA5-Land sono state osservate alle scale temporali mensile e stagionale. La performance è migliorata significativamente quando le stime di interpolazione sono state corrette mediante osservazioni locali. La distribuzione spaziale degli errori di stima associati alla procedur di rianalisi climatica hanno mostrato una correlazione positiva, significativa rispetto alla variazione di altitudine.

Parole chiave: Sentinel-2; Indici di vegetazione; Irrigazione di precisione; Dati meteorologici osservati; Dati mancanti; Rianalisi climatica; Classificazione non-supervisionata; Umidità del suolo; Aree irrigue; Gestione delle risorse idriche.

1 Introduction

1.1 Preface

As reported in *The State of Food Security and Nutrition in the World 2021* of the Food and Agriculture Organization of the United Nations, there are currently nearly 60 million of undernourished people in the World and this number continues to increase slowly. Much of the recent increase in food insecurity is related to the greater number of conflicts, often exacerbated by climate-related shocks, and to the economic slowdowns. Consequently, it is expected that the global number of undernourished people in 2030 would exceed 840 million. Additionally, COVID-19 pandemic was spreading across the globe, clearly threatening the food security. Preliminary assessments based on the latest available global economic prospects suggest an increase in 2020 between 83 and 132 million people to the total number of undernourished in the World, depending on the economic growth scenario.

The 2030 Agenda for Sustainable Development of the United Nations (https://sdgs.un.org/) recognizes the global food security as part of the Sustainable Development Goals (SDGs). Specifically, SDG2 aims to end hunger, achieve food security, improve nutrition and promote sustainable agriculture. The projected increase of the World population growth rate suggests that higher food demand is expected in the future, with a direct effect on agricultural water usage (Mancosu et al., 2015). In fact, water represents the essential driving force of agriculture sector (Wriedt et al., 2009). To ensure food production for the future generations, agriculture will require at least an increase of 50 % in water resources, especially in arid and semi-arid regions (Ozdogan et al., 2010).

However, across the World, the availability and the access to suitable water resources are at risk, due to a combination of excessive

demographic pressure and unsustainable agricultural practices (Dubois, 2011). Moreover, being in a climate change context where more frequent and severe droughts are expected to occur, water scarcity is destined to become worse (Mancosu et al., 2015). According to Theodoropoulos and Skoulikidis (2014), 36% of the global population already lives in water scarce regions and is expected to increase to 52% by 2050. The lack of efficient water management not only threatens the Earth's resources but may compromise the well-being of millions of people globally.

Because of all these factors, the debate on the allocation of water resources between the different economic sectors will be intensified, as well as the requirements of increasing the water use efficiency in all of them (Fader et al., 2016). In this sense, improvements in water management are essential to increase the sustainability of irrigated agriculture (Hsiao et al., 2007), especially in semi-arid areas, where water shortage is a limiting factor for crop production (Singh et al., 2017)

In Europe, appropriate measures have been undertaken for addressing sustainable water uses. In this sense, the 6th Environment Action Programme (EAP; 1600/2002/EC) and the Water Framework Directive (WFD; 2000/60/EC) set out the main policy objectives for ensuring a more sustainable and integrated approach for managing water resources (Wriedt et al., 2009). Specifically, WFD is the major legislative initiative, intended to resolve the piecemeal approach to European water legislation that has been developed since 1975 (Acreman and Ferguson, 2010). Although it has been adopted about 20 years ago, a precise quantification of water amount used for irrigation has not been achieved yet (Zucaro and Pontrandolfi, 2006). In Italy, as a response to the strong pressures raised from the European Commission, the Ministry of Agricultural, Food and Forestry Policies (MiPAAF) approved the Ministry Decree on July 31, 2015 for forcing Italian regions to: i) monitor the irrigated areas, and ii) determine the

irrigation volumes.

However, the availability of precise and updated data of irrigated areas (e.g. location and size) represents a critical issue, since this information is often fragmented and mostly derived from obsolete and/or time-consuming field measurements, that do not take into account the spatial component. For instance, the National Institute of Agricultural Economics (INEA) has contributed to design the irrigation water policy in Italy by supporting MiPAAF. Since the 1960's, INEA has conducted the census of irrigated areas, producing the Map of irrigation in Italy. Currently, the most complete and updated database that supports Governmental Institutions is the National Information System for Water Management in Agriculture (SIGRIAN; https://sigrian.crea.gov.it/), which collect the information coming from water management authorities (i.e. Reclamation Consortia and other Irrigation agencies). Nevertheless, the level of detail of the SIGRIAN database is often not enough accurate for a proper evaluation of irrigation water uses.

At the farm scale, huge progresses have been made for reaching water saving measures in irrigated agriculture, including the adoption of irrigation scheduling based on automated drip irrigation systems (Chaudhry & Garg, 2019). However, farmers often rely only on intuition to determine irrigation amounts (McCown et al., 2012).

Under this scenario, satellite Remote Sensing (RS) techniques offer great tools for retrieving spatially distributed information about the irrigated areas (Ozdogan et al., 2010), as well as for quantifying the Crop Water Requirements (CWR) at high temporal resolution and at different spatial scales thanks to the growing number of available satellites (Gong et al., 2019; Khanal et al., 2020). Therefore, RS represents a potential tool to assist EU member states to meet their obligations under the WFD (Chen et al., 2004) and the individual farmers to improve precision irrigation criteria.

Generally, most available RS-based models for estimating the

crop evapotranspitation (ET_c) require a complete set of agro-meteorological data, including air temperature (T_{air}), wind speed (u), solar radiation (R_s), and relative humidity (RH) (e.g. Ramírez-Cuesta et al., 2019a; Vuolo et al., 2015). Furthermore, precipitation data is required to determine the Irrigation Water Requirements (IWR). Traditionally, agro-meteorological variables are measured by automatic weather stations, which are not evenly spatially distributed. Moreover, meteorological data are often affected by substantial time gaps. In order to overcome these limitations, the use of alternative data sources (e.g. forecast data, reanalysis data) may offer consistent series of multiple agro-meteorological parameters all around the globe.

1.2 State of the art

1.2.1 Remote Sensing of irrigated agriculture

RS is the science of acquiring and analysing information about objects or phenomena without entering in contact with them (Lillesand and Kiefer, 1979). Specifically, it refers to the identification of Earth features by detecting the electromagnetic radiation that is reflected and/or emitted by its surface. Due to the synoptic nature of the data and readily available archives of imagery, RS offers great tools for monitoring irrigation. Additionally, remotely sensed data are also less expensive and time-consuming than traditional statistical surveys that may require aerial photography over large areas, making RS particularly valuable (Ozdogan et al., 2010).

Fig. 1.1 shows a summary of the main RS approaches for supporting irrigated agriculture, i.e. the identification of the irrigated areas and the estimation of the CWR.

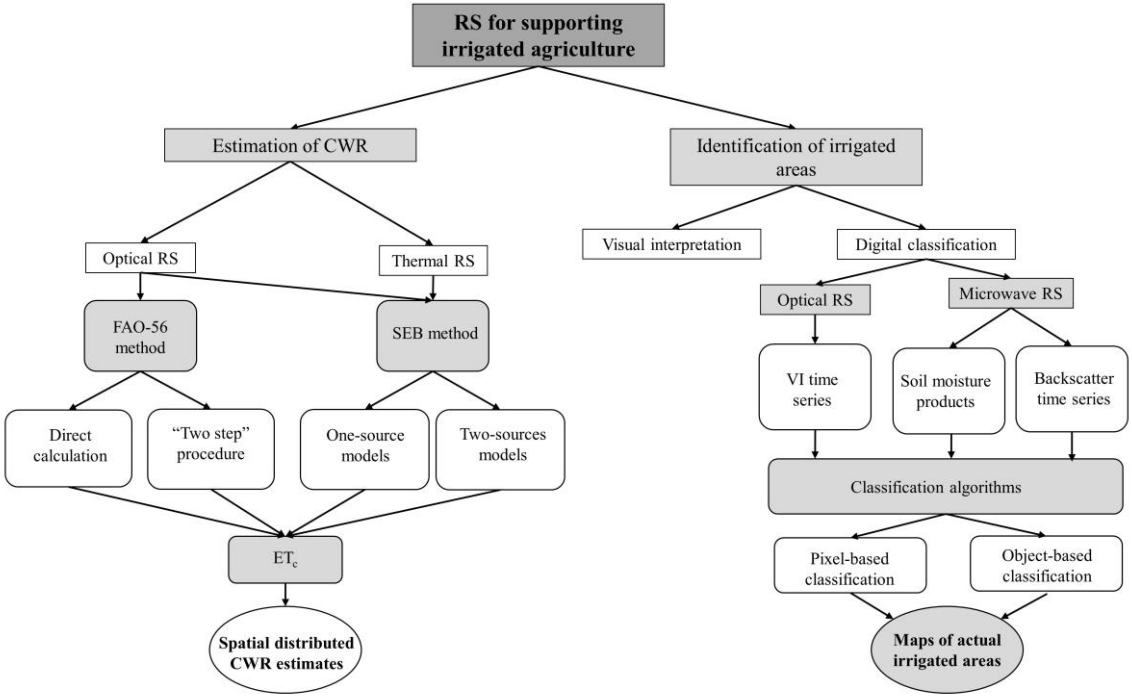

Fig. 1.1. Main RS approaches for supporting the irrigated agriculture

Several studies in literature have shown that satellite RS offers useful and efficient methods for mapping irrigated areas and estimate CWR. Although there are many RS models and approaches, there is no consensus on which one is the more suitable. Each method has both advantages and disadvantages relative to the others. Future researches are oriented to integrate different methods by taking advantage of their respective advantages and compensating for their limitations.

1.2.1.1 Estimation of Crop Water Requirements

CWR can be defined as the amount of water required to manage the losses due to ET_c. ET_c, that is the evapotranspiration from disease-free, well-fertilized crops, grown in large fields, under optimum soil water conditions, and achieving full production under the given climatic conditions, was recognised as significant *proxy* for scheduling irrigation (Allen et al., 1998; Gong et al., 2019). In the last years, several satellite-based models have been developed for determining spatially distributed ET_c estimates at different spatial scales. The most common approaches are the FAO-56 method and the Surface Energy Balance (SEB) method. However, there is no consensus on which approach is the more suitable because each of them has its own advantages and limitations.

FAO-56 method, based on Penman-Monteith (P-M) equation, is the standard procedure for estimating ET_c (Allen et al., 1998). Two main approaches can be distinguished: the "direct calculation" and the "two-step" procedure. The direct calculation, or one-step approach, computes ET_c estimates applying the P-M equation with appropriate values of canopy variables, such as crop height, surface albedo (α) and Leaf Area Index (LAI), and meteorological data. The two-step procedure estimates ET_c as a product of two factors: the evaporative power of the atmosphere, the ET_0, and the crop coefficient (K_c), which includes: a transpiration component, i.e. the basal crop coefficient (K_{cb}), and a soil evaporative component, i.e. the evaporation

coefficient (K_e) (Allen et al., 2011; Calera et al., 2017; D'Urso et al., 2010).

In the direct calculation, the canopy parameters are related to the surface properties, and specifically the surface and canopy resistances, as well as the net radiation (D'Urso et al.,1999). Since for a crop in standard conditions, a minimum value of stomatal resistance can be considered for most herbaceous crops (≈100 sm^{-1}), the surface resistance became a function of LAI only. During recent years, several authors used visible (VIS) and near-infrared (NIR) information to estimate α and LAI, allowing to adapt the P-M equation to be used directly with RS (Vanino et al., 2018; Vuolo et al., 2015).

In the two-step procedure, some pioneers (Bausch and Neale, 1987; Heclman et al., 1982; Neale et al., 1990) provided empirical evidence about the direct relationship between the K_{cb} values with the VI derived from multispectral satellite images. It results from the ability of VIs to measure the radiation absorbed by the vegetation, as the main driver of the evapotranspiration process (Pôças et al., 2020). Among the VI, the Normalized Difference Vegetation Index (NDVI) or the Soil Adjusted Vegetation Index (SAVI), derived from spectral observations in the VIS and NIR region, are the most used (D'Urso and Calera, 2006). Recently, several RS-based models applied this kind of approach. For instance, Ramírez-Cuesta et al. (2019b) developed an ArcGIS toolbox (ArcDualK_c model) which integrates the two-step procedure with satellite data, retrieving accurate ET_c estimates in a lettuce plot and in a peach orchard located in Spain.

On the other hand, SEB methods represent one of the oldest RS-based approach. They asses ET_c as a residual of the land surface energy balance equation (Bastiaanssen et al., 1998), by using ground-based ancillary data and remotely sensed data in the VIS, NIR and thermal-infrared (TIR) bands. The surface temperature values, derived from the TIR imagery, and the aerodynamic temperature, depending on surface aerodynamic roughness, wind speed and the coupling of

soil and canopy elements to the atmosphere, play a key role. Two main models are based on SEB, the One-source SEB models and the Two-sources SEB models. One-source SEB models consider the surface as a whole, and so without distinguishing the separate contributions from soil and vegetation components. The main contributions were the Surface Energy Balance Algorithm for Land (SEBAL; Bastiaanssen et al., 1998), and the Mapping Evapotranspiration with high Resolution and Internalized Calibration (METRIC; Allen et al., 2007). SEBAL requires infrared images and field information on shortwave atmospheric transmittance, surface temperature and vegetation height, for estimating the spatial variation of most essential hydrometeorological parameters empirically. METRIC is based on SEBAL and calibrates the SEB internally using two anchor pixels (hot and cold pixels) for reducing computational biases inherent to the RS-based energy balance. Recently, Ramírez-Cuesta et al. (2020) implemented METRIC in an ArcGIS Toolbox (METRIC-GIS), testing the energy balance components in semi-arid conditions in Spain.

On the contrary, two-sources SEB models divide the surface into two layers, usually soil surface and canopy, in which the energy and vapor fluxes interact between the components. The earliest two-source SEB models include those of Kustas (1990) and Norman et al. (1995). Based on the first contributions, several studies were carried out to improve the models (Anderson et al., 1997; Su, 2002; Sun et al., 2009). In the last years, some authors applied different SEB models comparing the performance. For instance, Wagle et al. (2017) applied five different SEB models for estimating daily ET_c in high biomass sorghum, in Chickasha. Consoli and Vanella (2014) and Gonzalez-Dugo et al. (2009) computed ET_c using one-source and two-source models, in Italy and Iowa, respectively, showing the suitability of SEB under conditions of moisture stress, compared to FAO-56 two-step procedure.

However, the current limited spatial resolution in thermal domain restricts the use of these models at field scale, especially when the plot size is smaller than the pixel resolution (Ramírez-Cuesta et al., 2019a).

1.2.1.2 Identification of irrigated areas

Irrigated areas are defined as those agricultural lands that receive water supplies by artificial means to offset periods of precipitation shortfalls during the crop growing period (Ozdogan et al., 2010). Irrigated agriculture is essential for increasing crop production and ensuring the global food yield (Cai & Rosegrant, 2002; Jin et al., 2016). For this reason, detailed spatial information on the irrigated areas is essential for supporting agriculture water management (Ambika et al., 2016). In particular, accurate mapping of irrigated areas could allow a better understanding of water use and food production patterns, supporting stakeholders to formulate more suitable water management strategies to achieve higher crop water productivity (Chance et al., 2017).

Different approaches can be applied for identifying the irrigated areas, varying in scale (i.e. local, regional and global), data and process requirements (Ozdogan et al., 2010).

Two types of mapping methods emerge as most common: visual interpretation and digital classification. Visual interpretation represents the traditional approach. It has been applied for identifying the irrigated areas in many researches (Draeger, 1977; Kolm and Case, 1984; Rundquist et al., 1989; Thelin and Heimes, 1987; Thiruvengadachari, 1981). Despite its accuracy, due to human expertise, visual interpretation is a cost and time-intensive process.

On the other hand, digital classification is used for overcoming these matters. Optical RS has been used for digital classification of irrigated areas by several authors (Akbari et al., 2006; Bolognesi et al., 2020; Jin et al., 2016; Nhamo et al., 2018). Single-date imagery

acquired during the peak of the crop growing season can be used for the classification of irrigated areas, although multi-temporal imagery approach (time series) is preferred as it covers the different phenology stages of the crops. The most common approach is based on the multi-temporal analysis of NDVI, due its ability to show a considerable difference between irrigated and non-irrigated pixels (Ozdogan et al., 2006, 2010). In fact, NDVI has the capability to measure green biomass and the existing strong correlation between green biomass and the available moisture for vegetation (Pervez & Brown, 2010). For instance, Bolognesi et al. (2020) applied this approach for mapping the actual extent of irrigated areas in Italy in semi-arid conditions. In their study, rainfed areas and irrigated areas were classified on the basis of the analysis of NDVI time series and accumulated rainfall data.

However, this approach shows some limitations, especially in areas where the same crop type is grown with and without irrigation during the same growing season. In these areas, as suggested by Ozdogan et al. (2010), the temporal NDVI profiles of both irrigated and non-irrigated crops may show an identical pattern, emphasizing the need for a more sensitive index to make this distinction. Additionally, optical RS applications depend on atmospheric conditions. For areas with frequent cloud cover, these methods may not be adaptable (Gao et al., 2018).

The use of microwave RS offers a good alternative to optical RS for mapping irrigated areas also under cloudy conditions, due to the ability of microwaves to penetrate through vegetation canopy and underlying soil, especially at lower frequencies (Sadeghi et al., 2015, 2017). Specifically, microwave domain measurements can be used to estimate soil moisture dynamics because the pronounced contrast between the dielectric constant values of the wet and dry soils (Baghdadi & Zribi, 2016; Lakhankar et al., 2009). Kumar et al. (2015) investigated the capability of several microwave remotely sensed soil

moisture products, including Advanced SCATterometer (ASCAT), Advanced Microwave Scanning Radiometer – Earth Observing System (AMSR-E), European Space Agency Climate Change Initiative Soil Moisture (ESA CCI SM), and Soil Moisture and Ocean Salinity (SMOS), while Lawston et al. (2017) showed the capability of the enhanced version of Soil Moisture Active Passive (SMAP) to detect the irrigation signal. Although these products have shown great potential for monitoring soil moisture dynamics they consider both rainfall and irrigation effects on soil moisture (Karthikeyan et al., 2020) and may require calibrations to account for surface roughness which causes perturbation of the microwave signal (Shi et al., 2006). Additionally, the application of microwave-based retrieval of soil moisture is not well suited for small-scale applications because the very coarse resolution, especially when compared with the higher spatial resolution outputs of optical methods (Sadeghi et al., 2017; Yue et al., 2019). More recently, several authors exploited instead Sentinel-1 Synthetic Aperture Radar (SAR) time series to map irrigated fields (Bazzi et al., 2019a,b; Gao et al., 2018). Specifically, based on the multi-temporal analysis of backscatter time series using vertical-vertical (VV) and vertical-horizontal (VH) polarizations, their studies showed that VV resulted more sensitive for characterizing the soil moisture conditions, while VH was more sensitive for monitoring the vegetation status. However, more studies exploiting this approach are required (Dari et al., 2021).

Both optical and microwave RS methods are used as inputs for mapping the irrigated areas and for distinguishing the different crops applying several classification algorithms. Usually, two main classification methods are distinguished - the pixel-based (P-B) classification and the object-based (O-B) classification. The traditional methods of classifying RS images are based upon P-B classification. In this method, each individual image pixel is analysed and classified according to its spectral features. P-B classification

methods have the limits of not considering the spatial relationships of landscape features (Schiewe et al., 2001). On the other hand, O-B classification has been identified as a method for incorporating spatial context into the classification process (Powell and Brooks, 2008). The assumption of O-B classification is that a pixel is very likely to belong to the same class as its neighbouring pixel. This method incorporates two steps - segmentation and classification. In the segmentation phase, homogeneous image objects are derived from both spectral and spatial information, while in the classification phase, image objects are classified in classes of the same semantic significance using established classification algorithms (Benz et al., 2004; Civco et al., 2002; Powell and Brooks, 2008).

In current classification methods, two basic categories exist - the unsupervised classification and the supervised classification. The unsupervised classification is a type of P-B classification that uses clustering to identify groups of pixels with similar pattern. Within the several clustering algorithms that are given in literature, the most common is k-means (Dari et al., 2021; Ragettli et al., 2018). Unsupervised classification is quite quick and easy to run, and it does not require an extensive prior knowledge of the area to classify. On the contrary, the identification and labelling of the classes after the classification is expected. The supervised classification instead, involves the use of training areas associated with specific classes, provided by the user, from which spectral signatures are determined. Then, the computer algorithm uses the spectral signatures from these training areas for classifying the whole image. The most common supervised classification algorithms include Artificial Neural Networks (ANN), Support Vector Machine (SVM) and Random Forest (RF) (Bolognesi et al., 2020; Magidi et al., 2021; Zurqani et al., 2021). Despite supervised classification is more accurate than unsupervised classification, it requires ground reference data to build rule-based classifiers, and thus, the transferability in time and space of

these approaches is not always guaranteed, especially under different climate conditions (Ragettli et al., 2018; Pageot et al., 2020).

1.2.2 Meteorological data sources

Nowadays, an optimal irrigation management mainly depends on accurate estimates of the ET_0, that is the evapotranspiration rate from a reference surface, not short of water (Allen et al., 1998). It is commonly calculated by using the P-M equation and popularized by the FAO-56 paper as a reference methodology for calculating CWR (Allen et al., 1998). The use of the P-M approach requires a reliable and complete set of site-specific agrometeorological data, including T_{air}, u, R_s, and RH.

Usually, agrometeorological variables are measured by automatic weather stations. Their data integrity must be ensured by proper data quality assessment and control procedures (De Pauw et al., 2000; Doraiswamy et al., 2020). However, ground-based observations could be affected by several errors, mainly due to the sensor properties, such as their accuracy, settings, instrument drift or temporal data sampling frequency (Beven, 1979; Hupet and Vanclooster, 2001; Meyer et al., 1989). Other shortcomings are related to the agrometeorological time-series consistency. The time series can suffer from substantial time gaps (Capra et al., 2013) and often protocols for correcting and/or estimating poor quality or missing data need to be applied (see, e.g., Pereira et al., 2015). Moreover, the agrometeorological data representativeness of well-watered conditions needs to be checked before implementing them in the ET_0 approach (Pereira et al., 2015). Despite the utmost importance of observed agrometeorological data for agriculture purposes, the agrometeorological networks are often sparse over the territory, especially in arid zones (De Pauw et al., 2000). Sometimes, data access is another critical point for end-users because data is managed and distributed by different regional services at the National level (Pelosi et al., 2021).

To compensate for the lack of spatial and temporal distributed information, alternative weather data sources have steadily developed, such as the use of interpolation methods from gauge-based observations, the adoption of satellite-based datasets, or the creation of gridded datasets obtained by adjusting the spatial interpolation estimates with satellite observations (Pelosi et al., 2020). Moreover, during the last century, great advances have been reached in agrometeorological data forecasting using global and regional numerical weather prediction (NWP) models (Srivastava et al., 2013).

NWP are based on numerical integration of the hydrodynamic equations governing atmospheric motions using deterministic or probabilistic approaches, requiring well-defined initial conditions (Benjamin et al., 2019). These NWP models can refer to different spatial and temporal scales (from mesoscale to local or microscale), varying their parametrizations and horizontal and vertical resolutions. Across Europe, different consortiums provide meteorological forecasting services, such as HIgh Resolution Limited Area Model (HIRLAM), Aire Limitée Adaptation dynamique Développement InterNational (ALADIN), European Centre for Medium-Range Weather Forecasts (ECMWF), and European Consortium for Small-scale Modelling (COSMO). The opportunity of integrating weather forecasts into irrigation scheduling has become more usable in recent years. In fact, the adoption of NWP models for forecasting ET_0 with days ahead is particularly relevant for providing irrigation advices to farmers in operative scenarios, because it permits the irrigation scheduling based on expected weather conditions rather than on intuition or past weather data. Several studies have already exploited their potential for supporting sustainable irrigation management (e.g. Chirico et al., 2018; Lorite et al., 2015; Medina et al., 2018; Negm et al., 2017; Pelosi et al., 2016; Vanella et al., 2020). As an example, Vanella et al. (2020) showed that the use of forecast agrometeorological estimates provided by COSMO, opens promising

perspectives for assessing the ET_0 in different agriculture contexts, particularly under conditions of water scarcity, instead than using past agrometeorological data.

However, caution need to be referred to forecast uncertainties because they could affect decision making in agricultural systems, causing, for instance, inaccuracies on irrigation requirement estimations (Cao et al., 2019) and on crop growth predictions (McDonnell et al., 2019). Sources of uncertainties on forecasted agrometeorological variables can be ascribed to specific micro-climate conditions (e.g., Coleman and DeCoursey, 1976; Irmak et al., 2006; Liang et al., 2008) and/or to their sensitivity during the season of the year (e.g., Bakhtiari and Liaghat, 2011; Ramirez-Cuesta et al., 2017; Yang et al., 2016). In addition, the quality of the forecasted variables used as input for ET_0 depends on terrain complexity (e.g. wind speed, Drechsel et al., 2012; Cai et al., 2007; Ramirez-Cuesta et al., 2017; Yang et al., 2016) or forecasting lead times (e.g. from 3-day to 9-day, Cao et al., 2019; Chirico et al., 2018; Lorite et al., 2015; Luo et al., 2014, 2015; Pelosi et al., 2016; Perera et al., 2014; Xiong et al., 2016; Yang et al., 2016).

Besides the forecast data, the use of atmospheric reanalysis is another alternative weather data source. Atmospheric reanalysis has generated increasing interest in the recent decade, due to its ability to provide complete and consistent time-series of multiple meteorological parameters at a global scale by covering several decades (Tarek et al., 2020). From a theoretical point of view, the reanalysis process is a retrospective analysis of past historical data. This process makes use of the ever-increasing computational resources, recent versions of NWP models and assimilation schemes. In general, the reanalysis approaches assimilate a wide array of atmospheric and ocean measured and remotely sensed information within a dynamical–physical coupled numerical model (Poli et al., 2016). One of the recognized advantages of using reanalysis

approaches is that their outputs are not directly dependent on the density of ground-based observational networks. Thus they have the potential to provide variables in areas with little and/or no surface coverage (Tarek et al., 2020). Moreover, Pelosi et al. (2020) reported that reanalysis data can represent an efficient data source for planning and design studies applied to irrigation water management.

Currently, several modelling centres provide reanalysis products at variable spatial and temporal scales (Lindsay et al., 2014; Chaudhuri et al., 2013). As an example, the ECMWF periodically applies its forecast models and data assimilation systems to reanalyse archived observations for generating global data sets describing the recent history of the atmosphere, land surface, and oceans. The latest released ECMWF reanalysis products are ERA5 single level (ERA5) and ERA5 Land (ERA5-L), which are being produced within the Copernicus Climate Change Service and freely distributed since 2019 (https://climate.copernicus.eu/). The first dataset, ERA5, covers the entire globe from 1979 at a spatial resolution of about 30 km (depending on latitude). The second dataset, ERA5-L, has been produced by replaying the land component of the ERA5 climate reanalysis, with a horizontal spatial resolution of 9 km. Specifically, ERA5-L uses T_{air}, RH and air pressure, in a process of atmospheric forcing, as input to control the simulated land fields. These atmospheric variables are corrected to account for the altitude difference between the grid of the forcing and the higher resolution grid of ERA5-L (Muñoz-Sabater, 2019). A comprehensive review of the state-of-the-art associated with the use of ERA5-L for land and environmental applications is presented by Muñoz-Sabater et al. (2021). They demonstrated the added value of ERA5-L reanalysis products, in comparison to ERA-Interim and ERA5, for estimating a wide range of *in situ* observations, even if they have not evaluated the performance of the reanalysis products in predicting ET fluxes.

1.3 Aim of the Thesis

Under this state-of-the-art, the general aim of the Thesis was to develop and test a methodological approach, based on the use of RS and alternative meteorological data sources for supporting the planning and the monitoring of irrigation water uses at different spatial scales. In detail, the Thesis would set the basis for assisting: (i) individual farmers at better planning the irrigation scheduling and, (ii) water management authorities at monitoring irrigated areas, and detecting eventual unauthorized water uses. This will allow the promotion of efficient water saving strategies and the accomplishment of the requirements of the water-related policies, improving the sustainability of the irrigated agriculture.

The specific objectives of the Thesis are:

(i) to assess the reliability of RS models combined with forecast meteorological data for obtaining *a priori* spatially distributed ET_c estimates at the farm scale;

(ii) to develop and test a stand-alone optical RS method able to detect the irrigated areas under different climate conditions.

(iii) to explore the effectiveness of using the climate reanalysis data as a potential data source for predicting the main agrometeorological variables and estimating the ET_0 at the district scale, in different climate contexts within the Italian territory;

(iv) to assess the use of the climate reanalysis and the spatial interpolation methods for retrieving spatially continuous distributed precipitation estimates at the basin scale;

1.4 Thesis outline

The present Thesis has been arranged as a scientific papers collection, providing single and self-standing Chapters which represent published or accepted scientific articles, that meet the objectives of the Thesis. The full citation of the articles is reported in the first page of each Chapter. In order to facilitate the reading, a short overview of the described studies is reported below:

Chapter 2 - This study aims at assessing the reliability of the ArcDualK_c model, based on the FAO-56 dual crop coefficient, for deriving spatially distributed estimates of K_c and ET_c in a deficit irrigated (DI) orange orchard. These were obtained using Sentinel-2 satellite imagery in combination with measured and forecast meteorological data provided by the nearest weather station and by COSMO model, respectively.

Chapter 3 - This study aims at developing and testing a stand-alone optical RS approach able to detect the irrigated areas under different climate conditions. Specifically, it combines the use of the unsupervised classification and the OPtical TRApezoid Model (OPTRAM) for distinguishing and mapping high-resolution irrigated and non-irrigated areas.

Chapter 4 - This study explores the reliability and consistency of the global ERA5 single levels and ERA5-Land reanalysis datasets in predicting the main agrometeorological estimates commonly used for crop water requirements calculation. In particular, the reanalysis data was compared, variable-by-variable, with *in situ* agrometeorological observations obtained from automatic weather stations.

Chapter 5 - This study provides a specific focus on precipitation variable, that has not treated on chapter 4. Specifically, the use of alternative data sources, i.e. interpolation methods and ERA5-Land reanalysis data, was combined for improving the spatially distributed

precipitation estimates at the spatial basin scale.

Chapter 6 - This Chapter summarizes the main conclusions provided separately by each presented study, highlighting the main findings of the Thesis and the future perspectives.

Chapter 7 - This Chapter reports the other research and academic activities carried out during the 3 years of the Ph.D. course.

References

Acreman, M. C., & Ferguson, A. J. D. (2010). Environmental flows and the European water framework directive. *Freshwater Biology*, *55*(1), 32-48.

Akbari, M., Mamanpoush, A. R., Gieske, A., Miranzadeh, M., Torabi, M., & Salemi, H. R. (2006). Crop and land cover classification in Iran using Landsat 7 imagery. *International Journal of Remote Sensing*, *27*(19), 4117-4135.

Allen, R. G., Pereira, L. S., Howell, T. A., & Jensen, M. E. (2011). Evapotranspiration information reporting: I. Factors governing measurement accuracy. *Agricultural Water Management*, *98*(6), 899-920.

Allen, R. G., Pereira, L. S., Raes, D., & Smith, M. (1998). Crop evapotranspiration-Guidelines for computing crop water requirements-FAO Irrigation and drainage paper 56. *Fao, Rome*, *300*(9), D05109.

Allen, R. G., Tasumi, M., & Trezza, R. (2007). Satellite-based energy balance for mapping evapotranspiration with internalized calibration (METRIC)—Model. *Journal of irrigation and drainage engineering*, *133*(4), 380-394.

Ambika, A. K., Wardlow, B., & Mishra, V. (2016). Remotely sensed high resolution irrigated area mapping in India for 2000 to 2015. Scientific data, 3(1), 1-14.

Anderson, M. C., Norman, J. M., Diak, G. R., Kustas, W. P., & Mecikalski, J. R. (1997). A two-source time-integrated model for estimating surface fluxes using thermal infrared remote sensing. *Remote sensing of environment*, *60*(2), 195-216.

Baghdadi, N., & Zribi, M. (2016). *Land surface remote sensing in continental hydrology*. Elsevier.

Bakhtiari, B., & Liaghat, A. M. (2011). Seasonal sensitivity analysis for climatic variables of ASCE-Penman-Monteith model in a semi-arid

climate. *Journal of Agricultural Science and Technology*, *13*(7), 1135-1145.

Bastiaanssen, W. G., Menenti, M., Feddes, R. A., & Holtslag, A. A. M. (1998). A remote sensing surface energy balance algorithm for land (SEBAL). 1. Formulation. *Journal of hydrology*, *212*, 198-212.

Bausch, W. C., & Neale, C. M. (1987). Crop coefficients derived from reflected canopy radiation: a concept. *Transactions of the ASAE*, *30*(3), 703-0709.

Bazzi, H., Baghdadi, N., El Hajj, M., Zribi, M., Minh, D. H. T., Ndikumana, E., Courault, D., & Belhouchette, H. (2019a). Mapping paddy rice using Sentinel-1 SAR time series in Camargue, France. *Remote Sensing*, *11*(7), 887.

Bazzi, H., Baghdadi, N., Ienco, D., El Hajj, M., Zribi, M., Belhouchette, H., Escorihuela, M. J., & Demarez, V. (2019b). Mapping irrigated areas using Sentinel-1 Time series in Catalonia, Spain. *Remote Sensing*, *11*(15), 1836.

Benjamin, S. G., Brown, J. M., Brunet, G., Lynch, P., Saito, K., & Schlatter, T. W. (2019). 100 years of progress in forecasting and NWP applications. *Meteorological Monographs*, *59*, 13-1.

Benz, U. C., Hofmann, P., Willhauck, G., Lingenfelder, I., & Heynen, M. (2004). Multi-resolution, object-oriented fuzzy analysis of remote sensing data for GIS-ready information. *ISPRS Journal of photogrammetry and remote sensing*, *58*(3-4), 239-258.

Bolognesi F., S., Pasolli, E., Belfiore, O. R., De Michele, C., & D'Urso, G. (2020). Harmonized Landsat 8 and Sentinel-2 Time Series Data to Detect Irrigated Areas: An Application in Southern Italy. *Remote Sensing*, *12*(8), 1275.

Cai, X., & Rosegrant, M. W. (2002). Global water demand and supply projections: part 1. A modeling approach. Water International, 27(2), 159-169.

Cai, J., Liu, Y., Lei, T., & Pereira, L. S. (2007). Estimating reference evapotranspiration with the FAO Penman–Monteith equation using

daily weather forecast messages. *Agricultural and Forest Meteorology*, *145*(1-2), 22-35.

Calera, A., Campos, I., Osann, A., D'Urso, G., & Menenti, M. (2017). Remote sensing for crop water management: from ET modelling to services for the end users. *Sensors*, *17*(5), 1104.

Cao, J., Tan, J., Cui, Y., & Luo, Y. (2019). Irrigation scheduling of paddy rice using short-term weather forecast data. *Agricultural water management*, *213*, 714-723.

Chance, E. W., Cobourn, K. M., Thomas, V. A., Dawson, B. C., & Flores, A. N. (2017). Identifying irrigated areas in the snake river plain, Idaho: evaluating performance across composting algorithms, spectral indices, and sensors. Remote sensing, 9(6), 546.

Chaudhry, S., & Garg, S. (2019). Smart irrigation techniques for water resource management. In *Smart Farming Technologies for Sustainable Agricultural Development* (pp. 196-219). IGI Global.

Chen, Q., Zhang, Y., Ekroos, A., & Hallikainen, M. (2004). The role of remote sensing technology in the EU water framework directive (WFD). *Environmental Science & Policy*, *7*(4), 267-276.

Chirico, G. B., Pelosi, A., De Michele, C., Bolognesi, S. F., & D'Urso, G. (2018). Forecasting potential evapotranspiration by combining numerical weather predictions and visible and near-infrared satellite images: An application in southern Italy. *The Journal of Agricultural Science*, *156*(5), 702-710.

Civco, D. L., Hurd, J. D., Wilson, E. H., Song, M., & Zhang, Z. (2002, April). A comparison of land use and land cover change detection methods. In *ASPRS-ACSM Annual Conference* (Vol. 21).

Coleman, G., & DeCoursey, D. G. (1976). Sensitivity and model variance analysis applied to some evaporation and evapotranspiration models. *Water Resources Research*, *12*(5), 873-879.

Consoli, S., & Vanella, D. (2014). Comparisons of satellite-based models for estimating evapotranspiration fluxes. *Journal of hydrology*, *513*, 475-489.

D'Urso, G., Richter, K., Calera, A., Osann, M. A., Escadafal, R., Garatuza-Pajan, J., Hanich, L., Perdigao, A., Tapia, J.B., & Vuolo, F. (2010). Earth Observation products for operational irrigation management in the context of the PLEIADeS project. *Agricultural water management*, *98*(2), 271-282.

D'Urso, G., & Calera Belmonte, A. (2006). Operative approaches to determine crop water requirements from Earth Observation data: methodologies and applications. In *AIP conference proceedings* (Vol. 852, No. 1, pp. 14-25). American Institute of Physics.

D'Urso, G., Menenti, M., & Santini, A. (1999). Regional application of one-dimensional water flow models for irrigation management. *Agricultural Water Management*, *40*(2-3), 291-302.

Draeger, W. C. (1977). Monitoring irrigated land acreage using Landsat imagery: An application example.

Drechsel, S., Mayr, G. J., Messner, J. W., & Stauffer, R. (2012). Wind speeds at heights crucial for wind energy: measurements and verification of forecasts. *Journal of Applied Meteorology and Climatology*, *51*(9), 1602-1617.

Dubois, O. (2011). *The state of the world's land and water resources for food and agriculture: managing systems at risk*. Earthscan.

Fader, M., Shi, S., Bloh, W. V., Bondeau, A., & Cramer, W. (2016). Mediterranean irrigation under climate change: more efficient irrigation needed to compensate for increases in irrigation water requirements. *Hydrology and Earth System Sciences*, *20*(2), 953-973.

FAO, IFAD, UNICEF, WFP and WHO. (2021). *The State of Food Security and Nutrition in the World 2021. Transforming food systems for food security, improved nutrition and affordable healthy diets for all*. Rome, FAO.

Gao, Q., Zribi, M., Escorihuela, M. J., Baghdadi, N., & Segui, P. Q. (2018). Irrigation mapping using Sentinel-1 time series at field scale. *Remote Sensing*, *10*(9), 1495.

Gong, X., Liu, H., Sun, J., Gao, Y., & Zhang, H. (2019). Comparison of Shuttleworth-Wallace model and dual crop coefficient method for estimating evapotranspiration of tomato cultivated in a solar greenhouse. *Agricultural Water Management*, *217*, 141-153.

Gong, X., Liu, H., Sun, J., Gao, Y., & Zhang, H. (2019). Comparison of Shuttleworth-Wallace model and dual crop coefficient method for estimating evapotranspiration of tomato cultivated in a solar greenhouse. *Agricultural Water Management*, *217*, 141-153.

Gonzalez-Dugo, M. P., Neale, C. M. U., Mateos, L., Kustas, W. P., Prueger, J. H., Anderson, M. C., & Li, F. (2009). A comparison of operational remote sensing-based models for estimating crop evapotranspiration. *Agricultural and Forest Meteorology*, *149*(11), 1843-1853.

Heclman, J. L., Heilman, W. E., & Moore, D. G. (1982). Evaluating the Crop Coefficient Using Spectral Reflectance 1. *Agronomy Journal*, *74*(6), 967-971.

Hsiao, T. C., Steduto, P., & Fereres, E. (2007). A systematic and quantitative approach to improve water use efficiency in agriculture. *Irrigation science*, *25*(3), 209-231.

Irmak, S., Payero, J. O., Martin, D. L., Irmak, A., & Howell, T. A. (2006). Sensitivity analyses and sensitivity coefficients of standardized daily ASCE-Penman-Monteith equation. *Journal of Irrigation and Drainage Engineering*, *132*(6), 564-578.

Jin, N., Tao, B., Ren, W., Feng, M., Sun, R., He, L., Zhuang, W., & Yu, Q. (2016). Mapping irrigated and rainfed wheat areas using multi-temporal satellite data. *Remote Sensing*, *8*(3), 207.

Khanal, S., KC, K., Fulton, J. P., Shearer, S., & Ozkan, E. (2020). Remote sensing in agriculture—accomplishments, limitations, and opportunities. *Remote Sensing*, *12*(22), 3783.

Kolm, K. E., & Case, H. L. (1984). The identification of irrigated crop types and estimation of acreages from Landsat imagery. *Photogrammetric engineering and remote sensing*, *50*(10), 1479-1490.

Kustas, W. P. (1990). Estimates of evapotranspiration with a one-and two-layer model of heat transfer over partial canopy cover. *Journal of Applied Meteorology*, *29*(8), 704-715.

Liang, L., Li, L., Zhang, L., Li, J., & Li, B. (2008). Sensitivity of penman-monteith reference crop evapotranspiration in Tao'er River Basin of northeastern China. *Chinese Geographical Science*, *18*(4), 340-347.

Lillesand, T. M., & Kiefer, R. W. (1979). Remote sensing and image interpretation(Book). *New York, John Wiley and Sons, Inc., 1979. 624 p*.

Lorite, I. J., Ramírez-Cuesta, J. M., Cruz-Blanco, M., & Santos, C. (2015). Using weather forecast data for irrigation scheduling under semi-arid conditions. *Irrigation science*, *33*(6), 411-427.

Luo, Y., Chang, X., Peng, S., Khan, S., Wang, W., Zheng, Q., & Cai, X. (2014). Short-term forecasting of daily reference evapotranspiration using the Hargreaves–Samani model and temperature forecasts. *Agricultural Water Management*, *136*, 42-51.

Luo, Y., Traore, S., Lyu, X., Wang, W., Wang, Y., Xie, Y., Jiao, X., & Fipps, G. (2015). Medium range daily reference evapotranspiration forecasting by using ANN and public weather forecasts. *Water resources management*, *29*(10), 3863-3876.

Mancosu, N., Snyder, R. L., Kyriakakis, G., & Spano, D. (2015). Water scarcity and future challenges for food production. *Water*, *7*(3), 975-992.

McCown, R. L., Carberry, P. S., Dalgliesh, N. P., Foale, M. A., & Hochman, Z. (2012). Farmers use intuition to reinvent analytic decision support for managing seasonal climatic variability. *Agricultural systems*, *106*(1), 33-45.

McDonnell, J., Brophy, C., Ruelle, E., Shalloo, L., Lambkin, K., & Hennessy, D. (2019). Weather forecasts to enhance an Irish grass growth model. *European Journal of Agronomy*, *105*, 168-175.

Neale, C. M., Bausch, W. C., & Heermann, D. F. (1990). Development of reflectance-based crop coefficients for corn. *Transactions of the ASAE*, *32*(6), 1891-1900.

Nhamo, L., Van Dijk, R., Magidi, J., Wiberg, D., & Tshikolomo, K. (2018). Improving the accuracy of remotely sensed irrigated areas using post-classification enhancement through UAV capability. *Remote Sensing*, *10*(5), 712.

Norman, J. M., Kustas, W. P., & Humes, K. S. (1995). Source approach for estimating soil and vegetation energy fluxes in observations of directional radiometric surface temperature. *Agricultural and Forest Meteorology*, *77*(3-4), 263-293.

Ozdogan, M., Woodcock, C. E., Salvucci, G. D., & Demir, H. (2006). Changes in summer irrigated crop area and water use in Southeastern Turkey from 1993 to 2002: Implications for current and future water resources. *Water resources management*, *20*(3), 467-488.

Ozdogan, M., Yang, Y., Allez, G., & Cervantes, C. (2010). Remote sensing of irrigated agriculture: Opportunities and challenges. *Remote sensing*, *2*(9), 2274-2304.

Pageot, Y., Baup, F., Inglada, J., Baghdadi, N., & Demarez, V. (2020). Detection of irrigated and rainfed crops in temperate areas using Sentinel-1 and Sentinel-2 time series. *Remote Sensing*, *12*(18), 3044.

Pelosi, A., Medina, H., Villani, P., D'Urso, G., & Chirico, G. B. (2016). Probabilistic forecasting of reference evapotranspiration with a limited area ensemble prediction system. *Agricultural water management*, *178*, 106-118.

Perera, K. C., Western, A. W., Nawarathna, B., & George, B. (2014). Forecasting daily reference evapotranspiration for Australia using numerical weather prediction outputs. *Agricultural and forest meteorology*, *194*, 50-63.

Pôças, I., Calera, A., Campos, I., & Cunha, M. (2020). Remote sensing for estimating and mapping single and basal crop coefficientes: A review on spectral vegetation indices approaches. *Agricultural Water Management*, *233*, 106081.

Powell, R., & Brooks, C. (2008). Land use land cover mapping in the Tiffin River Watershed, 2004-2006.

Ragettli, S., Herberz, T., & Siegfried, T. (2018). An unsupervised classification algorithm for multi-temporal irrigated area mapping in central Asia. *Remote Sensing*, *10*(11), 1823.

Ramírez-Cuesta, J. M., Allen, R. G., Intrigliolo, D. S., Kilic, A., Robison, C. W., Trezza, R., Santos, C., & Lorite, I. J. (2020). METRIC-GIS: An advanced energy balance model for computing crop evapotranspiration in a GIS environment. *Environmental Modelling & Software*, *131*, 104770.

Ramírez-Cuesta, J. M., Allen, R. G., Zarco-Tejada, P. J., Kilic, A., Santos, C., & Lorite, I. J. (2019a). Impact of the spatial resolution on the energy balance components on an open-canopy olive orchard. *International Journal of Applied Earth Observation and Geoinformation*, *74*, 88-102.

Ramírez-Cuesta, J. M., Mirás-Avalos, J. M., Rubio-Asensio, J. S., & Intrigliolo, D. S. (2019b). A novel ArcGIS toolbox for estimating crop water demands by integrating the dual crop coefficient approach with multi-satellite imagery. *Water*, *11*(1), 38.

Ramírez-Cuesta, J. M., Cruz-Blanco, M., Santos, C., & Lorite, I. J. (2017). Assessing reference evapotranspiration at regional scale based on remote sensing, weather forecast and GIS tools. *International journal of applied earth observation and geoinformation*, *55*, 32-42.

Rundquist, D. C., Hoffman, R. O., Carlson, M. P., and Cook, A. E. (1989). "Nebraska Center-Pivot Inventory: An Example of Operational Satellite Remote Sensing on a Long-Term Basis." *Photogrammetric Engineering and Remote Sensing*, *55*, 587-590.

Sadeghi, M., Babaeian, E., Tuller, M., & Jones, S. B. (2017). The optical trapezoid model: A novel approach to remote sensing of soil moisture applied to Sentinel-2 and Landsat-8 observations. *Remote sensing of environment*, *198*, 52-68.

Schiewe, J., Tufte, L., & Ehlers, M. (2001). Potential and problems of multi-scale segmentation methods in remote sensing. *GeoBIT/GIS*, *6*(01), 34-39.

Singh, S., Boote, K. J., Angadi, S. V., & Grover, K. K. (2017). Estimating water balance, evapotranspiration and water use efficiency of spring safflower using the CROPGRO model. *Agricultural Water Management*, *185*, 137-144.

Su, Z. (2002). The Surface Energy Balance System (SEBS) for estimation of turbulent heat fluxes. *Hydrology and earth system sciences*, *6*(1), 85-99.

Sun, Z., Wang, Q., Matsushita, B., Fukushima, T., Ouyang, Z., & Watanabe, M. (2009). Development of a simple remote sensing evapotranspiration model (Sim-ReSET): algorithm and model test. *Journal of Hydrology*, *376*(3-4), 476-485.

Thelin, G. P., & Heimes, F. J. (1987). *Mapping irrigated cropland from Landsat data for determination of water use from the High Plains aquifer in parts of Colorado, Kansas, Nebraska, New Mexico, Oklahoma, South Dakota, Texas, and Wyoming* (No. 1400). US Government Printing Office.

Theodoropoulos, C., & Skoulikidis, N. (2014, October). Environmental flows: the European approach through the Water Framework Directive 2000/60/EC. In *Proceedings of the 10th International Congress of the Hellenic Geographical Society* (pp. 1140-1152).

Thiruvengadachari, S. (1981). Satellite sensing of irrigation patterns in semiarid areas- An Indian study. *Photogrammetric Engineering and Remote Sensing*, *47*(10), 1493-1499.

Vanella, D., Intrigliolo, D. S., Consoli, S., Longo-Minnolo, G., Lizzio, G., Dumitrache, R. C., ... & Ramírez-Cuesta, J. M. (2020). Comparing the use of past and forecast weather data for estimating reference evapotranspiration. *Agricultural and Forest Meteorology*, *295*, 108196.

Vanino, S., Nino, P., De Michele, C., Bolognesi, S. F., D'Urso, G., Di Bene, C., Pennelli, B., Vuolo, F., Farina, B., Pulighe, G., & Napoli, R.

(2018). Capability of Sentinel-2 data for estimating maximum evapotranspiration and irrigation requirements for tomato crop in Central Italy. *Remote Sensing of Environment*, *215*, 452-470.

Vuolo, F., D'Urso, G., De Michele, C., Bianchi, B., & Cutting, M. (2015). Satellite-based irrigation advisory services: A common tool for different experiences from Europe to Australia. *Agricultural Water Management*, *147*, 82-95.

Wagle, P., Bhattarai, N., Gowda, P. H., & Kakani, V. G. (2017). Performance of five surface energy balance models for estimating daily evapotranspiration in high biomass sorghum. *ISPRS Journal of Photogrammetry and Remote Sensing*, *128*, 192-203.

Wriedt, G., Van der Velde, M., Aloe, A., & Bouraoui, F. (2009). Estimating irrigation water requirements in Europe. *Journal of Hydrology*, *373*(3-4), 527-544.

Xiong, Y., Luo, Y., Wang, Y., Traore, S., Xu, J., Jiao, X., & Fipps, G. (2016). Forecasting daily reference evapotranspiration using the Blaney–Criddle model and temperature forecasts. *Archives of Agronomy and Soil Science*, *62*(6), 790-805.

Yang, Y., Cui, Y., Luo, Y., Lyu, X., Traore, S., Khan, S., & Wang, W. (2016). Short-term forecasting of daily reference evapotranspiration using the Penman-Monteith model and public weather forecasts. *Agricultural water management*, *177*, 329-339.

Zucaro, R., & Pontrandolfi, A. (2006). Italian policy framework for water in agriculture. *Water and Agriculture Sustainability, Markets and Policies: Sustainability, Markets and Policies*, *411*.

2 Integrating forecast meteorological data into the ArcDualK_c model for estimating spatially distributed evapotranspiration rates of a citrus orchard[1]

Abstract

In the last years, several satellite-based models, using measured or forecast meteorological data, have been developed for determining spatially distributed ET_c estimates. The study herein presented aims at assessing the reliability of the ArcDualK_c model, based on the FAO-56 dual K_c, for deriving spatially distributed estimates of K_c and ET_c in a DI orange orchard. Daily ET_c and dual-K_c values were obtained using Sentinel-2 satellite imagery in combination with measured and forecast meteorological data provided by the nearest weather station and by COSMO model, respectively. Overestimations on K_c and ET_c resulted from the study when using forecast instead of measured meteorological data (average PBIAS of 7.62% and 26.24%, respectively); this might be caused by some inaccuracies in meteorological predictions. The K_e derived by the ArcDualK_c model resulted similar between the DI and the fully irrigated treatments. Differences up to 6% in terms of K_c and ET_c were identified among the irrigation strategies, mainly due to variations of the K_{cb}. Despite the reliability of the ArcDualK_c model, the obtained results might be

[1] A modified version of this Chapter was published as Longo-Minnolo, G., Vanella, D., Consoli, S., Intrigliolo, D. S., & Ramírez-Cuesta, J. M. (2020). Integrating forecast meteorological data into the ArcDualKc model for estimating spatially distributed evapotranspiration rates of a citrus orchard. *Agricultural Water Management, 231*, 105967. https://doi.org/10.1016/j.agwat.2019.105967

influenced by the heterogeneity of Sentinel-2 pixel, containing vegetated and bare soil surfaces, highlighting the need to integrate the model with ground-based data or by using higher-resolution images.

Keywords: Remote sensing data; Modelling; Sentinel-2; Crop coefficients; Precision irrigation

2.1 Introduction

Irrigation contributes to the greatest amount of water consumption among several economic sectors (Dubois, 2011) especially in semi-arid areas, where water deficit is a limiting factor for crop production (Singh et al., 2017). A well scheduled and dosed irrigation regime is essential for matching crop water requirements (Gu et al., 2017), and *vice-versa* accurate estimations of crop evapotranspiration (ET_c) represent a significant *proxy* for scheduling irrigation (Gong et al., 2019).

Several satellite-based models have been developed in the last 30 years for determining spatially distributed ET_c estimates at different spatial scales (Zhang et al., 2016; Mokhtari et al., 2018; Olivera-Guerra et al., 2018; Ramírez-Cuesta et al., 2019a). In general, these models are divided in two categories: those based on the SEB and those based on VI. The first category computes the latent heat flux and thus ET_c using ground-based ancillary data and remotely sensed data in the VIS, NIR and TIR portions of the electromagnetic spectrum (Zhang et al., 2016). However, the current limited spatial resolution in thermal domain restricts the use of these models at field scale, especially when the plot size is smaller than the pixel resolution (Ramírez-Cuesta et al., 2019a). The second category of models computes ET_c from empirical site-specific relationships between the fraction of ground covered by vegetation and VI derived from the canopy reflectance in VIS and NIR. These models are usually based

on the FAO-56 approach (Allen et al., 1998), which estimates ET_c by multiplying ET_0 by a single or dual K_c. In the dual K_c approach, K_c accounts for both plant transpiration (T) and soil evaporation (E) terms, represented by K_{cb} and K_e, respectively (Allen et al., 2018).

The dual K_c approach is often applied for its simplicity and operational basis (Consoli et al., 2016; Olivera-Guerra et al., 2018). In fact, it requires few inputs including phenological stages, irrigation amounts and standard meteorological data, even if a site-specific soil water balance is needed (Vanella et al., 2019). However, weather data, when available, are affected by large uncertainties, since they are estimated by spatial interpolation of sparse meteorological ground stations (Lorite et al., 2015). Nowadays, in order to overcome the limitation of available meteorological data, numerical weather prediction models are used to provide reliable forecast data (Pelosi et al., 2016; Chirico et al., 2018). Across Europe, different consortiums provide meteorological forecasting services, such as HIRLAM, ALADIN, ECMWF, COSMO. The use of forecast meteorological data for obtaining *a priori* ET_c estimations can provide a great tool for managing irrigation scheduling and facing with extreme events (Chirico et al., 2018).

In this study, spatially distributed estimates of K_c and ET_c were retrieved at farm level by a geographic information system (GIS) procedure integrated into the ArcDualK_c model (Ramírez-Cuesta et al., 2019b), which incorporated RS and separately measured and forecast meteorological data within the FAO-56 dual K_c approach. The main objectives of the study were (i) to assess the reliability of the ArcDualK_c model combined with forecast meteorological data provided by COSMO model for obtaining *a priori* spatially distributed K_c and ET_c, and (ii) to evaluate the ArcDualK_c model performance to predict ET fluxes and K_c values of deficit irrigated plots in semi-arid Mediterranean conditions.

2.2 Materials and methods

2.2.1 Site description

The study was carried out in an orange orchard (*Citrus sinensis* (L.) Osbeck cv 'Tarocco Sciara') during the period May-October 2017 (Day of the year, DOY_s 128-288). The orchard, of around 1 ha, is located in Eastern Sicily (Southern Italy, Lentini, SR; 37°20' N, 14°53' E) and managed by Italian Council for Agricultural Research and Agricultural Economics Analyses (CREA-OFA, Acireale). The climate of the area is typical semi-arid Mediterranean, characterized, for the study period by average air temperature, relative humidity and cumulative precipitation of 24.8 °C, 63.6%, 182.2 mm, respectively. The soil texture is sandy loam, with θ_{FC} and θ_{WP} values of 0.28 and 0.14 $m^3\ m^{-3}$, respectively (Aiello et al., 2014).

Different irrigation treatments were applied in the orange orchard (Fig. 2.1): (i) full irrigation (T1), supplying 100% of ET_c using a surface drip irrigation system; (ii) sustained DI (T2), replacing 75% of ET_c using a sub-surface drip irrigation system; (iii) regulated DI (T3), supplying 50% of ET_c in those vegetative phases less sensitive to water stress conditions (normally the end of the physiological fruit drop) and 100 % of ET_c during the remaining period; (iv) partial root-zone drying (T4), supplying 50% of ET_c alternatively on one side of the root-zone, while the other side was kept dry (Consoli et al., 2014; Consoli et al., 2017), and vice-versa every two weeks.

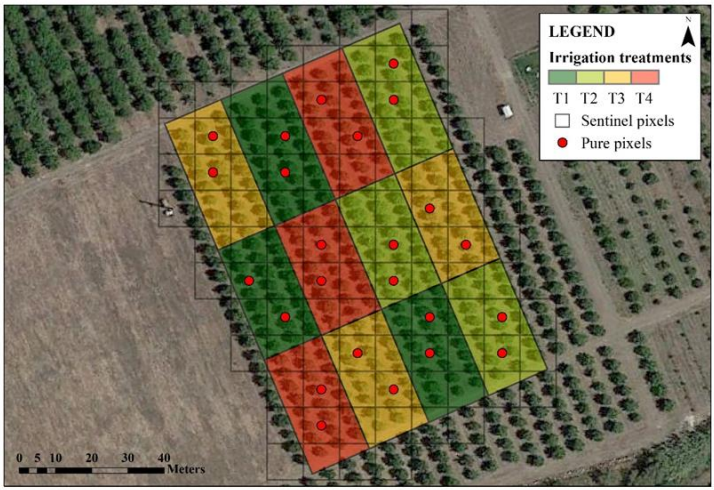

Fig.2.1. Irrigation treatments (T1 - full irrigation; T2 - sustained deficit irrigation; T3 - regulated deficit irrigation; T4 - partial root-zone drying) and satellite pixel grid superimposed at the study area. Location of pure pixels is reported as red points.

2.2.2 ArcDualK_c model description

The original dual K_c approach proposed in the FAO Irrigation and Drainage Paper No. 56 (Allen et al., 1998), determines ET_c on the basis of ET_0, by separating K_c into K_{cb}, which describes crop transpiration, and K_e, which accounts for soil evaporation:

$$ET_c = (K_{cb} + K_e)\, ET_0 \quad (1)$$

In this study, an ArcGIS toolbox (ArcDualK_c) developed by Ramírez-Cuesta *et al*., (2019b) was used in order to integrate the FAO-56 dual K_c approach with satellite data in a GIS environment (ArcMap 10, ESRI©). The ArcDualK_c model has been already tested, retrieving accurate crop water demand estimates, in a lettuce plot and in a peach

orchard located in South-eastern Spain (Los Alcáceres, Murcia) (Ramírez-Cuesta *et al*., (2019b)).

The ArcDualK_c routine includes 2 sub-models: the first, was used to compute K_{cb} outputs ($K_{cb,\ ArcDualKc}$), while the second was run for obtaining K_e ($K_{e,\ ArcDualKc}$), dual K_c (dual $K_{c,\ ArcDualKc}$) and ET_c estimations.

In general, K_{cb} represents the baseline potential K_c in absence of the additional effects of soil wetting by irrigation or precipitation. According to Allen et al. (1998), this coefficient is usually considered as a tabulated value ($K_{cb,\ tab}$) (i.e. 0.65, 0.60 and 0.65, at initial, middle and final stages, respectively, for *Citrus*, with 70% canopy and no ground cover).

In this study, $K_{cb,\ ArcDualKc}$ was computed, within the first ArcDualK_c sub-model, by using RS data, as function of SAVI (Gonzalez-Dugo et al., 2009; Consoli & Vanella, 2014 a, b):

$$K_{cb,ArcDualKc} = \frac{K_{cb,max}}{F_{c,max}} \left(\frac{SAVI - SAVI_{min}}{SAVI_{max} - SAVI_{min}} \right) \quad (2)$$

where, $SAVI_{max}$ e $SAVI_{min}$ refer to a high LAI and bare soil, respectively; $F_{c,max}$ is the maximum value of ground cover fraction (F_c) at which K_{cb} is maximal ($K_{cb,max}$). $K_{cb,max}$ values (i.e. $K_{cb,\ adj}$) were obtained by adopting the approach proposed by Allen et al. (1998), that adjusts $K_{cb,\ tab}$ at the middle and final stages considering the local RH and u_2 conditions at the study area, as follows:

$$K_{cb,adj} = K_{cb,tab} + [0.04\ (u_2 - 2) - 0.004\ (RH_{min} - 45)] \left(\frac{h}{3}\right)^{0.3} \quad (3)$$

SAVI was calculated, according to Huete (1988), as follows:

$$SAVI = \left(\frac{\rho_{NIR} - \rho_{RED}}{\rho_{NIR} + \rho_{RED} + L} \right) (1 + L) \quad (4)$$

where, ρ_{NIR} and ρ_{RED} are the NIR and red reflectance of RS data; L is a soil normalization factor fixed at 0.5.

F_c was defined as function of the NDVI (Gutman & Ignatov, 1998), as follows:

$$F_c = \frac{NDVI - NDVI_{min}}{NDVI_{max} - NDVI_{min}} \quad (5)$$

with $NDVI_{max}$ and $NDVI_{min}$ fixed to 1.00 and 0.01, respectively and NDVI values derived as in Rouse et al., (1974):

$$NDVI = \frac{\rho_{NIR} - \rho_{RED}}{\rho_{NIR} + \rho_{RED}} \quad (6)$$

Model calibration was necessary to refer $K_{cb,ArcDualKc}$ values, exclusively, to the local conditions. Initially, the ArcDualK_c first sub-model was run using default parameters (eq. 2). For the $K_{cb,ArcDualKc}$ calibration, $SAVI_{max}$ corresponded to the maximum value identified in the satellite image, whereas a constant value of 0.1 was assigned to $SAVI_{min}$. $F_{c,max}$ was then calculated by inverting eq. 2, considering SAVI parameter as the maximum SAVI value obtained among the 6 pure pixels of T1 treatment, assuming that in these pixels there are no water stress conditions (i.e. $K_{cb,ArcDualKc} = K_{cb,max}$) (Fig. 2.1).

In the second ArcDualK_c sub-model, a daily soil water balance (SWB) was run for calculating the amount of soil water content available for evaporation in the soil surface layer (i.e. K_e), as follows:

$$K_{e,ArcDuakKc} = \left(K_{c,max} - K_{cb}\right) K_r \quad (7)$$

where, $K_{c,max}$ represents the maximum K_c value following precipitation or irrigation, adjusted for local RH and u_2 conditions, calculated as indicated by Allen *et al*. (1998):

$$K_{c,max} = \max\left(\left\{1.2 + [0.04\,(u_2 - 2) - 0.004\,(RH_{min} - 45)]\,\left(\frac{h}{3}\right)^{0.3}\right\}, \{K_{cb} + 0.05\}\right) \quad (8)$$

K_r is an evaporation reduction coefficient related to the topsoil water depletion (Allen et al., 1998), as follows:

$$K_r = \frac{TEW - D_{e,i}}{TEW - REW} \quad (9)$$

where, TEW (total evaporable water) is the maximum cumulative depth of evaporation from the soil surface layer when the topsoil has been completely wetted, with TEW = 1000 (θ_{FC} – 0.5 θ_{WP}) Z_e; θ_{FC} and θ_{WP} are the soil field capacity and wilting point, respectively; Z_e is equal to 0.1 m as reported by Allen et al. (1998); REW (readily evaporable water) is the maximum water depth that can evaporate from the soil surface layer in the energy limiting stage (Allen et al., 1998 suggest to fix a REW value of 10 mm for sandy loam soil); $D_{e,i}$ represents the cumulative depletion of evaporation from soil surface estimated from a daily SWB, as follows:

$$D_{e,i} = D_{e,i-1} - P_i - I_i + ET \quad (10)$$

where, $D_{e,i}$ and $D_{e,i-1}$ refer to soil moisture depletion at the end of the day (i) and at the previous time steps (i-1); P_i and I_i refer to precipitation and irrigation on day i.; capillary rise, deep percolation and runoff were neglected (Consoli & Vanella, 2014 a, b).

2.2.3 Remote sensing data

In order to spatialize the dual K_c and ET_c estimates, the ArcDualK_c procedure was implemented using Sentinel-2 products (Level 1-C), provided by the European Space Agency (ESA,

https://sentinel.esa.int/). These RS products have a spatial resolution of 10 m in the VIS-NIR regions, with temporal resolution of 5 days (considering both Sentinel 2A and 2B satellites). Tab. 2.1 reports the available images within the study period, selected on the basis of clear sky condition (DOY, acquisition date and Satellite platform were reported for each image).

Tab. 2.1. Available Sentinel 2A/B satellite images in May-October 2017 at the experimental site.

DOY	Acquisition date	Satellite
128	08/05/2017	Sentinel2A
138	18/05/2017	Sentinel2A
148	28/05/2017	Sentinel2A
158	07/06/2017	Sentinel2A
168	17/06/2017	Sentinel2A
178	27/06/2017	Sentinel2A
183	02/07/2017	Sentinel2B
188	07/07/2017	Sentinel2A
193	12/07/2017	Sentinel2B
203	22/07/2017	Sentinel2B
208	27/07/2017	Sentinel2A
213	01/08/2017	Sentinel2B
218	06/08/2017	Sentinel2A
223	11/08/2017	Sentinel2B
228	16/08/2017	Sentinel2A
233	21/08/2017	Sentinel2B
238	26/08/2017	Sentinel2A
243	31/08/2017	Sentinel2B
248	05/09/2017	Sentinel2A
253	10/09/2017	Sentinel2B
258	15/09/2017	Sentinel2A
273	30/09/2017	Sentinel2B
283	10/10/2017	Sentinel2B
288	15/10/2017	Sentinel2A

Only pure pixels (covering a sole irrigation treatment) were used for extracting $K_{c,\ ArcDualKc}$ (and its components: $K_{cb,\ ArcDualKc}$ and $K_{e,\ ArcDualKc}$) and ET_c values from RS images, in order to avoid edge-pixel contamination. Specifically, 6 pure pixels per treatment were

selected as samples for further analysis and comparisons, with a total of 24 pixels for the 1 ha orchard under study (Fig. 2.1).

2.2.4 Measured and forecast meteorological data

Measured and forecast daily ET_0 estimates were used for feeding the ArcDualK_c model (Fig. 2.2). These values were computed by Ref-ET software (Allen, 2009), using separately ground-based and forecast meteorological data, by following the P-M equation (Allen et al., 1998):

$$ET_0 = \frac{0.408\,\Delta\cdot(R_n - G) + \gamma\cdot\frac{37}{T+273}\cdot u_2\cdot(e_s - e_a)}{\Delta + \gamma\cdot(1+0.34u_2)} \quad (11)$$

where, R_n is the net radiation at the reference crop surface (MJ m^{-2} h^{-1}); G is the soil heat flux density (MJ m^{-2} h^{-1}); T is the mean hourly air temperature T_{air} (°C); Δ is the slope of saturation vapour pressure curve at T_{air} (kPa $°C^{-1}$); γ is the psychrometric constant (kPa $°C^{-1}$); e_s is the saturation vapour pressure at T_{air} (kPa); e_a is the average hourly actual vapour pressure (kPa); and u_2 is the average hourly wind speed at 2 m height (m s^{-1}).

In particular, measured weather data were provided by a ground-based automatic meteorological station located about 2 km far from the experimental site (37.35°N, 14.91°E, 50 m a.s.l.) and managed by the Sicilian Agro-meteorological Information Service (SIAS, www.sias.regione.sicilia.it). Forecast meteorological data were provided by the atmospheric prediction COSMO model (https://www.cosmo-model.org/). Specifically, COSMO is a deterministic limited-area non-hydrostatic fully compressible atmospheric prediction model for forecasting operations on meso–β (20–200 Km) and meso–γ (2–20 Km) scales (Schättler et al., 2008; Steppeler et al., 2003). In this study, the COSMO model was run at 7

km horizontal resolution and the forecast was made for each hour until 78 hours anticipation, which corresponds with lead times from 1 to 3 days (1-day, 2-days, 3-days). Moreover, forecast cumulated precipitation, until the forecast time (P, mm) was incorporated into the ArcDualK_c second sub-model.

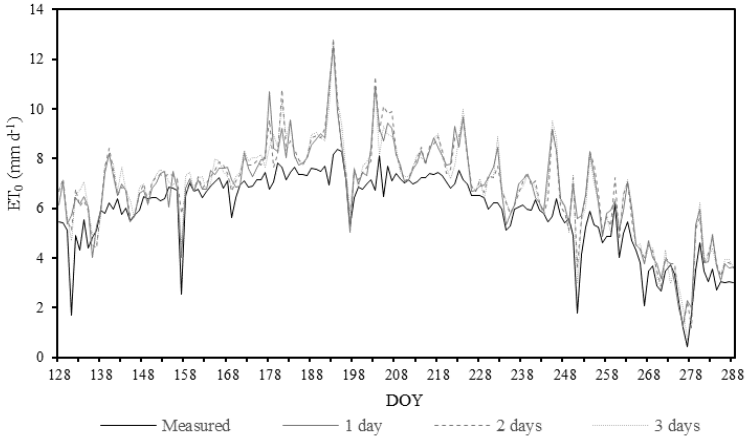

Fig. 2.2. Temporal evolution of daily ET_0 (mm d^{-1}) computed using measured and forecast meteorological data at different leading times (1-day, 2-days, 3-days).

2.2.5 Statistical performance

The performance of the ArcDualK_c model was evaluated by comparing separately its outputs ($K_{cb,\ ArcDualKc}$, $K_{e,\ ArcDualKc}$, $K_{c,\ ArcDualKc}$ and ET_c estimates) obtained, both by running the model with forecast meteorological data and with measured meteorological data.

The adopted statistical indicators were: regression slope (b), coefficient of determination (R^2; eq. 12), root-mean-square error (RMSE; eq.13), percent bias (PBIAS; eq.14); coefficient of variation (CV; eq.15).

$$R^2 = \frac{(\sum(S_i - \hat{S})(O_i - \hat{O}))^2}{\sum S_i - \hat{S})^2 \sum(O_i - \hat{O})^2} \quad (12)$$

$$RMSE = \sqrt{\frac{\sum_{i=1}^{n}(S_i - O_i)^2}{n}} \quad (13)$$

$$PBIAS = \frac{\sum(S_i - O_i)}{\sum O_i} \cdot 100 \quad (14)$$

where S_i is the simulated value, O_i is the observed value, $\hat{S}$ and $\hat{O}$ are the averages of the data arrays of S_i and O_i, and *n* is the numbers of observations. Specifically, the goodness of ArcDualK$_c$ model was evaluated respect to the FAO-56 tabulated values in terms of K_{cb} (Section 2.3.1), considering the $K_{cb,\ ArcDualKc}$ and $K_{cb,\ adj}$ as S_i and O_i values, respectively. On the other hand, when analysing the performance of ArcDualK$_c$ using measured and forecast meteorological data (Section 2.3.2.1), the first were considered as O_i whereas the forecast corresponded to S_i.

$$CV = \frac{SD}{AM} \cdot 100 \quad (15)$$

where, SD and AM are the standard deviation and the average of each data set.

2.3 Results

2.3.1 Comparison of K_{cb} obtained from ArcDualK_c and FAO-56 models

Fig. 2.3 shows the temporal evolution of the $K_{cb,ArcDualKc}$ values obtained using ground-based meteorological measures (a) and forecast-based meteorological estimations at different lead times (b, 1-day; c, 2-days; d, 3-days). In the same figure, $K_{cb,tab}$ and $K_{cb,adj}$ values are reported, together with $K_{cb,ArcDualKc}$ values at the different irrigation treatments (T1-T4). During the growing season 2017, using ground-based weather observations (a; Fig. 2.3), $K_{cb,ArcDualKc}$ varies from 0.50 to 0.56 in the development stage (*dev* in Fig. 2.3: DOY_s 128 - 149), from 0.52 to 0.67 in the middle stage (*mid* in Fig. 2.3: DOY_s 150 - 269) and from 0.45 to 0.57 in the final stage (*end* in Fig 2.3: DOY_s 270 - 288). Instead, using forecast meteorological estimations (b, c, d; Fig. 2.3), $K_{cb,ArcDualKc,}$ varies from 0.50 to 0.57 in the development stage (*dev* in Fig. 2.3: DOY_s 128 - 149), from 0.52 to 0.80 in the middle stage (*mid* in Fig. 2.3: DOY_s 150 - 269) and from 0.48 to 0.60 in the final stage (*end* in Fig. 2.3: DOY_s 270 - 288).

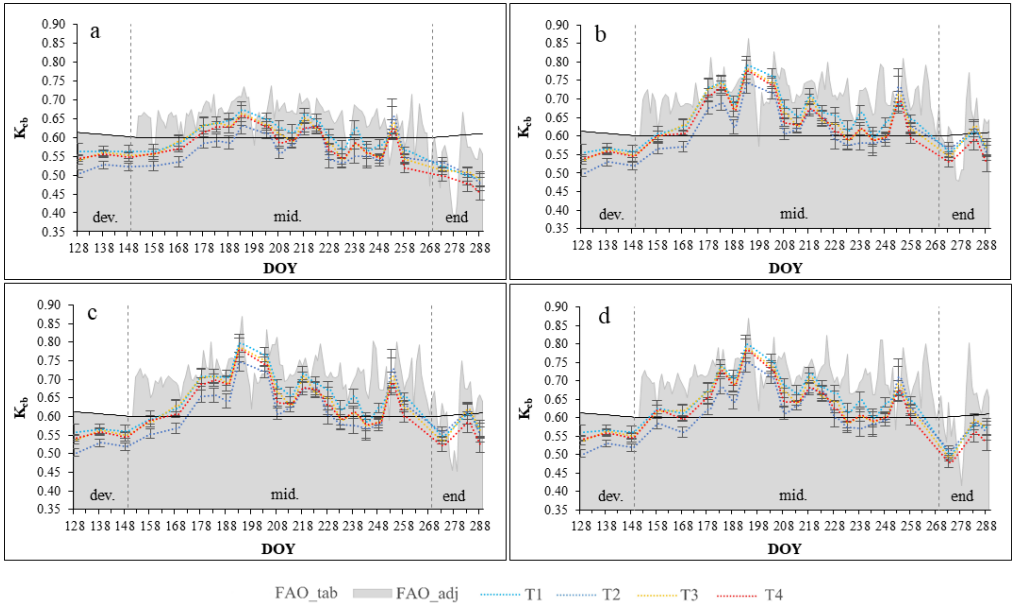

Fig. 2.3. Temporal evolution of K_{cb} obtained by the ArcDualK_c model ($K_{cb,ArcDualKc}$) at the different irrigation treatments (T1 - full irrigation; T2 - sustained deficit irrigation; T3 - regulated deficit irrigation; T4 - partial root-zone drying) from DOY 128 to 288 (2017), using (a) meteorological measurements and (b-d) forecast meteorological estimations at 1-day, 2-days and 3-days lead times.

Tab. 2.2 reports the statistical performances (RMSE, PBIAS, CV) of the comparison between $K_{cb,\ ArcDualKc}$ and the $K_{cb,adj}$ obtained using as input measured and forecast meteorological data, respectively, at different lead times (1-day, 2-days, 3-days; "All days" refers to all leading times together). Statistical indicators refer to the different irrigation treatments supplied at the study site (T1-T4; ALL denotes all treatments together).

Tab. 2.2. Statistical performance of the K_{cb} derived by ArcDualK_c model ($K_{cb,ArcDualKc}$) compared with locally adjusted FAO-56 K_{cb} ($K_{cb,\ adj}$) obtained using as input measured and forecast meteorological data, respectively, at different lead times (1-day, 2-days, 3-days; "All days" refers to all leading times together).

		Measured	1-day	2-days	3-days	All days
T1*	**RMSE**	0.11	0.08	0.08	0.08	0.08
	PBIAS (%)	-14.15	-6.69	-6.98	-7.78	-6.96
	CV (%)	7.64	10.70	10.96	11.59	11.07
T2*	**RMSE**	0.14	0.11	0.11	0.11	0.11
	PBIAS (%)	-19.10	-12.01	-12.28	-14.36	-12.29
	CV (%)	7.66	11.20	11.45	11.64	11.41
T3*	**RMSE**	0.12	0.09	0.09	0.09	0.09
	PBIAS (%)	-15.93	-8.60	-8.90	-10.06	-8.88
	CV (%)	7.95	11.18	11.32	11.87	11.44
T4*	**RMSE**	0.13	0.09	0.09	0.10	0.09
	PBIAS (%)	-17.19	-10.01	-10.30	-11.75	-10.28
	CV (%)	8.31	11.05	11.21	11.95	11.39
ALL*	**RMSE**	0.13	0.09	0.09	0.09	0.09
	PBIAS (%)	-16.59	-9.33	-9.62	-10.94	-9.60
	CV (%)	8.17	11.21	11.41	11.93	11.52

* T1-T4 refer to full irrigation, sustained deficit irrigation, regulated deficit irrigation and partial root-zone drying treatments, respectively; ALL denotes all treatments together.

Generally, good performances were obtained when comparing $K_{cb,\ ArcDualKc}$ and $K_{cb,adj}$ for all the irrigation treatments (ALL, Tab. 2.2),

with RMSE values of 0.09 and 0.13 by using forecast and measured meteorological data, respectively. However, underestimations were observed by using both forecast and measured meteorological data (PBIAS of -9.60% and -16.59%, respectively). The $K_{cb,\ ArcDualKc}$ variability within the study area, assessed through the CV, was 11.52% and 8.17% from forecast and measured meteorological data, respectively.

Using measured meteorological data, the underestimations of $K_{cb,ArcDualKc}$ were higher at the DI treatments (T2-T4; PBIAS ranging from -15.93 to -19.10% and RMSE from 0.09 to 0.11) respect to T1 (PBIAS -6.96% and RMSE 0.08). Similarly, using forecast meteorological data, the underestimations of $K_{cb,ArcDualKc}$ were higher at the DI treatments (T2-T4; PBIAS ranging from -8.88 to -12.29% and RMSE from 0.09 to 0.11) than at T1 (PBIAS -6.96% and RMSE 0.08). No relevant differences were observed in terms of lead time, using both the approaches (Tab. 2.2).

2.3.2 ET_c and crop coefficients comparison

Tab. 2.3 shows the average values (CV values in brackets) of $K_{cb,ArcDualKc}$, $K_{e,ArcDualKc}$, $K_{c,ArcDualKc}$ and daily ET_c (mm d^{-1}) estimates, obtained by running the ArcDualK_c model, separately with measured and forecast meteorological data at different lead times (1-day to 3-days and all days).

Specifically, $K_{cb,ArcDualKc}$ oscillated from 0.56 (using measured data) to 0.64 (using 1-day time lead forecast meteorological data), and it resulted always lower when using measured meteorological data as input for the ArcDualK_c model (Fig 2.3 and Tab. 2.3). $K_{e,ArcDualKc}$, independently of the meteorological data source, had values of 0.06-0.07, and showed no significant differences among the irrigation treatments (Tab. 2.3). These results led to values of $K_{c,ArcDualKc}$ and daily ET_c ranging from 0.62 to 0.70 and from 3.61 to 4.85 mm day^{-1},

respectively (Figs. 2.4 and 2.5 and Tab. 2.3). Due to the lower values of $K_{cb,\ ArcDualKc}$ and daily ET_0 (Fig. 2.2) obtained using measured meteorological data, the daily ET_c values resulted always lower than when using forecast meteorological data (Figs. 2.4 and 2.5 and Tab. 2.3).

Tab 2.3. Average values (and coefficient of variation, CV) of Kcb, Ke, Kc and daily ETc (mm d-1) obtained from the ArcDualKc model using measured and forecast meteorological data at different lead times (1-day, 2-days, 3-days; "All days" refers to all leading times together) as inputs.

		T1*	T2*	T3*	T4*	ALL*
K_{cb}	**Measured**	0.59 (0.08)	0.56 (0.08)	0.58 (0.11)	0.57 (0.08)	0.57 (0.08)
	1-day	0.64 (0.11)	0.60 (0.11)	0.64 (0.11)	0.62 (0.11)	0.62 (0.11)
	2-days	0.64 (0.11)	0.60 (0.11)	0.63 (0.11)	0.62 (0.11)	0.62 (0.11)
	3-days	0.64 (0.11)	0.60 (0.12)	0.62 (0.12)	0.61 (0.12)	0.62 (0.12)
	All days	0.64 (0.11)	0.60 (0.11)	0.63 (0.11)	0.62 (0.11)	0.62 (0.12)
K_e	**Measured**	0.06 (0.88)	0.06 (0.87)	0.06 (0.93)	0.06 (0.88)	0.06 (0.88)
	1-day	0.06 (1.01)	0.06 (1.01)	0.06 (1.01)	0.06 (1.01)	0.06 (1.01)
	2-days	0.06 (0.97)	0.06 (0.97)	0.06 (0.97)	0.06 (0.97)	0.06 (0.97)
	3-days	0.07 (0.91)	0.07 (0.91)	0.07 (0.91)	0.07 (0.91)	0.07 (0.91)
	All days	0.06 (0.96)	0.06 (0.96)	0.06 (0.96)	0.07 (0.96)	0.06 (0.96)
K_c	**Measured**	0.65 (0.11)	0.62 (0.12)	0.64 (0.14)	0.63 (0.11)	0.64 (0.11)
	1-day	0.70 (0.14)	0.66 (0.14)	0.69 (0.14)	0.68 (0.14)	0.68 (0.14)
	2-days	0.70 (0.14)	0.67 (0.15)	0.69 (0.14)	0.68 (0.14)	0.68 (0.14)
	3-days	0.70 (0.14)	0.67 (0.15)	0.69 (0.14)	0.68 (0.14)	0.69 (0.14)
	All days	0.70 (0.14)	0.67 (0.15)	0.69 (0.14)	0.68 (0.14)	0.68 (0.14)
ET_c (mm d^{-1})	**Measured**	3.82 (0.32)	3.61 (0.31)	3.75 (0.36)	3.71 (0.32)	3.72 (0.32)
	1-day	4.80 (0.34)	4.53 (0.34)	4.71 (0.34)	4.65 (0.34)	4.67 (0.34)
	2-days	4.84 (0.35)	4.57 (0.35)	4.75 (0.35)	4.69 (0.35)	4.71 (0.35)
	3-days	4.85 (0.35)	4.58 (0.34)	4.76 (0.35)	4.70 (0.35)	4.72 (0.35)
	All days	4.83 (0.34)	4.56 (0.34)	4.74 (0.35)	4.68 (0.35)	4.70 (0.35)

* T1-T4 refer to full irrigation, sustained deficit irrigation, regulated deficit irrigation and partial root-zone drying treatments, respectively; ALL denotes all treatments together.

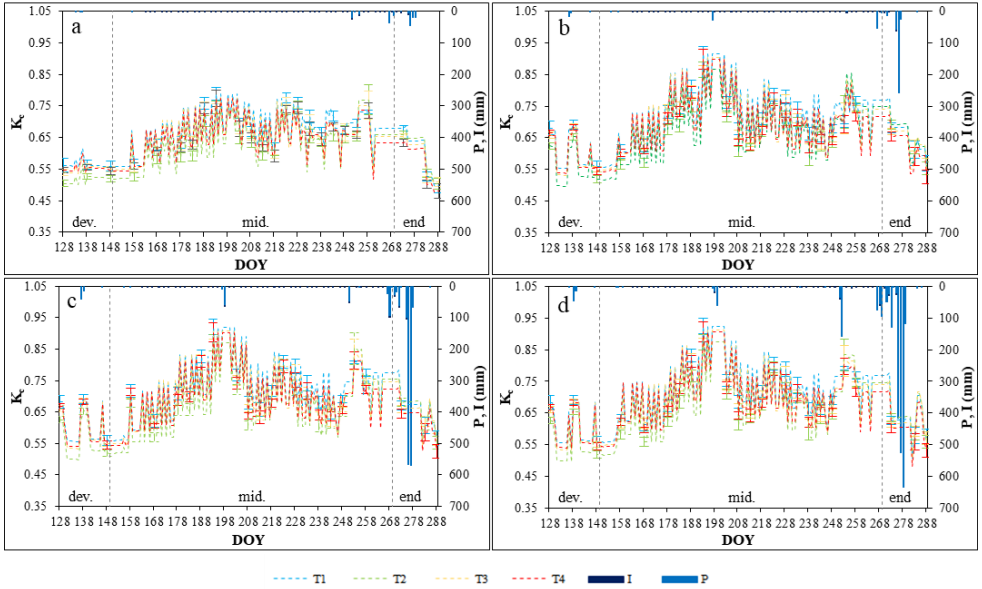

Fig. 2.4. Temporal evolution of the K_c obtained by the ArcDualK_c model ($K_{c,ArcDualKc}$) at the different irrigation treatments (T1 - full irrigation; T2 - sustained deficit irrigation; T3 - regulated deficit irrigation; T4 - partial root-zone drying) from DOY 128 to 288 (2017), using (a) measured and (b-d) forecast meteorological data at 1-day, 2-days and 3-days lead times. I and P refer to irrigation and precipitation, respectively.

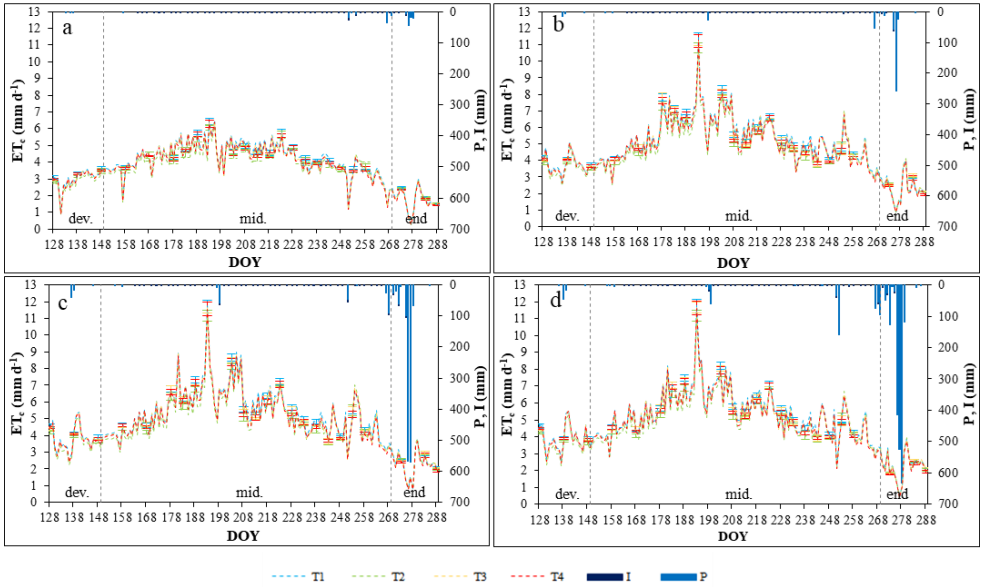

Fig. 2.5. Temporal evolution of ETc computed by the ArcDualKc model (mm d-1) at the different irrigation treatments (T1 - full irrigation; T2 - sustained deficit irrigation; T3 - regulated deficit irrigation; T4 - partial root-zone drying) from DOY 128 to 288 (2017), using (a) measured and (b-d) forecast meteorological data at 1-day, 2-days and 3-days lead times. I and P refer to irrigation and precipitation, respectively.

Figs. 2.6 and 2.7 show examples of the spatially distributed of $K_{c,ArcDualKc}$ and daily ET_c (mm d^{-1}) estimates obtained by the ArcDualK_c model at the experimental site, using separately as input measured (a, c, e) and forecast meteorological data (b, d, f). Figs. 2.6 and 2.7 refers to DOYs 138, 218 and 283. Average values of $K_{c,ArcDualKc,}$ using measured meteorological data, were, respectively, of 0.55, 0.59 and 0.52 in DOY 138, 218 and 283 (Fig. 2.6), corresponding to daily ET_c of 3.3, 4.4 and 1.8 mm·day^{-1} (Fig. 2.7). Higher values of $K_{c, ArcDualKc}$ and ET_c were obtained when using forecast meteorological data, with means of, respectively, 0.68, 0.69 and 0.60 (Fig. 2.6) and 3.98, 6.08, 2.83 mm day^{-1} (Fig. 2.7) in DOY 138, 218 and 283, respectively. In general, the irrigation treatments were quite homogeneous in all DOYs, with the exception of the edges of the field, where the effects of the surrounding plots increase the heterogeneity (Figs. 2.6 and 2.7).

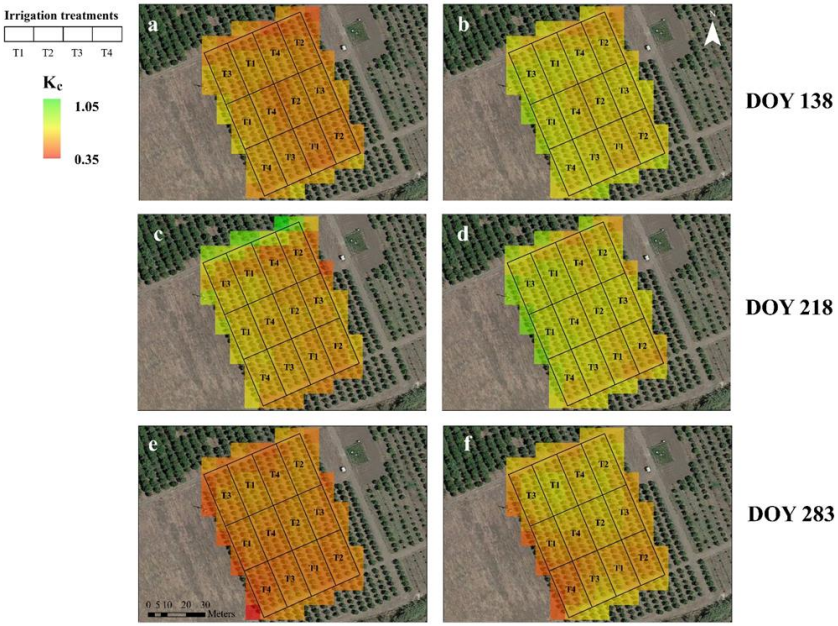

Fig. 2.6. Maps of K_c estimates from the ArcDualK_c model ($K_{c,ArcDualKc}$) obtained using measured meteorological data (a, c, e) and averaged (1-day to 3-day lead times) forecast meteorological data (b, d, f) in DOY$_s$ 138, 218 and 283. T1-T4 refer to full irrigation, sustained deficit irrigation, regulated deficit irrigation and partial root-zone drying treatments, respectively.

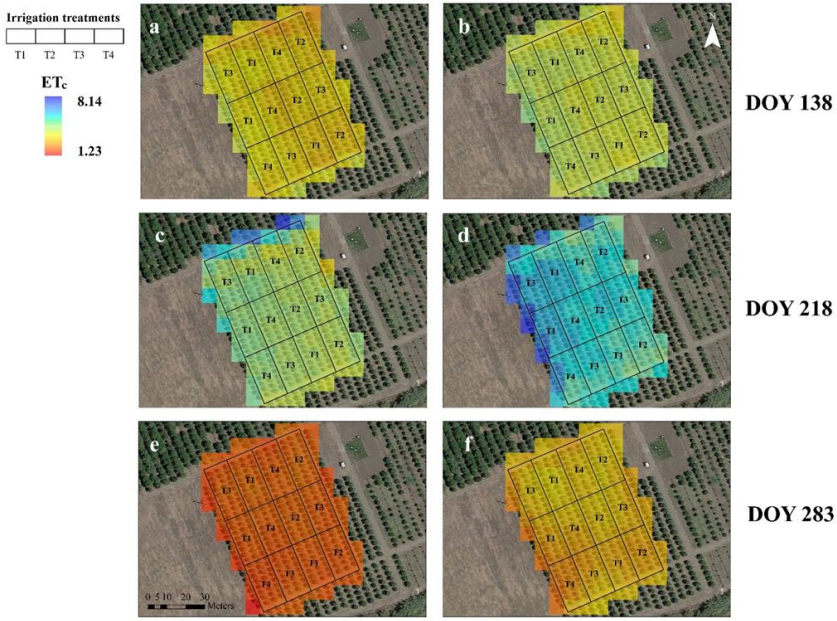

Fig. 2.7. Maps of daily ET$_c$ estimates from the ArcDualK$_c$ model (mm d^{-1}) obtained with measured meteorological data (a, c, e) and averaged (1-day to 3-day lead times) forecast meteorological data (b, d, f) in DOY$_s$ 138, 218 and 283. T1-T4 refer to full irrigation, sustained deficit irrigation, regulated deficit irrigation and partial root-zone drying treatments, respectively.

2.3.2.1 Measured versus forecast meteorological data

The daily ET_0 values obtained using measured and forecast meteorological data were 5.83 mm d^{-1} (CV 0.28) and 6.81 mm d^{-1} (CV 0.27), respectively. Referring to the specific lead times of the forecast meteorological data, ET_0 varied from 6.78 to 6.82 mm d^{-1} (CV 0.27-0.28) from 1 day to 3 days. As shown in Tab. 2.3, slight differences were observed by comparing measured and forecast meteorological data (all days), with $K_{cb,ArcDualKc}$ values of 0.57 (±0.08) and 0.62 (± 0.12), respectively. No substantial differences for $K_{e,ArcDualKc}$ were detected, with values of 0.06 using measured and forecast meteorological data. Similar differences were observed for $K_{c,ArcDualKc}$, which varies from 0.64 (±0.11) to 0.68 (±0.14) and in $ET_{c,}$ which oscillates from 3.73 (± 0.32) to 4.70 (±0.35) mm d^{-1}, using measured and forecast meteorological data respectively.

In terms of lead time (1-day, 2-days, 3-days), no relevant differences were observed for $K_{cb,ArcDualKc}$, (0.62; CV 0.11-0.12), $K_{e,ArcDualKc}$ (0.06-0.07; CV 0.91-1.01) and $K_{c,ArcDualKc}$ (0.68-0.69; CV of 0.14). These coefficients together with the daily ET_0 estimations led to small ET_c discrepancies, with values ranging from 4.67 to 4.72 mm d^{-1} (CV 0.34-0.35), from 1 to 3 days ahead, respectively.

Tab. 2.4 reports the statistical indices (b, R^2, RMSE, PBIAS) calculated by the ArcDualK_c model ($K_{cb,\ ArcDualKc}$, dual $K_{c,\ ArcDualKc}$, ET_c) at different lead times (1-day, 2-days, 3-days, all days) *versus* those values obtained with the measured meteorological data as input.

Generally, overestimations were observed in terms of $K_{cb,\ ArcDualKc}$ and ET_c by using forecast meteorological data, with PBIAS ranging within 8.80-8.07% and 25.40-26.86% from 1 to 3 days ahead, respectively. $K_{e,\ ArcDualKc}$ values were, instead, underestimated at 1-day forecast, with a PBIAS of -3.10% and overestimated at 2 and 3 days forecast, with PBIAS ranging within of 1.12-8.27% from 2 to 3 days ahead. RMSE values were steady for $K_{cb,ArcDualKc}$, $K_{e,ArcDualKc}$ and

$K_{c,ArcDualKc}$ values in terms of lead time (0.06, 0.04 and 0.07-0.08 respectively), while they ranged from 1.23 mm d^{-1} to 1.29 mm d^{-1} for ET_c, considering the different lead times.

Tab. 2.4. Statistical performance (b, R^2, RMSE and PBIAS) of K_c and ET_c estimates obtained by the ArcDualK_c model using as input measured and forecast meteorological data, respectively, at different lead times (1-day, 2-days, 3-days; "All days" refers to all leading times together).

		K_{cb}				K_e				K_c				ET_c (mm d^{-1})			
		1day	2 days	3 days	All days	1 day	2 days	3 days	All days	1 day	2 days	3 days	All days	1 day	2 days	3 days	All days
T1*	**b**	1.09	1.09	1.08	1.09	0.91	0.94	0.98	0.94	1.07	1.08	1.08	1.08	1.25	1.26	1.27	1.26
	R^2	0.73	0.74	0.74	0.74	0.55	0.55	0.53	0.54	0.71	0.70	0.66	0.69	0.76	0.77	0.80	0.74
	RMSE	0.06	0.06	0.06	0.06	0.04	0.04	0.04	0.04	0.07	0.07	0.08	0.07	1.27	1.32	1.30	1.30
	PBIAS (%)	8.78	8.58	8.08	8.48	-2.87	1.50	8.66	2.43	7.44	7.66	7.87	7.66	25.45	26.51	26.90	26.29
T2*	**b**	1.09	1.09	1.08	1.09	0.90	0.93	0.97	0.93	1.07	1.08	1.08	1.08	1.25	1.26	1.26	1.26
	R^2	0.75	0.76	0.74	0.75	0.53	0.53	0.52	0.53	0.73	0.71	0.67	0.70	0.75	0.76	0.79	0.77
	RMSE	0.06	0.06	0.06	0.06	0.04	0.04	0.04	0.04	0.07	0.07	0.07	0.07	1.20	1.26	1.23	1.23
	PBIAS (%)	8.85	8.65	8.08	8.53	-3.50	0.60	7.75	1.61	7.36	7.59	7.79	7.58	25.42	26.50	26.86	26.26
T3*	**b**	1.09	1.09	1.08	1.09	0.91	0.93	0.98	0.94	1.08	1.08	1.08	1.08	1.25	1.26	1.26	1.26
	R^2	0.75	0.76	0.75	0.75	0.55	0.55	0.53	0.54	0.70	0.68	0.64	0.68	0.77	0.77	0.80	0.78
	RMSE	0.06	0.06	0.06	0.06	0.04	0.04	0.04	0.04	0.07	0.07	0.08	0.07	1.25	1.30	1.28	1.28
	PBIAS (%)	8.81	8.60	8.08	8.50	-2.95	1.22	8.39	2.22	7.48	7.69	7.90	7.69	25.44	26.49	26.88	26.27
T4*	**b**	1.09	1.09	1.08	1.09	0.91	0.93	0.97	0.94	1.07	1.08	1.08	1.08	1.25	1.26	1.26	1.26
	R^2	0.74	0.75	0.76	0.75	0.54	0.54	0.52	0.54	0.70	0.69	0.65	0.68	0.77	0.77	0.80	0.78
	RMSE	0.06	0.06	0.06	0.06	0.04	0.04	0.04	0.04	0.07	0.07	0.08	0.07	1.23	1.29	1.27	1.26
	PBIAS (%)	8.75	8.54	8.05	8.45	-3.06	1.17	8.27	2.13	7.34	7.56	7.81	7.57	25.30	26.37	26.81	26.16
ALL*	**b**	1.09	1.09	1.08	1.09	0.91	0.93	0.97	0.94	1.07	1.08	1.08	1.08	1.25	1.26	1.26	1.26
	R^2	0.75	0.76	0.76	0.76	0.54	0.54	0.52	0.54	0.72	0.66	0.66	0.69	0.76	0.77	0.80	0.78
	RMSE	0.06	0.06	0.06	0.06	0.04	0.04	0.04	0.04	0.07	0.07	0.08	0.07	1.23	1.29	1.27	1.27
	PBIAS (%)	8.80	8.59	8.07	8.49	-3.10	1.12	8.27	2.10	7.41	7.62	7.84	7.62	25.40	26.47	26.86	26.24

* T1-T4 refer to full irrigation, sustained deficit irrigation, regulated deficit irrigation and partial root-zone drying treatments, respectively; ALL denotes all treatments together.

2.3.2.2 Deficit irrigation versus full irrigation

By comparing $K_{cb,\ ArcDualKc}$ of the different irrigation treatments, slight differences were observed using both measured and forecast meteorological data (Tab 2.3); at full irrigation (T1) $K_{cb,\ ArcDualKc}$ was of 0.61 whereas it varied between 0.60 to 0.63 (± 0.11) in all the DI treatment (T2-T4). $K_{e,\ ArcDualKc}$ values were quite constant for all the irrigation treatments, with values of 0.06-0.07 (± 0.96). The underestimations observed in K_{cb} at the DI treatments resulted in lower $K_{c,ArcDualKc}$ and ET_c rates compared to the full irrigation (up to 5% and 6%, respectively), with average $K_{c,ArcDualKc}$ of 0.67-0.69 (± 0.14-0.15) *versus* 0.70 (± 0.14), respectively; ET_c values were in the range 4.56-4.74 (± 0.34-0.35) mm d^{-1} in the DI treatment *versus* 4.83(± 0.34) mm d^{-1} in T1. The obtained results were quite similar using measured meteorological data as input for computing the $K_{cb,\ ArcDualKc}$, with values of 0.59 (± 0.08) in T1 and varying from 0.56 to 0.58 (± 0.08-0.11) in the DI treatments (T2-T4). No differences between T1 and T2-T4 were observed in terms of $K_{e,ArcDualKc}$, with a mean of 0.06 (± 0.87-0.93). $K_{c,ArcDualKc}$ and ET_c values (T2-T4) decreased up to 6% in the DI treatments if compared to T1, with average $K_{c,ArcDualKc}$ of 0.62-0.64 (± 0.11-0.14) in T2-T4 *versus* 0.65 (± 0.11) in T1 and average ET_c of 3.6-3.7 mm d^{-1} (± 0.33) in T2-T4 *versus* 3.8 mm d^{-1} (± 0.32) in T1.

2.4 Discussion

The $K_{cb,ArcDualKc}$ values obtained in the study were lower than those tabulated by the FAO-56 paper and adjusted during the development and final phenological stages for local meteorological conditions. The observed discrepancies were mainly caused by the model calibration procedure, which selects, within the full irrigation treatment T1, pixels that better represent potential irrigation conditions (i.e. maximum SAVI and F_c). On the contrary, $K_{cb,\ ArcDualKc}$

values on mid plant stage resulted higher than $K_{cb,tab}$ mainly due to the specificity of the local climate condition (Consoli et al., 2006a) characterised by semi-arid Mediterranean climate conditions, that most probably does not match the sub-humid climate conditions (with RH_{min} of about 45% and with calm to moderate u_2 of 2 m s^{-1}) at the base of $K_{cb,adj}$ calculation. In fact, more arid climate conditions with greater wind speed would result in higher values of $K_{cb,adj}$ (Allen et al., 1998). Several authors have reported higher values for $K_{cb,adj}$ respect to $K_{cb,tab,}$ highlighting the crucial role of the specific climatic adjustment of $K_{cb,tab}$ values (Benli et al., 2006; Paço et al., 2009). However, $K_{cb,ArcDualKc}$ values resulted lower than $K_{cb,adj}$ during the middle season, as consequence of the model calibration procedure effect identified also in the other phenological stages. Thus, K_{cb} is influenced by the vegetation reflectance condition occurred at the field site; within the first ArcDualK_c sub-model, it was computed as a function of F_c and SAVI, resulting in smaller values respect to the $K_{cb,adj}$ values.

In the present study, the ArcDualK_c model was able to distinguish the different irrigation treatments supplied at the study site in terms of $K_{cb,ArcDualKc}$ as indicator of transpiration due to the imposed water deficit conditions (Comstock, 2002). Thus, results showed $K_{cb,\ ArcDualKc}$ values up to 6% higher in T1 respect to DI treatments (T2-T4). On the contrary, no differences were observed in $K_{e,\ ArcDualKc}$ terms, since the evaporation process occurs on a limited extension referred to the surface wetted by the drippers that, in the ArcDualK_c model, is assumed to be constant, independently of the irrigation treatment. The above-mentioned discrepancies among treatments, mainly in terms of $K_{cb,\ ArcDualKc}$, led to differences of 5% in $K_{c,ArcDualKc}$ and 6% in ET_c estimates between the T1 and the DI treatments (T2-T4). These results confirm that, as suggested by other authors (Rallo et al., 2014, 2017), agro-hydrological models can be considered as an easy-to-use tool for

indirect evaluations of soil and crop water status.

The use of forecast meteorological data for *a priori* ET_c estimations could be useful for providing irrigation advices to farmers in operative scenarios, since it allows to plan irrigation water supply based on expected realistic meteorological conditions rather than on past and/or current meteorological data (Chirico et al., 2018). In this study, $K_{cb,ArcDualKc}$ values, computed using forecast meteorological data (RH and u_2) as input, resulted 8% higher than those obtained using measured weather data; this can be due to the uncertainties in the agro-meteorological forecasted parameters, which are used in the ArcDualK_c model (T_{air}, RH, R_s, u_2, P). The application of COSMO model has produced overestimation of T_{air} (8%), u_2 (31%) and P (up to 100%), whereas it has underestimated RH and R_s (26% and 11%, respectively). Several authors reported the same behaviour in their studies (Luo et al., 2014; Xiong et al., 2016; Yang et al., 2016). However, even if large inaccuracies were observed in some agrometeorological variables, the estimates of $K_{cb,ArcDualKc}$ using forecast data did not differ too much (8%) from those values obtained by using the measured data, as a consequence of the compensation of the expected error (i.e. the underestimation of RH of 26% was offset by an overestimation of u_2, up 31%).

Furthermore, the inaccuracies in the predicted agrometeorological variables also influenced the ET_0 estimates calculated with the P-M equation, resulting in an overestimation of up to 17%.

In terms of lead-time, a different behaviour was observed for the values of $K_{e,ArcDualKc}$, which showed an increase in the trend from 1-day to 3-days (Tab. 2.3), mainly due to an increase in the occurrence of the precipitations predicted by COSMO model (from 1 to 3 days the onset of precipitation increased by about 50%; Figs. 2.4 and 2.5).

Consequently, the lead time had a slight effect on $K_{c,\ ArcDualKc}$

and ET_c, with discrepancies less than 2% between lead times of 1-day and 3-days (Tab. 2.3). This decreasing trend in the accuracy of the single agrometeorological prediction variable has also been observed in other studies (Lorite et al., 2015; Pelosi et al., 2016; Xiong et al., 2016; Cao et al., 2019), who found differences up to 25% in u_2 (Lorite *et al*., 2015) when the forecast horizon increased from 1 to 3 days.

Despite the reliability of ArcDualK_c in modelling ET_c at field level, the results could be influenced by the pixel size of Sentinel-2, which contains both vegetated and bare soil surfaces. In this sense, the ArcDualK_c model could be improved by integrating the data obtained from ground measurements (e.g. electrical resistivity tomography, ERT; lisimetry; sap flow and eddy covariance, (Motisi et al., 2012; Consoli & Papa, 2013), to obtain more accurate soil parameters (Campos et al., 2016; Zhang et al., 2017; Vanella et al., 2019) or more reliable crop coefficient values instead of using those tabulated on FAO-56 paper (Consoli et al., 2006b; Peddinti & Kambhammettu, 2019).

This information would help to better understand the specificity of the site, increasing the accuracy of the ET_c estimates. Other improvements could be based on the use of images with higher spatial resolution that would allow the distinction between vegetation and bare soil (Gago et al., 2015) or on the integration of different satellite platforms in order to increase temporal resolution (Shelestov et al., 2017; Ramírez-Cuesta et al., 2019b), which would allow a better characterization of the crop coefficient curve. This fact is particularly relevant in areas frequently covered by clouds where only a few clear sky images are available during the entire growing season (Karlsen et al., 2018).

2.5 Conclusion

The ArcDualK_c model has provided reliable spatial distributed ET_c and K_c (and its components) estimates by combining RS images and measured or predicted meteorological data. Despite significant errors were obtained in daily ET_0 estimates due to forecast inaccuracies of meteorological variables provided by COSMO model, the use of forecast meteorological data resulted only in slight overestimates of $K_{cb,ArcDualKc}$, $K_{c,ArcDualKc}$ and ET_c, when compared with the use of measured meteorological data. In addition, the ArcDualK_c model was able to identify the different irrigation treatments respect to $K_{cb,ArcDualKc}$; whereas no differences were found in $K_{e,ArcDualKc}$ estimates. Finally, slight differences (between 5 and 6%) were obtained in terms of $K_{c,ArcDualKc}$ and ET_c in the irrigation control treatment and in the deficit irrigated ones. The ArcDualK_c model can be then considered reliable for improving precision irrigation and water resource management in the context of deficit irrigation strategies, including also the possibility of employing forecasted meteorological data as alternative of ground-based observation of meteorological variables.

It is finally expected that the accuracies of the ArcDualK_c model in estimating ET_c will improve in the near future as its inputs are better characterized both reducing the uncertainties of the prediction models and increasing the spatial and temporal resolutions of remote sensing data.

References

Aiello, R., Bagarello, V., Barbagallo, S., Consoli, S., Di Prima, S., Giordano, G., & Iovino, M. (2014). An assessment of the Beerkan method for determining the hydraulic properties of a sandy loam soil. *Geoderma*, *235*, 300-307.

Allen, R. G., Pereira, L. S., Raes, D., & Smith, M. (1998). Crop evapotranspiration-Guidelines for computing crop water requirements-FAO Irrigation and drainage paper 56. *Fao, Rome*, *300*(9), D05109.

Allen, R. G. (2009). REF-ET: Reference Evapotranspiration Calculation Software for FAO and ASCE standardized Equations. University of Idaho.

Benli, B., Kodal, S., Ilbeyi, A., & Ustun, H. (2006). Determination of evapotranspiration and basal crop coefficient of alfalfa with a weighing lysimeter. *Agricultural water management*, *81*(3), 358-370.

Campos, I., González-Piqueras, J., Carrara, A., Villodre, J., & Calera, A. (2016). Estimation of total available water in the soil layer by integrating actual evapotranspiration data in a remote sensing-driven soil water balance. *Journal of Hydrology*, *534*, 427-439.

Cao, J., Tan, J., Cui, Y., & Luo, Y. (2019). Irrigation scheduling of paddy rice using short-term weather forecast data. *Agricultural Water Management*, *213*, 714-723.

Chirico, G. B., Pelosi, A., De Michele, C., Bolognesi, S. F., & D'Urso, G. (2018). Forecasting potential evapotranspiration by combining numerical weather predictions and visible and near-infrared satellite images: An application in southern Italy. *The Journal of Agricultural Science*, *156*(5), 702-710.

Comstock, J. P. (2002). Hydraulic and chemical signalling in the control of stomatal conductance and transpiration. *Journal of Experimental Botany*, *53*(367), 195-200.

Consoli, S., O'Connell, N., & Snyder, R. (2006a). Estimation of evapotranspiration of different-sized navel-orange tree orchards using energy balance. *Journal of irrigation and drainage engineering*, *132*(1), 2-8.

Consoli, S., O'Connell, N., & Snyder, R. (2006b). Measurement of light interception by navel orange orchard canopies: case study of Lindsay, California. *Journal of irrigation and drainage engineering*, *132*(1), 9-20.

Consoli, S., & Papa, R. (2013). Corrected surface energy balance to measure and model the evapotranspiration of irrigated orange orchards in semi-arid Mediterranean conditions. *Irrigation science*, *31*(5), 1159-1171.

Consoli, S., & Vanella, D. (2014a). Comparisons of satellite-based models for estimating evapotranspiration fluxes. *Journal of hydrology*, *513*, 475-489.

Consoli, S., & Vanella, D. (2014b). Mapping crop evapotranspiration by integrating vegetation indices into a soil water balance model. *Agricultural Water Management*, *143*, 71-81.

Consoli, S., Stagno, F., Roccuzzo, G., Cirelli, G. L., & Intrigliolo, F. (2014). Sustainable management of limited water resources in a young orange orchard. *Agricultural Water Management*, *132*, 60-68.

Consoli, S., Licciardello, F., Vanella, D., Pasotti, L., Villani, G., & Tomei, F. (2016). Testing the water balance model criteria using TDR measurements, micrometeorological data and satellite-based information. *Agricultural Water Management*, *170*, 68-80.

Consoli, S., Stagno, F., Vanella, D., Boaga, J., Cassiani, G., & Roccuzzo, G. (2017). Partial root-zone drying irrigation in orange orchards: Effects on water use and crop production characteristics. *European journal of agronomy*, *82*, 190-202.

Dubois, O. (2011). *The state of the world's land and water resources for food and agriculture: managing systems at risk*. Earthscan.

Gago, J., Douthe, C., Coopman, R., Gallego, P., Ribas-Carbo, M., Flexas, J., Escalona, J., Medrano, H. (2015). UAVs challenge to assess water stress for sustainable agriculture. *Agricultural water management*, *153*, 9-19.

Gong, X., Liu, H., Sun, J., Gao, Y., & Zhang, H. (2019). Comparison of Shuttleworth-Wallace model and dual crop coefficient method for estimating evapotranspiration of tomato cultivated in a solar greenhouse. *Agricultural Water Management*, *217*, 141-153.

Gonzalez-Dugo, M. P., Neale, C. M. U., Mateos, L., Kustas, W. P., Prueger, J. H., Anderson, M. C., & Li, F. (2009). A comparison of operational remote sensing-based models for estimating crop evapotranspiration. *Agricultural and Forest Meteorology*, *149*(11), 1843-1853.

Gu, Z., Qi, Z., Ma, L., Gui, D., Xu, J., Fang, Q., Yuan, S., Feng, G. (2017). Development of an irrigation scheduling software based on model predicted crop water stress. *Computers and Electronics in Agriculture*, *143*, 208-221.

Gutman, G., & Ignatov, A. (1998). The derivation of the green vegetation fraction from NOAA/AVHRR data for use in numerical weather prediction models. *International Journal of remote sensing*, *19*(8), 1533-1543.

Huete, A. R. (1988). A soil-adjusted vegetation index (SAVI). *Remote sensing of environment*, *25*(3), 295-309.

Karlsen, S. R., Anderson, H.B., Van der Wal, R., & Hansen, B. B. (2018). A new NDVI measure that overcomes data sparsity in cloud-covered regions predicts annual variation in ground-based estimates of high arctic plant productivity. *Environmental Research Letters*, *13*(2), 025011.

Lorite, I. J., Ramírez-Cuesta, J. M., Cruz-Blanco, M., & Santos, C. (2015). Using weather forecast data for irrigation scheduling under semi-arid conditions. *Irrigation science*, *33*(6), 411-427.

Luo, Y., Chang, X., Peng, S., Khan, S., Wang, W., Zheng, Q., & Cai, X. (2014). Short-term forecasting of daily reference evapotranspiration using the Hargreaves–Samani model and temperature forecasts. *Agricultural Water Management*, *136*, 42-51.

Mokhtari, A., Noory, H., Vazifedoust, M., & Bahrami, M. (2018). Estimating net irrigation requirement of winter wheat using model-and satellite-based single and basal crop coefficients. *Agricultural water management*, *208*, 95-106.

Motisi, A., Consoli, S., Rossi, F., Minacapilli, M., Cammalleri, C., Papa, R., Rallo, G., & D'urso, G., (2012). Eddy covariance and sap flow measurement of energy and mass exchange of woody crops in a Mediterranean environment. *Acta Horticulturae. 951*,121–127.

Olivera-Guerra, L., Merlin, O., Er-Raki, S., Khabba, S., & Escorihuela, M. J. (2018). Estimating the water budget components of irrigated crops: Combining the FAO-56 dual crop coefficient with surface temperature and vegetation index data. *Agricultural water management*, *208*, 120-131.

Paço, T. A., Ferreira, M. I., & Conceição, N. (2006). Peach orchard evapotranspiration in a sandy soil: Comparison between eddy covariance measurements and estimates by the FAO 56 approach. *Agricultural Water Management*, *85*(3), 305-313.

Peddinti, S. R., & Kambhammettu, B. P. (2019). Dynamics of crop coefficients for citrus orchards of central India using water balance and eddy covariance flux partition techniques. *Agricultural water management*, *212*, 68-77.

Pelosi, A., Medina, H., Villani, P., D'Urso, G., & Chirico, G. B. (2016). Probabilistic forecasting of reference evapotranspiration with a limited area ensemble prediction system. *Agricultural water management*, *178*, 106-118.

Rallo, G., Baiamonte, G., Juárez, J. M., & Provenzano, G. (2014). Improvement of FAO-56 model to estimate transpiration fluxes of drought tolerant crops under soil water deficit: application for olive

groves. *Journal of Irrigation and Drainage Engineering*, *140*(9), A4014001.

Rallo, G., González-Altozano, P., Manzano-Juárez, J., & Provenzano, G. (2017). Using field measurements and FAO-56 model to assess the eco-physiological response of citrus orchards under regulated deficit irrigation. *Agricultural water management*, *180*, 136-147.

Ramírez-Cuesta, J. M., Allen, R. G., Zarco-Tejada, P. J., Kilic, A., Santos, C., & Lorite, I. J. (2019a). Impact of the spatial resolution on the energy balance components on an open-canopy olive orchard. *International Journal of Applied Earth Observation and Geoinformation*, *74*, 88-102.

Ramírez-Cuesta, J., Mirás-Avalos, J., Rubio-Asensio, J., & Intrigliolo, D. (2019b). A Novel ArcGIS Toolbox for Estimating Crop Water Demands by Integrating the Dual Crop Coefficient Approach with Multi-Satellite Imagery. *Water*, *11*(1), 38.

Rouse, J. W., Haas, R. H., Schelle, J. A., Deering, D. W., & Harlan, J. C. (1974). Monitoring the vernal advancement or retrogradation of natural vegetation. *NASA/GSFC, Type III, Final report, Green-belt, MD*, *371*.

Schättler, U., Doms, G., & Schraff, C. (2008). A description of the nonhydrostatic regional COSMO-model part VII: user's guide. Deutscher Wetterdienst *Rep. COSMO-Model*, 4, 142.

Shelestov, A., Lavreniuk, M., Kussul, N., Novikov, A., Skakun, S. (2017). Exploring Google Earth Engine platform for big data processing: Classification of multi-temporal satellite imagery for crop mapping. *Frontiers in Earth Science*, *5*, 17.

Singh, S., Boote, K. J., Angadi, S. V., & Grover, K. K. (2017). Estimating water balance, evapotranspiration and water use efficiency of spring safflower using the CROPGRO model. *Agricultural water management*, *185*, 137-144.

Steppeler, J., Doms, G., Schättler, U., Bitzer, H. W., Gassmann, A., Damrath, U., & Gregoric, G. (2003). Meso-gamma scale forecasts using the

nonhydrostatic model LM. *Meteorology and atmospheric Physics*, 82(1-4), 75-96.

Vanella, D., Ramírez-Cuesta, J. M., Intrigliolo, D. S., & Consoli, S. (2019). Combining Electrical Resistivity Tomography and Satellite Images for Improving Evapotranspiration Estimates of Citrus Orchards. *Remote Sensing*, *11*(4), 373.

Xiong, Y., Luo, Y., Wang, Y., Traore, S., Xu, J., Jiao, X., & Fipps, G. (2016). Forecasting daily reference evapotranspiration using the Blaney–Criddle model and temperature forecasts. *Archives of Agronomy and Soil Science*, *62*(6), 790-805.

Yang, Y., Cui, Y., Luo, Y., Lyu, X., Traore, S., Khan, S., & Wang, W. (2016). Short-term forecasting of daily reference evapotranspiration using the Penman-Monteith model and public weather forecasts. *Agricultural water management*, *177*, 329-339.

Zhang, K., Kimball, J. S., & Running, S. W. (2016). A review of remote sensing based actual evapotranspiration estimation. *Wiley Interdisciplinary Reviews: Water*, *3*(6), 834-853.

3 A stand-alone remote sensing approach based on the use of the optical trapezoid model for detecting the irrigated areas[2]

Abstract

Under the current water scarcity scenario, the promotion of water saving strategies is essential for improving the sustainability of the irrigated agriculture. In particular, high resolution irrigated area maps are required for better understanding water uses and supporting water management authorities. The main purpose of this study was to provide a stand-alone remote sensing (RS) methodology for mapping irrigated areas. Specifically, an unsupervised classification approach on Normalized Difference Vegetation Index (NDVI) data was coupled with the OPtical TRApezoid Model (OPTRAM) for detecting actual irrigated areas without the use of any reference data. The proposed methodology was firstly applied and validated at the Marchfeld Cropland region (Austria) during the irrigation season 2021, showing a good agreement with an overall accuracy of 70%. Secondly, it was applied at the irrigation district Quota 102,50 (Italy) for the irrigation seasons 2019-2020. The results of the latter were instead compared with the data declared by the Reclamation Consortium, finding an overestimation of irrigated areas of 21%. In conclusion, this study suggests an easy-to-use approach, eventually independent of reference data such as agricultural statistical surveys or records and replicable

[2]A modified version of this Chapter was published as Longo-Minnolo, G., Consoli, S., Vanella, D., Ramírez-Cuesta, J. M., Greimeister-Pfeil, I., Neuwirth, M., & Vuolo, F. (2022). A stand-alone remote sensing approach based on the use of the Optical Trapezoid Model for detecting the irrigated areas. *Agricultural Water Management*, *274*, 107975. https://doi.org/10.1016/j.agwat.2022.107975

under different agricultural settings in continental or Mediterranean climates to support stakeholders for regular estimation of irrigated areas in different growing years or detecting eventual unauthorized water uses. However, some uncertainties should be considered, needing further analyses for improving the accuracy of the proposed approach.

Keywords: Satellite images; Rainfall; Unsupervised classification; NDVI; Water Content

3.1 Introduction

Water scarcity represents a global risk in terms of potential impact on the sustainable development of human society (Mekonnen & Hoekstra, 2016). Moreover, under climate change conditions, prolonged droughts are expected to occur in the future, with an increasing of crop dependency on water supply (Scanlon et al., 2012).

Irrigated agriculture is the principal consumer of freshwater resources. Its role is essential for increasing crop production and ensuring the global food yield (Cai & Rosegrant, 2002; Jin et al., 2016). Due to the global population growth and the discrepancy between crop water requirements and the actual irrigation applied, a better agricultural water management is required in order to fulfil the increasing demand for food production (Gao et al., 2018).

In this context, detailed spatial information on the irrigated areas is essential for supporting agriculture water management (Ambika et al., 2016). In particular, accurate mapping of irrigated areas could allow a better understanding of water use and food production patterns, supporting stakeholders to formulate more suitable water management strategies to achieve higher crop water productivity (Chance et al., 2017). However, the accurate extent and distribution of many irrigated areas remains often unknown despite the

significant impact of irrigation on food security and water resources (Bazzi et al., 2019b; Cai et al., 2017). In fact, even though huge efforts have been made in the last years in this regard, there is a general lack of accurate and current maps about irrigated areas, avoiding the full implementation and compliance of the Water Framework Directive (WFD) (Bolognesi et al., 2020; Magidi et al., 2021).

In Italy, the National Institute of Agricultural Economics (INEA) has contributed to design the irrigation water policy by supporting the Italian Ministry of Agricultural, Food and Forestry Policies (MiPAAF). Since the 1960's, INEA has conducted the census of irrigated areas, producing the Map of irrigation in Italy. Currently, the most complete and updated database that supports Governmental Institutions is the National Information System for Water Management in Agriculture (SIGRIAN; https://sigrian.crea.gov.it/), which collect the information coming from water management authorities (i.e. Reclamation Consortia and other Irrigation agencies). Nevertheless, the level of detail of the SIGRIAN database is often not enough accurate for a proper evaluation of irrigation water uses.

In Austria, Farm Structure Surveys are conducted as (i) full survey (census) on the basis of EU legislation every 10 years and (ii) sample survey at regular intervals (3 to 4 years) by Austria's Federal Statistical Office (Statistics Austria). Farm Structure Surveys conducted by questionnaires also comprise features with respect to irrigation, particularly the "total irrigable area" of an agricultural operation or the "actual irrigated area" of areas with field vegetables. However, overall, the data situation with respect to actual irrigated areas requires improvement especially with respect to the time gaps within the surveys that might miss particularly dry years with high irrigation needs.

Since the 1980s, remote sensing (RS) has been used to map land cover and agricultural areas at different spatial and temporal scales

(Pareeth et al., 2019). One of the main methods implemented to derive this information is based on the use of satellite-based optical data. Single-date imagery acquired during the peak of the crop growing season can be used for classifying the irrigated areas, although the use of multi-temporal imagery approach is preferred as it covers the different phenology stages of the crops (Ghassemi et al., 2022; Vuolo et al., 2018). A common approach is based on the analysis of the NDVI time series, due to its ability to show a considerable difference between irrigated and non-irrigated pixels (Ozdogan et al. 2006, 2010). The use of NDVI as an indicator of vegetation phenology provides a simple proxy for classifying complex landscapes (Chance et al., 2017). In particular, NDVI is considered a sufficiently good indicator of irrigation presence (Ozdogan et al., 2006) thanks to its capability to measure green biomass and the existing strong correlation between green biomass and the available moisture for vegetation (Pervez & Brown, 2010). For instance, Bolognesi et al. (2020) applied this approach for mapping the actual extent of irrigated areas in Italy in semi-arid conditions. In their study, rainfed areas and irrigated areas were classified on the basis of the analysis of NDVI time series and accumulated rainfall data. However, this approach highlights some limitations, especially in areas where the same crop type is grown with and without irrigation during the same growing season. In these areas in fact, as suggested by Ozdogan et al. (2010), the temporal NDVI profiles of both irrigated and non-irrigated crops may show an identical pattern, emphasizing the need for a more sensitive index to make this distinction. Additionally, optical RS applications depend on atmospheric conditions. For areas with frequent cloud cover, these methods may not be adaptable (Gao et al., 2018).

The use of microwave RS offers a good alternative to optical RS for mapping irrigated areas also under cloudy conditions, due to

the ability of microwaves to penetrate through vegetation canopy and underlying soil, especially at lower frequencies, where measurements are not impeded by clouds or darkness (Sadeghi et al., 2015, 2017). Specifically, microwave domain measurements can be used to estimate soil moisture dynamics because the pronounced contrast between the dielectric constant values of the wet and dry soils (Baghdadi & Zribi, 2016; Lakhankar et al., 2009). Kumar et al. (2015) investigated the capability of several microwave remotely sensed soil moisture products, including ASCAT (Advanced SCATterometer), AMSR-E (Advanced Microwave Scanning Radiometer – Earth Observing System), ESA CCI SM (European Space Agency Climate Change Initiative Soil Moisture), SMOS (Soil Moisture and Ocean Salinity), while Lawston et al. (2017) showed the capability of the enhanced version of SMAP (Soil Moisture Active Passive) to detect the irrigation signal. Although these products have shown greater potential for monitoring soil moisture dynamics, they consider both rainfall and irrigation effects on soil moisture (Karthikeyan et al., 2020) and may require calibrations to account for surface roughness which causes perturbation of the microwave signal (Shi et al., 2006). Additionally, the application of microwave-based retrieval of soil moisture is not well suited for small-scale applications because the very coarse resolution, especially when compared with the higher spatial resolution outputs of optical methods (Sadeghi et al., 2017; Yue et al., 2019). More recently, several authors (Bazzi et al., 2019a,b; Gao et al., 2018) exploited instead Sentinel-1 SAR (Synthetic Aperture Radar) time series to map irrigated fields. Specifically, based on the multi-temporal analysis of backscatter time series using vertical-vertical (VV) and vertical-horizontal (VH) polarizations, their studies showed that VV resulted more sensitive for characterizing the soil moisture conditions, while VH was more sensitive for monitoring the vegetation status. However, more studies exploiting this approach are

required (Dari et al., 2021).

Commonly, both optical and microwave RS data are used as inputs for mapping the irrigated areas and for distinguishing the different classes by applying supervised classification approaches. Because these approaches require ground reference data to build rule-based classifiers, their transferability in time and space is not always guaranteed, especially under different climate conditions (Ragettli et al., 2018; Pageot et al., 2020).

Recently, Sadeghi et al. (2017) proposed the physically-based OPTRAM. Specifically, this methodology is based on the pixel distribution within the NDVI and shortwave infrared transformed reflectance (STR) space, for estimating the soil moisture, by using only optical data. In the last years, OPTRAM has been successfully applied for mapping the soil moisture at high resolution in rainfed and irrigated fields (Ambrosone et al., 2020; Babaeian et al., 2019). The promising results obtained in these studies highlight the possibility of using OPTRAM also for discriminating between irrigated and non-irrigated areas. In fact, besides the visible (VIS) and near-infrared (NIR) bands of NDVI, it introduces additional information on the short-wave infrared (SWIR) with the STR index, which provides high sensitivity to soil moisture variation (Sadeghi et al., 2015).

In this context, the aims of this study were:

• to develop a stand-alone optical RS method able to detect the irrigated areas, based on the combined use of the unsupervised classification and OPTRAM;

• to validate and test the proposed method at different spatial level (i.e. field and district level, respectively), under different climate conditions.

Hence, the study would provide an easy-to-use method, not dependent on ground reference data and replicable under different contexts aiming at supporting the stakeholders for monitoring and

reporting the irrigated areas. This will allow the promotion of efficient water-saving strategies and the accomplishment of the requirements of water-related policies.

3.2 Materials and methods

3.2.1 Study area

The study was carried out at 2 different test sites (Fig. 3.1): the irrigation district "Quota 102,50" in Italy (2019-2020); and the "Marchfeld Cropland" region in Austria (2021).

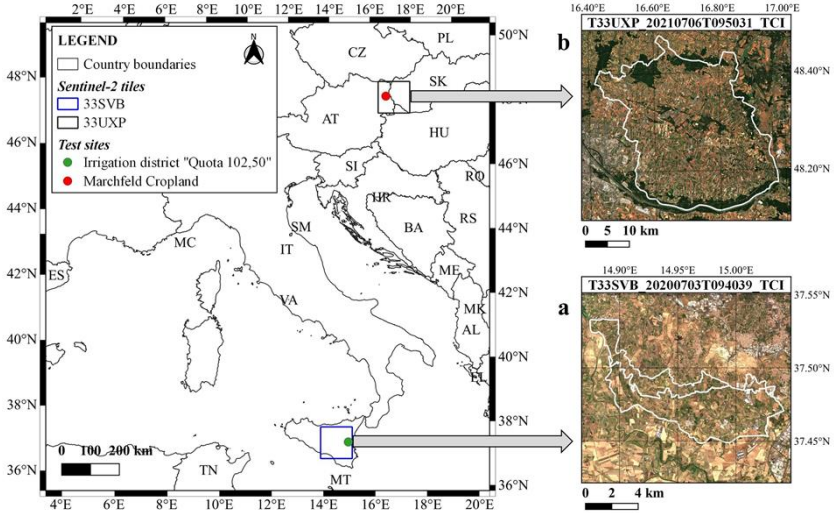

Fig. 3.1. Location of the two test sites: (a) irrigation district "Quota 102,50" in Italy; and (b) "Marchfeld Cropland" region in Austria.

The irrigation district "Quota 102,50" (managed by the Reclamation Consortium Sicilia Orientale) is located in Eastern Sicily (Lat. 37.44 °N – 37.54 °N, Long. 14.85 °E – 15.05 °E; WGS84, Fig 3.1a). The district is characterized by a total area of 5,050 ha and an irrigated area of about 2,300 ha, that is mainly cultivated with citrus,

olive and fruit groves. The irrigation season is generally from mid-May to mid-October, depending on the weather conditions. The climate is hot-summer Mediterranean (Csa) under the Köppen-Geiger classification, according to Beck et al. (2018). During the study period, the average annual precipitation values were of 597 and 656 mm for 2019 and 2020, respectively, with values of 201 and 202 mm recorded during the 2019-20 irrigation seasons.

The cropland area of Marchfeld is located in Lower Austria (Lat. 48.10 °N – 48.50 °N, Long. 16.40 °E – 17.00 °E; WGS84, Fig 3.1b). It covers an agricultural surface of about 60,000 ha, with an irrigated surface of about 21,000 ha. The main cultivated crops are vegetables, sugar beet, potatoes and winter cereals (Immitzer et al., 2016). The irrigation season is from mid-April to mid-July (Deissenberger, 2021). Conventionally, the area is characterised by a warm-summer humid continental climate (Dfb) (Beck et al., 2018). However, it is the driest region of Austria, with an average annual precipitation of 500 mm for the study period 2021, with 109 mm during the irrigation season.

3.2.2 Detection of the irrigated areas

Fig. 3.2 shows a flow chart of the proposed methodological approach. Specifically, the detection of the irrigated areas was performed by combining a preliminary unsupervised classification on a seasonal NDVI time series for identifying the potentially irrigated clusters, and the subsequent application of the OPTRAM model, on these clusters, for more specifically distinguishing the irrigated pixels from the non-irrigated pixels during the dry period of the irrigation season. The entire process required two types of data sources at the initial stage, i.e. Sentinel-2 satellite images and rainfall values, and then the soil parameters, i.e. wilting point (WP) and field capacity (FC), for applying OPTRAM approach.

Only clear sky satellite images covering the test areas within the reference study periods were used. For the Austrian test site, a pre-processing of the images for removing cloudy pixels was necessary due the unavailability of images with perfect clear sky conditions.

A preliminary analysis of rainfall values was conducted in order to identify the dry periods during the irrigation seasons. Specifically, these dry periods were characterised by a cumulated rainfall value during the 10 previous days of 0 mm at the irrigation district Quota 102,50 and lower than 4 mm at Marchfeld Cropland. A sub-dataset of satellite images was created within the dry periods, for dates with a daily rainfall value of 0 mm (Tab. S3.1). Finally, NDVI and STR values were calculated for each pixel of the potentially irrigated clusters, representing the input for the OPTRAM approach application.

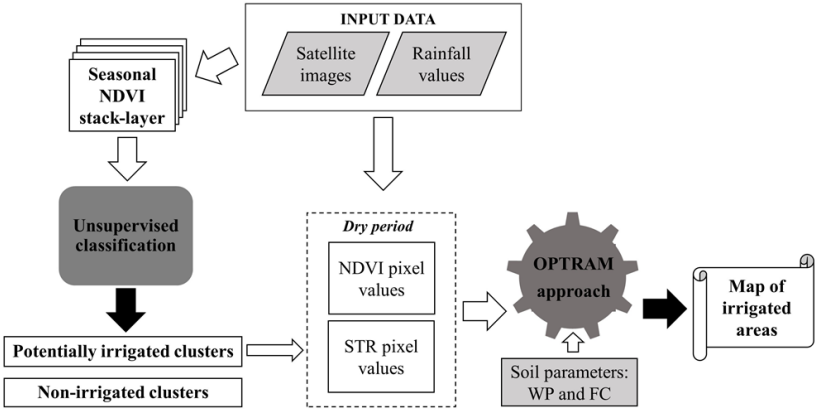

Fig. 3.2. Workflow of the proposed methodological approach for detecting the irrigated areas. Light grey boxes identify the inputs (the satellite images and the rainfall values, and the soil parameters WP and FC), whereas the dark grey boxes refer to the main processes (the unsupervised classification and the OPTRAM approach). The white boxes, instead, represent the intermediate outputs. The final output is the map of irrigated areas.

3.2.2.1 Dataset input

In this study, the multispectral images from Sentinel-2 European Space Agency's (ESA) satellite (https://sentinel.esa.int/web/sentinel/missions/sentinel-2) were used. The satellite is equipped with an opto-electronic multispectral sensor (MSI) for imaging the Earth surface with a spatial resolution of 10 - 60 m in the VIS, NIR and SWIR spectral zones. The temporal resolution of each single Sentinel-2 satellite (Sentinel-2 A and B) is 10 days, leading to a revisit time of 5 days with two satellites in operation. A total of 158 Sentinel-2 images were collected at the study areas: 65 and 62 images for the irrigation district Quota 102,50 during the years 2019-2020, respectively (T33SVB tile; Fig 3.1), and 31 images for Marchfeld Cropland region during the year 2021 (T33UXP tile; Fig 3.1). For each dataset, a time-series NDVI stack-layer was created using all the available images.

Rainfall data were collected from the closest ground-based automatic meteorological stations to the two test sites, i.e. 4 weather stations distant between 10-31 km from the irrigation district Quota 102,50 (Fig. S3.1a) and 4 weather stations distant between 18-36 km from the Marchfeld Cropland region (Fig. S3.1b), managed respectively by the Sicilian Agro-meteorological Information Service (SIAS, www.sias.regione.sicilia.it) and the Central Institute for Meteorology and Geodynamics (ZAMG, www.zamg.ac.a).

In Fig. 3.3, the observed daily rainfall values and the identified dry periods during the irrigation season were reported. In the Supplementary material section (at the end of the Thesis), Table S3.1 reports the Sentinel-2 images used in the study for the two test sites. For each image, the type of Sentinel satellite (A or B), the daily rainfall value (mm) and the cumulated rainfall value (mm) in the previous 10 days are reported. The dry dates selected during the irrigation season for applying OPTRAM are also indicated.

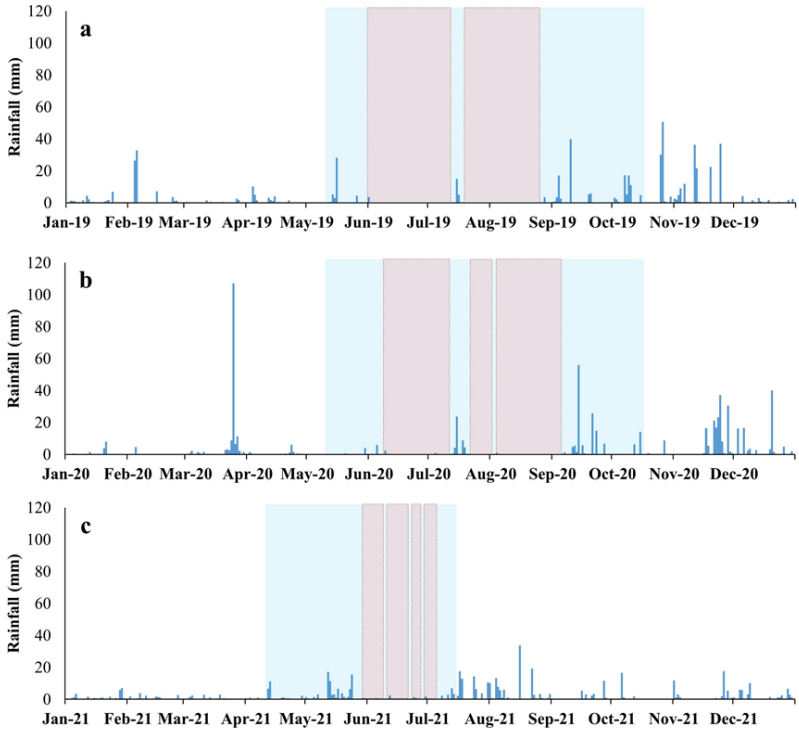

Fig. 3.3. Daily rainfall values observed at the irrigation district Quota 102,50 during the years 2019 (a) and 2020 (b) and at Marchfeld Cropland region during the year 2021 (c). The light blue rectangles indicate the irrigation seasons at the test sites, whereas the grey rectangles indicate the dry periods.

3.2.2.2 Unsupervised classification

As reported in Fig. 3.2, the application of the unsupervised classification on the NDVI time series represented the first main step of the proposed methodological approach with the aim to grouping similar NDVI patterns in unlabelled clusters. As reported by Bolognesi et al. (2020) and Chance et al. (2017), the presence of green and healthy vegetation during the dry season, when no precipitation events are observed, can be attributed to irrigation water applications.

In this context, the following first hypothesis can be applied: "*during the irrigation season, low and decreasing temporal NDVI profiles could refer to non-irrigated areas, whereas high and increasing temporal NDVI profiles could refer to irrigated areas*". According to this hypothesis, clusters can be labelled as non-irrigated or potentially irrigated depending on the NDVI trends observed during the irrigation season. A value of 0.3 was set as NDVI threshold for distinguishing the high and low NDVI temporal profiles. In fact, according to Campoy et al. (2020), González-Gómez et al. (2018) and Lobell et al. (2013), this value represents the green-up of vegetation. The algorithm used in this study was the ISODATA (Ball & Hall, 1965), requiring only the raster and the number of clusters as input. The number of clusters was decided to minimize the standard deviation (in terms of NDVI) of each one, in order to have clusters as clear as possible. Specifically, a number of 20 clusters was used, from which temporal average patterns of NDVI were extracted. During the irrigation seasons at the two test sites, clusters were labelled as: i) non-irrigated, when NDVI trends were lower than 0.3 or decreasing; and ii) potentially irrigated, when NDVI trends were higher than 0.3 or increasing. Pixels representing non-agricultural lands, such as water (negative NDVI values) and built-up (NDVI values ranging from 0.0 to 0.1), were removed by using the NDVI temporal profile analysis.

3.2.2.3 Optical Trapezoid Model

In a second step, the clusters labelled as "potentially irrigated" were further analysed to better discriminate between irrigated and non-irrigated pixels through the use of the OPTRAM, with additional information based on the VIS-NIR and SWIR bands.

OPTRAM is based on the pixel distribution within the NDVI-STR space. Assuming a linear relationship between soil and vegetation water content, the STR-NDVI feature space forms a

trapezoid shape (Sadeghi et al., 2017). The upper and the lower sides of the STR-NDVI feature space, indicating the wet and the dry edges, respectively, were used to solve the water content (W) for each pixel as a function of NDVI and STR:

$$W = \frac{i_d + s_d NDVI - STR}{i_d - i_w + (s_d - s_w) NDVI} \quad (1)$$

where i_d, s_d, and i_w, s_w parameters, are respectively the intercept and the slope of the dry and wet edges of the STR-NDVI feature space.

By using cluster-specific linear parametrizations of OPTRAM and introducing a threshold value based on the soil water content (SWC) status, well-watered vegetation and stressed vegetation can be discriminated on the STR-NDVI feature space during the irrigation season, under dry conditions (e.g. 10 days with no precipitation events recorded).

In fact, thresholds of SWC indicate the water availability for crop consumption and their identification ensure the maintenance of soil moisture conditions that avoid physiological stress (Datta et al., 2017; Thompson et al., 2007). According to several authors (Jabro et al., 2020; Lozoya et al., 2014), WP is that threshold at which plants cannot longer adsorb water from the soil and start to wilt. Specifically, at WP threshold, transpiration and all the other processes vital to plant survival come to stop, causing a significant reduction in crop growth. If SWC remains below the WP for an extended period, crops will eventually die (Datta et al., 2017).

Thus, the second hypothesis of the proposed approach was the following: "*during the irrigation season, in absence of precipitation events for an extended period, if W is greater than WP there is available water in the soil due to the irrigation practice and vegetation may be well-watered, whereas if W is lower than WP there is no available water and vegetation may be under stress conditions*". On

the basis of this second hypothesis, pixels were classified as irrigated or non-irrigated, when W, calculated as a function of NDVI-STR by applying OPTRAM, exceeded or not the WP, respectively (Fig. 3.4).

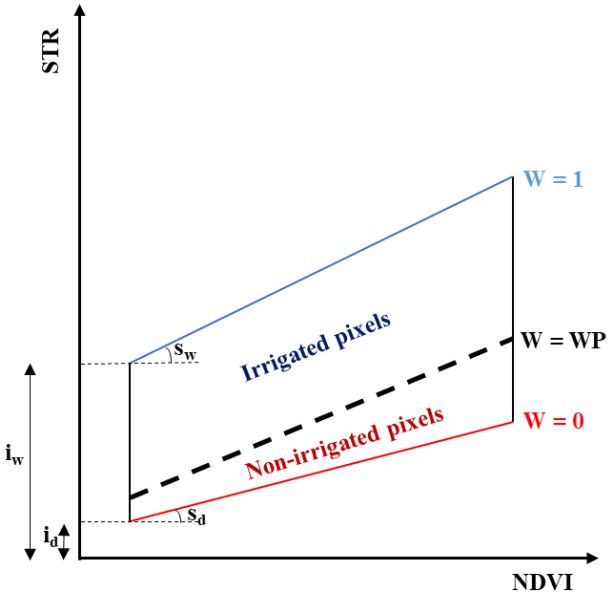

Fig 3.4. The updated OPtical TRApezoid Model (OPTRAM) approach proposed in the study. The blue and red lines are the wet and the dry edge, respectively, representing the maximum (W = 1) and the minimum (W = 0) water content (W) at which pixels refer to well-watered or stressed vegetation, respectively. The black dotted line indicates W at the wilting point (W = WP), considered as threshold value for discriminating the irrigated and the non-irrigated pixels.

In this study, OPTRAM was applied for each date of the dry period during the irrigation season, in order to determine W for the pixels of each cluster (considering only potentially irrigated clusters). The W values were converted into SWC values through a linear regression analysis performed using the WP and the FC data retrieved by the

European Soil Database (https://esdac.jrc.ec.europa.eu/resource-type/european-soil-database-soil-properties). The WP threshold values were of 23.27% and 11.85% for the Marchfeld Cropland region and the irrigation District Quota 102,50, respectively.

For each test site and irrigation season, the differences between SWC and WP values were calculated for the pixels of the selected Sentinel-2 satellite images (i.e., 4 images for the Marchfeld Cropland region during 2021 and 7 images for the irrigation district Quota 102,50 during both 2019-2020). The final label was assigned by considering an average value of the difference SWC – WP on the several dates, as follows:

i) irrigated, when the average of the differences (SWC – WP) ≥ 0;

ii) non-irrigated, when the average of the differences (SWC – WP) < 0.

At the Marchfeld Cropland region, in order to validate the proposed methodological approach at field level, a crop mask (https://geometadatensuche.inspire.gv.at/) was used for separating the single fields. Each field was finally labelled by considering the most frequent pixel values (irrigated or non-irrigated). On the other hand, at the irrigation district Quota 102,50 no crop mask was employed and each pixel was finally labelled as irrigated or non-irrigated. However, a sub-districts mask provided by the Reclamation Consortium was used (Fig. S3.4), and only pixels within this mask were considered in order to validate at district level.

3.2.3 Statistical assessment

The validation of the results obtained in the study was performed at two different levels: i) accuracy assessment of the detection of the irrigated areas at field level for the Marchfeld Cropland region; ii) evaluation of the estimated irrigated areas surface

at district level for the irrigation district Quota 102,50.

Specifically, the accuracy assessment at the Marchfeld Cropland region was performed using a binary confusion matrix between the estimated irrigated/non-irrigated areas with the methodological approach and the reference data collected during a campaign in the framework of another study (BML 2022). A total of 2560 reference fields were used, of which 160 irrigated and 2400 non-irrigated. The campaign aimed at putting together a comprehensive database of georeferenced observation of the irrigation status of several fields. In order to take account growing seasons and harvest dates of different crop types, the campaign was running during three months in summer 2021. For each observation, the following information was documented: i) observation data and time, ii) crop type, iii) type of irrigation system, iv) irrigation ongoing or turned off. A quality check was also performed on the reference database, e.g. with respect to the correct georeferencing of the collected points. This was done using field photos taken alongside the data collection. All points with unclear georeference were excluded from further analyses. While the irrigated fields were observed during the measurements campaign, and thus considered very reliable, an uncertainty degree should be contemplated for the non-irrigated fields, since they were derived from a database where farms register their fields and attributes.

In order to quantitatively evaluate the goodness of the results, several metrics, including accuracy (ACC, %; eq.2), precision (PPV, %; eq.3), recall (TPR, %; eq.4) and F1 score (F1, %; eq.5) were calculated by the confusion matrix, as follow:

$$\mathrm{ACC} = \frac{\mathrm{TP+TN}}{\mathrm{TP+TN+FP+FN}} \quad (2)$$

$$\mathrm{PPV} = \frac{\mathrm{TP}}{\mathrm{TP+FP}} \quad (3)$$

$$\mathrm{TPR} = \frac{\mathrm{TP}}{\mathrm{TP+FN}} \quad (4)$$

$$\mathrm{F1} = \frac{2\mathrm{TP}}{2\mathrm{TP+FP+FN}} \quad (5)$$

where TP, TN, FP and FN indicate respectively the true positive, true negative, false positive and false negative. However, when the dataset is unbalanced, the previous metrics can be misleading. In order to overcome this issue, relative values were calculated normalizing by the number of elements in each class, e.g. TP and FN were divided by the sum of the reference irrigated areas (TP+FN), whereas FP and TN were divided by the sum of the reference non-irrigated areas (FP+TN). In fact, the normalization, taking into account the unbalanced availability of the classes of the binary confusion matrix, allows a better interpretation of the results. Since the final results could be sensitive to the value of WP, a sensitivity analysis was also performed varying the WP threshold in the range of 10%, 15%, 20%, 25%, 30%, 35%, and the same metrics were determined.

On the other hand, for the irrigation district Quota 102,50, the total surface of the irrigated areas (ha) obtained by applying the proposed approach was compared to the data declared by the Consortium.

3.3 Results

3.3.1 Marchfeld Cropland

Fig. 3.5 shows the temporal NDVI profiles of the 20 clusters obtained by applying the ISODATA classification on the study area for the year 2021. Cluster 1 was forthwith excluded because it represents water bodies (negative NDVI values). During the irrigation season, NDVI trends were decreasing or constant and lower than 0.3 for the clusters 2, 3, 5, 6, 7, 10, 11, 17, and 18. Considering the first hypothesis, they were labelled as "non-irrigated". On the other hand, NDVI trends were constant and higher than 0.3 or increasing for the clusters 4, 8, 9, 12, 13, 14, 15, 16, 19, and 20, and they were labelled as "potentially irrigated". In order to facilitate the interpretation of Fig. 3.5, the labels assigned for each cluster are reported in Tab. 3.1. Fig. S3.2 shows instead the preliminary map of the potentially irrigated areas at the Marchfeld Cropland region.

Tab. 3.1. Labelling and number of pixels of the clusters at the Marchfeld Cropland region during the year 2021. In white and grey, the non-irrigated clusters and the potentially irrigated clusters, respectively. In black, the excluded cluster.

Cluster	Label (n° of pixels)	Cluster	Label (n° of pixels)
1	52861	**11**	229838
2	6705	**12**	444469
3	858812	**13**	43171
4	875378	**14**	3569
5	791086	**15**	3015
6	998990	**16**	119043
7	303157	**17**	42954
8	1042842	**18**	2175
9	422500	**19**	534
10	425310	**20**	52861

A cluster-specific linear parametrization of OPTRAM on "potentially irrigated" clusters was performed in order to derive the wet and dry edges. Specifically, pixels of potentially irrigated clusters were distributed within the STR-NDVI feature space of OPTRAM (Fig. 3.6), where the wet and dry edges were determined by a visual inspection, as suggested by Sadeghi et al. (2017). In fact, the authors showed as this approach is better than least-square regression since oversatured or shadowed pixels scattered around the main point cloud of each trapezoid can be omitted. The obtained OPTRAM parameters (i.e., i_d, s_d, i_w, s_w) are reported in Tab. S3.2.

By using OPTRAM parameters of Tab. S3.2, W values were calculated for each pixel of the selected clusters and then converted into SWC values.

By calculating the difference between the average SWC value and the WP and applying the second hypothesis, agricultural lands were labelled as "irrigated" or "non-irrigated". The final map of the irrigated areas obtained for the test site is reported in Fig. 3.7. As shown in this figure, there is a prevalence of non-irrigated areas at Marchfeld region during the irrigation season of 2021. In fact, the surfaces of the non-irrigated areas and the irrigated areas were of 64% and 36%, respectively, of the total surface of the agricultural lands.

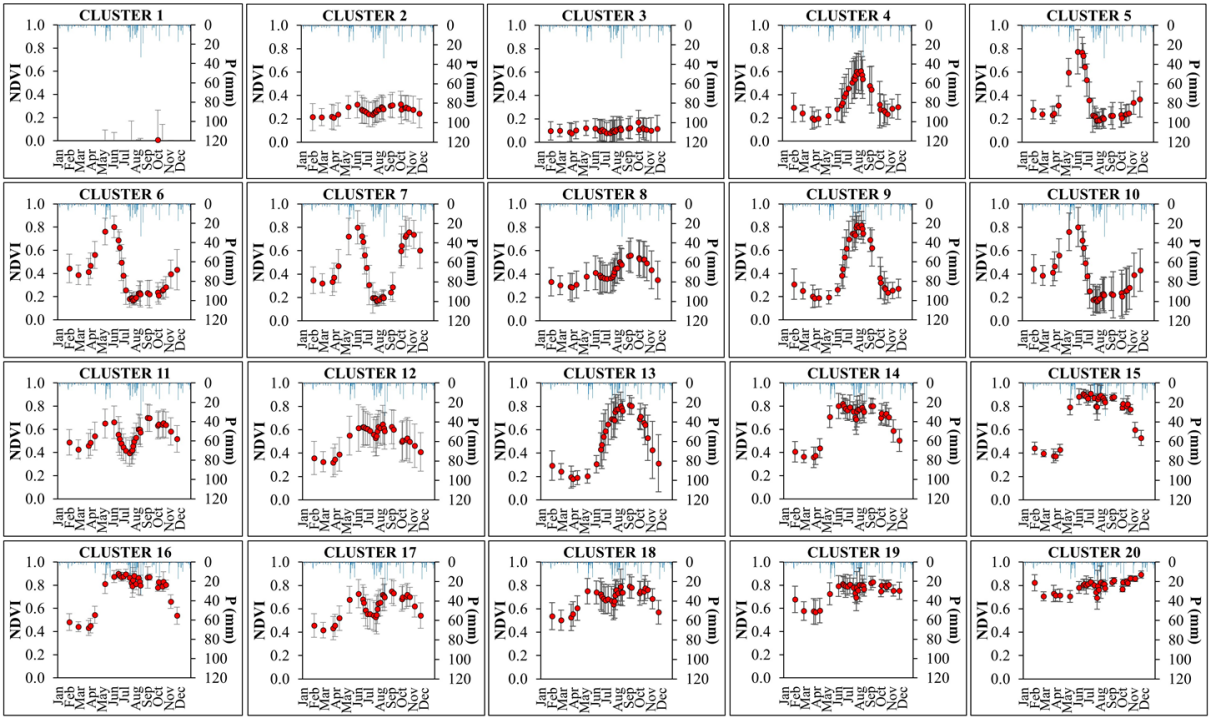

Fig. 3.5. Temporal NDVI profiles (red dots) of the 20 clusters at the Marchfeld region for the year 2021. The blue bars represent the daily rainfall that occurred in the study area.

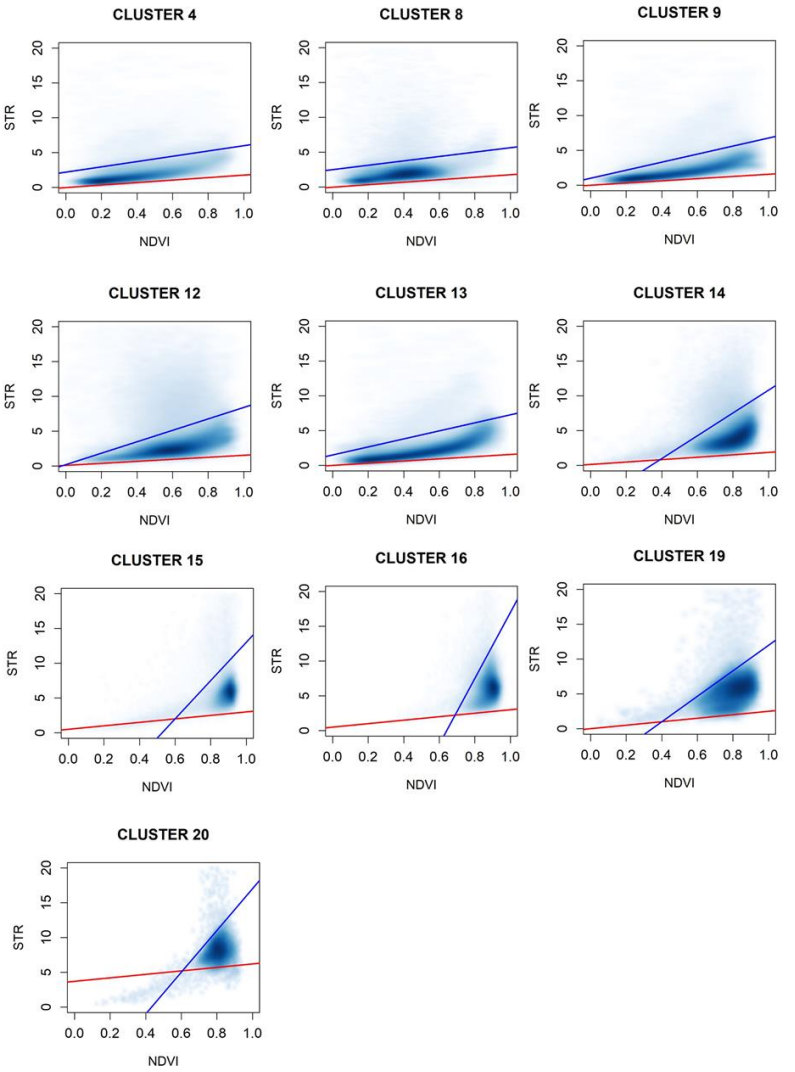

Fig. 3.6. Pixel distribution within the STR-NDVI feature space of the selected clusters at Marchfeld Cropland region during the selected dry period of the irrigation season of 2021. Data are visualized as density scatterplots, associated with the wet (in blue) and dry (in red) edges.

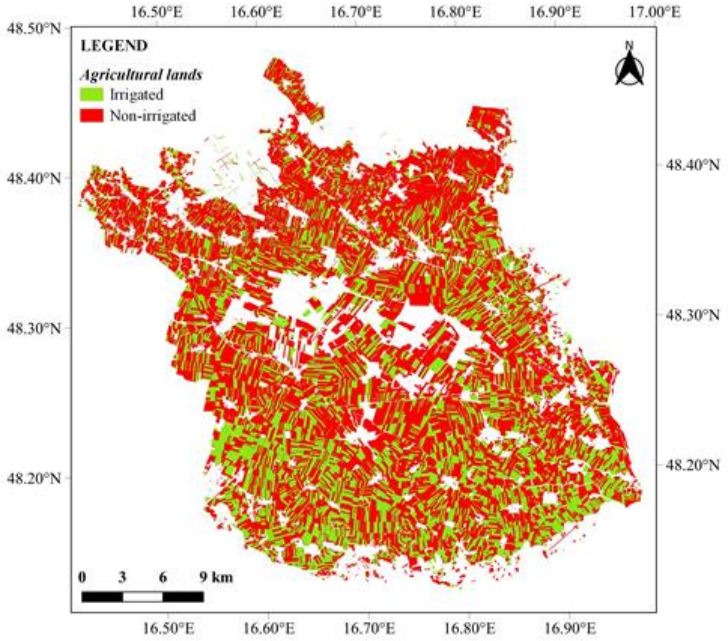

Fig. 3.7. Map of the irrigated (in green) and non-irrigated (red) areas identified at Marchfeld Cropland region during the irrigation season of 2021.

Fig. 3.8 shows the binary confusion matrix between the estimated and the reference irrigated/non-irrigated areas. An overall ACC of 71% was obtained, with PPV, TPR, F1 values of 72%, 68% and 70%, respectively (Fig. 3.9). Finally, Fig. 3.9 shows the sensitivity of metrics by varying the original WP threshold (23%) in the range of 10%, 15%, 20%, 25%, 30%, 35%. ACC, TPR and F1 values decreased from 74% to 58%, from 80% to 26% and from 76% to 39%, respectively, in the WP range of 10%, 15%, 20%, 25%, 30%, 35%. PPV values instead, increased from 71% to 75%, respectively, in the range of 10%, 15%, 20%, 25%, 30%, 35%.

REFERENCE DATA	PROPOSED APPROACH: *Irr.*	PROPOSED APPROACH: *Non-irr.*
Irr.	112 (0.68)	53 (0.32)
Non-irr.	631 (0.26)	1814 (0.74)

Fig. 3.8. Confusion matrix between the estimated and the reference irrigated (Irr.) /non-irrigated (Non-irr.) areas. In brackets the relative values.

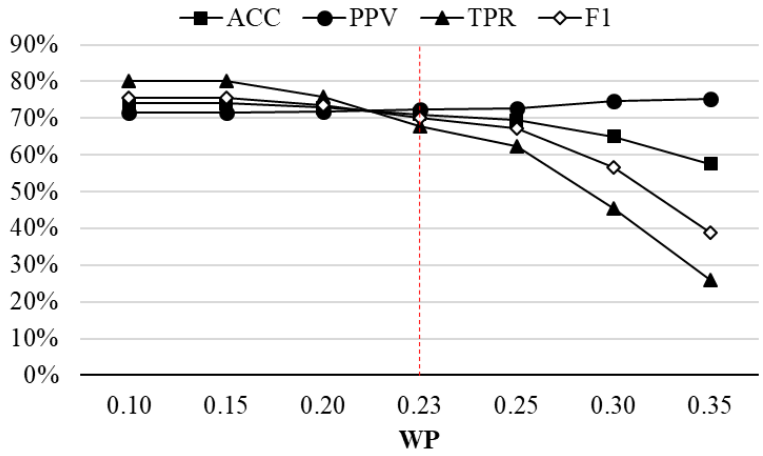

Fig. 3.9. Sensitivity of metrics (ACC, PPV, TPR, F1) obtained at the Marchfeld Cropland region by varying the original WP threshold (23%) in the range of 10%, 15%, 20%, 25%, 30%, 35%.

3.3.2 Irrigation district Quota 102,50

Figs. 3.10-3.11 show the temporal NDVI profiles of the 20 clusters obtained by applying the ISODATA classification to the study area, for the year 2019 and 2020, respectively. Cluster 1 was excluded for both the years because it represents built-up (NDVI values ranging from 0.0 to 0.1). Decreasing or constant and lower than 0.3 NDVI trends were observed for clusters 1, 2, 3, 4, 5, 7, 8, 9, 11 and 12 during the irrigation season 2019, and for clusters 1, 2, 3, 4, 5, 6, 7, 10, 11 and 13 during the irrigation season 2020, labelling them as "non-irrigated". Otherwise, constant and higher than 0.3 or increasing NDVI trends were observed for clusters 10, 13, 14, 15, 16, 17, 18, 19 and 20 during the irrigation season 2019, and for clusters 8, 9, 12, 14, 15, 16, 17, 18, 19 and 20 during the irrigation season 2020. These clusters were labelled as "potentially irrigated". Tab. 3.2 reports the labels assigned for each cluster. Fig. S3.3 shows instead the preliminary maps of the potentially irrigated areas at the irrigation district Quota 102,50.

Tab. 3.2. Labelling and number of pixels of the clusters at the irrigation district Quota 10250 during the years 2019-2020. In white and grey, the non-irrigated clusters and the potentially irrigated clusters, respectively. In black, the excluded clusters.

Cluster	Label (n° of pixels)		Cluster	Label (n° of pixels)	
	2019	***2020***		***2019***	***2020***
1	6815	8891	**11**	10827	15874
2	12410	2413	**12**	31365	24029
3	15384	12605	**13**	9374	38340
4	2336	14032	**14**	53691	45553
5	4656	6913	**15**	44642	18179
6	23271	7199	**16**	6027	43309
7	4587	15083	**17**	73894	73614
8	12425	19785	**18**	22164	10587
9	15216	26808	**19**	80729	52329
10	39932	14072	**20**	35062	55192

Pixels of potentially irrigated clusters were distributed within the STR-NDVI feature space of OPTRAM (Figs. 3.12-3.13), and the wet and dry edges were determined by a visual inspection, obtaining the parameters i_d, s_d, i_w, s_w reported in Tab. S3.3. Note that the W values were calculated, and then converted into SWC values, for the pixels of the selected clusters, for all the selected dates of the dry period during the irrigation seasons 2019-2020, using the parameters reported in Tab. S3.3. The final maps of the irrigated areas obtained by applying the second hypothesis and labelling the agricultural lands as irrigated or non-irrigated are showed in Fig.3.4 for the irrigation seasons 2019-2020..

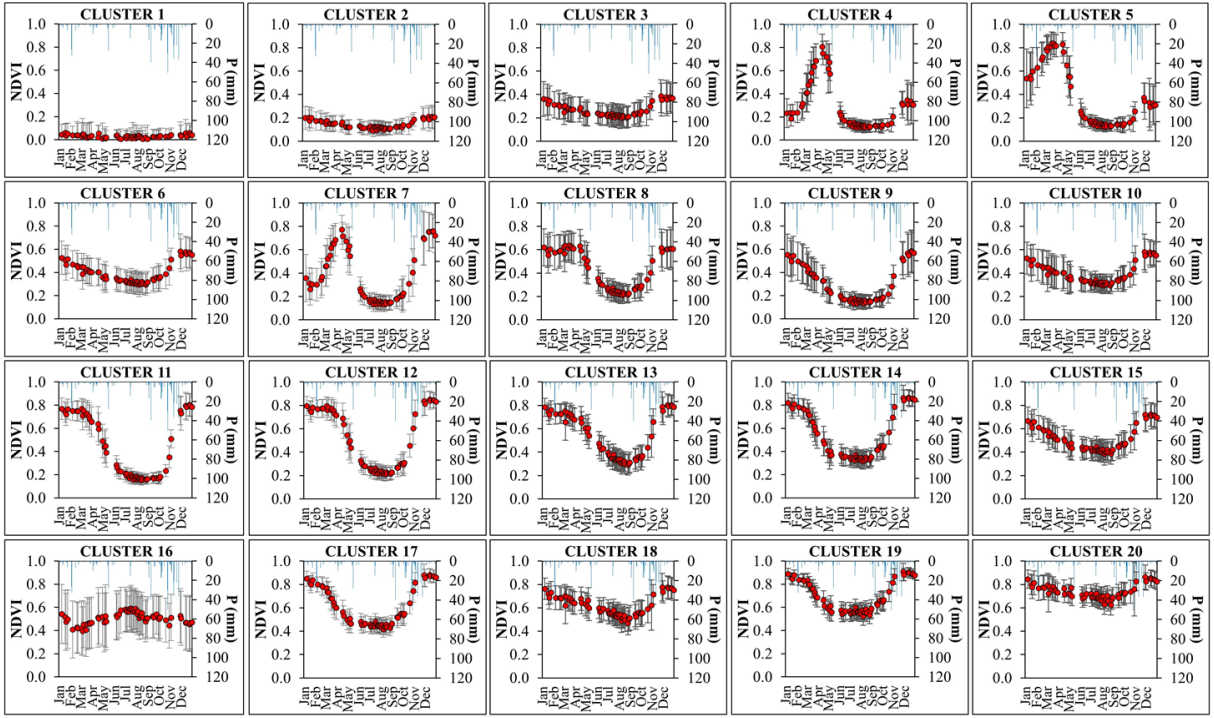

Fig. 3.10. Temporal NDVI profiles (red dots) of the 20 clusters at the irrigation district Quota 102,50 for the year 2019. The blue bars represent the daily rainfall that occurred in the study area.

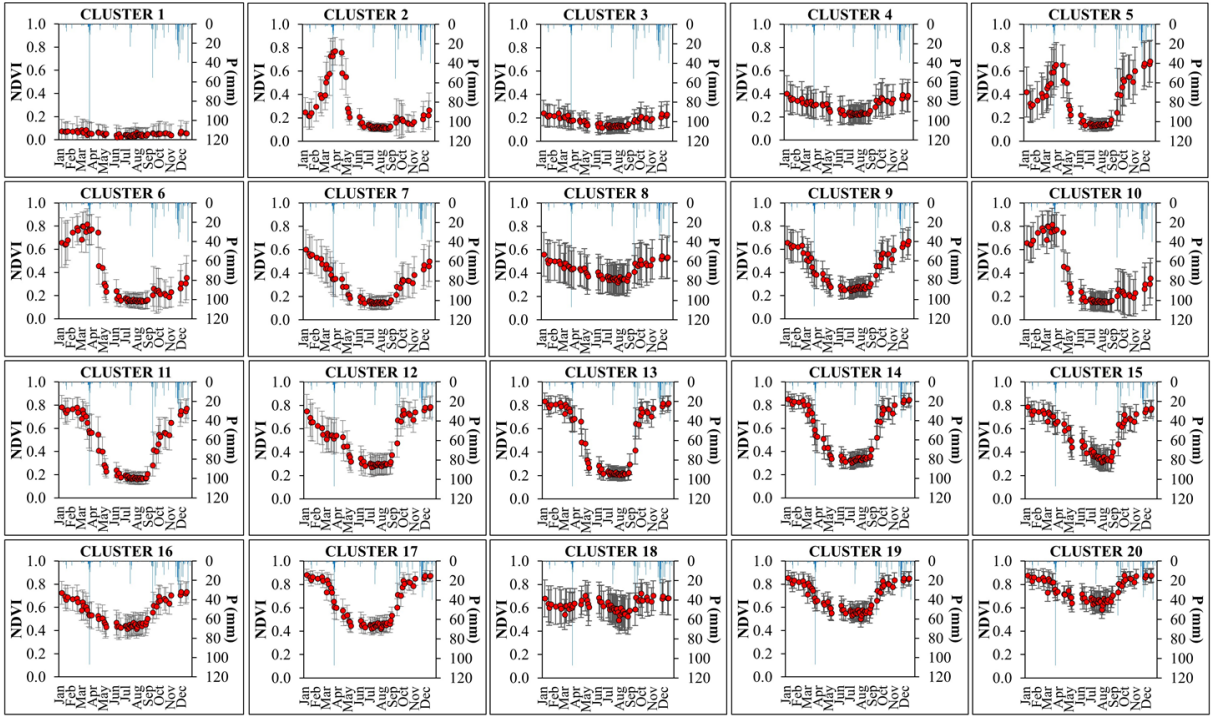

Fig. 3.11. Temporal NDVI profiles (red dots) of the 20 clusters at the irrigation district Quota 102,50 for the year 2020. The blue bars represent the daily rainfall that occurred in the study area.

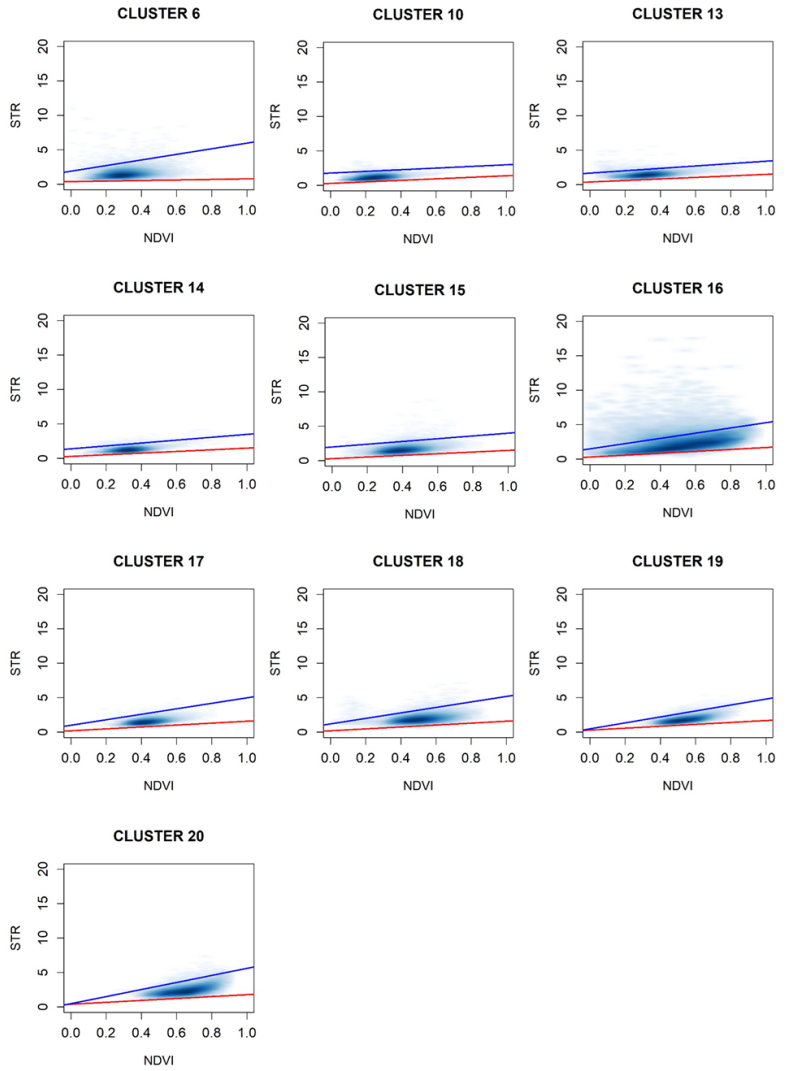

Fig. 3.12. Pixel distribution within the STR-NDVI feature space of the selected clusters at the irrigation district Quota 102,50 during the selected dry period of the irrigation season of 2019. Data are visualized as density scatterplots, associated with the wet (in blue) and dry (in red) edges.

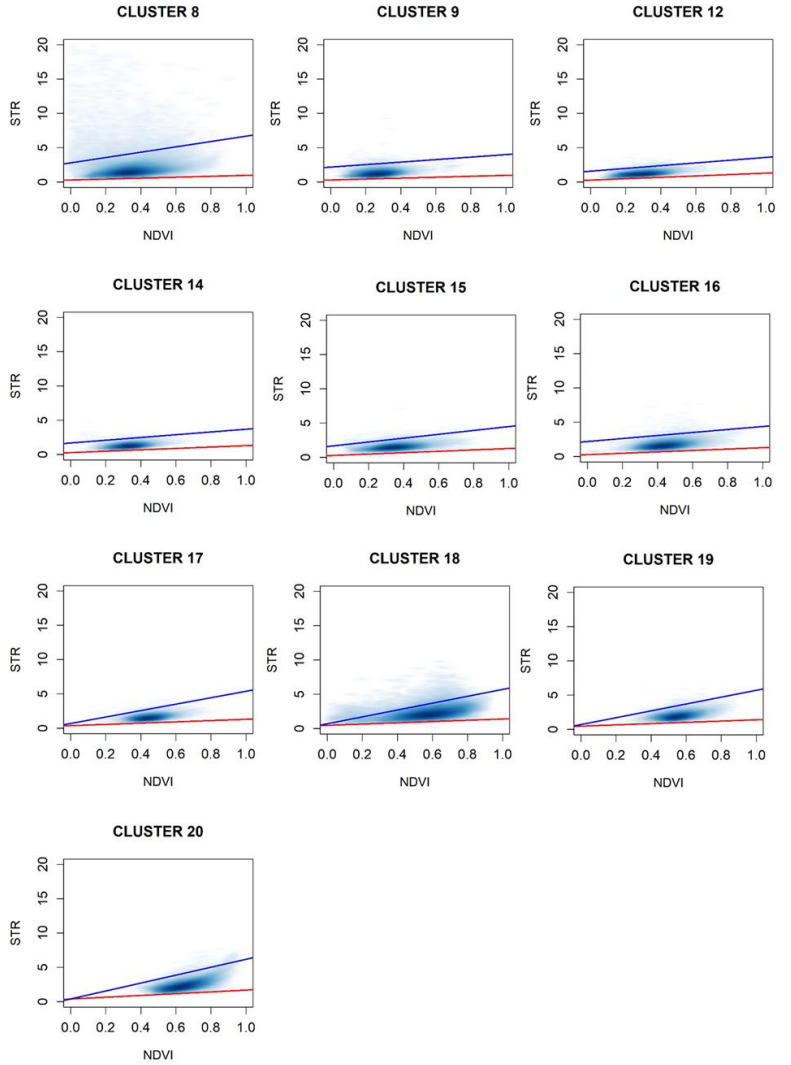

Fig. 3.13. Pixel distribution within the STR-NDVI feature space of the selected clusters at the irrigation district Quota 102,50 during the selected dry period of the irrigation season of 2020. Data are visualized as density scatterplots, associated with the wet (in blue) and dry (in red) edges.

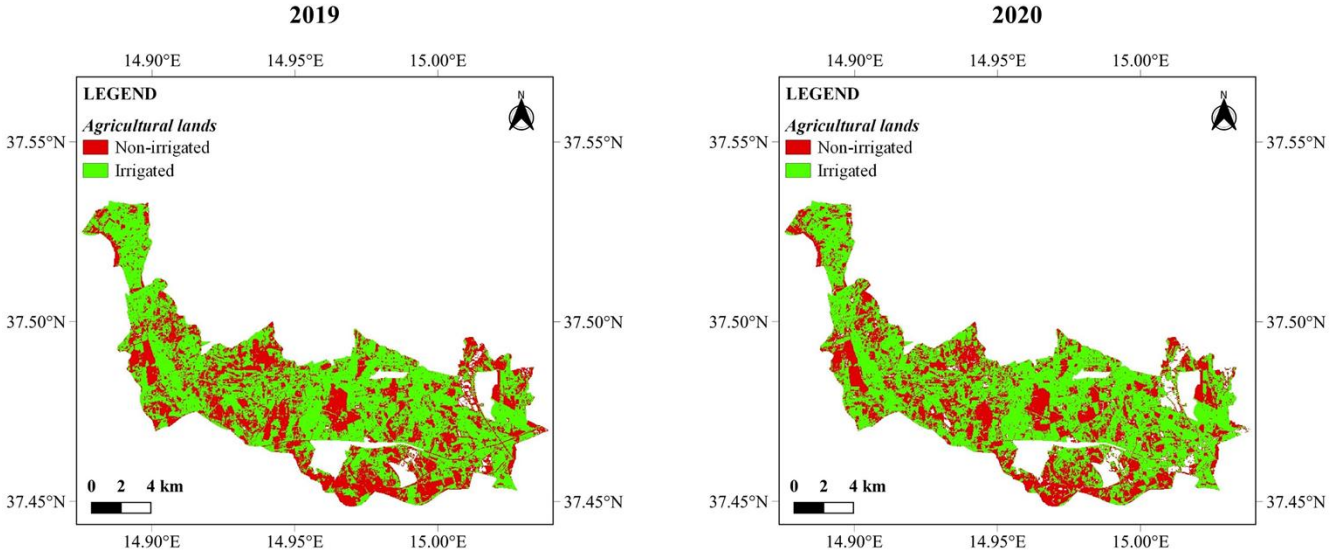

Fig. 3.14. Map of the irrigated (green) and non-irrigated (red) areas obtained at the irrigation district Quota 102,50 during the irrigation seasons 2019-2020.

The surfaces of the irrigated areas were of 61% and 60% on the total surface for the years 2019 and 2020, respectively. Additionally, Fig. S3.1 shows for each sub-district of the Quota 102,50, the irrigated surface variation (%) between 2019 and 2020. This variation was calculated as ratio between the difference of irrigated surface on the two irrigation seasons and the total surface of the sub-district.

Tab. 3.3 shows the comparison between the estimated irrigated areas and the declared irrigated areas by the Reclamation Consortium. An overestimation was observed for both the years, showing that the irrigated areas estimated with the proposed approach were grater than 20.98% and 21.16% compared to the declared irrigated areas for the seasons 2019 and 2020, respectively.

Tab. 3.3. Surfaces (ha) of the estimated and declared irrigated areas at the irrigation district Quota 102,50 for the irrigation seasons 2019-2020.

	Estimated irrigated areas (ha)	**Declared irrigated areas (ha)**	**Absolute error (ha)**
2019	2851.72	2253.32	598.40
2020	2804.60	2211.20	593.40

3.4 Discussion

In the current water scarcity scenario, the need of up-to-date and accurate maps of the irrigated areas is essential for supporting stakeholders to formulate suitable water management strategies. In the last years, many studies have demonstrated the potential of vegetation indices derived from optical RS to detect irrigated areas (Bolognesi et al., 2020; Htitiou et al., 2019; Magidi et al., 2021; Zurqani et al., 2021). Htitiou et al. (2019) applied an approach based on phenological metrics derived separately from Landsat-8 and Sentinel-2 NDVI time series, using with random forest (RF) classification for identifying and mapping irrigated crops in semi-arid conditions. The best performances were obtained for Sentinel-2 data, with an overall accuracy of 93%. In the same climate conditions, Bolognesi et al. (2020) proposed a machine learning classification-based approach based on NDVI time series derived from harmonized Landsat-8 and Sentinel-2 images. By comparing six different types of classifiers, the authors obtained the best performance with RF, reaching an overall accuracy of about 90% in detecting irrigated areas. Recently, Magidi et al. (2021) proposed an approach for classifying irrigated areas under temperate and subtropical climate conditions. They applied RF in conjunction with Google Earth Engine (GEE) platform, using Landsat-8 and Sentinel-2 NDVI time series and other static input data, obtaining an overall accuracy of 88%. Similarly, Zurqani et al. (2021) developed a framework for mapping and quantifying irrigated areas in humid and subtropical climate conditions, based on the use of several Sentinel-2 spectral indices and other RS datasets on GEE platform. Specifically, they produced irrigated and non-irrigated land cover maps by applying RF supervised classification for three years with an overall accuracy of 83.73%, 86.18% and 84.55%, for the years 2016, 2017 and 2018, respectively. Despite the high accuracies obtained, the

approaches proposed by these studies require training process and rules on decision tree structures. Additionally, they did not analyse the case when the same crop type is grown with and without irrigation in the same growing season, which could mean similar temporal NDVI profiles as suggested by Ozdogan et al. (2010). For instance, Ozdogan & Gutman (2008), mapping irrigated areas in Central Nebraska, showed temporal NDVI profiles of irrigated and non-irrigated corn fields with a very similar pattern. Therefore, the authors suggested the use of a more sensitive index to make this distinction.

In this study, a new stand-alone optical RS approach to map irrigated areas was proposed. Compared to previous studies, it does not require any training and is easily replicable in different contexts, using only satellite images, rainfall data, and WP and FC data. Moreover, when no ground measurements are available for deriving rainfall values, alternative data sources such as the climate reanalysis could be used. For example, as suggested by Longo-Minnolo et al. (2022), ERA5-Land reanalysis offers valid rainfall estimates with high probability of detection of the precipitation events. In order to map the irrigated areas without using reference data, a preliminary clustering classification was used. Thus, crop type is not directly considered. The unsupervised classification has been widely adopted for irrigated area mapping, although never in fully automated schemes. For instance, Ragettli et al. (2018) proposed a method implemented on GEE, based on unsupervised classification and multi-temporal satellite image analysis, which made it possible to obtain irrigation maps at 30m of resolution with an accuracy of 77-96% from 2000 to 2017. Specifically, they applied the unsupervised classification for creating samples to use as input for RF. In the study herein proposed, for recognizing the non-irrigated and the potentially irrigated areas we used the unsupervised classification and the analysis of the temporal NDVI profiles and the rainfall events. Thus, for each cluster of the

unsupervised classification labelled as potentially irrigated, which basically represents one or more crop types with the same phenology and green biomass conditions, OPTRAM was applied for deriving the moisture variation and detecting the actual irrigated areas. The resulting map for the Austrian site during the irrigation season 2021 was reasonable accurate, with an overall accuracy of 70% and a precision for detecting the actual irrigated areas of 71%, showing quite lower performances compared to the previous studies that use supervised classification algorithms. It should be noticed that the effects of imbalance on performance metrics was faced by normalizing the classes of the confusion matrix (Luque et al., 2019). A similar accuracy (about 78%) was obtained by Dari et al. (2021) by applying an approach based only on the use of K-means algorithm, RS soil moisture products and a land surface model, but obtaining maps with lower resolution. The maps for the Italian site, instead, showed an overestimation of irrigated areas of about 21% during both the irrigation seasons 2019-2020, with respect to the data declared by the Reclamation Consortium. The overestimation may be in part due to the presence of non-declared irrigated areas since several farmers could use own water sources. In Sicily in fact, autonomous irrigation managed by private consortia or owner of single farms is quite widespread and prevails in many areas compared with collective irrigation, with abstraction of water from small reservoirs and/or wells (Zucaro et al., 2014).

Some uncertainties in the methodology should be also considered. A first source of errors could come from inaccuracies of the unsupervised classification which does not allow a clear crop type distinction, affecting OPTRAM parameters (i_d, s_d, i_w, s_w). In this sense, the use of a detailed crop type map derived by supervised approaches could guarantee higher accuracy since OPTRAM method would be specifically applied for each crop allowing a better discrimination

between irrigated and non-irrigated classes (this approach was however not tested in this study). Despite this, the use of a ground-truth dataset should be taken into account. Secondly, the visual inspection for determining the wet and dry edges of OPTRAM suggested by Sadeghi et al. (2017) could introduce user-related bias, leading to some degree of uncertainty of model outputs. However, as demonstrated by Babaeian et al. (2018) performing a sensitivity analysis by varying the visually-fitted parameters, the visual inspection results in acceptable soil moisture estimates, despite the its perceived user bias. In fact, OPTRAM outputs are not highly sensitive to the dry and wet edge model parameters. Additionally, the reliability of WP and FC of the European Soil Database used for calibrating W calculated by OPTRAM, is undefined. In fact, due the coarse resolution (1 km), these products could be not representative of the study areas, affecting the SWC values. As a consequence, the use of a not accurate WP as threshold value in the second hypothesis we presented, could lead to a not proper estimation of irrigated area affecting the final irrigation maps, as showed by the sensibility analysis. Lastly, since soil moisture is highly influenced by rainfall (Acharya et al., 2022), the accuracy and resolution of the rainfall dataset used in the selection of the dry periods could affect SWC values calculated by OPTRAM.

These limitations clearly need further investigations in order to enhance the methodological approach proposed. Additionally, since the mapping of irrigated areas at large spatial scales is still a great challenge, the enhanced method could be tested at bigger scale. Recently, Zhang et al. (2022) proposed an approach based on the integrate use of remote sensing, irrigation suitability, and irrigated area statistics for developing an irrigated cropland map in mainland China. Despite the good results, the authors highlight the heavy dependence of their method on irrigated area statistics and the

subjectivity of irrigation suitability analysis, as well as the lack of sufficient ground truth data. Thus, the stand-alone RS approach presented in this study, could provide a valuable contribute to the scientific community regarding irrigation mapping even in the large spatial domain.

3.5 Conclusion

This paper introduces a new approach for mapping irrigated areas at high resolution under different climate conditions. Based on the use of the unsupervised classification on NDVI time series and OPTRAM, the main advantage of this methodology is the requirement of only few input data, i.e. cloud-free optical satellite images, rainfall values and soil water parameters, without needing any reference crop type data and thus allowing its transferability in time and space.

The approach was applied and tested in Marchfeld Cropland region in Austria, under a Dfb climate, obtaining a map of the irrigated areas for the irrigation season 2021 with an overall accuracy of 70% and a capability in detecting the actual irrigated areas of 71%. The proposed approach was also applied in the irrigation district Quota 102,50 in Italy, under Csa climate, where the results were compared with the irrigation data of the Reclamation Consortium, finding an overestimation (by RS) of irrigated areas of 21% during the irrigation seasons 2019-2020.

Despite the lower accuracy compared to studies that use supervised classification approaches, these results demonstrate the potential of using OPTRAM for irrigation purposes. Future research could enhance the methodology by studying in detail how crop types affect OPTRAM performances and how to solve the main uncertainties related to the soil water parameters. Additionally, all the enhanced framework could be implemented on GEE platform or similar cloud computing for larger scale applications.

In conclusion, this approach could allow the promotion of data-driven decision for water use and allocation leading to efficient water saving strategies and improving the sustainability of the irrigated agriculture. It could be used as an operational monitoring system by water management authorities for regular reporting of irrigated areas,

representing a potential tool to assist EU member states for meeting their obligations under the WFD.

References

Acharya, U., Daigh, A. L., & Oduor, P. G. (2022). Soil Moisture Mapping with Moisture-Related Indices, OPTRAM, and an Integrated Random Forest-OPTRAM Algorithm from Landsat 8 Images. *Remote Sensing*, *14*(15), 3801.

Ambika, A. K., Wardlow, B., & Mishra, V. (2016). Remotely sensed high resolution irrigated area mapping in India for 2000 to 2015. *Scientific data*, *3*(1), 1-14.

Ambrosone, M., Matese, A., Di Gennaro, S. F., Gioli, B., Tudoroiu, M., Genesio, L., Miglietta, F., Baronti, S., Maienza, A., Ungaro, F., & Toscano, P. (2020). Retrieving soil moisture in rainfed and irrigated fields using Sentinel-2 observations and a modified OPTRAM approach. *International Journal of Applied Earth Observation and Geoinformation*, *89*, 102113.

Babaeian, E., Sadeghi, M., Franz, T. E., Jones, S., & Tuller, M. (2018). Mapping soil moisture with the OPtical TRApezoid Model (OPTRAM) based on long-term MODIS observations. *Remote sensing of environment*, *211*, 425-440.

Babaeian, E., Sidike, P., Newcomb, M. S., Maimaitijiang, M., White, S. A., Demieville, J., Ward, R. W., Sadeghi, M., LeBauer, D. S., Jones, S. B., Sagan, V., & Tuller, M. (2019). A new optical remote sensing technique for high-resolution mapping of soil moisture. *Frontiers in big Data*, 37.

Baghdadi, N., & Zribi, M. (2016). *Land surface remote sensing in continental hydrology*. Elsevier.

Ball, G. H., & Hall, D. J. (1965). *ISODATA, a novel method of data analysis and pattern classification*. Stanford research inst Menlo Park CA.

Bazzi, H., Baghdadi, N., El Hajj, M., Zribi, M., Minh, D. H. T., Ndikumana, E., Courault, D., & Belhouchette, H. (2019a). Mapping paddy rice using Sentinel-1 SAR time series in Camargue, France. *Remote Sensing*, *11*(7), 887.

Bazzi, H., Baghdadi, N., Ienco, D., El Hajj, M., Zribi, M., Belhouchette, H., Escorihuela, M.J., & Demarez, V. (2019b). Mapping irrigated areas using Sentinel-1 time series in Catalonia, Spain. *Remote Sensing*, *11*(15), 1836.

Beck, H. E., Zimmermann, N. E., McVicar, T. R., Vergopolan, N., Berg, A., & Wood, E. F. (2018). Present and future Köppen-Geiger climate classification maps at 1-km resolution. *Scientific data*, *5*(1), 1-12.

BML (Ed.) (2022). Projekt AREAL. Halbautomatische satellitengestützte Ausweisung bewässerter Flächen - Potenzial und Grenzen. Bundesministerium für Land- und Forstwirtschaft, Regionen und Wasserwirtschaft. Wien, Österreich.

Bolognesi F., S., Pasolli, E., Belfiore, O. R., De Michele, C., & D'Urso, G. (2020). Harmonized landsat 8 and sentinel-2 time series data to detect irrigated areas: An application in Southern Italy. *Remote Sensing*, *12*(8), 1275.

Cai, X., & Rosegrant, M. W. (2002). Global water demand and supply projections: part 1. A modeling approach. *Water International*, *27*(2), 159-169.

Cai, X., Magidi, J., Nhamo, L., & van Koppen, B. (2017). *Mapping irrigated areas in the Limpopo Province, South Africa* (Vol. 172). International Water Management Institute (IWMI).

Chance, E. W., Cobourn, K. M., Thomas, V. A., Dawson, B. C., & Flores, A. N. (2017). Identifying irrigated areas in the snake river plain, Idaho: evaluating performance across composting algorithms, spectral indices, and sensors. *Remote sensing*, *9*(6), 546.

Dari, J., Quintana-Seguí, P., Escorihuela, M. J., Stefan, V., Brocca, L., & Morbidelli, R. (2021). Detecting and mapping irrigated areas in a Mediterranean environment by using remote sensing soil moisture and a land surface model. *Journal of Hydrology*, *596*, 126129.

Datta, S., Taghvaeian, S., & Stivers, J. (2017). *Understanding soil water content and thresholds for irrigation management*. Oklahoma Cooperative Extension Service.

Deissenberger. (2021). *Remote monitoring of irrigated areas in the Marchfeld region*.

Gao, Q., Zribi, M., Escorihuela, M. J., Baghdadi, N., & Segui, P. Q. (2018). Irrigation mapping using Sentinel-1 time series at field scale. *Remote Sensing*, *10*(9), 1495.

Ghassemi, B., Immitzer, M., Atzberger, C., & Vuolo, F. (2022). Evaluation of Accuracy Enhancement in European-Wide Crop Type Mapping by Combining Optical and Microwave Time Series. *Land*, *11*(9), 1397.

Htitiou, A., Boudhar, A., Lebrini, Y., Hadria, R., Lionboui, H., Elmansouri, L., Tychon, B., & Benabdelouahab, T. (2019). The performance of random forest classification based on phenological metrics derived from Sentinel-2 and Landsat 8 to map crop cover in an irrigated semi-arid region. *Remote Sensing in Earth Systems Sciences*, *2*(4), 208-224.

Immitzer, M., Vuolo, F., & Atzberger, C. (2016). First experience with Sentinel-2 data for crop and tree species classifications in central Europe. *Remote sensing*, *8*(3), 166.

Jabro, J. D., Stevens, W. B., Iversen, W. M., Allen, B. L., & Sainju, U. M. (2020). Irrigation scheduling based on wireless sensors output and soil-water characteristic curve in two soils. *Sensors*, *20*(5), 1336.

Jin, N., Tao, B., Ren, W., Feng, M., Sun, R., He, L., Zhuang, W., & Yu, Q. (2016). Mapping irrigated and rainfed wheat areas using multi-temporal satellite data. *Remote Sensing*, *8*(3), 207.

Karthikeyan, L., Chawla, I., & Mishra, A. K. (2020). A review of remote sensing applications in agriculture for food security: Crop growth and yield, irrigation, and crop losses. *Journal of Hydrology*, *586*, 124905.

Kumar, S. V., Peters-Lidard, C. D., Santanello, J. A., Reichle, R. H., Draper, C. S., Koster, R. D., Nearing, G., & Jasinski, M. F. (2015). Evaluating the utility of satellite soil moisture retrievals over irrigated areas and the ability of land data assimilation methods to

correct for unmodeled processes. *Hydrology and Earth System Sciences*, *19*(11), 4463-4478.

Lawston, P. M., Santanello Jr, J. A., & Kumar, S. V. (2017). Irrigation signals detected from SMAP soil moisture retrievals. *Geophysical Research Letters*, *44*(23), 11-860.

Lakhankar, T., Krakauer, N., & Khanbilvardi, R. (2009). Applications of microwave remote sensing of soil moisture for agricultural applications. *International Journal of Terraspace Science and Engineering*, 2(1), 81-91.

Longo-Minnolo, G., Vanella, D., Consoli, S., Pappalardo, S., & Ramírez-Cuesta, J. M. (2022). Assessing the use of ERA5-Land reanalysis and spatial interpolation methods for retrieving precipitation estimates at basin scale. *Atmospheric Research*, *271*, 106131.

Lozoya, C., Mendoza, C., Mejía, L., Quintana, J., Mendoza, G., Bustillos, M., Arras, O., & Solís, L. (2014). Model predictive control for closed-loop irrigation. *IFAC Proceedings Volumes*, *47*(3), 4429-4434.

Luque, A., Carrasco, A., Martín, A., & de Las Heras, A. (2019). The impact of class imbalance in classification performance metrics based on the binary confusion matrix. *Pattern Recognition*, *91*, 216-231.

Magidi, J., Nhamo, L., Mpandeli, S., & Mabhaudhi, T. (2021). Application of the random forest classifier to map irrigated areas using google earth engine. *Remote Sensing*, *13*(5), 876.

Mekonnen, M. M., & Hoekstra, A. Y. (2016). Four billion people facing severe water scarcity. *Science advances*, *2*(2), e1500323.

Ozdogan, M., Woodcock, C. E., Salvucci, G. D., & Demir, H. (2006). Changes in summer irrigated crop area and water use in Southeastern Turkey from 1993 to 2002: Implications for current and future water resources. *Water resources management*, *20*(3), 467-488.

Ozdogan, M., & Gutman, G. (2008). A new methodology to map irrigated areas using multi-temporal MODIS and ancillary data: An

application example in the continental US. *Remote Sensing of Environment*, *112*(9), 3520-3537.

Ozdogan, M., Yang, Y., Allez, G., & Cervantes, C. (2010). Remote sensing of irrigated agriculture: Opportunities and challenges. *Remote sensing*, *2*(9), 2274-2304.

Pageot, Y., Baup, F., Inglada, J., Baghdadi, N., & Demarez, V. (2020). Detection of irrigated and rainfed crops in temperate areas using Sentinel-1 and Sentinel-2 time series. *Remote Sensing*, *12*(18), 3044.

Pareeth, S., Karimi, P., Shafiei, M., & De Fraiture, C. (2019). Mapping agricultural landuse patterns from time series of Landsat 8 using random forest based hierarchial approach. *Remote Sensing*, *11*(5), 601.

Pervez, M. S., & Brown, J. F. (2010). Mapping irrigated lands at 250-m scale by merging MODIS data and national agricultural statistics. *Remote Sensing*, *2*(10), 2388-2412.

Ragettli, S., Herberz, T., & Siegfried, T. (2018). An unsupervised classification algorithm for multi-temporal irrigated area mapping in central Asia. *Remote Sensing*, *10*(11), 1823.

Sadeghi, M., Babaeian, E., Tuller, M., & Jones, S. B. (2017). The optical trapezoid model: A novel approach to remote sensing of soil moisture applied to Sentinel-2 and Landsat-8 observations. *Remote sensing of environment*, *198*, 52-68.

Sadeghi, M., Jones, S. B., & Philpot, W. D. (2015). A linear physically-based model for remote sensing of soil moisture using short wave infrared bands. *Remote Sensing of Environment*, 164, 66-76.

Scanlon, B. R., Faunt, C. C., Longuevergne, L., Reedy, R. C., Alley, W. M., McGuire, V. L., & McMahon, P. B. (2012). Groundwater depletion and sustainability of irrigation in the US High Plains and Central Valley. *Proceedings of the national academy of sciences*, *109*(24), 9320-9325.

Shi, J., Jiang, L., Zhang, L., Chen, K. S., Wigneron, J. P., Chanzy, A., & Jackson, T. J. (2006). Physically based estimation of bare-surface soil moisture with the passive radiometers. *IEEE transactions on geoscience and remote sensing*, 44(11), 3145-3153.

Thompson, R. B., Gallardo, M., Valdez, L. C., & Fernández, M. D. (2007). Using plant water status to define threshold values for irrigation management of vegetable crops using soil moisture sensors. *Agricultural Water Management*, *88*(1-3), 147-158.

Vuolo, F., Neuwirth, M., Immitzer, M., Atzberger, C., & Ng, W. T. (2018). How much does multi-temporal Sentinel-2 data improve crop type classification?. *International journal of applied earth observation and geoinformation*, *72*, 122-130.

Yue, J., Tian, J., Tian, Q., Xu, K., & Xu, N. (2019). Development of soil moisture indices from differences in water absorption between shortwave-infrared bands. *ISPRS Journal of Photogrammetry and Remote Sensing*, 154, 216-230.

Zhang, L., Zhang, K., Zhu, X., Chen, H., & Wang, W. (2022). Integrating remote sensing, irrigation suitability and statistical data for irrigated cropland mapping over mainland China. *Journal of Hydrology*, 128413.

Zucaro, R., Pontrandolfi, A., Gallinoni, C., Vollaro, M., Dodaro, G. M., Pacicco, C. L., & Maurano, L. (2014). Atlas of Italian irrigation systems. *Politiche per l'ambiente e l'agricoltura. Risorse idriche*.

Zurqani, H. A., Allen, J. S., Post, C. J., Pellett, C. A., & Walker, T. C. (2021). Mapping and quantifying agricultural irrigation in heterogeneous landscapes using Google Earth Engine. *Remote Sensing Applications: Society and Environment*, *23*, 100590.

4 Comparing the use of ERA5 reanalysis dataset and ground-based agrometeorological data under different climates and topography in Italy[3]

Abstract

Study Region: The study region is represented by seven irrigation districts distributed under different climate and topography conditions in Italy.

Study Focus: This study explores the reliability and consistency of the global ERA5 single levels and ERA5-Land reanalysis datasets in predicting the main agrometeorological estimates commonly used for crop water requirements calculation. In particular, the reanalysis data was compared, variable-by-variable (e.g., R_s; T_{air}; RH; u_{10}; ET_0), with *in situ* agrometeorological observations obtained from 66 automatic weather stations (2008-2020). In addition, the presence of a climate-dependency on their accuracy was assessed at the different irrigation districts.

New Hydrological Insights for the Region: A general good agreement was obtained between observed and reanalysis agrometeorological variables at both daily and seasonal scales. The best performance was obtained for T_{air}, followed by RH, R_s, and u_{10} for both reanalysis datasets, especially under temperate climate conditions. These

[3]A modified version of this Chapter was published as Vanella, D., Longo-Minnolo, G., Belfiore, O. R., Ramírez-Cuesta, J. M., Pappalado, S., Consoli, S., D'Urso, G., Chirico, G. B., Coppola, A., Comegna, A., Toscano, A., Quarta, R., Provenzano, G., Ippolito, M., Castagna, A., & Gandolfi, C. (2022). Comparing the use of ERA5 reanalysis dataset and ground-based agrometeorological data under different climates and topography in Italy. *Journal of Hydrology: Regional Studies, 42*, 101182. https://doi.org/10.1016/j.ejrh.2022.101182

performances were translated into slightly higher accuracy of ET_0 estimates by ERA5-Land product, confirming the potential of using reanalysis datasets as an alternative data source for retrieving the ET_0 and overcoming the unavailability of observed agrometeorological data.

Keywords: Weather ground-based observation; reanalysis dataset; data-processing; modelling and simulation; water management; irrigation

4.1 Introduction

The quantitative estimation of the evapotranspiration (ET) fluxes exchanged within the soil-plant-atmosphere *continuum* is a precondition for rational irrigation scheduling, crop yield forecasting, and hydrological modelling applications (Hupet and Vanclooster 2001). Nowadays, the ET_0 formulation, proposed by P-M and popularized by the FAO-56 paper as a reference methodology for calculating crop water requirements (Allen et al. 1998), is still largely used for practical purposes (Pereira et al. 2015). The use of the P-M approach calls for the necessity of having a reliable and complete set of site-specific agrometeorological data. In fact, the P-M approach calculates the ET_0 for a standard surface, requiring a complete set of ground-based agrometeorological data, such as T_{air}, u, t R_s, and RH, to parameterize the surface and aerodynamic resistances. Commonly, agrometeorological variables are measured by automatic weather stations. Their data integrity is ensured by proper data quality assessment and control procedures (De Pauw et al. 2000). However, ground-based observations could be affected by several errors, mainly due to the sensor properties, such as their accuracy, settings, instrument drift or temporal data sampling frequency (Beven, 1979; Hupet and Vanclooster, 2001; Meyer et al., 1989). Other shortcomings

are related to the agrometeorological time-series consistency. The time series can suffer from substantial time gaps (Capra et al. 2013) and often protocols for correcting and/or estimating poor quality or missing data need to be applied (see, e.g., Pereira et al. 2015). Moreover, the agrometeorological data representativeness of well-watered conditions needs to be checked before implementing them in the ET_0 approach (Pereira et al. 2015). Despite the utmost importance of observed agrometeorological data for agriculture purposes, the agrometeorological networks are often sparse over the territory, especially in arid zones (De Pauw et al. 2000). Sometimes, data access is another critical point for end-users because data is managed and distributed by different regional services at the National level (Pelosi et al. 2021). To compensate for the lack of spatial and temporal distributed information, other weather data sources have steadily developed, such as the use of interpolation methods from gauge-based observations, the adoption of satellite-based datasets, or the creation of gridded datasets obtained by adjusting the spatial interpolation estimates with satellite observations (Pelosi et al. 2020). Moreover, during the last century, great advances have been reached in agrometeorological data forecasting using global and regional NWP models. Several studies have already exploited their potential for supporting sustainable irrigation management (e.g. Negm et al. 2017; Chirico et al., 2018; Longo- Minnolo et al., 2020; Medina et al., 2018; Pelosi et al., 2016; Vanella et al., 2020). As an example, Vanella et al., (2020) showed that the use of forecast agrometeorological estimates provided by COSMO, opens promising perspectives for assessing the ET_0 in different agriculture contexts, particularly under conditions of water scarcity, instead than using past agrometeorological data. Besides the NWP models, the use of atmospheric reanalysis is another alternative weather data source. Atmospheric reanalysis has generated increasing interest in the recent decade, due to its ability to provide

complete and consistent time-series of multiple meteorological parameters at a global scale by covering several decades (Tarek et al. 2020). From a theoretical point of view, the reanalysis process is a retrospective analysis of past historical data. This process makes use of the ever-increasing computational resources, recent versions of NWP models and assimilation schemes. In general, the reanalysis approaches assimilate a wide array of atmospheric and ocean measured and remotely sensed information within a dynamical–physical coupled numerical model (Poli et al. 2016). One of the recognized advantages of using reanalysis approaches is that their outputs are not directly dependent on the density of ground-based observational networks. Thus they have the potential to provide variables in areas with little and/or no surface coverage (Tarek et al. 2020). Moreover, Pelosi et al. (2020) reported that reanalysis data can represent an efficient data source for planning and design studies applied to irrigation water management.

Currently, several modelling centres provide reanalysis products at variable spatial and temporal scales (Lindsay et al., 2014; Chaudhuri et al., 2013). As an example, the ECMWF periodically applies its forecast models and data assimilation systems to reanalyse archived observations for generating global data sets describing the recent history of the atmosphere, land surface, and oceans. The latest released ECMWF reanalysis products are ERA5 single levels (ERA5) and ERA5 Land (ERA5-L), which are being produced within the Copernicus Climate Change Service and freely distributed since 2019. The first dataset, ERA5, covers the entire globe from 1979 at a spatial resolution of about 30 km (depending on latitude). The second dataset, ERA5-L, has been produced by replaying the land component of the ERA5 climate reanalysis, with a horizontal spatial resolution of 9 km. Specifically, ERA5-L uses T_{air}, RH and air pressure, in a process of atmospheric forcing, as input to control the simulated land fields.

These atmospheric variables are corrected to account for the altitude difference between the grid of the forcing and the higher resolution grid of ERA5-L (Muñoz-Sabater, 2019). A comprehensive review of the state-of-the-art associated with the use of ERA5-L for land and environmental applications is presented by Muñoz-Sabater et al. (2021). They demonstrated the added value of ERA5-L reanalysis products, in comparison to ERA-Interim and ERA5, for estimating a wide range of *in situ* observations, even if they have not evaluated the performance of the reanalysis products in predicting ET fluxes.

The specific objective of this study was to explore the effectiveness of using the most advanced global ECMWF reanalysis data (ERA5 single levels and ERA5-L) as a potential data source for predicting the main agrometeorological variables and estimating the ET_0 in different climate contexts within the Italian territory, at daily and seasonal scales. In addition, visual GIS based user-friendly tools have been developed in this study for guiding the users in the reanalyses data pre-processing steps.

4.2 Materials and methods

The methodological approach proposed in this study was carried out in the framework of the research project INtegrated Computer modeling and monitoring for Irrigation Planning in Italy (INCIPIT). The general aim of the INCIPIT project is to identify a shared set of modelling tools and monitoring techniques for the assessment of irrigation water uses in seven irrigation districts distributed over the Italian territory. In this context, time series of daily values of the agrometeorological variables registered in 66 weather stations, referred to as the INCIPIT irrigation districts (Tab. 4.1 and Fig. 4.1), were collected. The use of the new generation ECMWF reanalysis datasets was then evaluated in comparison to the retrieved ground-based agrometeorological data for the ET_0 estimation.

4.2.1 Ground-based agrometeorological variables at the study sites

The observed agrometeorological data was acquired on a daily scale from 66 weather stations located in six different Italian administrative regions (Campania, Emilia-Romagna, Lombardy, Apulia, Sardinia, and Sicily), within the reference period 2008-2020 (from January 1st 2008 to December 31st 2020). Due to the trans-regional component of this study, the observed agrometeorological data were provided from multiple ground-based sources managed by different Regional meteorological agencies located in each of the irrigation districts of interest (Fig. 4.1 and Tab. 4.1).

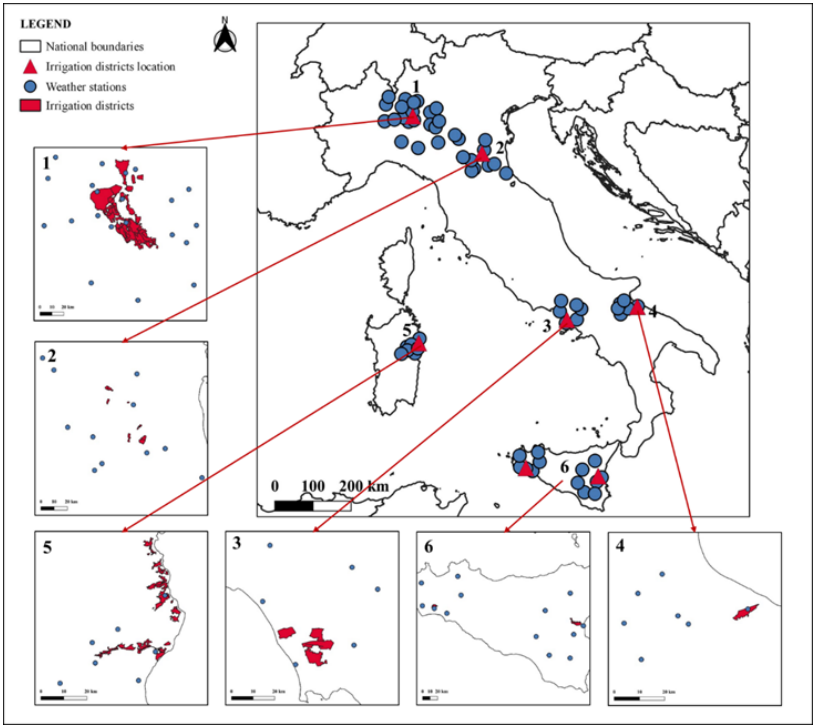

Fig. 4.1. Location of the weather stations selected over the investigated irrigation districts within the Italian peninsula: (1) Lombardy; (2) Emilia-Romagna; (3) Campania; (4) Apulia; (5) Sardinia; and (6) Sicily (Eastern and Western sides).

The set of agrometeorological variables under investigation was composed of R_s (W m^{-2}), maximum and minimum T_{air} measured at 2 m (°C), maximum and minimum RH (%), u measured at 2 m (u_2, m s^{-1}) and 10 m (u_{10}, m s^{-1}), respectively, and ET_0 estimates calculated with the P-M approach (mm d^{-1}).

The selection of the weather stations was based on a twofold criterion. Firstly, they were identified by setting a maximum distance

(50 km) between the centroid of each of the 7 irrigation districts under study (whose coordinates are reported in Tab. 4.1) and the candidate weather stations. Secondly, the selection was refined based on the temporal consistency (i.e. continuous time series) and completeness (i.e. the complete set of data) of the available agrometeorological series. Under these criteria, more than 50 million records were acquired from 66 weather stations, covering a great range of climatic conditions, mainly in terms of the different irrigation district geographic locations (i.e., northern, central and insular Italy) and elevation features (Tab. 4.1). Note that the available dataset for Sardinia sites was only composed of the ET_0 estimates.

In particular, under the improved Köppen-Geiger classification, recently provided at 1-km resolution by Beck et al. (2018), a number of 7 weather stations located in Apulia are characterized by arid, steppe, cold climate (BSk); 24 sites, placed in Campania, Sicily (Eastern and Western part) and Sardinia, are featured by Csa; and 32 sites, located in Emilia-Romagna and Lombardy, are referred to no dry season, hot summer temperate climate conditions (Cfa).

The quality of the ground-based data was checked according to the procedure proposed in Allen (1996). Daily ground-based data was aggregated in 4 periods for seasonality analyses on the astronomical basis, as follows: winter (1st January–19th March and 21st-31st December), spring (20th March–20th June), summer (21st June– 22nd September), and autumn (23rd September–20th December).

Tab. 4.1. Denominations and locations of the investigated irrigation districts, climate characterization and number of referred weather stations, including the name of the regional meteorological agencies

Italian Region		Irrigation districts	Latitude (°)	Longitude (°)	Average altitude (± standard error) (m, a.s.l.)	Climate condition	Number of weather station	Regional meteorological agencies
Lombardy		n. 4 districts – Adda river basin	45.37	9.54	150.0 ± 28.5	Temperate, no dry season, hot summer (Cfa)	21	Arpa Lombardia (https://www.arpalombardia.it/)
Emilia-Romagna		n. 7 districts – Consorzio di Bonifica Renana	44.52	11.24	274.2 ± 113.9		14	Arpae Emilia-Romagna (https://simc.arpae.it/dext3r/)
Campania		Consorzio di Bonifica del Bacino Inferiore del Volturno	41.20	14.15	64.5 ± 26.8	Temperate, dry and hot summer (Csa)	6	Protezione Civile Campania
Sicily	Western	n. 1 district “1A” – Consorzio di Bonifica Sicilia Occidentale	37.78	12.95	247.0 ± 94.3		5	Servizio Informativo Agrometeorologico Siciliano (www.sias.regione.sicilia.it)
	Eastern	n. 1district “Quota 102.50” – Consorzio di Bonifica Sicilia Orientale	37.39	14.74	435.3 ± 135.2		7	
Sardinia		n. 2 districts “Cedrino” and “Posada” - Consorzio di Bonifica della Sardegna Centrale	40.39	15.48	553.9 ± 139.6		6	Sardegna Arpa (http://www.sar.sardegna.it/)
Apulia		n. 1 district 10 -Consorzio di Bonifica della Capitanata	41.3	15.75	120.0 ± 37.5	Arid, steppe, cold (BSk)	7	Consorzio di Bonifica della Capitanata

4.2.2 Reanalysis datasets description

The technical characteristics of the used reanalysis datasets (ERA5 single levels and ERA5-L) and the related data-processing steps are described in Sections 4.2.2.1 and 4.2.2.2, respectively.

4.2.2.1 Reanalysis data collection and characteristics

In this study, the most advanced global reanalysis data produced in Europe by ECMWF has been used: ERA5 single levels (Hersbach et al., 2020) and ERA5-L (Muñoz-Sabater, 2019). The main technical details of these reanalysis datasets are reported in Tab. 4.2.

Tab. 4.2. Main technical details of the reanalysis datasets used in this study

Reanalysis dataset characteristics	ERA5	ERA5-L
Data type	Gridded	
Projection	Regular latitude-longitude grid	
Horizontal coverage	Global	
Horizontal resolution (atmosphere)	0.25° x 0.25°	0.1° x 0.1°
Temporal coverage	1979 to present	1950 to present
Temporal resolution	Hourly	

The ERA5 dataset is the 5th generation of ECMWF global reanalysis succeeding ERA-Interim and covering the entire globe from 1979, at a spatial resolution of about 30 km. The ERA5-L dataset is generated for the entire globe with a native horizontal resolution of about 9 km (released on a regular 0.1◦ x 0.1◦ grid) by replaying the land component of ERA5 climate reanalysis, from 1981 to 2–3 months before the present. Specifically, the atmospheric forcing in ERA5-L is provided by land fields of ERA5 atmospheric variables. In ERA5, T_{air},

air humidity and air pressure are corrected to account for the elevation difference between the grid of the forcing and the higher-resolution grid of ERA5-L, according to the so-called lapse rate correction (Muñoz-Sabater, 2019). Although ERA5-L runs at the enhanced spatial resolution, there is a limit that data are not provided for numerical grid points falling on the sea surface or in the proximity of the coastline (Pelosi et al. 2020).

The ERA5 and ERA5-L reanalysis datasets were freely downloaded from the Climate Change Service Copernicus platform (https://cds.climate.copernicus.eu/cdsapp#!/search?type=dataset) through the Climate Data Store web interface v.1.0 in Network common data form (NetCDF) format for the entire Italian domain (1221.79 x 916.46 km), as for the ground-based observations, within the reference period 2008-2020. The hourly agrometeorological variables of interest were: the T_{air} ('2m_temperature', t2m, °C) and the dew point temperatures (T_{dew}, named as '2m_dewpoint_temperature d2m, m s^{-1}'); the R_s ('surface_solar_radiation_downwards', ssrd, J m^{-2}) and; the vertical and horizontal component of the wind speed ('10m_u_component_of_wind', U10, m s^{-1}, and '10m_v_component_of_wind', V10, m s^{-1}).

4.2.2.2 Data pre-processing steps

Both hourly ERA5 single levels and ERA5-L data were aggregated at a daily time step to be compared variable-by-variable with the ground-based observations.

The daily minimum and maximum T_{air} and T_{dew} values were obtained from the hourly data. The daily T_{air} comparisons were carried out considering the average of the daily maximum (T_{max}) and minimum temperatures (T_{min}). The daily R_s values were aggregated on 24 hours basis. The daily RH was calculated as the ratio between the actual (e_a) and the saturation ($e_o(T)$) vapour pressure using the average

T_{air} and T_{dew} derived on 24 hours basis as inputs, according to the formula proposed in Allen et al. (1998):

$$RH = 100 \cdot \frac{e_a}{e_o(T)} \quad (1)$$

$$e_a = e^o(T_{dew}) = 0.6108 \cdot \exp\left(\frac{17.27\, T_{dew}}{T_{dew} + 237.3}\right) \quad (2)$$

$$e_o(T) = 0.6108 \cdot \exp\left(\frac{17.27\, T_{air}}{T_{air} + 237.3}\right) \quad (3)$$

The daily wind speed at 10 m (u_{10}, m s^{-1}) was calculated using the horizontal and vertical components (V10 and U10) retrieved by ERA5 and ERA5-L datasets, as reported in Allen et al. (1998). Note that the wind speed comparison between the ground-based and reanalysis observations was performed on the u_{10} basis. The wind speed at 2 m (u_2) was rescaled, from the logarithmic wind profile, for being used as input in the ET_0 calculation using the P-M approach (see Section 4.2.3).

The above-mentioned reanalysis datasets data pre-processing steps were performed using five *ad hoc* GIS-based toolboxes developed in ArcPy (ESRI©) (see *Supplementary materials* at the end of the Thesis). The reanalysis post-processed data were extracted from the overall domain at the weather stations' location variable-by-variable (Fig. 4.1). Finally, as for the daily ground-based data, the reanalysis data were aggregated in four periods for seasonality analyses using the same time step as used for the ground-based data.

4.2.3 Calculating daily ET_0 estimates

Although ERA5 single levels and ERA5-L provide potential evapotranspiration data (ET_p), this variable is conceptually different from ET_0 estimates as defined in the FAO-56 paper (Allen et al., 1998). In particular, ET_p is computed in ERA5 based on surface

energy balance calculations with the vegetation parameters set to "crops/mixed farming" and assuming "no stress from soil moisture" (Hersbach et al. 2018), whereas, ET_p in ERA5-L is computed as open water evaporation assuming that the atmosphere is not affected by the artificial surface condition (Muñoz 2019). Thus, in this study daily ET_0 estimates were obtained by implementing the reanalysis of agrometeorological data through the Penman-Monteith (PM) method (Penman, 1956; Monteith, 1965), as follows:

$$ET_0 = \frac{0.408\,\Delta\cdot(R_n - G) + \gamma\cdot\frac{C_n}{T+273}\cdot u_2\cdot(e_s - e_a)}{\Delta + \gamma\cdot(1 + C_d u_2)} \quad (4)$$

where, R_n is the net radiation at the grass surface and G is the soil heat flux density (in MJ m^{-2} d^{-1} for a 24-h daily time step); C_n and C_d are constants, equal to 900 and 0.34, respectively, which vary according to the time step, the reference crop type and daytime/night-time ratio; T is the mean daily T_{air} (°C); Δ is the slope of the saturation vapour pressure curve at T_{air} (kPa $°C^{-1}$); γ is the psychrometric constant (kPa $°C^{-1}$); e_s is the saturation vapour pressure at T_{air} (kPa); e_a is the average daily actual vapour pressure (kPa); and u_2 is the average daily wind speed at 2 m height (m s^{-1}).

Note that the daily ET_0 ground-based estimates (mm d^{-1}) were provided at all site locations by the Regional meteorological agencies (Tab. 4.1), except for Campania and Emilia-Romagna regions for which daily ET_0 values were estimated by Eq. 4 using the agrometeorological information measured *in situ*.

4.2.4 Statistical indicators

The comparisons between the reanalysis-based agrometeorological estimations, from ERA5 and ERA5-L, respectively, and the ground-based observations were assessed using

different statistical metrics, such as the b forced by the origin; R^2; RMSE (Eq. 5); the mean absolute error (MAE; Eq. 6); PBIAS (Eq. 7); and the normalized root-mean-square error (NRMSE; Eq. 8), calculated as follows:

$$\mathrm{RMSE} = \sqrt{\frac{\sum_{i=1}^{n}(S_i - O_i)^2}{n}} \quad (5)$$

$$\mathrm{MAE} = \frac{1}{n}\sum|S_i - O_i| \quad (6)$$

$$\mathrm{PBIAS} = \frac{\sum(S_i - O_i)}{\sum O_i} \cdot 100 \quad (7)$$

$$\mathrm{NRMSE} = \frac{\mathrm{RMSE}}{\bar{O}} \quad (8)$$

where S_i is the simulated value by ERA5 and ERA5-L dataset, respectively, O_i is the observed value from the ground-based agrometeorological stations, where $\hat{S}$ and $\hat{O}$ are the averages of the data arrays of S_i and O_i, and n is the number of observations.

The difference in reproducing the agrometeorological variables by ERA5 and ERA5-L products, respectively, was assessed by applying the least-squares linear regression method and by comparing the outputs of the regression lines in terms of b (for p-values < 0.05). This statistical analysis was conducted using the R software (R Core team, 2020).

The evaluation of the topographic effect on the agrometeorological variables obtained by the reanalysis datasets was assessed by comparing the elevation of the selected weather stations (Tab. 4.1) with the average elevation observed at the cell-size of the ERA5 single levels and ERA5-L datasets (30 and 9 km), respectively (see "*Supplementary materials*"). In particular, the main zonal statistics (count, mean, minimum, maximum, standard deviation, and

median values) of the elevation values were extracted at the level of the cell containing the weather stations (Tab. 4.1) from a digital elevation model (DEM), with a spatial resolution of 75 m, released by the Italian Ministry of the Environment and the Protection of the Territory and the Sea.

4.3 Results

4.3.1 Agrometeorological variable-by-variable comparisons

The description of the main results obtained by comparing the ERA5 and ERA5-L reanalysis agrometeorological estimates (T_{air}, R_s, u_2, RH and ET_0), respectively, and the relative ground-based variables are reported hereafter variable-by-variable for the irrigation districts under study (Tab. 4.1), referring to the period 2008-2020.

The overall performance (in terms of RMSE, MAE, PBIAS and NRMSE values) of the comparisons are given in Tab. 4.3 and 3.4 at the different explored time scales (daily and seasonal). Note that Sardinia sites are not included in Tab. 4.3 and 3.4 because no data was available. Figs 4.2-4.6 report the scatterplots outputted by comparing the daily ERA5 and ERA5-L estimates, respectively, *versus* the observed variables for the irrigation districts under study, as well as the parameters of the regression analyses (b and R^2).

In general, the results of the least-squares linear regression analysis carried out to compare the daily reanalysis datasets (i.e., ERA5 and ERA5-L) *versus* the observed agrometeorological data showed significant differences in terms of slopes values for all the variables of interest also at the seasonal level.

Tab. 4.3. Daily and seasonal performance obtained by comparing the predicted agrometeorological estimates from the ERA5 reanalysis dataset and the ground-based observations; RMSE, MAE, PBIAS and NRMSE refer to the root mean square error, the mean absolute error, the percent bias and the normalized root-mean-square error, respectively.

Italian region		Time-scale	Air temperature (T_{air})				Solar radiation (R_s)				Wind speed (u_{10})				Relative humidity (RH)			
			RMSE °C	MAE °C	PBIAS %	NRMSE	RMSE W m^{-2}	MAE W m^{-2}	PBIAS %	NRMSE	RMSE m s^{-1}	MAE m s^{-1}	PBIAS %	NRMSE	RMSE %	MAE %	PBIAS %	NRMSE
Lombardy		daily	1.62	1.20	-0.38	0.11	35.03	26.41	1.76	0.23	0.69	0.52	-15.69	0.45	8.62	6.70	-2.95	0.12
		winter	1.63	1.24	6.97	0.32	25.59	19.30	11.86	0.32	0.71	0.52	-14.35	0.46	8.96	6.93	-4.42	0.11
		spring	1.62	1.16	-2.58	0.10	42.82	33.49	1.25	0.20	0.78	0.60	-21.24	0.44	8.26	6.40	-2.25	0.12
		summer	1.74	1.27	-1.33	0.07	41.86	33.34	-3.22	0.17	0.64	0.50	-18.39	0.43	9.35	7.40	-1.96	0.14
		autumn	1.47	1.11	1.96	0.14	24.86	18.89	9.39	0.33	0.63	0.47	-6.37	0.47	7.80	6.04	-3.00	0.10
Emilia-Romagna		daily	1.78	1.38	6.62	0.13	29.83	21.99	-0.09	0.18	1.39	0.93	-34.72	0.57	8.93	7.06	4.58	0.13
		winter	1.85	1.44	17.74	0.37	22.42	16.52	5.39	0.26	1.50	0.95	-33.60	0.61	9.76	7.41	5.18	0.13
		spring	1.77	1.33	5.35	0.11	38.07	28.92	0.70	0.17	1.42	1.00	-35.60	0.54	8.32	6.78	3.61	0.13
		summer	1.78	1.40	4.19	0.08	32.84	25.38	-3.58	0.13	1.25	0.93	-37.16	0.53	8.77	7.13	3.73	0.15
		autumn	1.73	1.35	8.95	0.16	21.68	16.30	3.42	0.25	1.40	0.84	-31.95	0.63	8.88	6.94	5.60	0.12
Campania		daily	2.26	1.83	-9.22	0.14	33.54	24.75	4.61	0.20	0.82	0.56	-18.13	0.43	7.87	6.16	-0.39	0.10
		winter	2.09	1.65	-12.54	0.23	26.88	20.90	13.89	0.29	1.02	0.65	-16.70	0.47	8.53	6.64	-1.56	0.11
		spring	2.55	2.14	-11.66	0.15	41.16	31.50	3.59	0.18	0.81	0.57	-23.63	0.41	7.54	5.86	2.77	0.10
		summer	2.43	1.99	-7.51	0.10	32.09	23.57	-0.46	0.12	0.63	0.48	-23.32	0.35	7.09	5.59	1.20	0.10
		autumn	1.92	1.50	-7.20	0.13	32.23	22.87	12.89	0.34	0.80	0.53	-8.12	0.45	8.30	6.60	-3.57	0.10
Sicily	**Western**	daily	1.56	1.24	2.47	0.09	30.16	21.89	2.28	0.15	1.46	1.05	-7.75	0.45	11.13	8.50	8.78	0.17
		winter	1.64	1.31	9.37	0.15	28.20	21.97	4.73	0.23	1.71	1.24	-1.13	0.48	7.97	6.34	3.82	0.11
		spring	1.48	1.18	0.37	0.08	39.38	28.32	5.22	0.15	1.38	0.99	-12.95	0.40	12.46	9.71	11.86	0.20
		summer	1.57	1.26	-0.65	0.06	25.18	17.68	0.78	0.09	1.11	0.84	-17.11	0.37	14.08	10.87	15.30	0.24
		autumn	1.54	1.23	5.40	0.09	25.35	19.51	-2.71	0.19	1.61	1.14	0.01	0.51	8.52	6.85	5.46	0.12
	Eastern	daily	1.47	1.19	0.38	0.09	33.11	24.43	1.89	0.17	1.35	1.12	-35.75	0.48	9.63	7.75	7.55	0.15
		winter	1.56	1.29	2.16	0.16	29.12	22.33	1.60	0.23	1.40	1.12	-29.53	0.46	9.49	7.53	7.09	0.13
		spring	1.42	1.13	0.42	0.08	42.74	31.45	5.12	0.17	1.35	1.15	-36.10	0.46	9.10	7.28	5.54	0.15
		summer	1.39	1.10	-0.95	0.06	30.69	22.33	1.33	0.11	1.37	1.19	-45.24	0.54	10.42	8.53	10.21	0.19
		autumn	1.52	1.24	1.52	0.10	27.35	21.44	-3.12	0.21	1.26	1.02	-32.31	0.48	9.45	7.66	7.70	0.13
Apulia		daily	1.46	1.15	4.14	0.09	45.03	30.72	-5.21	0.24	1.57	1.17	-19.43	0.58	19.02	15.30	-18.46	0.24
		winter	1.41	1.13	7.13	0.17	37.27	26.24	-4.77	0.33	1.81	1.31	-20.48	0.59	16.31	13.70	-15.42	0.19
		spring	1.55	1.21	4.60	0.09	54.82	38.86	-2.64	0.22	1.37	1.07	-17.74	0.49	21.73	17.74	-22.18	0.28
		summer	1.35	1.08	2.31	0.05	51.29	34.70	-6.32	0.18	1.54	1.18	-24.97	0.57	20.59	15.65	-21.36	0.30
		autumn	1.50	1.20	5.23	0.11	32.71	23.01	-8.31	0.28	1.53	1.11	-13.39	0.65	16.81	14.11	-15.74	0.19

Tab. 4.4. Daily and seasonal performance obtained by comparing the predicted agrometeorological estimates from the ERA5-L reanalysis dataset and the ground-based observations; RMSE, MAE, PBIAS and NRMSE refer to the root mean square error, the mean absolute error, the percent bias and the normalized root-mean-square error, respectively.

Italian region		Time-scale	Air temperature (T_{air})				Solar radiation (R_s)				Wind speed (u_{10})				Relative humidity(RH)			
			RMSE °C	MAE °C	PBIAS %	NRMSE	RMSE W m^{-2}	MAE W m^{-2}	PBIAS %	NRMSE	RMSE m s^{-1}	MAE m s^{-1}	PBIAS %	NRMSE	RMSE %	MAE %	PBIAS %	NRMSE
Lombardy		daily	1.80	1.42	-6.10	0.13	34.68	26.13	1.83	0.22	0.90	0.71	-29.11	0.58	8.43	6.59	2.03	0.11
		winter	1.76	1.35	-8.77	0.34	25.46	19.21	11.58	0.32	0.86	0.67	-25.24	0.56	8.70	6.74	1.03	0.11
		spring	2.07	1.68	-9.02	0.12	42.39	33.10	1.40	0.19	1.04	0.85	-36.42	0.58	8.38	6.54	4.58	0.12
		summer	1.86	1.48	-4.70	0.08	41.30	32.81	-3.06	0.17	0.90	0.73	-33.99	0.60	8.97	7.08	2.64	0.13
		autumn	1.47	1.14	-3.37	0.14	24.69	18.78	9.33	0.33	0.76	0.58	-17.58	0.57	7.58	5.97	0.30	0.09
Emilia-Romagna		daily	1.84	1.36	1.35	0.13	33.99	23.99	0.08	0.20	1.61	1.21	-45.22	0.66	10.83	8.56	9.07	0.16
		winter	2.08	1.50	6.36	0.41	26.10	18.35	5.85	0.30	1.69	1.19	-42.70	0.68	12.55	9.76	10.08	0.17
		spring	1.72	1.32	-1.37	0.11	44.33	31.97	0.89	0.19	1.66	1.30	-46.15	0.62	10.52	8.51	9.92	0.17
		summer	1.72	1.28	0.70	0.07	36.22	27.07	-3.51	0.14	1.53	1.24	-49.27	0.64	9.64	7.75	7.84	0.16
		autumn	1.83	1.35	4.68	0.17	24.26	17.74	3.63	0.28	1.57	1.08	-42.05	0.71	10.57	8.30	8.41	0.14
Campania		daily	2.60	2.18	-11.75	0.16	33.81	24.97	4.64	0.20	1.03	0.8	-30.59	0.54	8.23	6.28	3.22	0.11
		winter	2.58	2.11	-19.73	0.28	27.02	21.03	13.70	0.29	1.14	0.82	-24.34	0.53	9.55	7.12	4.10	0.12
		spring	2.95	2.59	-14.33	0.17	41.39	31.65	3.63	0.18	1.08	0.88	-39.80	0.54	8.52	6.59	6.46	0.12
		summer	2.53	2.16	-7.96	0.10	32.40	23.78	-0.37	0.12	0.95	0.79	-41.16	0.53	6.74	5.34	1.88	0.10
		autumn	2.28	1.85	-10.42	0.16	32.60	23.26	12.92	0.35	0.95	0.69	-16.33	0.53	7.96	6.13	0.64	0.10
Sicily	**Western**	daily	1.37	1.09	-1.36	0.08	30.31	21.89	2.63	0.15	1.54	1.19	-7.19	0.47	9.72	7.99	9.32	0.15
		winter	1.44	1.13	-0.15	0.13	28.46	22.14	5.19	0.23	1.71	1.33	1.71	0.47	9.11	7.43	6.84	0.12
		spring	1.36	1.08	-2.47	0.08	39.75	28.45	5.61	0.15	1.44	1.11	-13.21	0.42	10.27	8.49	11.58	0.16
		summer	1.33	1.06	-1.61	0.05	25.12	17.50	1.02	0.09	1.30	1.04	-18.87	0.44	9.82	8.02	11.43	0.17
		autumn	1.36	1.09	-0.52	0.08	25.28	19.41	-2.28	0.19	1.67	1.29	1.39	0.53	9.61	7.96	7.91	0.13
	Eastern	daily	1.31	1.05	-1.51	0.08	33.47	24.76	2.00	0.17	1.54	1.3	-41.43	0.55	11.52	9.29	10.45	0.18
		winter	1.32	1.06	-4.68	0.14	29.11	22.38	1.56	0.23	1.50	1.22	-31.06	0.49	12.41	10.16	12.44	0.17
		spring	1.28	1.03	-0.47	0.08	42.78	31.49	5.20	0.17	1.56	1.34	-42.29	0.53	9.67	7.79	7.93	0.16
		summer	1.36	1.08	-0.70	0.05	31.40	22.82	1.50	0.12	1.68	1.49	-56.64	0.66	11.57	9.28	10.08	0.21
		autumn	1.28	1.02	-2.16	0.08	28.19	22.16	-2.98	0.22	1.39	1.14	-35.86	0.53	12.30	10.03	11.09	0.17
Apulia		daily	1.97	1.44	-2.46	0.12	44.98	30.67	-5.29	0.24	1.75	1.34	-23.50	0.64	15.98	12.03	-11.92	0.20
		winter	1.86	1.38	-6.46	0.22	37.22	26.20	-4.99	0.33	1.95	1.45	-21.52	0.63	12.00	9.54	-7.37	0.14
		spring	2.20	1.58	-3.48	0.13	54.72	38.74	-2.66	0.22	1.59	1.27	-22.22	0.57	17.27	13.36	-13.46	0.22
		summer	1.90	1.40	-1.07	0.08	51.25	34.64	-6.34	0.18	1.76	1.39	-34.50	0.65	19.75	14.45	-17.89	0.29
		autumn	1.88	1.40	-1.49	0.13	32.71	23.03	-8.51	0.28	1.68	1.26	-14.31	0.71	13.41	10.63	-9.95	0.15

4.3.1.1 Air temperature (T_{air})

4.3.1.1.1 T_{air}: ERA5 versus ground-observations

Daily average T_{air} values were estimated with good accuracy by the ERA5 reanalysis dataset at all the irrigation districts under study (Tab. 4.3), showing average RMSE values of 1.46 °C, 1.70 °C and 1.76 °C; and MAE values of 1.15 °C, 1.29 °C and 1.42 °C under Bsk, Cfa and Csa climate conditions, respectively. The average values of NRMSE varied between 0.09 and 0.14; reaching minimum and maximum values under Bsk and Csa-Cfa climate conditions, respectively. The PBIAS values varied from 0.38% (in Eastern Sicily study sites) to 6.62% (in Emilia-Romagna study sites) and -9.22% (in Campania study sites); showing average values of -2.12%, 3.12% and 4.14% under Csa, Cfa and Bsk climate conditions, respectively, with average R^2 values varying between 0.94 (Csa) and 0.97 (Bsk). b values ranged from 0.91 to 1.04, indicating a site-specific underestimation of 9% and overestimation of 4% in Campania and Emilia-Romagna study sites, respectively (Fig. 4.2a-f).

On a seasonal basis, the best T_{air} performance was observed in autumn, showing average RMSE, MAE, PBIAS, b and R^2 values of 1.61 °C, 1.27 °C, 2.64%, 1.01 and 0.89, respectively. Similar performances were obtained in spring-summer seasons (with average RMSE, MAE, PBIAS, b and R^2 values of 1.72 °C, 1.35 °C, -0.62%, 0.99 and 0.79, respectively), while a slightly lower accuracy was observed in winter (with average RMSE, MAE, PBIAS, b and R^2 values of 1.70 °C, 1.34 °C, 5.14%, 1.00 and 0.72, respectively). The same trend was observed in terms of NRMSE values. Specifically, the T_{air} predictions reached the best performance in Apulia study sites during winter and summer (with RMSE and MAE values of 1.35 and 1.08 °C, respectively), followed by spring and autumn in Eastern Sicily and Lombardy study sites; whereas the lowest T_{air} performance

was obtained in Campania study sites during all seasons (Tab. 4.3).

4.3.1.1.2 T_{air}: ERA5-L versus ground-observations

Daily average T_{air} values were predicted with acceptable accuracy by the ERA-L reanalysis dataset at all the irrigation districts under study (Tab. 4.4), resulting in average RMSE values of 1.76 °C, 1.82 °C and 1.97 °C; and MAE values of 1.44 °C, 1.39 °C and 1.44 °C under Csa, Cfa and Bsk climate conditions, respectively. The average NRMSE values varied between 0.08 and 0.16; with similar values under Csa, Cfa and Bsk climate conditions The PBIAS values ranged between 1.35% (in Emilia-Romagna study sites) to -11.75% (in Campania study sites); showing average values of -4.87%, -2.38% and 2.46% in Csa, Cfa and Bsk climate conditions, respectively. The average R^2 values ranged from 0.93 (Csa) to 0.95 (Cfa and Bsk); and b values ranged from 0.89 to 0.99, indicating a maximum and minimum underestimation of 11% and 1% in Campania and Emilia-Romagna study sites, respectively (Fig. 4.2g-l).

Seasonally greater T_{air} predictions were retrieved in summer and autumn seasons, resulting in average RMSE, MAE, PBIAS, b and R^2 values of 1.73 °C, 1.36 °C, -2.39%, 0.97 and 0.81, respectively; whereas, slightly lower T_{air} performance were observed in spring and winter seasons, showing average RMSE, MAE, PBIAS, b and R^2 values of 1.89°C, 1.48 °C, -5.38%, 0.93 and 0.80, respectively. A similar trend was observed in terms of NRMSE values. Specifically, the T_{air} predictions reached the best performance at Eastern Sicily study sites during spring and autumn-winter periods (with average RMSE, MAE, PBIAS, b and R^2 values of 1.28 °C, 1.02 °C, -1.31%, 0.98 and 0.92, respectively) and in summer in Western Sicily study sites (Tab. 4.4); whereas the lowest T_{air} performance was obtained in Campania study sites during all seasons (Tab. 4.4).

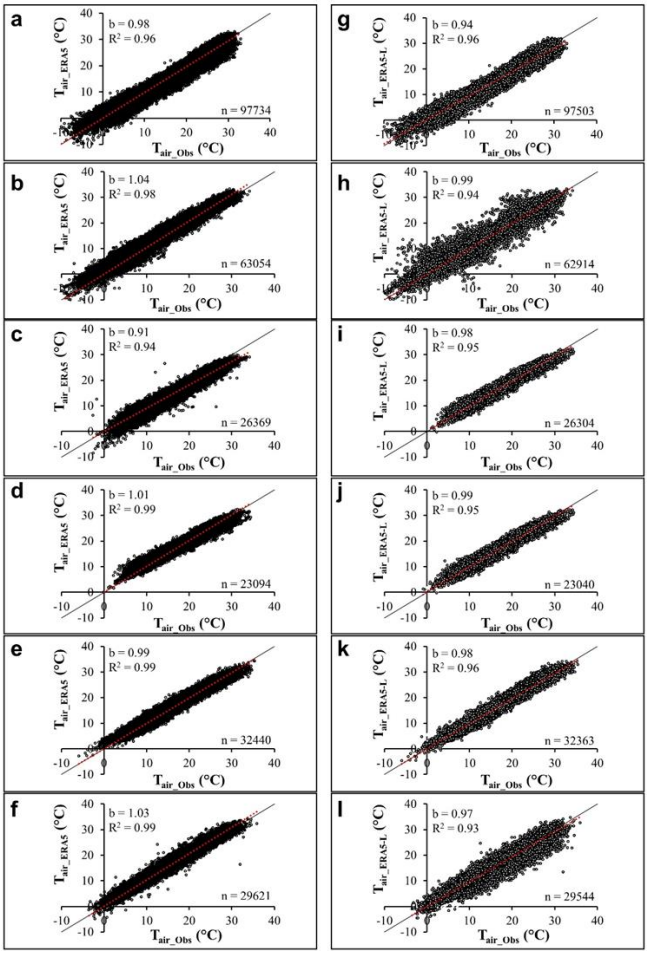

Fig. 4.2. Daily average predicted air temperature (T_{air_ERA5} and $T_{air\_ERA5\text{-}L}$, °C) *versus* observed (T_{air_Obs}, °C) values at the irrigation districts located in Lombardy (a, g), Emilia-Romagna (b, h); Campania (c, i), Western Sicily (d, j), Eastern Sicily (e, k) and Apulia (f, l) within the period 2008-2020. The black line and red line represent the 1:1 line and linear regression line, respectively. The terms b, R^2 and n refer to the slope of the regression equation through the origin, the coefficient of determination and the number of observations, respectively.

4.3.1.2 Solar radiation (R_s)

4.3.1.2.1 R_s: ERA5 versus ground-observations

ERA5 dataset showed good performance in estimating daily R_s under all the examined climate conditions (Tab. 4.3), showing average RMSE values of 32.27 W m^{-2}, 32.43 W m^{-2}, and 45.03 W m^{-2}; MAE of 23.67 W m^{-2}, 24.20 W m^{-2} and 30.72 W m^{-2}, and NRMSE of 0.17, 0.21 and 0.24 in Csa, Cfa and Bsk, respectively. Average PBIAS values ranged between 0.83% (Cfa) to 2.93% (Csa) and -5.21% (Bsk), corresponding to R^2 values of 0.88, 0.86 and 0.80, respectively. b terms presented the same trend with values from 1.00 to 0.96 and 0.91 under Csa, Cfa and Bsk climate conditions, respectively.

Seasonally, the best R_s performance was retrieved in autumn (with average RMSE, MAE and PBIAS values of 27.36 W m^{-2}, 20.34 W m^{-2}, and 1.93%, respectively; and b and R^2 terms of 0.88 and 0.67, respectively) at all site locations (except for Campania locations), followed by winter and summer. Slightly lower R_s performance was obtained in spring, resulting in average RMSE, MAE, PBIAS, b and R^2 values of 43.17 W m^{-2}, 32.09 W m^{-2}, 2.20%, 0.96 and 0.48, respectively. In absolute terms, the best R_s predictions were reached in Western Sicily study sites during summer (also in terms of NRMSE values) and in Emilia-Romagna study sites for the other seasons (Tab. 4.3); whereas the lowest R_s performance was obtained in Bsk climate condition (Apulia study sites) during all seasons and in Campania sites for the autumn season in terms of NRMSE (Tab. 4.3).

4.3.1.2.2 R_s: ERA5-L versus ground-observations

Daily R_s values were predicted with good accuracy by the ERA5-L reanalysis dataset at all study sites (Tab. 4.4), resulting in average RMSE values of 32.53 W m^{-2}, 34.33 W m^{-2} and 44.98 W m^{-2}, and NRMSE values of 0.17, 0.21 and 0.24 under Csa, Cfa and Bsk climate conditions, respectively. Average MAE values ranged from

23.87 W m^{-2} (Csa) to 25.06 W m^{-2} (Cfa) and 30.67 W m^{-2} (Bsk); and PBIAS values varied between 0.96% (Cfa) to 3.09% (Csa) and -5.29% (Bsk). The R^2 values and b terms varied from 0.80 to 0.86 and 0.87, and from 0.91 to 0.96 and 1.00, under Bsk, Csa and Cfa climate conditions, respectively (Fig. 4.3g-l).

At the seasonal level, the R_s predictions reached the best performance in autumn at all climate conditions (except for Campania locations also in terms of NRMSE), with average RMSE, MAE and PBIAS values of 27.96 W m^{-2}, 20.73 W m^{-2}, and 2.02%, respectively; and b and R^2 terms of 0.92 and 0.65. The lower performance was observed in spring under all climate conditions, with average RMSE, MAE and PBIAS values of 44.23 W m^{-2}, 32.57 W m^{-2}, and 2.35%, respectively; and b and R^2 terms of 0.98 and 0.46, respectively. (Tab. 4.4). Intermediate R_s performances were observed in winter and summer (Tab. 4.4). Partially different results were observed in terms of NRMSE showing greater performances in summer followed by spring and winter-autumn seasons. The R_s predictions reached the best performance in Western Sicily during spring and summer periods (Tab. 4.4) and in autumn and winter seasons under Cfa climate conditions (Lombardy and Emilia-Romagna study sites); whereas the lowest R_s performance was obtained under Bsk climate condition (Apulia study sites) during all seasons also in terms of NRMSE values (Tab. 4.4).

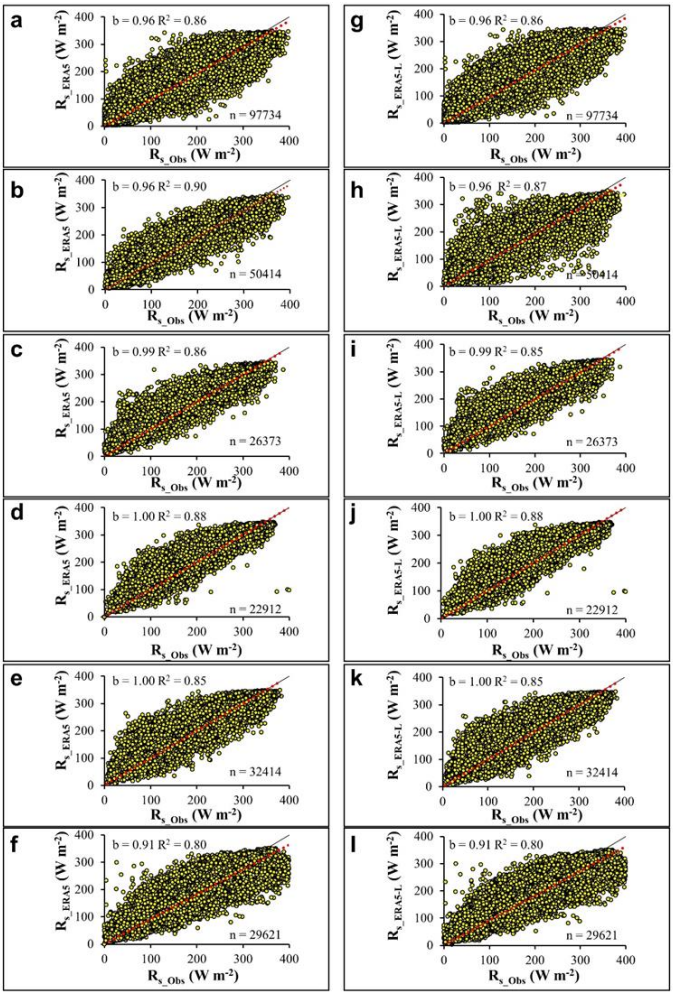

Fig. 4.3. Daily predicted solar radiation (R_{s_ERA5} and $R_{s\_ERA5\text{-}L}$, W m^{-2}) *versus* observed (R_{s_Obs}, W m^{-2}) values at the irrigation districts located in Lombardy (a, g), Emilia-Romagna (b, h); Campania (c, i), Western Sicily (d, j), Eastern Sicily (e, k) and Apulia (f, l) for the period 2008-2020. The black line and red line represent the 1:1 line and linear regression line, respectively. The terms b, R^2 and n refer to the slope of the regression equation through the origin, the coefficient of determination and the number of observations, respectively.

4.3.1.3 Wind speed (u_{10})

4.3.1.3.1 u_{10}: ERA5 versus ground-observations

The performances of the ERA5 dataset in predicting daily u_{10} values are shown in Tab. 4.3 and Fig. 4.4a-f. The ERA5 accuracy shows a specific pattern as a function of the climate conditions, resulting in average RMSE values of 1.04 m s^{-1}, 1.21 m s^{-1} and 1.57 m s^{-1} under Cfa, Csa, and Bsk climate conditions, respectively. Similar behaviour is observed in terms of average MAE values, ranging from 0.73 m s^{-1} (Cfa) to 0.91 m s^{-1} (Csa) and 1.17 m s^{-1} (Bsk). Inversely, PBIAS values were equal to -19.43%, -20.54%, and -25.21% from Bsk to Csa and Cfa climate conditions, respectively. Lower R^2 values were obtained at all study sites, with b terms ranging from 0.66 and 0.74 in Cfa-Bsk and Csa climate conditions, respectively. A similar trend was observed in terms of NRMSE values.

ERA5 performance increased in summer-autumn/spring periods (with average RMSE, MAE, PBIAS, NRMSE, b and R^2 values of 1.16 m s^{-1}, 0.87 m s^{-1}, -22.53%, 0.46, 0.70 and 0.18, respectively). Lower performance was observed in winter, resulting in average RMSE, MAE, PBIAS, NRMSE, b and R^2 values of 1.36 m s^{-1}, 0.97 m s^{-1}, -19.30%, 0.51, 0.71 and 0.22, respectively. In particular, relatively better performance was observed in Campania (summer) and Lombardy study sites (for the rest of the seasons) (Tab. 4.3), whereas, lower performance was registered during winter and summer in Apulia study sites, during spring for Emilia-Romagna and autumn for Western Sicily study sites, respectively (Tab. 4.3).

4.3.1.3.2 u_{10}: ERA5-L versus ground-observations

The accuracy and performance indicators of the ERA5-L dataset in predicting daily u_{10} values are shown in Tab. 4.4 and Fig. 4.4g-l. Similarly to ERA5, the ERA5-L accuracy shows a specific pattern as a function of the climate conditions, resulting in average

RMSE values of 1.26 m s^{-1}, 1.37 m s^{-1} and 1.75 m s^{-1} in Cfa, Csa, and Bsk climate conditions, respectively; showing similar trends in terms of average MAE values, that ranged from 0.96 m s^{-1} (Cfa) to 1.10 m s^{-1} (Csa) and 1.34 m s^{-1} (Bsk). Conversely, PBIAS values varying between -23.50% (Bsk) to -26.40% (Csa) and -37.17% (Cfa); with R^2 and NRMSE values varying from 0.06 (Bsk) to 0.25 (Cfa) and 0.45 (Csa) and from 0.64 to 0.62 and 0.52, under Bsk, Cfa and Csa climate conditions, respectively. b terms ranged from 0.58 (Cfa) to 0.64 (Bsk) and 0.72 (Csa), indicating an underestimation varying from 28% to 36 and 42%, under Csa, Bsk and Cfa climate conditions, respectively.

At the seasonal level, the u_{10} predictions reached the best performance in autumn, with average RMSE, MAE and PBIAS values of 1.34 m s^{-1}, 1.01 m s^{-1}, and -20.79%, respectively; and b and R^2 terms of 0.68 and 0.26, respectively. Lower performance was observed in winter, resulting in average RMSE, MAE, PBIAS, b and R^2 values of 1.47 m s^{-1}, 1.11 m s^{-1}, -23.86%, 0.70 and 0.32, respectively. Moderate u_{10} performances were observed in the other seasons (Tab. 4.4). Slight differences were observed in terms of NRMSE values. Specifically, the u_{10} predictions reached the best and worst performance at Lombardy and Apulia study sites, respectively, during all seasons (Tab. 4.4).

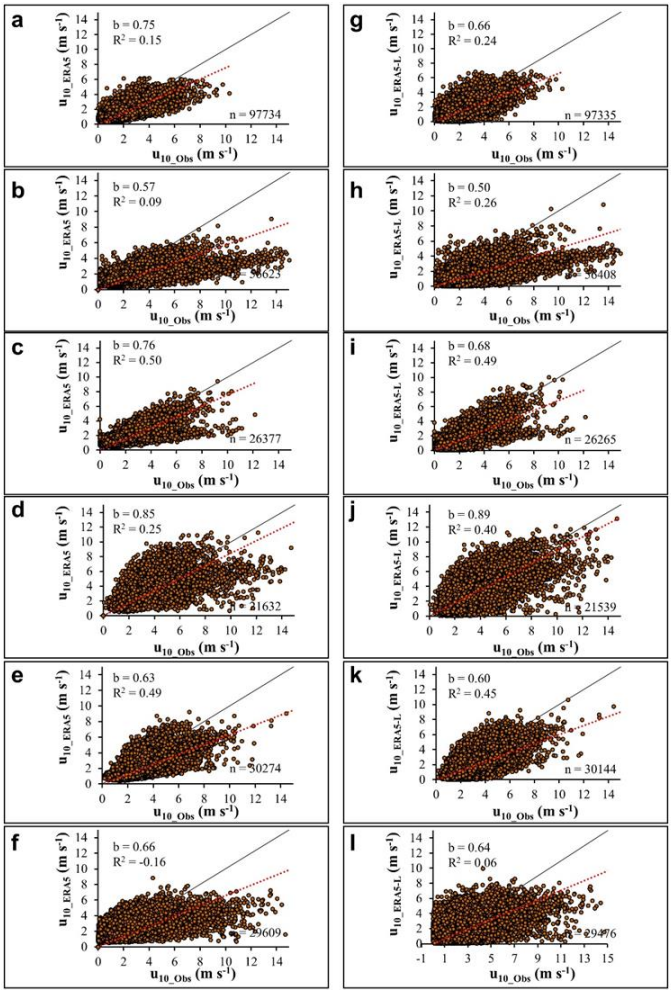

Fig. 4.4. Daily predicted wind speed (u_{10_ERA5} and u_{10_ERA5-L}, m s^{-1}) *versus* observed (u_{10_Obs}, m s^{-1}) values at the irrigation districts located in Lombardy (a, g), Emilia-Romagna (b, h); Campania (c, i), Western Sicily (d, j), Eastern Sicily (e, k) and Apulia (f, l) within the period 2008-2020. The black line and red line represent the 1:1 line and linear regression line through the origin, respectively. The terms b, R^2 and n refer to the slope of the regression equation, the coefficient of determination and the number of observations, respectively.

4.3.1.4 Relative humidity (RH)

4.3.1.4.1 RH: ERA5 versus ground-observations

Good accuracy was observed in the estimation of daily RH values by ERA5 at all study sites (Tab. 4.3), resulting in a similar trend of RMSE and MAE, with values of these indicators ranging from 8.78% to 9.55% and 19.02%, and from 6.88% to 7.47% and 15.30% under Cfa, Csa and Bsk climate conditions, respectively. Similar behaviour was observed in terms of NRMSE, PBIAS and b values, showing better performances from Cfa to Csa and Bsk climates (Fig. 4.5a-f). b terms and R^2 values ranged from 0.81 to 1.04, and from 0.34 to 0.66, respectively.

On a seasonal basis, the ERA5 accuracy was better in autumn and winter (average RMSE, MAE and NMRSE values of 10.07%, 8.06% and 0.13), followed by spring and summer seasons (average RMSE, MAE and NMRSE values of 11.23%, 8.96% and 0.16, respectively). In particular, the best ERA5 performance was retrieved at Campania (spring-summer), Lombardy (autumn) and Western Sicily (winter) study sites. Lower accuracy was obtained at Apulia study sites for all seasons.

4.3.1.4.2 RH: ERA5-L versus ground-observations

The daily RH estimates predicted by ERA5-L in comparison to the ground-based measurements resulted in RMSE values ranging between 9.63% and 9.82% under Cfa and Csa climate conditions, respectively, reaching 15.98% in Bsk conditions (Fig. 4.5g-l). Similar trend was observed in terms of NRMSE values. This behaviour resulted in MAE and PBIAS values of 7.57%, 7.85%, 12.03% and 5.55%, 7.66%, -11.92% under Cfa, Csa and Bsk conditions, respectively. Similar trends were observed for the b and R^2 terms, showing values of 1.04-1.06 and 0.86 and 0.41-0.52 and 0.27 under Cfa-Csa and Bsk conditions, with overestimation of 4-6% in Cfa and

Csa and underestimation of 14% at Apulia study site (Bsk).

At the seasonal level, the overall best RH performance was observed in autumn (Tab. 4.4), with average RMSE, MAE, PBIAS and NRMSE values of 10.24%, 8.17%, 3.07% and 0.13, respectively. Similar performances were retrieved in winter and spring, with slightly lower ERA5-L accuracy during summer (Tab. 4.4). Specifically, the best performance was observed at Campania (in summer) and Lombardy study sites (in the other seasons); whereas lower performance at Emilia-Romagna (in winter) and Apulia study sites (in the other seasons) (Tab. 4.4).

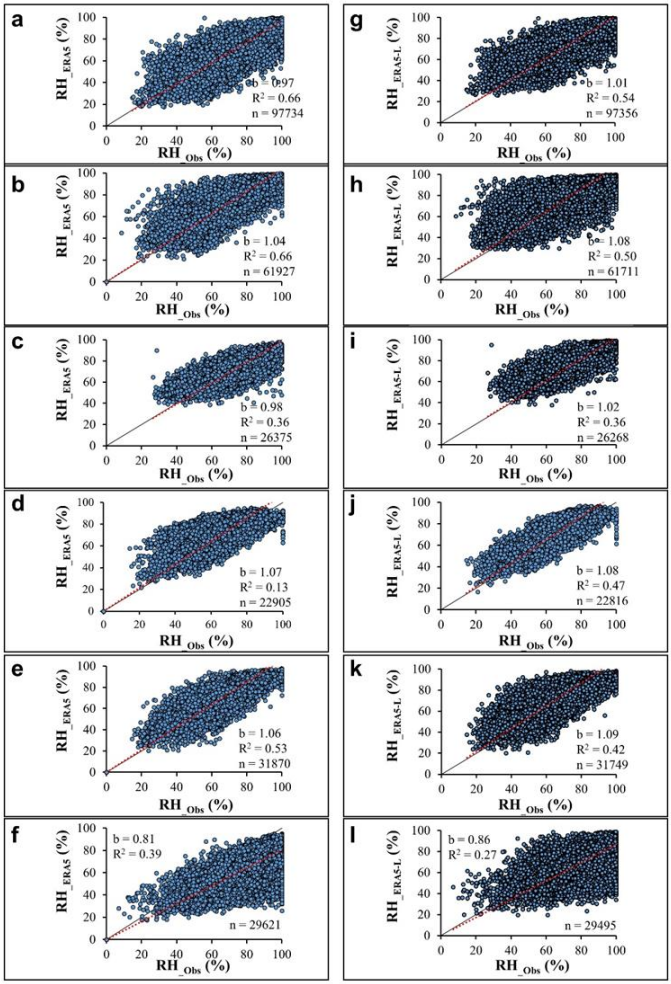

Fig. 4.5. Daily predicted relative air humidity ($RH_{\_ERA5}$ and $RH_{\_ERA5\text{-}L}$, %) *versus* observed ($RH_{\_Obs}$, %) values at the irrigation districts located in Lombardy (a, g), Emilia-Romagna (b, h); Campania (c, i), Western Sicily (d, j), Eastern Sicily (e, k) and Apulia (f, l) for the period 2008-2020. The black and red lines represent the 1:1 and the linear regression line through the origin, respectively. The terms b, R^2 and n refer to the slope of the regression equation, the coefficient of determination and the number of observations, respectively.

4.3.1.5 Reference evapotranspiration (ET_0)

4.3.1.5.1 ET_0: ERA5 versus ground-observations

Daily ET_0 estimates obtained using as inputs the agrometeorological information provided by the ERA5 dataset showed good accuracy in comparison to the ground-based ET_0 estimates (Tab. 4.5 and Fig. 4.6a-m). In particular, the daily ET_0 estimates reached the best performance under Csa-Cfa climate conditions (with average RMSE, MAE and NRMSE values of 0.66 mm d^{-1}, 0.48 mm d^{-1}, and 0.23, respectively). Lower performance was observed at Bsk, resulting in average RMSE, MAE and NRMSE values of 0.90 mm d^{-1}, 0.67 mm d^{-1}, and 0.31, respectively. Positive average PBIAS values were obtained at Bsk (7.90%), whereas negative average PBIAS values of -4.25% and -9.64% resulted under Csa and Cfa climate conditions.

At the seasonal level, the ET_0 performance was greater during winter and autumn periods (with average RMSE, MAE, BIAS, b and R^2 values of 0.47 mm d^{-1}, 0.34 mm d^{-1}, 1.98%, 0.93 and 0.58, respectively), and lower, but still satisfactory, in spring and summer (with average RMSE, MAE, BIAS, b and R^2 values of 0.85 mm d^{-1}, 0.67 mm d^{-1}, -5.58%, 0.93 and 0.59, respectively). Similar values were observed in terms of NRMSE values among the seasons (Tab. 4.5). Better accuracy was obtained at Lombardy (winter-autumn seasons), Campania (summer) and Eastern Sicily (spring) study sites; whereas, lower accuracy was reached at Apulia study sites for all seasons (Tab. 4.5).

4.3.1.5.2 ET_0: ERA5-L versus ground-observations

Overall, ERA5-L provided daily ET_0 estimates with good accuracy (Tab. 4.5 and Fig. 4.6h-n). Specifically, the daily ET_0 estimates reached the best performance under Csa and Cfa conditions (with average RMSE, MAE and NRMSE values of 0.63 mm d^{-1}, 0.46

mm d^{-1} and 0.22, respectively) (Tab. 4.5 and Fig. 6h-n). The lower performance was observed at Bsk, with average RMSE, MAE and NRMSE values of 0.88 mm d^{-1}, 0.64 mm d^{-1} and 0.30, respectively. Positive average PBIAS values were obtained under Bsk (5.86%); whereas under Csa and Cfa climate conditions resulted in values ranging from -2.53% to -10.81%, respectively.

At the seasonal level, the ET_0 performance resulted better in winter and autumn (with average RMSE, MAE, BIAS, b and R^2 values of 0.50 mm d^{-1}, 0.36 mm d^{-1}, -3.84%, 0.90 and 0.64, respectively), and lower, but still quite satisfactory, in spring and summer (with average RMSE, MAE, BIAS, b and R^2 values of 0.77 mm d^{-1}, 0.60 mm d^{-1}, -3.53%, 0.94 and 0.63, respectively). As for the ERA5, similar values were observed in terms of NRMSE values among the seasons (Tab. 4.5). Greater accuracy was obtained at Lombardy (winter-autumn seasons) and Western Sicily (spring-summer seasons) study sites, while lower accuracy was obtained at Apulia study sites for all seasons (Tab. 4.5).

Tab. 4.5. Daily and seasonal (winter, spring, summer and autumn) performance obtained by the comparison between predicted crop reference evapotranspiration (ET_0) by ERA5 and ERA-L reanalysis dataset, respectively, and the ground-based observations; RMSE, MAE, PBIAS and NRMSE refer to the root mean square error, the mean absolute error, the percent bias and the normalized root-mean-square error, respectively.

Italian region	Time-scale	ERA5				ERA5-L			
		RMSE	MAE	PBIAS	NRMSE	RMSE	MAE	PBIAS	NRMSE
		mm d^{-1}		%		mm d^{-1}		%	
Lombardy	daily	0.62	0.42	-6.28	0.25	0.61	0.42	-7.92	0.25
	winter	0.29	0.19	-0.36	0.34	0.30	0.21	-9.45	0.35
	spring	0.75	0.58	-7.38	0.21	0.75	0.59	-8.68	0.21
	summer	0.88	0.69	-7.94	0.20	0.85	0.67	-7.55	0.19
	autumn	0.32	0.21	0.42	0.33	0.31	0.21	-5.45	0.32
Emilia-Romagna	daily	0.70	0.51	-13.00	0.24	0.70	0.52	-13.70	0.24
	winter	0.40	0.28	-15.04	0.37	0.44	0.31	-20.70	0.41
	spring	0.77	0.62	-11.67	0.20	0.79	0.64	-12.37	0.20
	summer	0.97	0.79	-13.33	0.19	0.94	0.76	-12.68	0.18
	autumn	0.44	0.31	-14.24	0.33	0.45	0.31	-16.92	0.34
Campania	daily	0.65	0.48	-11.25	0.23	0.62	0.45	-10.44	0.22
	winter	0.43	0.30	-9.95	0.35	0.47	0.32	-15.58	0.38
	spring	0.77	0.63	-12.57	0.21	0.73	0.59	-11.16	0.20
	summer	0.82	0.69	-12.39	0.17	0.73	0.58	-9.33	0.15
	autumn	0.43	0.29	-4.79	0.30	0.47	0.31	-8.08	0.33

Sicily	**Western**	daily	0.69	0.51	-3.32	0.20	0.57	0.43	-1.06	0.17
		winter	0.44	0.34	7.91	0.28	0.40	0.31	2.91	0.25
		spring	0.74	0.57	-5.57	0.17	0.59	0.45	-1.81	0.14
		summer	0.91	0.71	-7.55	0.16	0.71	0.54	-2.46	0.13
		autumn	0.56	0.42	4.90	0.28	0.53	0.39	1.49	0.26
	Eastern	daily	0.62	0.46	-6.62	0.19	0.57	0.42	-4.21	0.18
		winter	0.38	0.29	-5.20	0.25	0.37	0.28	-8.36	0.24
		spring	0.63	0.49	-3.49	0.16	0.60	0.46	0.55	0.15
		summer	0.87	0.68	-9.03	0.16	0.75	0.58	-4.98	0.14
		autumn	0.46	0.35	-7.47	0.25	0.46	0.34	-9.18	0.25
Sardinia		daily	0.71	0.52	4.20	0.26	0.68	0.50	5.60	0.24
		winter	0.56	0.41	16.80	0.47	0.45	0.33	5.91	0.37
		spring	0.74	0.57	0.83	0.21	0.74	0.58	4.94	0.21
		summer	0.90	0.67	1.54	0.19	0.92	0.71	6.74	0.20
		autumn	0.59	0.43	10.94	0.38	0.48	0.36	3.24	0.31
Apulia		daily	0.90	0.67	7.90	0.31	0.88	0.64	5.86	0.30
		winter	0.60	0.48	23.67	0.51	0.55	0.42	10.91	0.47
		spring	1.03	0.81	10.83	0.28	0.99	0.77	9.18	0.27
		summer	1.18	0.89	-0.37	0.22	1.18	0.90	1.04	0.22
		autumn	0.66	0.50	20.15	0.47	0.61	0.45	12.30	0.44

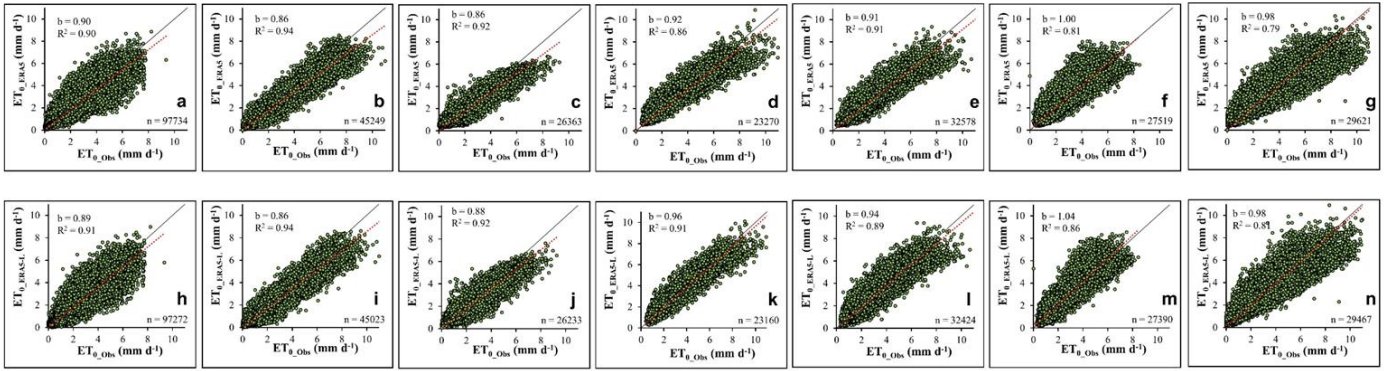

Fig. 4.6. Daily predicted crop reference evapotranspiration (ET_{0_ERA5} and $ET_{0\_ERA5\text{-}L}$, mm d^{-1}) *versus* observed (ET_{0_Obs}, mm d^{-1}) values at the irrigation districts located in Lombardy (a, h), Emilia-Romagna (b, i); Campania (c, j), Western Sicily (d, k), Eastern Sicily (e, l), Sardinia (f, m) and Apulia (g, n) for the period 2008-2020. The black and red lines represent the 1:1 and the linear regression line through the origin, respectively. The terms b, R^2 and n refer to the slope of the regression equation, the coefficient of determination and the number of observations, respectively.

4.4 Discussion

Climate reanalysis data have been widely used for hydrological and meteorological applications. However, it is still difficult to quantitatively estimate their accuracy due to their variability both at spatial and temporal scales, especially under complex topography and pronounced climatic heterogeneity (i.e., the rainfall) (Jiao et al. 2021). Often, ground variables are taken into account in the reanalysis process (such as air pressure, T_{air}, RH and u_{10}) to improve the reanalysis data quality. However, if the data assimilation approach can improve data accuracy, by adding physically meaningful information from the predictive model, this is still subject to uncertainty. The main sources of uncertainty are due to numerical simulations, assimilation schemes and errors associated with the observation systems (Dee et al. 2011). In this sense, some studies showed that it is difficult to completely replace observational data with reanalysis information for describing the true state of the atmosphere (Bengtsson et al. 2004), e.g., for long-term climate trend studies (Liu et al., 2018) and/or for capturing seasonal and inter-annual changes (Jiao et al. 2021).

This study explored the potential of using the new released ECMWF climate reanalysis datasets (i.e., ERA5 and ERA5-L) for proving daily and seasonal agrometeorological information (T_{air}, R_s, RH, u_{10} and ET_0) by determining their performance against measured ground-based observations within the Italian territory in the reference period 2008 – 2020. Moreover, since new user requirements are constantly emerging in society (Muñoz-Sabater et al. 2021), *ad hoc* user-interfaces GIS-based user-friendly tools have been developed in this study for supporting the needs of a diverse set of users, next to the climate and weather research motivations, within the reanalysis data pre-processing steps (Figs. S4.1-S4.4).

Herein, a generally good agreement was observed between the

ability of ERA5 and ERA5-L products in reproducing the agrometeorological variables of interest (commonly used for ET calculation) in comparison to the ground-based observations collected at 66 study sites distributed over 7 irrigation districts. Specifically, the daily T_{air} estimates offered the most accurate reanalysis predictions, followed by the RH, R_s, and u_{10} variables, which still provided satisfactory results (Tabs 4.3-4.4, Figs 4.3-4.5). Similar (i.e., for RH) or slightly improved statistical metrics were obtained by ERA5 in comparison to ERA5-L (i.e., showing lower RMSE values than ERA5-L, for T_{air} and R_s, respectively, in 67% and 83% of the total number of the investigated irrigation districts). This can be attributed to the fact these variables are more homogeneous at the spatial scales provided by ERA5 products in comparison to ERA5-L (Fig. 5.S in *Supplementary materials*). The u_{10} performance was always more consistent for ERA5 than ERA5-L in comparison to the observations at all irrigation districts, most likely because ERA5-L does not consider the influence of the sea surface in its products (Muñoz-Sabater 2019). Altogether, the daily T_{air}, R_s, RH, and u_{10} estimates were more accurate during the autumn season for both reanalysis datasets (Tabs 4.3-4.4).

The influence of topographic features on the accuracy of the reanalysis data was also investigated, following the evidence that it could be significant provided by previous studies. For example, Gao and Hao (2014) evaluated the relationship existing between the elevation of the climate reanalysis data from ERA-Interim and the observed station's elevation. These authors pointed out that differences in elevation can affect the accuracy of the reanalysis data, especially in areas with relatively higher altitudes. Analogous considerations are reported by Longo-Minnolo et al. (2022) for a Sicilian watershed, with elevation values ranging between 0 and 3,313 m a.s.l., for which the highest RMSE values were observed in the

ERA5-L cells with relatively higher variations in altitude. To overcome these shortcomings in mountainous areas, other authors suggest applying altitude correction procedures, especially for water vapour, precipitation and T_{air} estimates (Zhao et al. 2008; Feng et al., 2012; Hu et al. 2013; Negm et al. 2018). For altitudes below 1,000 m (a.s.l.), however, Jiao et al. (2021) found a good agreement between climate reanalysis and observational data. Similar results emerged from this study, where no specific relationships were obtained between the elevation changes and the goodness of reanalysis datasets in reproducing the agrometeorological variables of interest, at the site-by-site scale, within the seven irrigation districts under investigation (Tab. 4.1). These findings show that the accuracy of the reanalyses products is strongly connected with the climatic conditions rather than the topographic distribution of the selected study sites. Due to the above-mentioned explanations and for maintaining the integrity of the reanalysis datasets, no topography corrections were applied in this study.

The performance of reanalysis data strongly depends on the different climate conditions characterizing the investigated sites, as shown by Tarek et al. (2020). Specifically, these authors observed that T_{air} and precipitation estimated by ERA5 are systematically more performant in comparison to ERA-Interim at all the 13 Northern America climate zones under study. In addition, they reported that *in situ* measurements are higher than ERA5 for Cfa and hot-summer humid continental (Dfa) climate zones; elsewhere, these differences are less pronounced. In this sense, they did not experience the difference in hydrological modelling performance using both ERA5 products and observations over 9 of the 13 climate zones. For the remaining regions (Bsk, Cfa, Dfa, and warm-summer humid continental climate, Dfb), the use of observations resulted in improved hydrological modelling performance. In agreement with Tarek et al.

(2020), in our study site-specific performance depended on the different investigated climate conditions (Tab. 4.1). In particular, the major part of the variables of interest (R_s, RH, u_{10} and ET_0) resulted in greater and lower performance under Csa and Bks climate conditions, respectively, by both reanalysis datasets, except for T_{air} estimates provided by ERA5 that shows an inverted pattern due to the influence of the sea temperature in this product (Hersbach et al. 2020). Intermediate performance was observed under Cfa climate zones.

The good quality of the reanalysis data was translated into reliable daily and seasonal ET_0 estimates (with an underestimation from 2 up to 13% for the climate classes under study). Specifically, as for the other variables, ET_0 estimates were more accurate in autumn/winter than in spring/summer by both reanalysis datasets in terms of RMSE values (Tab. 4.5 and Fig. 4.6). In addition, ERA5-L reproduces with greater accuracy and higher spatial resolution the ET_0 observations at most of the study sites even under different climate conditions, i.e., showing lower RMSE values than ERA5 in 86% of the total number of the irrigation districts under study. Thus, the high accuracy obtained in this study when estimating ET_0 by reanalysis products (resulting in RMSE and NRMSE values ranging between 0.57 and 0.90 mm d^{-1} and from 0.17 to 0.31, respectively) suggests the potential use of this information for calculating the daily crop evapotranspiration rates aiming at supporting the irrigation scheduling. In this sense, Rolle et al. (2021) have recently estimated the global irrigation requirement of 26 crops by implementing the Hargreaves-Samani method (Hargreaves and Samani 1985) to calculate ET_0, by using information on T_{air} and R_s retrieved by the ERA5 dataset. Other studies assessed the use of a blended set of weather input data composed of ERA5-L outputs and different sources of climate data (i.e., reanalysis data and satellite-based radiation data) to evaluate the ET_0 for the Campania region (Pelosi et al. 2020; Pelosi

& Chirico, 2021). Pelosi et al. (2021) combined the ERA5-L products with multispectral satellite imagery for estimating the past crop evapotranspiration. Under this scenario, the results of the present study may contribute to the informed use of reanalysis data in water management applications in Italy and elsewhere.

4.5 Conclusion

This study explores the performance of the ERA5 single levels and ERA5-L in depicting the agrometeorological data from 2008 to 2020 in comparison to observational data measured at 66 sites distributed over 7 irrigation districts over the Italian territory. Specifically, the main findings that can be drawn from this study are the following:

- the daily average T_{air} estimates offered the most accurate reanalysis predictions, followed by RH, R_s, and u_{10} variables. This was translated into reliable daily ET_0 estimates resulting in RMSE and NRMSE values ranging between 0.57 and 0.90 mm d^{-1} and from 0.17 to 0.31, respectively;
- similar or slightly improved statistical metrics were obtained by ERA5 in comparison to ERA5-L in estimating RH, T_{air} and R_s; whereas the u_{10} and ET_0 performances were more consistent by ERA5 and ERA5-L, respectively, when compared to the observations at the majority of the irrigation districts under study;
- the R_s, RH, u_{10} and ET_0 estimates resulted in higher and lower performance under Csa and Bks climate conditions, respectively, by both reanalysis datasets; conversely, a reverse pattern was obtained for T_{air} estimates provided by ERA5, being more accurate under Bsk. Intermediate performance was observed under Cfa climate zones.

These results help to improve our understanding of the uncertain sources of reanalysis data under different climate conditions, the rational application of these datasets and the potential improvements for the next product generation. In addition, they open promising perspectives for the use of reanalysis data as an alternative data source to estimate ET_0 for irrigation water management in different climate contexts, overcoming the limited availability of observed agrometeorological data in many areas.

References

Allen, R. G., Pereira, L. S., Raes, D., & Smith, M. (1998). Crop evapotranspiration-Guidelines for computing crop water requirements-FAO Irrigation and drainage paper 56. *Fao, Rome*, *300*(9), D05109.

Allen, R. G. (1996). Assessing integrity of weather data for reference evapotranspiration estimation. *Journal of irrigation and drainage engineering*, *122*(2), 97-106.

Beck, H. E., Zimmermann, N. E., McVicar, T. R., Vergopolan, N., Berg, A., & Wood, E. F. (2018). Present and future Köppen-Geiger climate classification maps at 1-km resolution. *Scientific data*, *5*(1), 1-12.

Bengtsson, L., Hagemann, S., & Hodges, K. I. (2004). Can climate trends be calculated from reanalysis data?. *Journal of Geophysical Research: Atmospheres*, *109*(D11).

Beven, K., 1979. A sensitivity analysis of the Penman-Monteith actual evapotranspiration estimates. Journal of Hydrology 44, 169-190.

Capra, A., Consoli, S., & Scicolone, B. (2013). Long-term climatic variability in Calabria and effects on drought and agrometeorological parameters. *Water Resources Management*, *27*(2), 601-617.

Chaudhuri, A. H., Ponte, R. M., Forget, G., & Heimbach, P. (2013). A comparison of atmospheric reanalysis surface products over the ocean and implications for uncertainties in air–sea boundary forcing. *Journal of Climate*, *26*(1), 153-170.

Chirico, G. B., Pelosi, A., De Michele, C., Bolognesi, S. F., & D'Urso, G. (2018). Forecasting potential evapotranspiration by combining numerical weather predictions and visible and near-infrared satellite images: An application in southern Italy. *The Journal of Agricultural Science*, *156*(5), 702-710.

De Pauw, E., Göbel, W., & Adam, H. (2000). Agrometeorological aspects of agriculture and forestry in the arid zones. *Agricultural and Forest Meteorology*, *103*(1-2), 43-58.

Dee, D.P., Uppala, S.M., Simmons, A.J., Berrisford, P., Poli, P., Kobayashi, S., Andrae, U., Balmaseda, M.A., Balsamo, G., Bauer, P., Bechtold, P., Beljaars, A.C.M., van de Berg, L., Bidlot, J., Bormann, N., Delsol, C., Dragani, R., Fuentes, M., Geer, A.J., Haimberger, L., Healy, S.B., Hersbach, H., Hólm, E.V., Isaksen, L., Kållberg, P., Köhler, M., Matricardi, M., McNally, A.P., Monge-Sanz, B.M., Morcrette, J.-J., Park, B.-K., Peubey, C., de Rosnay, P., Tavolato, C., Thépaut, J.-N., & Vitart, F. (2011). The ERA-Interim reanalysis: Configuration and performance of the data assimilation system. *Quarterly Journal of the royal meteorological society*, *137*(656), 553-597.

Feng, L., & Zhou, T. (2012). Water vapor transport for summer precipitation over the Tibetan Plateau: Multidata set analysis. *Journal of Geophysical Research: Atmospheres*, *117*(D20).

Gao, L., & Hao, L. (2014). Verification of ERA-Interim reanalysis data over China. *J. Subtrop. Resour. Environ*, *9*, 75-81.

Hargreaves, G. H., & Samani, Z. A. (1985). Reference crop evapotranspiration from temperature. Applied engineering in agriculture, 1(2), 96-99.

Hersbach, H., Bell, B., Berrisford, P., Biavati, G., Horányi, A., Muñoz Sabater, J., Nicolas, J., Peubey, C., Radu, R., Rozum, I., Schepers, D., Simmons, A., Soci, C., Dee, D., Thépaut, J-N. (2018): ERA5 hourly data on single levels from 1979 to present. *Copernicus Climate Change Service (C3S) Climate Data Store (CDS),10*.

Hersbach, H., Bell, B., Berrisford, P., Hirahara, S., Horányi, A., Muñoz-Sabater, J., Nicolas, J., Peubey, C., Radu, R., Schepers, D., Simmons, A., Soci, C., Abdalla, S., Abellan, X., Balsamo, G., Bechtold, P., Biavati, G., Bidlot, J., Bonavita, M., De Chiara, G., Dahlgren, P., Dee, D., Diamantakis, M., Dragani, R., Flemming, J., Forbes, R., Fuentes, M., Geer, A., Haimberger, L., Healy, S., Hogan, R.J., Hólm, E., Janisková, M., Keeley, S., Laloyaux, P., Lopez, P., Lupu, C., Radnoti, G., de Rosnay, P., Rozum, I., Vamborg, F., Villaume, S., & Thépaut, J.N. (2020). The ERA5 global reanalysis. *Quarterly Journal of the Royal Meteorological Society*, *146*(730), 1999-2049.

Hu, Z., Ni, Y., Shao, H., Yin, G., Yan, Y., & Jia, C. (2013). Applicability study of CFSR, ERA-Interim and MERRA precipitation estimates in Central Asia. Arid land geography, 36(4), 700-708. Hupet, F., & Vanclooster, M. (2001). Effect of the sampling frequency of meteorological variables on the estimation of the reference evapotranspiration. *Journal of Hydrology*, *243*(3-4), 192-204.

Jiao, D., Xu, N., Yang, F., & Xu, K. (2021). Evaluation of spatial-temporal variation performance of ERA5 precipitation data in China. *Scientific Reports*, *11*(1), 1-13.

Lindsay, R., Wensnahan, M., Schweiger, A., & Zhang, J. (2014). Evaluation of seven different atmospheric reanalysis products in the Arctic. *Journal of Climate*, *27*(7), 2588-2606.

Liu, Z., Liu, Y., Wang, S., Yang, X., Wang, L., Baig, M. H. A., Chi, W., & Wang, Z. (2018). Evaluation of spatial and temporal performances of ERA-Interim precipitation and temperature in mainland China. *Journal of Climate*, *31*(11), 4347-4365.

Longo-Minnolo, G., Vanella, D., Consoli, S., & Ramírez-Cuesta, J. M. (2022). Assessing the use of ERA5-Land reanalysis and spatial interpolation methods for retrieving precipitation estimates at basin scale. *Atmospheric Research*, *271*, 106131.

Longo-Minnolo, G., Vanella, D., Consoli, S., Intrigliolo, D. S., & Ramírez-Cuesta, J. M. (2020). Integrating forecast meteorological data into the ArcDualK_c model for estimating spatially distributed evapotranspiration rates of a citrus orchard. *Agricultural Water Management*, *231*, 105967.

Medina, H., Tian, D., Srivastava, P., Pelosi, A., & Chirico, G. B. (2018). Medium-range reference evapotranspiration forecasts for the contiguous United States based on multi-model numerical weather predictions. *Journal of hydrology*, *562*, 502-517.

Meyer, S. J., Hubbard, K. G., & Wilhite, D. A. (1989). Estimating potential evapotranspiration: the effect of random and systematic errors. *Agricultural and forest meteorology*, *46*(4), 285-296.

Monteith, J. L. (1965). Evaporation and environment. In *Symposia of the society for experimental biology* (Vol. 19, pp. 205-234). Cambridge University Press (CUP) Cambridge.

Muñoz-Sabater, J., Dutra, E., Agustí-Panareda, A., Albergel, C., Arduini, G., Balsamo, G., Boussetta, S., Choulga, M., Harrigan, S., Hersbach, H., Martens, B., Miralles, D. G., Piles, M., Rodríguez-Fernández, N. J., Zsoter, E., Buontempo, C., & Thépaut, J.-N. L. (2021). ERA5-Land: A state-of-the-art global reanalysis dataset for land applications. *Earth System Science Data Discussions*, 1-50.

Muñoz-Sabater, J., (2019). ERA5-Land hourly data from 1981 to present. *Copernicus Climate Change Service (C3S) Climate Data Store (CDS)*.

Negm, A., Jabro, J., & Provenzano, G. (2017). Assessing the suitability of American National Aeronautics and Space Administration (NASA) agro-climatology archive to predict daily meteorological variables and reference evapotranspiration in Sicily, Italy. *Agricultural and Forest Meteorology*, *244*, 111-121.

Negm, A., Minacapilli, M., & Provenzano, G. (2018). Downscaling of American National Aeronautics and Space Administration (NASA) daily air temperature in Sicily, Italy, and effects on crop reference evapotranspiration. *Agricultural Water Management*, *209*, 151-162.

Pelosi, A., Medina, H., Villani, P., D'Urso, G., & Chirico, G. B. (2016). Probabilistic forecasting of reference evapotranspiration with a limited area ensemble prediction system. *Agricultural water management*, *178*, 106-118.

Pelosi, A., Terribile, F., D'Urso, G., & Chirico, G. B. (2020). Comparison of ERA5-Land and UERRA MESCAN-SURFEX reanalysis data with spatially interpolated weather observations for the regional assessment of reference evapotranspiration. *Water*, *12*(6), 1669.

Pelosi, A., Bolognesi, S. F., D'Urso, G., & Chirico, G. B. (2021, November). Assessing crop evapotranspiration by combining ERA5-Land meteorological reanalysis data and visible and near-infrared satellite

imagery. In *2021 IEEE International Workshop on Metrology for Agriculture and Forestry (MetroAgriFor)* (pp. 285-289). IEEE.

Pelosi, A., & Chirico, G. B. (2021). Regional assessment of daily reference evapotranspiration: Can ground observations be replaced by blending ERA5-Land meteorological reanalysis and CM-SAF satellite-based radiation data?. *Agricultural Water Management*, *258*, 107169.

Penman, H. L. (1956). Estimating evaporation. *Eos, Transactions American Geophysical Union*, *37*(1), 43-50.

Pereira, L. S., Allen, R. G., Smith, M., & Raes, D. (2015). Crop evapotranspiration estimation with FAO56: Past and future. *Agricultural Water Management*, *147*, 4-20.

Poli, P., Hersbach, H., Dee, D. P., Berrisford, P., Simmons, A. J., Vitart, F., Laloyaux, P., Tan, D. G. H., Peubey, C., Thépaut, J.N., Trémolet, Y., Holm, E.V., Bonavita, M., Isaksen, L., & Fisher, M. (2016). ERA-20C: An atmospheric reanalysis of the twentieth century. *Journal of Climate*, *29*(11), 4083-4097.

R Core Team. (2020). R: A Language and Environment for Statistical Computing. Vienna, Austria. Retrieved from https://www.R-project.org/

Rolle, M., Tamea, S., & Claps, P. (2021). ERA5-based global assessment of irrigation requirement and validation. *PLoS One*, *16*(4), e0250979.

Tarek, M., Brissette, F. P., & Arsenault, R. (2020). Evaluation of the ERA5 reanalysis as a potential reference dataset for hydrological modelling over North America. *Hydrology and Earth System Sciences*, *24*(5), 2527-2544.

Vanella, D., Intrigliolo, D. S., Consoli, S., Longo-Minnolo, G., Lizzio, G., Dumitrache, R. C., Mateescu, E., Deelstra, J., & Ramírez-Cuesta, J. M. (2020). Comparing the use of past and forecast weather data for estimating reference evapotranspiration. *Agricultural and Forest Meteorology*, *295*, 108196.

Zhao, T., Guo, W., & Fu, C. (2008). Calibrating and evaluating reanalysis surface temperature error by topographic correction. *Journal of Climate*, *21*(6), 1440-1446.

5 Assessing the use of ERA5-Land reanalysis and spatial interpolation methods for retrieving precipitation estimates at basin scale[4]

Abstract

Precipitation data availability plays a crucial role in many climatic, hydrological and agricultural-related applications. In this study, the use of alternative data sources (i.e. interpolation methods and ERA5-L reanalysis data) was combined for improving the spatially distributed precipitation estimates at the Simeto river basin, located in Eastern Sicily (Italy). A total of 51 rain gauges were used to generate a monthly precipitation dataset for the reference period 2002-2019. Among the 6 tested interpolation methods, Natural Neighbour was the method that predicted precipitation the best at monthly level with a Distance between Indices of Simulation and Observation (DISO) of 0.51. Radial Basis Functions and Inverse Distance Weighting provided the highest precipitation accuracies, respectively, for winter and autumn (with DISO values of 0.44 and 0.50, respectively), and for spring and summer seasons (with DISO values of 0.50 and 0.63, respectively). Underestimations on the ERA5-L precipitation estimates were observed when compared to the most accurate interpolation methods both at monthly (25%) and seasonal temporal scales (21% in winter and summer, 36% in autumn), with the exception for spring. The performance was significantly improved

[4] A modified version of this Chapter was published as Longo-Minnolo, G., Vanella, D., Consoli, S., Pappalardo, S., & Ramírez-Cuesta, J. M. (2022). Assessing the use of ERA5-Land reanalysis and spatial interpolation methods for retrieving precipitation estimates at basin scale. *Atmospheric Research, 271*, 106131.
https://doi.org/10.1016/j.atmosres.2022.106131

when the interpolation estimates were corrected with local observations (with RMSD values ranging from 35.29 mm to 26.46 mm at monthly scale, and from 23.33 – 55.34 mm to 23.15 – 37.88 mm at seasonal level). The spatial distribution of the estimation errors associated to precipitation obtained from ERA5-L reanalysis revealed a significant positive correlation (p value < 0.05) with the altitude variation in each ERA5-L cell within the basin under study. These results confirm the good performance on the combined use of alternative precipitation data sources, while adjustments are required to reduce site-specific uncertainties due to local microclimatic conditions occurring at the basin scale.

Keywords: Precipitation; missing data; ERA5-L; interpolation methods; bias correction; spatial variability

5.1 Introduction

Precipitation plays a fundamental role in the hydrologic cycle, conditioning runoff, infiltration, evapotranspiration and water yield processes (Taesombat & Sriwongsitanon, 2009), representing the most important variable related to the atmospheric circulation (Kidd & Huffman, 2011). For this reason, an accurate precipitation dataset, that is complete and reliable on a temporal and spatial basis, is required for several climatic, hydrological and agricultural-related applications (Di Piazza et al., 2011; Yilmaz et al., 2005). Traditionally, this information has been obtained from gauges, including rain gauges, disdrometers and radar, which measure precipitation directly at the Earth's surface (Kidd, 2001; Tapiador et al., 2012). These gauge observations are not uniformly distributed in space and the availability, completeness and consistency of the data may not be adequate, leading to significant time gaps (Kidd et al., 2017; Kidd & Levizzani, 2011). To overcome these limitations, alternative data

sources, such as satellite-based, interpolation and reanalysis precipitation datasets have been proposed (Jiang et al., 2021). However, some uncertainties should be considered, as precipitation is one of the most challenging variables to estimate (Tapiador et al., 2012).

Methods based on satellite information provide spatially distributed and temporally complete datasets for many areas of the globe, offering a cost-effective way to measure precipitation and fill in data gaps (Kidd & Levizzani, 2011; Liu, 2015). Nowadays, several satellite precipitation datasets are available with different spatial coverage, spatial resolutions, and temporal spans and latencies (Mu et al., 2021), such as the Precipitation Estimation from Remotely Sensed Information using Artificial Neural Networks (PERSIANN; Sorooshian et al., 2000), the Tropical Rainfall Measuring Mission (TRMM) Multi-satellite Precipitation Analysis products (TMPA; Huffman et al., 2007), the Global Precipitation Measurement (GPM; Hou et al., 2008), the Global Satellite Mapping of Precipitation (GSMaP; Ushio et al., 2009) and the Multi-Source Weighted-Ensemble Precipitation (MSWEP; Beck et al., 2017). Despite being a potentially useful source of data, satellite products are limited by their short recording duration and contain significant random errors and biases, limiting their use for various study purposes (Liu et al., 2020; Sun et al., 2018).

On the other hand, spatial interpolation methods represent a good alternative to generate distributed and accurate spatial information using available measurements on certain areas (Antal et al., 2021; Chen et al., 2017). In general, spatial interpolation is based on Tobler's first law (Tobler, 1970) which stated that "everything is related to everything else, but near things are more related than distant things". Several interpolation methods have been used for spatializing the precipitation data, including deterministic, e.g. Inverse Distance

Weighting (IDW), Nearest Neighbour (NeN), Natural Neighbour (NN), Radial Basis Functions (RBF); and geostatistical, e.g. Ordinary Kriging (OK), CoKriging (CoOK) (de Amorim Borges et al., 2016; Hurtado et al., 2021; Lyra et al., 2018; Pellicone et al., 2018; Wagner et al., 2012). The selection of the most suitable interpolation technique varies from one study to another, as the performance of the methods depends on several factors, including the spatial and temporal resolution of the data and the selected parameters of the models (Ly et al., 2013). However, one of the critical issues when using interpolation methods, especially for precipitation estimation refers to the number and position of the gauges considered within the study area, which must be representative of the spatial distribution of precipitation (Ly et al., 2013; Wagner et al., 2012). Additionally, an accurate estimation of this variable is complicated in mountainous areas, where the precipitation pattern may be influenced by the irregular topography (Buytaert et al., 2006).

Recent advances in global and regional NWP models (Srivastava et al., 2013), have led to an increased use of climate reanalysis methods since they provide complete and consistent dataset able to overcome the main data limitations (i.e. spatial and temporal availability) of the other techniques (Gleixner et al., 2020). In fact, reanalysis data are produced by running the current NWP models that sequentially assimilate the observed data on the atmosphere and the surface, with the aim of recreating the state variables of the Earth's surface, oceans and atmosphere in the past (Pelosi et al., 2020).

Several organizations, including the National Centers for Environment Prediction/National Center for Atmospheric Research (NCEP/NCAR), the Japanese Meteorological Agency (JPA), the National Aeronautics and Space Administration (NASA) and the ECMWF, provide climate reanalysis useful for deriving precipitation at global and regional scale. Focusing on global reanalysis systems,

NCEP/NCAR released NCEP1 (Kalnay et al., 1996) and NCEP2 (Kanamitsu et al., 2002), with a resolution of 2.5° x 2.5° and 1.875° x 1.875°, respectively. JPA have provided the second Japanese global atmospheric reanalysis project, Japanese 55-year Reanalysis (JRA-55; Ebita et al., 2011), which overcome the lacks in the first Japanese reanalysis project providing a long-term comprehensive atmospheric dataset, with a resolution of 1.25° x 1.25°. In 2017, NASA released the Modern-Era Retrospective analysis for Research and Applications, Version 2 (MERRA-2; Gelaro et al., 2017), which replaced the original MERRA (Rienecker et al., 2011) because of the advances made in the assimilation system that enables integration of satellite observations, with the same resolution of 0.5° x 0.67°. ECMWF have provided several reanalysis products, beginning with First Global Atmospheric Research Program Global Experiment (FGGE; Bengtsson, 1982), followed by ERA-15 (Gibson et al., 1997), ERA-40 (Uppala et al., 2005), and ERA-Interim (Dee et al., 2011). In 2016, the fifth generation of the ECMWF reanalyses has been released, i.e. ERA5 (Hersbach et al., 2020) followed in 2019 by ERA5-L (Muñoz-Sabater, 2021). Compared to the above-mentioned datasets, ERA5 and ERA5-L have several advantages, including the use of advanced data assimilation technologies and a higher spatial and temporal resolution. In fact, ERA5 covers the entire globe with a resolution of 0.25° x 0.25°, whereas ERA5-L has a resolution of 0.1° x 0.1°, both datasets having a temporal scale of 1 hour. Specifically, ERA5-L has been produced using temperature, humidity and air pressure, in an atmospheric forcing process as input to control ERA5 simulated land fields. These atmospheric variables are corrected to account for the difference in altitude between the forcing and the higher resolution grid of ERA5-L (Muñoz-Sabater et al., 2021).

Recently, the use of precipitation data from climate reanalysis methods has been addressed by several authors for many hydrological

and meteorological applications. However, some uncertainties related to the reanalysis data should be considered due to the errors of models and observations in the data assimilation system, leading to biased precipitation estimates (Jiang et al., 2021; Nie et al., 2015). Generally, the performance of ERA5 and ERA5-L was greater compared to other climate reanalysis (Gleixner et al., 2020; Hamm et al., 2020). Despite that, their accuracy can be improved by correcting some biases effects (Jiang et al., 2021). Additionally, a comprehensive evaluation on the spatial distribution of precipitation from these reanalysis datasets is essential to analyse the orographic effect on their estimations (Chen et al., 2021).

The aim of this study was to improve monthly and seasonal estimates of spatially continuous distributed precipitation data at basin scale combining alternative data sources. Specifically, the interpolation methods and ERA5-L were assessed in order to reduce the precipitation data biases of the climate reanalysis and improve their accuracy. Furthermore, the spatial distribution of the estimation errors associated with ERA5-L was evaluated in order to detect a correlation with the variation in altitude.

5.2 Materials and methods

5.2.1 Study area

The case study is the Simeto river basin, located in Eastern Sicily (insular Italy) (Fig. 5.1). The drainage area of the basin and the perimeter are of 4,196 km2 and 323 km, respectively. The altitude ranges between 0 and 3,313 m a.s.l., with an average value of 535 m a.s.l. and a slope of 15%. Most of the Simeto river basin is set on the Apennines-Maghrebian Chain terrains, covered by post-orogenic Miocene and Pliocene units. Due to the different geological evolution, the main characteristics of the Simeto river basin are quite various, with a strong difference between the northern and the southern areas.

A detailed geological and morphological description of the study area was provided by Lentini et al. (1991, 1994). The climate is typical Mediterranean with annual average T_{air}, RH and cumulative P values of 16 °C, 66% and 770 mm, respectively, in the study period (2002-2019).

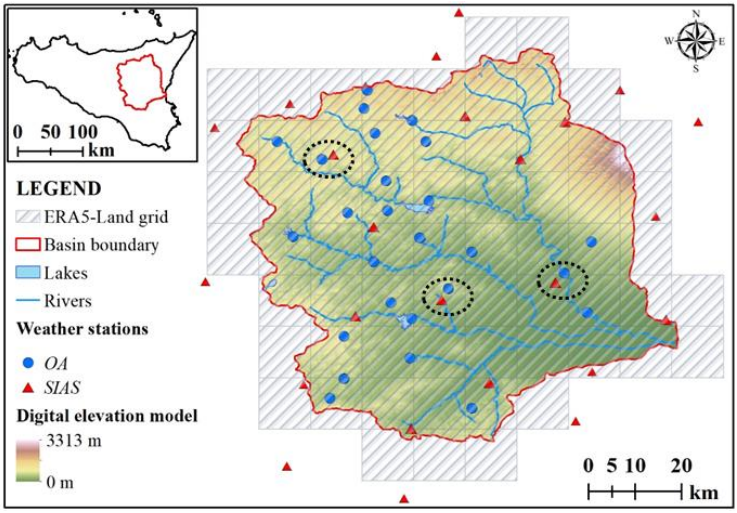

Fig. 5.1. Simeto river basin with the localization of the rain gauges (red triangles indicate the Sicilian Agrometeorological Information Service - SIAS network; blue dots indicate the Basin Authority of the hydrographic district of Sicily - OA network) and the grid of the ERA5-L reanalysis dataset. The dotted circles indicate the selected weather stations to evaluate the coherence between the networks.

5.2.2 Estimation of spatially distributed precipitation data

In order to improve the accuracy of the use of alternative data sources for estimating spatially distributed precipitation data at the basin scale, two main datasets were used: i) an interpolated precipitation dataset; and ii) the ERA5-L reanalysis precipitation dataset.

Fig. 5.2 shows a summary of the methodology followed in the study. The interpolated precipitation data set was generated from ground observations from two main networks, i.e. SIAS (www.sias.regione.sicilia.it) and the Basin Authority of the hydrographic district of Sicily (OA - *Autorità di Bacino del distretto idrografico della Sicilia*, ex *Osservatorio Acque*; www.regione.sicilia.it/istituzioni/regione/strutture-regionali/presidenza-regione/autorita-bacino-distretto-idrografico-sicilia). In particular, a subset containing 60% of the dataset of ground-based observations was used to perform the interpolation, while the remaining 40% was used to evaluate its accuracy. Six interpolation methods have been applied, i.e. IDW, NeN, NN, RBF, OK, CoOK. Once the best performing interpolator was identified, the interpolated precipitation estimates, both non-corrected ($P_{int,nc}$) and corrected ($P_{int,bias}$), were compared to the ERA5-L reanalysis estimates. The corrected interpolation estimates were obtained adjusting the bias as follows:

$$P_{int,bias} = a + b * P_{int,nc} \quad (1)$$

where a and b coefficients corresponded with the intercept and slope terms obtained from the correlation between the interpolation and validation subsets. The value of these parameters for the specific interpolation methods selected at different temporal levels are included in Tab. S4.1 (see *Supplementary materials* at the end of the

Thesis).

Then, the spatial distribution of the estimation errors associated with the climate reanalysis dataset in the study area was assessed for evaluating the correlation with the variation in altitude within each cell of ERA5-L (Fig. 5.2).

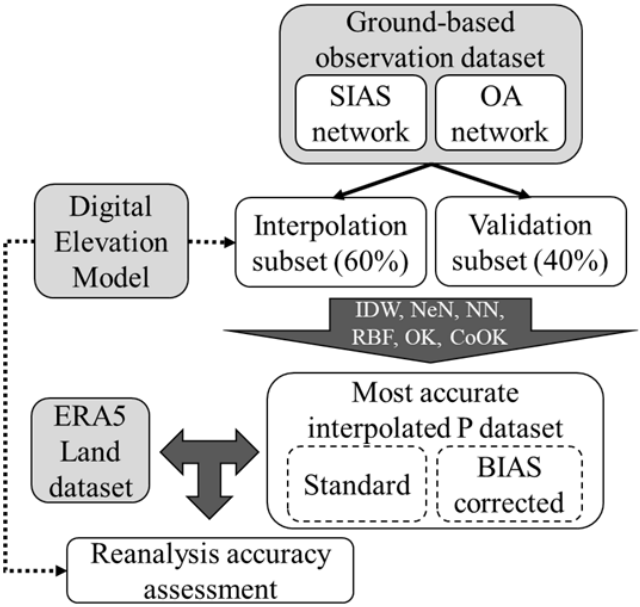

Fig. 5.2. Workflow applied for assessing the use of ERA5-L reanalysis and interpolation methods to estimate spatially distributed precipitation data at the study area. Grey boxes identify the inputs. SIAS and OA refer to the Sicilian Agrometeorological Information Service and the Basin Authority of the hydrographic district of Sicily, respectively. IDW, NeN, NN, RBF, OK and CoOK refer to Inverse Distance Weighting, Nearest Neighbour, Natural Neighbour, Radial Basis Functions, Ordinary Kriging and CoKriging methods, respectively.

5.2.2.1 Ground-based observations

The observed daily precipitation data used in this study were recorded at 51 rain gauges managed by SIAS and OA networks (Fig. 5.1, Tab. 5.2) for the reference period 2002-2019. In order to evaluate the coherence between both weather stations networks, a linear regression was performed between the daily precipitation values recorded by 3-pairs of weather stations belonging to the 2 networks (SIAS and OA), located at a maximum distance of 3 km (Fig. 5.1).

Fig. S4.1 shows a good agreement between daily rainfall measured by SIAS and OA networks. In general, the SIAS network has overestimated the precipitation values by 2%, with b and R^2 values of 1.02 and 0.82 respectively, and a RMSE value of 5.25 mm.

The daily precipitation values were, subsequently, aggregated on a monthly level and then grouped in 4 periods for seasonal analysis, as follows: winter (December, January, February), spring (March, April, May), summer (June, July, August), autumn (September, October, November). The consistency of the dataset was evaluated through a preliminary analysis to detect all the missing data during the study period 2002-2019. The weather stations exceeding 30% of missing daily values were excluded from the dataset for that specific month. No temporal interpolation was performed for data gap filling.

The obtained monthly dataset was divided into 2 main subsets: i) interpolation subset, consisting of 60% of the monthly precipitation values, used to perform the different interpolation methods; and ii) validation subset, consisting of 40% of monthly precipitation values, used to validate the results (Fig. 5.2). In this way, the validation was completely independent of the formulation of the interpolation method (Ly et al., 2012). The assignment of the weather stations to one or another subset was performed considering the spatial distribution of the weather stations. Thus, the most externally located weather stations (Fig. 5.1) were assigned to the interpolation subset in order to

perform the spatial interpolation covering the entire area minimizing the errors in the edge of the basin. Additionally, the completeness of the data series for all the study period was considered, favouring the allocation of weather stations with a more complete dataset to the interpolation subset. As shown in Tab. 5.1, SIAS weather stations mostly respected these criteria.

Tab. 5.1. Meteorological stations in the study area, including the identification number (Station ID) the name, the relative network (SIAS and OA), the type of subset (interpolation and validation), the coordinates (longitude, X and latitude, Y) in decimal degrees (°) (reference system: World Geographic System - WGS84) and the elevation (Z) (m, a.s.l.).

ID	Station name	Network	Subset	X(°)	Y(°)	Z(m)
77	Pomiere	OA	Validation	14.491	37.888	1348
78	Capizzi	OA	Validation	14.483	37.853	1161
92	Pietrarossa Diga	OA	Validation	14.573	37.369	197
112	Troina	OA	Validation	14.603	37.789	1008
114	Nicosia	OA	Validation	14.402	37.754	757
115	Agira	OA	Interpolation	14.528	37.655	785
116	Catenanuova	OA	Interpolation	14.692	37.575	202
117	Raddusa	OA	Validation	14.535	37.476	361
127	Cerami	OA	Interpolation	14.505	37.805	956
128	Gagliano Castelferrato	OA	Validation	14.526	37.713	831
130	Mineo	OA	Validation	14.693	37.271	484
133	Mirabella Imbaccari	OA	Validation	14.444	37.328	462
134	Castel di Iudica	OA	Interpolation	14.647	37.503	670
137	Paternò	OA	Interpolation	14.924	37.595	405
138	Presa Dittaino	OA	Interpolation	14.502	37.555	233
157	Pozzillo Diga	OA	Validation	14.609	37.674	359
164	Ancipa Diga	OA	Validation	14.576	37.830	949
173	Don Sturzo Diga	OA	Interpolation	14.576	37.445	213
174	Nicoletti Diga	OA	Interpolation	14.346	37.604	387
177	Sciaguana Diga	OA	Validation	14.592	37.602	261
179	Ponte Barca Traversa	OA	Validation	14.871	37.534	67
186	Simeto a Ponte Giarretta	OA	Validation	14.916	37.457	23
203	Contrada Cicera	OA	Validation	14.315	37.789	656
210	Nissoria	OA	Validation	14.451	37.651	672
214	Aidone	OA	Validation	14.445	37.411	835
215	S. Michele di Ganzaria	OA	Validation	14.418	37.291	355
216	Gela	SIAS	Interpolation	14.334	37.159	70
224	Bronte	SIAS	Validation	14.787	37.755	424
227	Caltagirone	SIAS	Interpolation	14.575	37.232	260
228	Catania	SIAS	Interpolation	15.069	37.443	10
230	Linguaglossa	SIAS	Interpolation	15.131	37.828	590
231	Maletto	SIAS	Interpolation	14.873	37.828	1040

232	Mazzarrone	SIAS	Interpolation	14.562	37.096	300
233	Mineo	SIAS	Interpolation	14.726	37.321	205
234	Paternò	SIAS	Interpolation	14.855	37.516	100
235	Pedara	SIAS	Interpolation	15.049	37.644	803
237	Randazzo	SIAS	Interpolation	14.980	37.889	680
238	Enna	SIAS	Interpolation	14.176	37.517	350
241	Nicosia	SIAS	Interpolation	14.424	37.764	700
242	Piazza Armerina	SIAS	Interpolation	14.367	37.317	540
243	Aidone	SIAS	Interpolation	14.467	37.451	350
245	Caronia	SIAS	Interpolation	14.487	37.897	1470
246	Cesarò	SIAS	Interpolation	14.680	37.839	820
252	Militello Rosmarino	SIAS	Interpolation	14.667	38.040	460
253	Mistretta	SIAS	Interpolation	14.340	37.863	690
259	S. Fratello	SIAS	Interpolation	14.624	37.955	1040
269	Gangi	SIAS	Interpolation	14.194	37.816	833
291	Francofonte	SIAS	Interpolation	14.894	37.246	100
292	Lentini	SIAS	Interpolation	14.926	37.342	50
312	Agira	SIAS	Validation	14.502	37.623	467
316	Ramacca Giumarra	SIAS	Validation	14.634	37.482	263

5.2.2.2 Spatial interpolation algorithms

In order to estimate the spatially distributed precipitation for the study area from the weather station data, 6 interpolation methods - IDW, NeN, NN, RBF, OK, CoOK - were applied, using the Spatial Analyst and the Geostatistical Analyst tools implemented in ArcGIS 10 (ESRI ©). The IDW method interpolates using a weighted average of the observations, weighing by the inverse distance between each observation and the point to be estimated (Shepard, 1968). In the current study, a power of 2 was used to perform the IDW interpolations. The NeN method is based on the assumption that the estimated precipitation value at a certain point corresponds to the observed value at the nearest weather station. It is performed by applying Delaunay tessellation (Watson, 1981) to create a network of Thiessen polygons by the perpendicular bisectors that connect neighbouring stations to other related stations. The NN method (Sibson, 1981) also interpolates using a weighted average of the observations as in IDW, but the weight for each station is proportionally based on the area determined by the construction of the Thiessen polygons rather than on the distance. The RBF interpolates using a weighted linear function of the distance between a specified number of nearby observed points and the point to be estimated, adding a bias. The function used in the study is the thin plate spline (TPS; Hutchinson and Gessler, 1994), which generates a smooth folded surface passing through each observed value.

Regarding the geostatistical interpolators, Kriging method (Metheron, 1971) uses a weighted average of observations, where the weights are evaluated using a semivariogram, which considers the spatial autocorrelation of the data. Alternatively, OK interpolates using a linear combination of observed values in which the mean is assumed to be constant, but unknown (Isaaks, 1989). In this study, a

stable function was used to model the empirical semivariogram, and the model parameters (including nugget and partial sill) were optimized using the cross-validation. Additionally, CoOK incorporates one or more auxiliary variables to perform the interpolation (Isaaks, 1989). In this study, a digital elevation model (DEM), with 20 m of spatial resolution (www.pcn.minambiente.it/mattm/servizio-di-scaricamento-wcs), was used as covariate.

5.2.2.3 ERA5-Land reanalysis dataset

ERA5-L is an integral and operational component of the Copernicus Climate Change Service (C3S), of the ECMWF. Data is available hourly and can be downloaded on a regular latitude/longitude grid of 0.1° x 0.1° via the Climate Data Store (CDS) catalogue (cds.climate.copernicus.eu) in GRIB or NetCDF format. The update frequency is monthly with a delay of about three months compared to the actual date.

In this study, hourly ERA5-L precipitation data, in NetCDF format, were collected for the period 2002-2019 for the entire study area (Fig. 5.1). These data were converted into TIFF format obtaining a multi-bands raster (24 bands) for each day of the study period, in which each single band identifies the cumulated precipitation value until that hour of the day. Thus, the 24th band of each raster represents the cumulative value of the precipitation of the whole day. Subsequently, the 24th bands of each multi-band raster were extracted and summed to obtain monthly single-band raster. These processes were performed using ArcGIS toolboxes specifically created for this purpose in GIS environment (ArcMap 10 ©), using ArcPy.

5.2.3 Statistical performance

The performance of each interpolation algorithm was evaluated using linear regressions, comparing the interpolated precipitation estimates (interpolation subset) with the observed data from the validation subset (Fig. 5.2; Tab. 5.1). In particular, b and R^2 were evaluated by forcing intercept to 0. In addition, the following statistical metrics were adopted to quantitatively describe the accuracy of the methods: RMSE (mm; Eq. (2)); MAE (mm; Eq. (3)), PBIAS (%; Eq. (4)).

$$\mathrm{RMSE} = \sqrt{\frac{\sum(P_i - O_i)^2}{n}} \quad (2)$$

$$\mathrm{MAE} = \sum \frac{|P_i - O_i|}{n} \quad (3)$$

$$\mathrm{PBIAS} = \frac{\sum(P_i - O_i)}{\sum O_i} \cdot 100 \quad (4)$$

where P_i is the predicted precipitation obtained by applying the interpolation algorithms (interpolation subset, Fig. 5.2), O_i is the observed precipitation from the weather stations (validation subset, Fig. 5.), and *n* is the number of observations.

To select the best interpolation method, the Taylor diagram (Taylor, 2001) and the DISO (Hu et al., 2019) were determined. Specifically, Taylor diagram provides a statistical summary of the estimation performance of the 6 interpolation methods applied in the study, using: i) the Pearson correlation coefficient (r), ii) the RMSE and iii) the standard deviation (σ). The result of each method is graphically displayed as a point and the one closest (i.e. lower DISO value) to the reference point (observed field) indicates the best results. DISO quantitatively shows the overall performance of the different methods, as follows:

$$\mathrm{DISO} = \sqrt{(\mathrm{r}-1)^2 + (\mathrm{RB})^2 + (\mathrm{NRMSE})^2} \quad (5)$$

where *RB* and *NRMSE* are the Normalized Absolute Error and the Normalized RMSE, calculated dividing both the Absolute Error and the RMSE by the mean value of the observations, respectively.

Finally, to assess the accuracy of the ERA5-L reanalysis dataset compared to the best interpolation algorithm, a linear regression was conducted, determining: b; R^2; Root Mean Square Difference (RMSD (mm); Eq. (6)), Mean Absolute Difference (MAD (mm); Eq. (7)), and Percentage Difference (PDIFERENCE (%); Eq. (8)).

$$\mathrm{RMSD} = \sqrt{\frac{\sum(\mathrm{P_{ERA5L,i}} - \mathrm{P_{INT,i}})^2}{\mathrm{n}}} \quad (6)$$

$$\mathrm{MAD} = \sum \frac{|\mathrm{P_{ERA5L,i}} - \mathrm{P_{INT,i}}|}{\mathrm{n}} \quad (7)$$

$$\mathrm{PDIFFERENCE} = \frac{\sum(\mathrm{P_{ERA5L,i}} - \mathrm{P_{INT,i}})}{\sum \mathrm{P_{INT,i}}} \cdot 100 \quad (8)$$

where $P_{ERA5L,i}$ and $P_{INT,i}$ are the precipitation values predicted by ERA5-L and the best interpolation method, respectively.

Furthermore, the probability of detection (POD (%)), indicating the probability of ERA5-L to detect the precipitation event, was calculated for the rainy days, as follows:

$$\mathrm{POD} = \frac{\mathrm{hit}}{\mathrm{hit+miss}} \quad (9)$$

where *hit* refers to the precipitation events simultaneously detected by both ERA5-L and the interpolation algorithm; and *miss* includes only those detected by one of the approaches but not by the other.

The significance of the correlation between the estimation error

associated with the ERA5-L reanalysis and the variation in altitude was evaluated using the p value (<0.05). Specifically, the variation in altitude within each ERA5-L cell was calculated as its standard deviation.

5.3 Results

5.3.1 Evaluation of the interpolated precipitation data

5.3.1.1 Monthly analysis

As shown in Fig. 5.4 and Tab. 5.2, the best performances were obtained using deterministic interpolation methods (IDW, NeN, NN and RBF), with b and R^2 values ranging from 1.08 to 1.14 and from 0.64 to 0.75, respectively. The accuracy was also evaluated in terms of RMSE, MAE and PBIAS, with values ranging from 25.70 to 32.84 mm, 17.66 to 20.95 mm and 13.52 to 20.06% respectively. The geostatistical methods (i.e. OK, CoOK), instead, showed lower accuracy and precision, with b and R^2 values respectively of 0.76 and 0.52 - 0.53. RMSE and MAE values oscillated between 63.96 - 64.33 mm and 49.32 - 49.48 mm, respectively, whereas PBIAS were of 17.05 and 17.40%, respectively.

Tab. 5.2. Statistical performance of monthly precipitation (mm) estimated by the interpolation methods for the reference period 2002-2019.

Interpolation method	b	R^2	RMSE (mm)	MAE (mm)	PBIAS (%)	DISO
IDW	1.13	0.75	26.05	18.26	20.06	0.53
NeN	1.12	0.64	32.84	20.95	17.33	0.65
NN	1.11	0.74	25.70	17.66	17.03	0.51
RBF	1.08	0.71	26.34	17.90	13.52	0.52
OK	0.77	0.52	64.33	49.48	17.05	1.51
CoOK	0.77	0.53	63.96	49.32	17.40	1.51

From the Taylor diagram (Fig. 5.3) it was inferred that IDW, NN, and RBF were the interpolation methods with the smallest RMSE and σ and highest r. The DISO analysis (Tab. 5.2) confirmed also the similar behaviour of NN, RBF and IDW, with values of 0.51, 0.52 and 0.53, respectively.

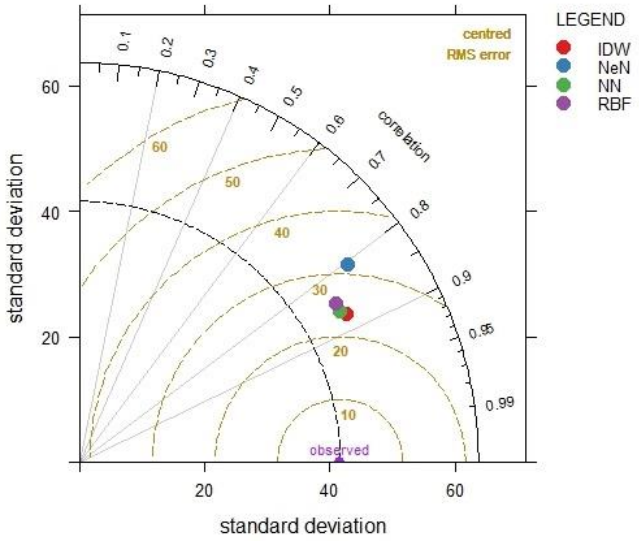

Fig. 5.3. Taylor diagram at monthly level of the deterministic interpolation methods applied at the study basin.

5.3.1.2 Seasonal analysis

In general, as shown in Fig. 5.4 and Tab. 5.3, for all seasons, the deterministic interpolation methods (IDW, NeN, NN and RBF) gave better results than the geostatistical ones (OK, CoOK).

In winter, b and R^2 values of IDW, NeN, NN and RBF ranged from 1.05 to 1.14 and 0.61 to 0.66, respectively. RBF was the most accurate, showing the lowest RMSE, MAE, and PBIAS values (26.47 mm, 18.68 mm, and 9.47%, respectively). Geostatistical approaches showed lower performance, with b and R^2 values of 0.81 and 0.22 – 0.23 respectively, and RMSE, MAE and PBIAS values ranging between 62.32 and 62.79 mm, 46.79 to 46.93 mm and 1.05 to 1.92%, respectively.

In spring, deterministic interpolators resulted in b values of 1.00 and R^2 varying from 0.59 to 0.68. RMSE, MAE and PBIAS values ranged from 15.50 to 19.41 mm, from 10.83 to 13.17 mm and from 6.28 to 7.93%. IDW resulted the most accurate in terms of RMSE (15.50 mm) and MAE (10.83 mm), but the worst among the deterministic interpolators in terms of PBIAS (7.93%). As in winter, OK and CoOK were less accurate than the deterministic approaches, resulting in precipitation overestimates of 19%, with R^2 of 0.66 – 0.68. Low accuracy was also indicated by the RMSE, MAE and PBIAS indices, with values of 63.04 – 63.33 mm, 47.65 – 47.86 mm and 92.82 – 92.97%, respectively.

In summer, all interpolation methods showed good accuracy with reference to values of b (1.06 – 1.13) and R^2 (0.40 – 0.83). However, RMSE, MAE and PBIAS were lower for the deterministic methods (20.67 – 29.96 mm, 14.79 – 19.37 mm and 16.60 – 23.48%, respectively) than for the geostatistical ones (65.48 – 66.18 mm, 53.60 – 54.02 mm, 87.64 – 88.54%, respectively). IDW showed the lowest RMSE and MAE values, but not for PBIAS (Tab. 5.4).

The worst performance for all methods was observed in

autumn. Specifically, IDW, NeN, NN and RBF showed b and R^2 between 1.12 and 1.18 and between 0.56 and 0.69. The low performance was detected also in terms of RMSE, MAE and PBIAS, with values ranging from 32.95 to 44.62 mm, from 23.34 to 29.10 mm and from 17.31 to 26.20%, respectively. Geostatistical interpolators showed b and R^2 values of 0.58 and 0.30 - 0.31 respectively, with RMSE, MAE and PBIAS values ranging from 68.05 to 68.18 mm, from 51.96 to 52.05 mm and from -21.51 to -21.23%, respectively.

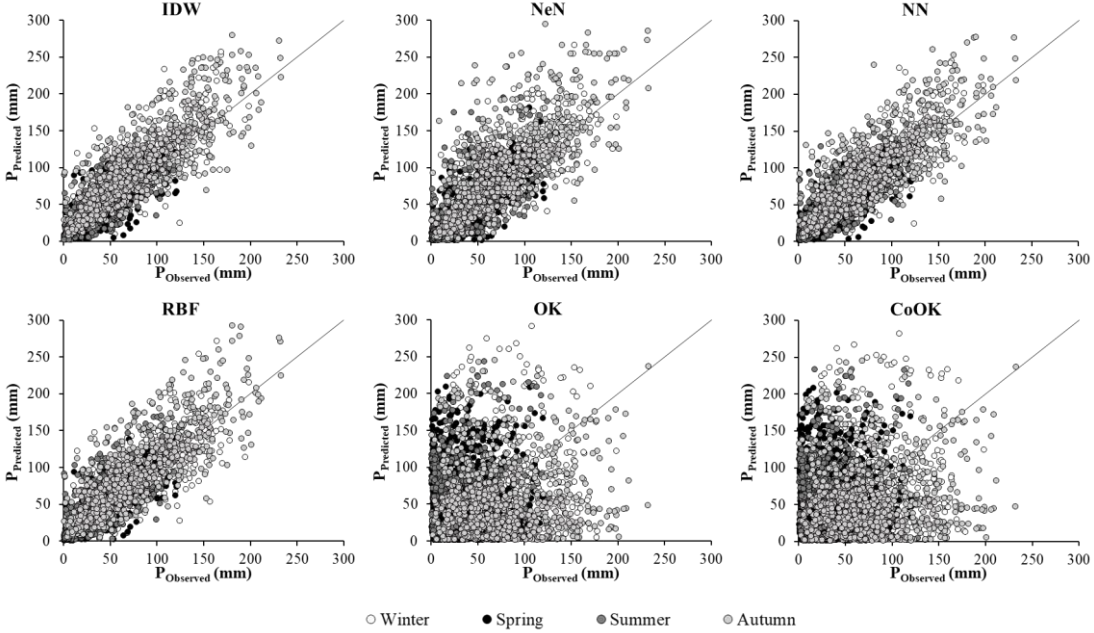

Fig. 5.4. Comparison of monthly precipitation (mm) estimated from the interpolation methods ($P_{Predicted}$) and measured in the ground-based meteorological stations ($P_{Observed}$), for the different seasons within the reference period 2002-2019 (number of observations: 803 for winter; 720 for spring; 550 for summer; 798 for autumn). The solid line is the 1:1 line.

Tab. 5.3. Statistics of the interpolation methods used to estimate precipitation for the reference period 2002-2019

Season	Interpolation method	b	R^2	RMSE (mm)	MAE (mm)	PBIAS (%)	DISO
Winter	IDW	1.14	0.66	28.79	20.72	20.26	0.49
	NeN	1.12	0.61	32.28	21.81	16.48	0.54
	NN	1.10	0.66	27.39	19.50	16.32	0.46
	RBF	1.05	0.64	26.47	18.68	9.47	0.44
	OK	0.81	0.22	62.79	46.93	1.05	1.24
	CoOK	0.81	0.23	62.32	46.79	1.92	1.23
Spring	IDW	1.00	0.68	15.50	10.83	7.93	0.50
	NeN	1.00	0.59	19.41	13.17	6.28	0.63
	NN	1.00	0.67	15.75	10.87	7.41	0.51
	RBF	1.00	0.67	16.23	11.16	5.52	0.52
	OK	1.19	0.66	63.33	47.86	92.82	2.35
	CoOK	1.19	0.68	63.04	47.65	92.97	2.35
Summer	IDW	1.08	0.59	20.67	14.79	19.09	0.63
	NeN	1.06	0.40	29.96	19.37	16.60	0.91
	NN	1.11	0.55	23.52	16.18	22.36	0.72
	RBF	1.13	0.52	26.34	17.87	23.48	0.80
	OK	1.13	0.79	66.18	54.02	88.54	2.28
	CoOK	1.12	0.83	65.48	53.60	87.64	2.27
Autumn	IDW	1.18	0.69	34.52	25.76	26.20	0.55
	NeN	1.17	0.56	44.62	29.10	24.05	0.69
	NN	1.14	0.68	33.37	23.81	20.86	0.51
	RBF	1.12	0.68	32.95	23.34	17.31	0.50
	OK	0.58	0.30	68.18	51.96	-21.51	1.31
	CoOK	0.58	0.31	68.05	52.05	-21.23	1.30

In Fig. 5.5, Taylor diagrams shows the performances of deterministic interpolation methods for all the seasons. These results confirmed what observed in terms of RMSE and MAE. For all seasons, deterministic interpolators presented lower DISO values (< 0.91) than the geostatistical ones (> 1.24). Additionally, deterministic interpolators' performance was dependent on the season of the year. Thus, in winter, spring and autumn, IDW, NN and RBF showed similar patterns in terms of DISO values, oscillating between 0.44 and 0.55. However, in summer, the differences among the deterministic approaches were more marked, with IDW presenting the lowest DISO value (i.e. 0.63). In all seasons, NeN was the deterministic interpolation method that provided the higher DISO values (0.54 – 0.91).

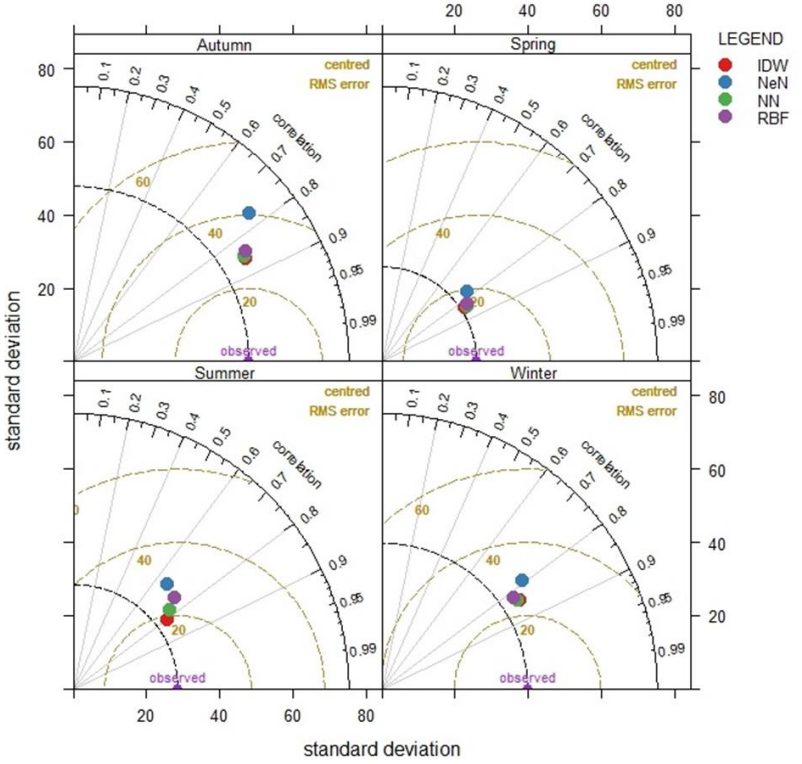

Fig. 5.5. Taylor diagram at seasonal level of the deterministic interpolation methods applied at the study area.

5.3.2 Estimation of spatially distributed precipitation data by combining interpolated and ERA5-Land dataset

5.3.2.1 Accuracy evaluation at monthly and seasonal level

As shown in Fig. 5.6 and Tab. 5.4, a low performance for simulating monthly precipitation was obtained at the study area by using ERA5-L when compared to non-corrected NN estimates, with b and R^2 values of 0.75 and 0.61, respectively. RMSD, MAD and PDIFFERENCE were of 35.29 mm, 22.30 mm and 13.66%, respectively. However, the precipitation events were detected in 94% of cases. On the other hand, the comparison of ERA5-L and NN estimates corrected by site-specific observations using the validation dataset, resulted in higher b, R^2 and POD values (0.93, 0.65 and 97%, respectively), whereas RMSD, MAD and PDIFFERENCE decreased to 26.46 mm, 17.88 mm and 1.17%, respectively.

Seasonally, as shown in Fig. 5.7 and Tab. 5.4, the best performance was observed in spring by comparing ERA5-L to the non-corrected IDW estimates, with b and R^2 values of 1.03 and 0.47, respectively. Additionally, RMSD, MAD and PDIFFERENCE values were 23.33 mm, 16.66 mm, and 25.53%, respectively, with a POD of 91%. Moderate underestimates were observed for the other seasons. In winter, the comparison between ERA5-L and non-corrected estimates from RBF, resulted in b and R^2 values of 0.79 and 0.62 respectively, with RMSD, MAD and PDIFFERENCE of 34.67 mm, 23.12 mm and -11.82%, respectively. Despite this low performance, the POD reached the 96%.

In summer, the comparison between ERA5-L and non-corrected IDW shows b and R^2 values of 0.79 and 0.61, respectively, with RMSD, MAD and PDIFFERENCE of 26.88 mm, 16.92 mm and -11.16%, with a POD value of 78%. In autumn, the comparison between ERA5-L and RBF is underperforming, with b and R^2 values

of 0.64 and 0.30, and RMSD, MAD and PDIFFERENCE of 55.34 mm, 38.23 mm and -23.18%, respectively. Despite the low accuracy in estimating precipitation values, the POD was 96%.

The statistical indicators generally improved when ERA5-L was compared to the corrected interpolation values obtaining higher values of b and R^2 and lower values of RMSD, MAD and PDIFFERENCE. In winter, comparing the climatic reanalysis with the corrected RBF estimates, the b and R^2 values were respectively 0.94 and 0.68, with RMSD, MAD and PDIFFERENCE of 25.73 mm, 18.38 mm and -2.34%, respectively, and a POD value of 100%. In summer, very high accuracy was observed comparing the climatic reanalysis with the corrected IDW estimates, with a b value of 1.02 and R^2 of 0.63. Additionally, the RMSD, MAD and PDIFFERENCE values were 23.80 mm, 15.16 mm and 2.44%, respectively; with a POD of 90%. In autumn, when comparing ERA5-L with the corrected RBF estimates, b and R^2 values of 0.82 and 0.54, respectively, were detected. The RMSD, MAD and PDIFFERENCE values were 37.88 mm, 27.22 mm, and -9.98%, respectively, with a POD of 100%. In spring, even if PDIFFERENCE increased from 25.23 to 35.20%, R^2 increased from 0.47 to 0.54 and RMSD and MAD values decreased from 23.33 to 23.15 mm and from 16.66 to 16.63 mm, respectively.

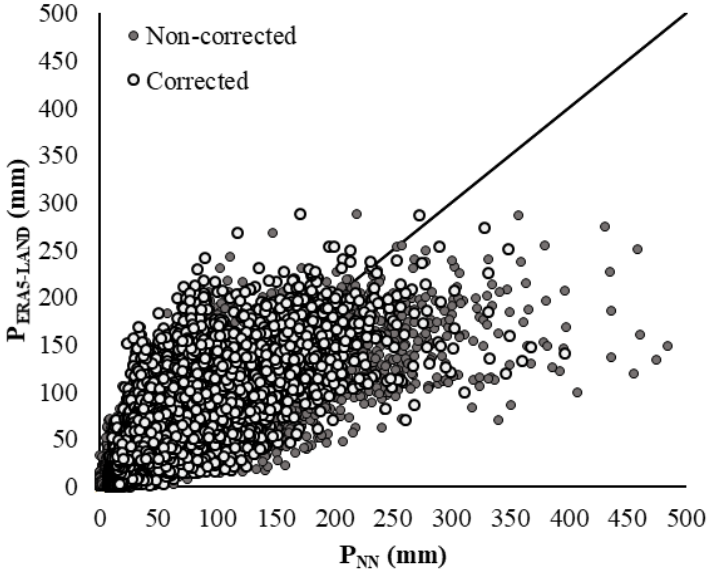

Fig. 5.6. Comparison of monthly precipitation (mm) from ERA5-L reanalysis ($P_{ERA5\text{-}LAND}$) and NN method (P_{NN}), for the reference period 2002-2019 (number of observations: 13284). Grey points refer to non-corrected interpolation estimates, whereas white points refer to corrected interpolation estimates. The solid line is the 1:1 line.

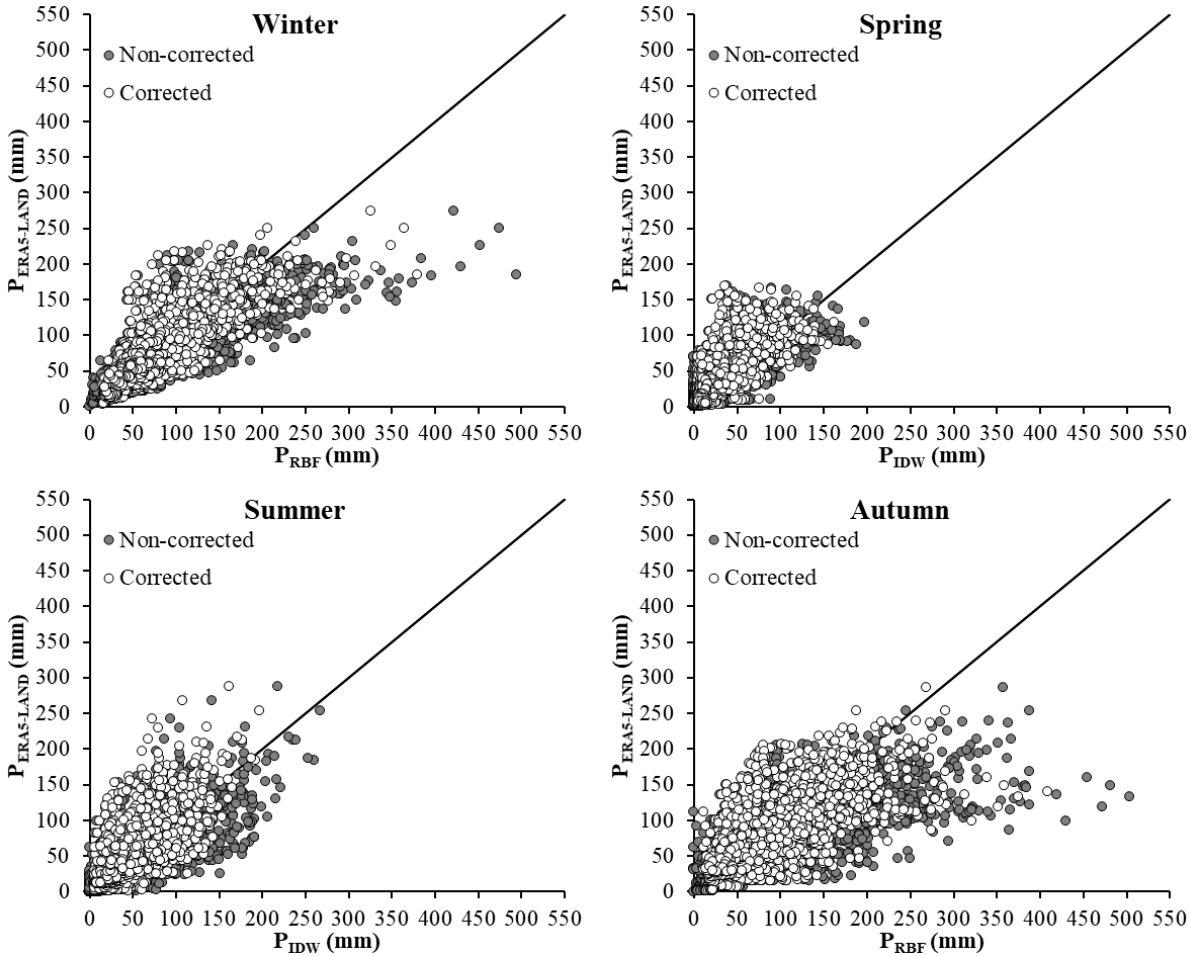

Fig. 5.7. Comparison of seasonal precipitation (mm) from ERA5-L reanalysis ($P_{ERA5\text{-}LAND}$) and the most accurate interpolation method for each season (RBF for winter and autumn – P_{RBF}; IDW for spring and summer – P_{IDW}), for the reference period 2002-2019 (number of observations: 3330 for winter; 3312 for spring; 3366 for summer; 3276 for autumn). Grey points refer to non-corrected interpolation estimates, whereas white points refer to corrected interpolation estimates. The solid line is the 1:1 line.

Tab 5.4. Main statistics of monthly and seasonal precipitation (mm) estimated by ERA5-L, in comparison with non-corrected and corrected interpolation data, for the reference period 2002-2019. In parenthesis, it is indicated the most accurate interpolation method used for performing the comparison in each temporal period.

		b	R^2	RMSD (mm)	MAD (mm)	PDIFFERENCE (%)	POD (%)
Non-corrected	Monthly (NN)	0.75	0.61	35.29	22.30	-13.66	94
	Winter (RBF)	0.79	0.62	34.67	23.12	-11.82	96
	Spring (IDW)	1.03	0.47	23.33	16.66	25.53	91
	Summer (IDW)	0.79	0.61	26.88	16.92	-11.16	78
	Autumn (RBF)	0.64	0.30	55.34	38.23	-23.18	96
Corrected	Monthly (NN)	0.93	0.65	26.46	17.88	1.17	97
	Winter (RBF)	0.94	0.68	25.73	18.38	-2.34	100
	Spring (IDW)	1.20	0.54	23.15	16.36	35.20	98
	Summer (IDW)	1.02	0.63	23.80	15.16	2.44	90
	Autumn (RBF)	0.82	0.54	37.88	27.22	-9.98	100

5.3.2.2 Spatial variability

Figs. 5.8 and 5.9 show the spatial distribution of RMSD associated with the ERA5-L reanalysis, during the reference period 2002-2019. A decrease in the RMSD was observed when the interpolation estimates, were corrected with local observations. Generally, the highest RMSD values were observed in the ERA5-L cells with higher variation in altitude, showing a significant direct correlation (p value < 0.05). In particular, the value of R^2 between the monthly RMSD and the variation in altitude was 0.52 (Fig. 5.10).

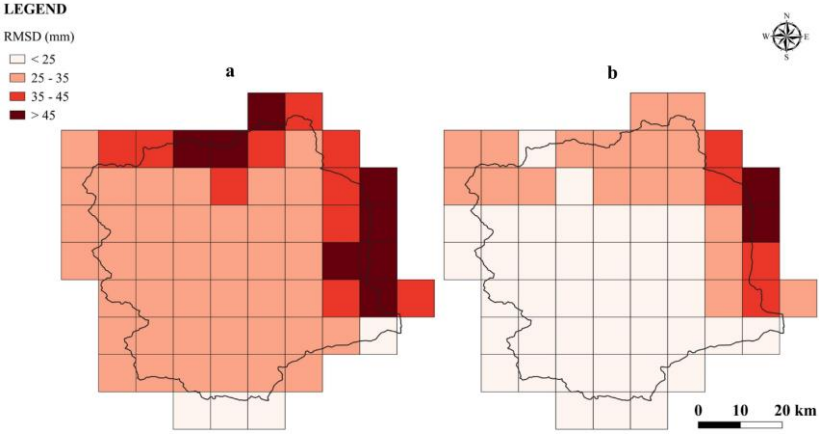

Fig. 5.8. Spatial distribution of RMSD (mm) over the study area at monthly level associated to ERA5-L reanalysis, by using (a) non-corrected and (b) corrected interpolated estimates (NN method), respectively.

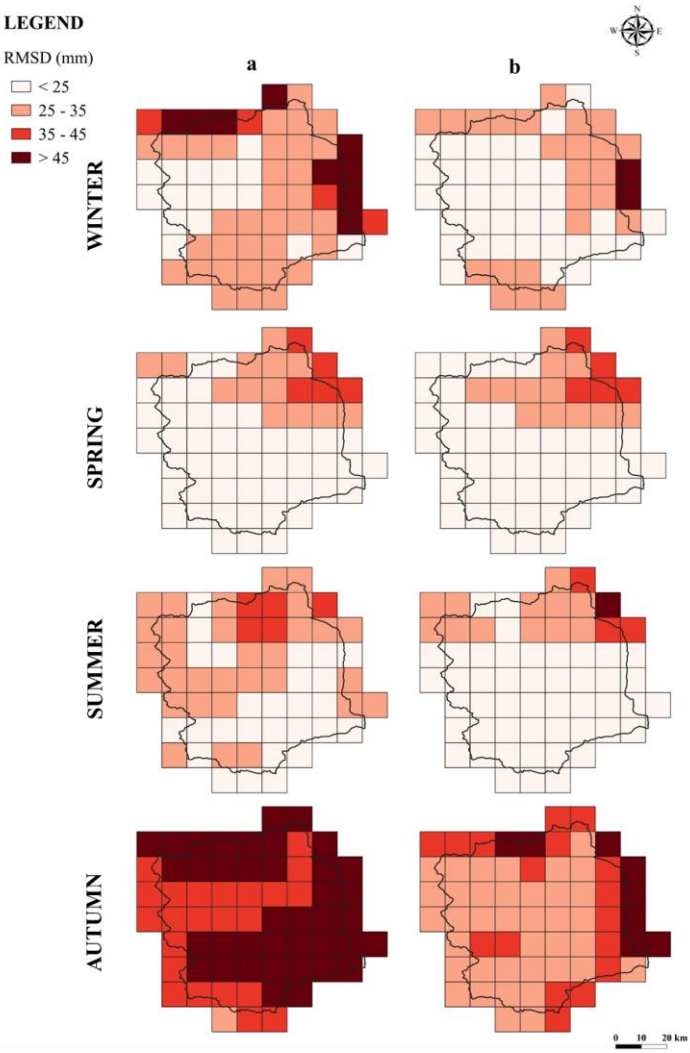

Fig. 5.9. Spatial distribution of RMSD (mm) over the study area at seasonal level, associated to ERA5-L reanalysis, by using (a) non-corrected and (b) corrected interpolated estimates (RBF method for winter and autumn, IDW method for spring and summer), respectively.

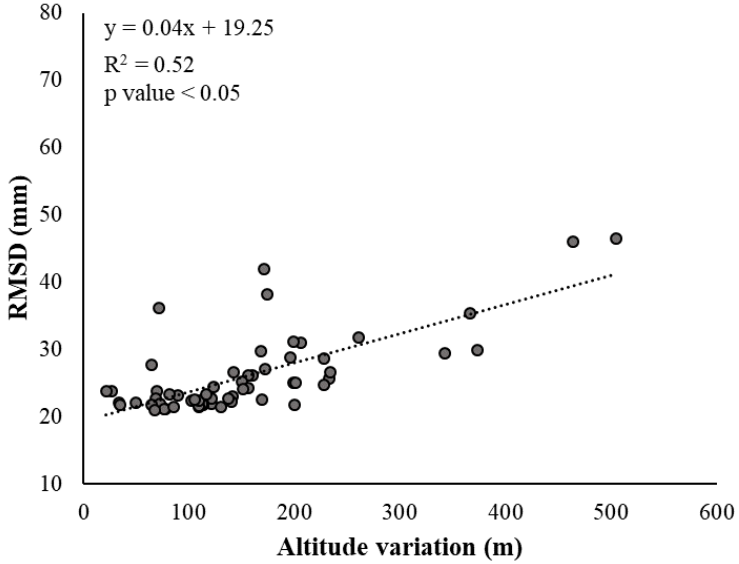

Fig. 5.10. Correlation between RSMD (mm) and altitude variation (m) within each ERA5-L cell, on a monthly basis within the study area.

5.4 Discussion

In this study, interpolated precipitation data showed that deterministic methods, including IDW, NN and RBF, and to a lesser extent NeN, provided most accurate results at monthly and seasonal level than geostatistical interpolators. The reliability of deterministic interpolators for estimating precipitation has been also proved by several authors. For example, Amorim Borges et al. (2016), compared IDW, RBF, OK, CoOK, detrended universal kriging (DUK), multiple linear regression (MReg), and residual interpolation using IDW (MRegIDW) and OK (MRegOK) for estimating annual and seasonal precipitation in Brazil. The results showed the good performance of the IDW, OK, MRegIDW and MRegOK methods at annual scale, with mean square error values of 3334.5, 3681.2, 2512.0 and 2956.9 mm, respectively, and r values of 0.95, 0.94, 0.97 and 0.96, respectively. Lyra et al. (2017) applied and compared 5 deterministic methods, including IDW, NN, NeN, RBF and triangulation with linear interpolation, to estimate monthly precipitation values in Brazil. The applied methods showed high accuracy with specific reference to RBF in terms of R^2 and RMSE. Amini et al. (2019) used 6 interpolation methods, namely IDW, NN, RBF, OK, universal kriging (UK), to map monthly basin-scale temperature and precipitation values in Iran. NN was found to be the most accurate interpolation method for predicting precipitation values, with a MAE value of 0.52 mm.

Contrarily to what obtained in the present study, Hurtado et al. (2021) found no performance differences between kriging and IDW methods. The goodness of these methods depends on several factors including the density of the data and the size and distribution of the sample (Hurtado et al., 2021). Indeed, as suggested by Li & Heap (2008), the performance of OK and CoOK improves with increasing sample size, as this affects the reliability of the semivariogram. In this

study, the size of the interpolation subset ranged from 13 to 23 rain gauges available over the different months, because of the different time intervals which may have influenced the performance of the geostatistical methods. Furthermore, and agreeing with the results obtained in our study, Ly et al. (2011) concluded that the use of altitude as a covariate in CoOK did not improve the accuracy of the interpolation for estimating precipitation values.

All of the previously cited researches used different statistics, including the RMSE, MAE and BIAS indices applied in this study, to select the most accurate interpolation method. As suggested by Zhou et al. (2021), it could result difficult to discriminate the performance using single metrics (Tabs 5.2 and 5.3). In fact, although IDW, NN and RBF have shown the greatest accuracies, it was difficult to establish the best interpolation method using these metrics separately because, each of them, showed better performance with reference to one index, but worse capabilities in the others. To overcome this limitation, alternative methodologies as the Taylor diagram or the DISO approach have been proposed to quantify the overall performance of the applied interpolators combining several statistical indicators (Hu et al., 2019; Amato et al., 2019; Antal et al. 2021; Kalmar et al., 2021). However, the similar statistical performances of deterministic methods used in our study made difficult to select a single interpolator as the most accurate, even using the Taylor diagram and DISO approach (Figs. 5.3 and 5.5 and Tabs. 5.2 and 5.3).

The reliability of the ECMWF reanalysis products for the estimation of spatially distributed precipitation data has been evaluated by different authors, at different spatial and temporal scales. Gleixner et al. (2020) assessed the overall performance of ERA5 for predicting temperature and precipitation in Africa. Comparing the climate reanalysis with the monthly grid observational datasets, r value of 0.97 and 0.96 were found for temperature and precipitation,

respectively. Jiang et al. (2021) evaluated the accuracy of ERA5 for precipitation estimates in different climate contexts on the Chinese mainland. The climate analysis was evaluated using grid precipitation products obtained by applying the IDW by means of pluviometric observations, on a daily basis. In general, their results showed r, RMSD and POD values of 0.78, 3.55 mm/d and 85%, respectively. In terms of spatial distribution, ERA5 showed higher values of RMSD in humid climate areas. Gao et al. (2020) compared the performance of several satellite and precipitation reanalysis products, including ERA5-L, against grid rain gauge data in southern China. Very low performance of ERA5-L was observed on a daily and hourly level. In fact, on a daily level, the values of r, RMSD and PDIFFERENCE were respectively 0.57, 13.41 mm/d and 26.16%. At hourly level, the values of r, RMSD and PDIFFERENCE were 0.22, 1.80 mm/h and 18.26%. In the proposed study, when comparing ERA5-L and the interpolated data in order to improve the precipitation estimates accuracy, underestimates on a monthly and seasonal level were observed, with the exception of the spring season (Figs 5.6 and 5.7, Tab. 5.4). Autumn and winter presented the largest errors (in terms of RMSD and MAD) due to the higher amount of precipitation occurred during these seasons in comparison to spring and summer. Other authors also detected this seasonal error trend using climate reanalysis data. Specifically, Jiao et al. (2021) and Izado et al. (2021) observed the highest errors during the rainy season whereas the lowest errors occurred in the dry season when evaluating the accuracy of ERA5 precipitation data in China and Iran, respectively.

Furthermore, the spatial distribution of the estimation error associated with ERA5-L was explored in the Simeto river basin, with the greatest RMSD values observed at high altitude areas (Figs. 5.8 and 5.9). Some studies showed that the accuracy of reanalysis data in mountainous terrain was generally lower than in flat terrain,

highlighting the altitudinal-dependence of reanalysis precipitation estimates (Liu et al., 2018; Li et al., 2020; Chen et al., 2021; Jiao et al., 2021). According to these authors, a significant positive correlation was observed in this study with the variation in altitude within each ERA5-L cell (Fig. 5.10). Moreover, the unevenly distribution of the error in the study area is also associated to the reference gridded product used for comparing the climate reanalysis. In this sense, according to Hofstra et al. (2008), such higher errors may be related to the lower meteorological station density at high altitude areas, which hinders the application of interpolation approaches in these regions; and to the use of interpolation methods that do not consider the effect of elevation.

However, the specific adjustments made on the interpolation dataset, with local observations, allowed the improvement of the performance (Tab. 5.4). In fact, the underestimates of precipitation have become milder in terms of b values and the accuracy was improved in terms of R^2, RMSD and MAD, as well as the probability of the climate reanalysis to detect the precipitation event in term of POD.

5.5 Conclusion

This research work evaluated the use of alternative data sources (including interpolated precipitation and reanalysis dataset) to improve the spatially distributed precipitation estimates at the Simeto river basin scale over an 18-year period, from 2002 to 2019. In particular, the performance of 6 interpolation methods (IDW, NeN, NN, RBF, OK, CoOK) was evaluated for the study area by linear regression analysis. The DISO indicator was used to select the best performing techniques. Subsequently, the best interpolation estimates were used as reference grid products to compare the reanalysis precipitation dataset, i.e. ERA5-L, for improving the accuracy of the

spatially distributed precipitation estimates at basin scale.

Overall, the results of the study confirmed a certain underestimation (25%) of precipitation. However, when local observations were used to correct the reference grid products, the performance has significantly improved and the underestimates have become milder (7%). In addition, the spatial distribution of the estimation error associated with ERA5-L suggested a dependence on the variation in altitude within each cell of ERA5-L.

In conclusion, the results of the study confirm the possibility of using interpolation methods and ERA5-L reanalysis as potential alternative data sources for the estimation of spatially distributed precipitation data at the basin scale, while specific adjustments are required to reduce site-specific uncertainties due to microclimatic conditions.

References

Amato, R., Steptoe, H., Buonomo, E., & Jones, R. (2019). High-resolution history: downscaling China's climate from the 20CRv2c reanalysis. *Journal of Applied Meteorology and Climatology*, *58*(10), 2141-2157.

Amini, M. A., Torkan, G., Eslamian, S., Zareian, M. J., & Adamowski, J. F. (2019). Analysis of deterministic and geostatistical interpolation techniques for mapping meteorological variables at large watershed scales. *Acta Geophysica*, *67*(1), 191-203.

Antal, A., Guerreiro, P. M., & Cheval, S. (2021). Comparison of spatial interpolation methods for estimating the precipitation distribution in Portugal. *Theoretical and Applied Climatology*, 1-14.

Beck, H. E., Van Dijk, A. I., Levizzani, V., Schellekens, J., Miralles, D. G., Martens, B., & Roo, A. D. (2017). MSWEP: 3-hourly 0.25 global gridded precipitation (1979–2015) by merging gauge, satellite, and reanalysis data. *Hydrology and Earth System Sciences*, *21*(1), 589-615.

Bengtsson, L. (1982). FGGE 4-dimensional data assimilation at ECMWF.

Buytaert, W., Celleri, R., Willems, P., De Bievre, B., & Wyseure, G. (2006). Spatial and temporal rainfall variability in mountainous areas: A case study from the south Ecuadorian Andes. *Journal of hydrology*, *329*(3-4), 413-421.

Chen, T., Ren, L., Yuan, F., Yang, X., Jiang, S., Tang, T., Liu, Y., Zhao, C., & Zhang, L. (2017). Comparison of spatial interpolation schemes for rainfall data and application in hydrological modeling. *Water*, *9*(5), 342.

Chen, Y., Sharma, S., Zhou, X., Yang, K., Li, X., Niu, X., Hu, X., & Khadka, N. (2021). Spatial performance of multiple reanalysis precipitation datasets on the southern slope of central Himalaya. *Atmospheric Research*, *250*, 105365.

de Amorim Borges, P., Franke, J., da Anunciação, Y. M. T., Weiss, H., & Bernhofer, C. (2016). Comparison of spatial interpolation methods for the estimation of precipitation distribution in Distrito Federal, Brazil. *Theoretical and applied climatology*, *123*(1-2), 335-348.

Dee, D.P., Uppala, S.M., Simmons, A.J., Berrisford, P., Poli, P., Kobayashi, S., Andrae, U., Balmaseda, M.A., Balsamo, G., Bauer, P., Bechtold, P., Beljaars, A.C.M., van de Berg, L., Bidlot, J., Bormann, N., Delsol, C., Dragani, R., Fuentes, M., Geer, A.J., Haimberger, L., Healy, S.B., Hersbach, H., Hólm, E.V., Isaksen, L., Kållberg, P., Köhler, M., Matricardi, M., McNally, A.P., Monge-Sanz, B.M., Morcrette, J.-J., Park, B.-K., Peubey, C., de Rosnay, P., Tavolato, C., Thépaut, J.-N., & Vitart, F. (2011). The ERA-Interim reanalysis: Configuration and performance of the data assimilation system. *Quarterly Journal of the royal meteorological society*, *137*(656), 553-597.

Di Piazza, A., Conti, F. L., Noto, L. V., Viola, F., & La Loggia, G. (2011). Comparative analysis of different techniques for spatial interpolation of rainfall data to create a serially complete monthly time series of precipitation for Sicily, Italy. *International Journal of Applied Earth Observation and Geoinformation*, *13*(3), 396-408.

Ebita, A., Kobayashi, S., Ota, Y., Moriya, M., Kumabe, R., Onogi, K., Harada, Y., Yasui, S., Miyaoka, K., Takahashi, K., Kamahori, H., Kobayashi, C., Endo, H., Soma, M., Oikawa, Y., & Ishimizu, T. (2011). The Japanese 55-year reanalysis "JRA-55": an interim report. *Sola*, *7*, 149-152.

Gao, Z., Huang, B., Ma, Z., Chen, X., Qiu, J., & Liu, D. (2020). Comprehensive comparisons of state-of-the-art gridded precipitation estimates for hydrological applications over southern China. *Remote Sensing*, *12*(23), 3997.

Gelaro, R., McCarty, W., Suárez, M. J., Todling, R., Molod, A., Takacs, L., Randles, C. A., Darmenov, A., Bosilovich, M. G., Reichle, R., Wargan, K., Coy, L., Cullather, R., Draper, C., Akella, S., Buchard, V., Conaty, A., da Silva, A. M., Gu, W., Kim, G., Koster, R., Lucchesi, R., Merkova, D., Nielsen, J. E., Partyka, G., Pawson, S., Putman, W., Rienecker, M., Schubert, S. D., Sienkiewicz, M., &

Zhao, B. (2017). The modern-era retrospective analysis for research and applications, version 2 (MERRA-2). *Journal of climate*, *30*(14), 5419-5454.

Gibson, J. K., Kallberg, P., Uppala, S., Hernandez, A., Nomura, A., & Serrano, E. (1997). ERA description. ECMWF Re-Analysis Project Report Series 1, ECMWF. *Reading, United Kingdom*, *74*.

Gleixner, S., Demissie, T., & Diro, G. T. (2020). Did ERA5 improve temperature and precipitation reanalysis over East Africa?. *Atmosphere*, *11*(9), 996.

Hamm, A., Arndt, A., Kolbe, C., Wang, X., Thies, B., Boyko, O., Reggiani, P., Scherer, D., Bendix, J., & Schneider, C. (2020). Intercomparison of gridded precipitation datasets over a sub-region of the Central Himalaya and the Southwestern Tibetan Plateau. *Water*, *12*(11), 3271.

Hersbach, H., Bell, B., Berrisford, P., Hirahara, S., Horányi, A., Muñoz-Sabater, J., Nicolas, J., Peubey, C., Radu, R., Schepers, D., Simmons, A., Soci, C., Abdalla, S., Abellan, X., Balsamo, G., Bechtold, P., Biavati, G., Bidlot, J., Bonavita, M., De Chiara, G., Dahlgren, P., Dee, D., Diamantakis, M., Dragani, R., Flemming, J., Forbes, R., Fuentes, M., Geer, A., Haimberger, L., Healy, S., Hogan, R.J., Hólm, E., Janisková, M., Keeley, S., Laloyaux, P., Lopez, P., Lupu, C., Radnoti, G., de Rosnay, P., Rozum, I., Vamborg, F., Villaume, S., & Thépaut, J.N. (2020). The ERA5 global reanalysis. *Quarterly Journal of the Royal Meteorological Society*, *146*(730), 1999-2049.

Hofstra, N., Haylock, M., New, M., Jones, P., & Frei, C. (2008). Comparison of six methods for the interpolation of daily, European climate data. *Journal of Geophysical Research: Atmospheres*, *113*(D21).

Hou, A. Y., Skofronick-Jackson, G., Kummerow, C. D., & Shepherd, J. M. (2008). Global precipitation measurement. In *Precipitation: Advances in measurement, estimation and prediction* (pp. 131-169). Springer, Berlin, Heidelberg.

Hu, Z., Chen, X., Zhou, Q., Chen, D., & Li, J. (2019). DISO: A rethink of Taylor diagram. *International Journal of Climatology*, *39*(5), 2825-2832.

Huffman, G. J., Bolvin, D. T., Nelkin, E. J., Wolff, D. B., Adler, R. F., Gu, G., Hong, Y., Bowman, K. P., & Stocker, E. F. (2007). The TRMM Multisatellite Precipitation Analysis (TMPA): Quasi-global, multiyear, combined-sensor precipitation estimates at fine scales. *Journal of hydrometeorology*, *8*(1), 38-55.

Hurtado, S. I., Zaninelli, P. G., Agosta, E. A., & Ricetti, L. (2021). Infilling methods for monthly precipitation records with poor station network density in Subtropical Argentina. *Atmospheric Research*, *254*, 105482.

Hutchinson, M. F., & Gessler, P. E. (1994). Splines—more than just a smooth interpolator. *Geoderma*, *62*(1-3), 45-67.

Isaaks, E. H., & Srivastava, M. R. (1989). *Applied geostatistics* (No. 551.72 ISA).

Izadi, N., Karakani, E. G., Saadatabadi, A. R., Shamsipour, A., Fattahi, E., & Habibi, M. (2021). Evaluation of ERA5 Precipitation Accuracy Based on Various Time Scales over Iran during 2000–2018. *Water*, *13*(18), 2538.

Jiang, Q., Li, W., Fan, Z., He, X., Sun, W., Chen, S., Wen, J., Gao, J., & Wang, J. (2021). Evaluation of the ERA5 reanalysis precipitation dataset over Chinese Mainland. *Journal of Hydrology*, *595*, 125660.

Jiao, D., Xu, N., Yang, F., & Xu, K. (2021). Evaluation of spatial-temporal variation performance of ERA5 precipitation data in China. *Scientific Reports*, *11*(1), 1-13.

Joyce, R. J., Janowiak, J. E., Arkin, P. A., & Xie, P. (2004). CMORPH: A method that produces global precipitation estimates from passive microwave and infrared data at high spatial and temporal resolution. *Journal of hydrometeorology*, *5*(3), 487-503.

Kalmár, T., Pieczka, I., & Pongrácz, R. (2021). A sensitivity analysis of the different setups of the RegCM4. 5 model for the Carpathian Region. *International Journal of Climatology*, *41*, E1180-E1201.

Kalnay, E., Kanamitsu, M., Kistler, R., Collins, W., Deaven, D., Gandin, L., Iredell, M., Saha, S., White, G., Woollen, J., Zhu, Y., Chelliah, M., Ebisuzaki, W., Higgins, W., Janowiak, J., Mo, K. C., Ropelewski, C., Wang, J., Leetmaa, A., Reynolds, R., Jenne, R., & Joseph, D. (1996). The NCEP/NCAR 40-year reanalysis project. *Bulletin of the American meteorological Society*, *77*(3), 437-472.

Kanamitsu, M., Ebisuzaki, W., Woollen, J., Yang, S. K., Hnilo, J. J., Fiorino, M., & Potter, G. L. (2002). Ncep–doe amip-ii reanalysis (r-2). *Bulletin of the American Meteorological Society*, *83*(11), 1631-1644.

Kidd, C. (2001). Satellite rainfall climatology: A review. *International Journal of Climatology: A Journal of the Royal Meteorological Society*, *21*(9), 1041-1066.

Kidd, C., & Huffman, G. (2011). Global precipitation measurement. *Meteorological Applications*, *18*(3), 334-353.

Kidd, C., & Levizzani, V. (2011). Status of satellite precipitation retrievals. *Hydrology and Earth System Sciences*, *15*(4), 1109-1116.

Kidd, C., Becker, A., Huffman, G. J., Muller, C. L., Joe, P., Skofronick-Jackson, G., & Kirschbaum, D. B. (2017). So, how much of the Earth's surface is covered by rain gauges?. *Bulletin of the American Meteorological Society*, *98*(1), 69-78.

Lentini, F., Carbone, S., Catalano, S., Grasso, M., & Monaco, C. (1991). Presentazione della carta geologica della Sicilia centro-orientale. *Memorie della Societa Geologica Italiana*, *47*, 145-156.

Lentini, F., Carbone, S., & Catalano, S. (1994). Main structural domains of the central Mediterranean region and their Neogene tectonic evolution. Bollettino di Geofisica Teorica ed Applicata, 36(141-44), 103-125.

Li, D., Yang, K., Tang, W., Li, X., Zhou, X., & Guo, D. (2020). Characterizing precipitation in high altitudes of the western Tibetan plateau with a focus on major glacier areas. *International Journal of Climatology*, *40*(12), 5114-5127.

Li, J., & Heap, A. D. (2008). A review of spatial interpolation methods for environmental scientists.

Liu, Z. (2015). Comparison of precipitation estimates between Version 7 3-hourly TRMM Multi-Satellite Precipitation Analysis (TMPA) near-real-time and research products. *Atmospheric Research*, *153*, 119-133.

Liu, Z., Liu, Y., Wang, S., Yang, X., Wang, L., Baig, M. H. A., Chi, W., & Wang, Z. (2018). Evaluation of spatial and temporal performances of ERA-Interim precipitation and temperature in mainland China. *Journal of Climate*, *31*(11), 4347-4365.

Liu, C. Y., Aryastana, P., Liu, G. R., & Huang, W. R. (2020). Assessment of satellite precipitation product estimates over Bali Island. *Atmospheric Research*, *244*, 105032.

Ly, S., Charles, C., & Degre, A. (2011). Geostatistical interpolation of daily rainfall at catchment scale: the use of several variogram models in the Ourthe and Ambleve catchments, Belgium. Hydrology and Earth System Sciences, 15(7), 2259-2274.

Ly, S., Charles, C., & Degré, A. (2013). Different methods for spatial interpolation of rainfall data for operational hydrology and hydrological modeling at watershed scale: a review. *Biotechnologie, Agronomie, Société et Environnement*, *17*(2), 392-406.

Lyra, G. B., Correia, T. P., de Oliveira-Júnior, J. F., & Zeri, M. (2018). Evaluation of methods of spatial interpolation for monthly rainfall data over the state of Rio de Janeiro, Brazil. *Theoretical and Applied Climatology*, *134*(3), 955-965.

Metheron, G. (1971). Theory of regionalized variables and its applications. *Cah. Centre Morrphol. Math.*, *5*, 211.

Mu, Y., Biggs, T., & Shen, S. S. (2021). Satellite-based precipitation estimates using a dense rain gauge network over the Southwestern Brazilian Amazon: Implication for identifying trends in dry season rainfall. *Atmospheric Research*, *261*, 105741.

Muñoz-Sabater, J., Dutra, E., Agustí-Panareda, A., Albergel, C., Arduini, G., Balsamo, G., Boussetta, S., Choulga, M., Harrigan, S., Hersbach, H., Martens, B., Miralles, D. G., Piles, M., Rodríguez-Fernández, N. J., Zsoter, E., Buontempo, C., & Thépaut, J.-N. L. (2021). ERA5-Land: A state-of-the-art global reanalysis dataset for land applications. *Earth System Science Data Discussions*, 1-50.

Nie, S., Luo, Y., Wu, T., Shi, X., & Wang, Z. (2015). A merging scheme for constructing daily precipitation analyses based on objective bias-correction and error estimation techniques. *Journal of Geophysical Research: Atmospheres*, *120*(17), 8671-8692.

Pellicone, G., Caloiero, T., Modica, G., & Guagliardi, I. (2018). Application of several spatial interpolation techniques to monthly rainfall data in the Calabria region (southern Italy). *International Journal of Climatology*, *38*(9), 3651-3666.

Pelosi, A., Terribile, F., D'Urso, G., & Chirico, G. B. (2020). Comparison of ERA5-Land and UERRA MESCAN-SURFEX reanalysis data with spatially interpolated weather observations for the regional assessment of reference evapotranspiration. *Water*, *12*(6), 1669.

Rienecker, M. M., Suarez, M. J., Gelaro, R., Todling, R., Bacmeister, J., Liu, E., Bosilovich, M. G., Schubert, S. D., Takacs, L., Kim, G., Bloom, S., Chen, J., Collins, D., Conaty, A., da Silva, A., Gu, W., Joiner, J., Koster, R. D., Lucchesi, R., Molod, A., Owens, T., Pawson, S., Pegion, P., Redder, C. R., Reichle, R., Robertson, F. R., Ruddick, A. G., Sienkiewicz, M., & Woollen, J. (2011). MERRA: NASA's modern-era retrospective analysis for research and applications. *Journal of climate*, *24*(14), 3624-3648.

Shepard, D. (1968, January). A two-dimensional interpolation function for irregularly-spaced data. In *Proceedings of the 1968 23rd ACM national conference* (pp. 517-524).

Sibson, R. (1981). A brief description of natural neighbour interpolation. *Interpreting multivariate data*.

Sorooshian, S., Hsu, K. L., Gao, X., Gupta, H. V., Imam, B., & Braithwaite, D. (2000). Evaluation of PERSIANN system satellite-based estimates of tropical rainfall. *Bulletin of the American Meteorological Society*, *81*(9), 2035-2046.

Srivastava, P. K., Han, D., Rico Ramirez, M. A., & Islam, T. (2013). Comparative assessment of evapotranspiration derived from NCEP and ECMWF global datasets through Weather Research and Forecasting model. *Atmospheric Science Letters*, *14*(2), 118-125.

Sun, Q., Miao, C., Duan, Q., Ashouri, H., Sorooshian, S., & Hsu, K. L. (2018). A review of global precipitation data sets: Data sources, estimation, and intercomparisons. *Reviews of Geophysics*, *56*(1), 79-107.

Taesombat, W., & Sriwongsitanon, N. (2009). Areal rainfall estimation using spatial interpolation techniques. *Science Asia*, *35*(3), 268-275.

Tapiador, F. J., Turk, F. J., Petersen, W., Hou, A. Y., García-Ortega, E., Machado, L. A., Angelis, C.F., Salio, P., Kidd, C., Huffman, G.J., & De Castro, M. (2012). Global precipitation measurement: Methods, datasets and applications. *Atmospheric Research*, *104*, 70-97.

Taylor, K. E. (2001). Summarizing multiple aspects of model performance in a single diagram. *Journal of Geophysical Research: Atmospheres*, *106*(D7), 7183-7192.

Tobler, W. R. (1970). A computer movie simulating urban growth in the Detroit region. *Economic geography*, *46*(sup1), 234-240.

Uppala, S.M., KÅllberg, P.W., Simmons, A.J., Andrae, U., Bechtold, V.D.C., Fiorino, M., Gibson, J.K., Haseler, J., Hernandez, A., Kelly, G.A., Li, X., Onogi, K., Saarinen, S., Sokka, N., Allan, R.P., Andersson, E., Arpe, K., Balmaseda, M.A., Beljaars, A.C.M., Berg, L.V.D., Bidlot, J., Bormann, N., Caires, S., Chevallier, F., Dethof, A., Dragosavac, M., Fisher, M., Fuentes, M., Hagemann, S., Hólm, E., Hoskins, B.J., Isaksen, L., Janssen, P.A.E.M., Jenne, R., Mcnally,

A.P., Mahfouf, J.-F., Morcrette, J.-J., Rayner, N.A., Saunders, R.W., Simon, P., Sterl, A., Trenberth, K.E., Untch, A., Vasiljevic, D., Viterbo, P., & Woollen, J. (2005). The ERA-40 re-analysis. *Quarterly Journal of the Royal Meteorological Society: A journal of the atmospheric sciences, applied meteorology and physical oceanography*, *131*(612), 2961-3012.

Ushio, T., Sasashige, K., Kubota, T., Shige, S., Okamoto, K. I., Aonashi, K., Inoue, T., Takahashi, N., Iguchi, T., Kachi, M., Oki, R., Morimoto, T., & Kawasaki, Z. I. (2009). A Kalman filter approach to the Global Satellite Mapping of Precipitation (GSMaP) from combined passive microwave and infrared radiometric data. *Journal of the Meteorological Society of Japan. Ser. II*, *87*, 137-151.

Wagner, P. D., Fiener, P., Wilken, F., Kumar, S., & Schneider, K. (2012). Comparison and evaluation of spatial interpolation schemes for daily rainfall in data scarce regions. *Journal of Hydrology*, *464*, 388-400.

Watson, D. F. (1981). Computing the n-dimensional Delaunay tessellation with application to Voronoi polytopes. *The computer journal*, *24*(2), 167-172.

Yilmaz, K. K., Hogue, T. S., Hsu, K. L., Sorooshian, S., Gupta, H. V., & Wagener, T. (2005). Intercomparison of rain gauge, radar, and satellite-based precipitation estimates with emphasis on hydrologic forecasting. *Journal of Hydrometeorology*, *6*(4), 497-517.

Zhou, Q., Chen, D., Hu, Z., & Chen, X. (2021). Decompositions of Taylor diagram and DISO performance criteria. *International Journal of Climatology*.

6 General conclusions

The herein Thesis explored a methodological approach based on the use of RS and alternative meteorological data sources with the aim of improving the sustainability of the irrigated agriculture at different spatial scales.

At the farm scale, a RS-based model (i.e. ArcDualK_c) was tested for determining reliable spatially distributed ET_c estimates, representing this variable a significant *proxy* for scheduling irrigation. A general good performance of ArcDualK_c was observed, even combining RS data and forecast meteorological data provided by COSMO. In fact, despite the inaccuracies of the non-hydrostatic limited-area atmospheric model, very slight overestimations in terms of ET_c and K_c were detected. Additionally, differences in terms of K_{cb} were found between the different irrigation strategies (DI strategies *versus* full irrigation) applied at the experimental site, highlighting the ability of ArcDualK_c in detecting site specific conditions.

A stand-alone optical RS approach for mapping at high resolution irrigated areas under different climate conditions was suggested. The proposed approach was based on the use of the unsupervised classification on NDVI time series and OPTRAM, with the main advantage of requiring only few input data (i.e. satellite images, rainfall values and soil parameters), without needing any reference cropland data. It was applied and tested firstly in Austria, under a Dfb climate, obtaining a good overall accuracy, and later in Italy, under Csa climate, where the results were compared with the Reclamation Consortium data, finding an overestimation of irrigated areas. However, future researches could enhance the methodology by studying in detail how crop types affect OPTRAM performances and how to solve the main uncertainties related to the soil parameters.

At the district scale, a deeper study on alternative meteorological data sources was carried out. Specifically, the

reliability of climate reanalysis (i.e. ERA5 datasets) was tested for predicting the main agrometeorological variables (R_s; T_{air}; RH; u_{10}; ET_0) into seven irrigation districts distributed under different climates and topography in Italy. The results showed accurate estimated of T_{air}, followed by RH, R_s, and u_{10} variables, resulting into reliable daily ET_0 estimates. Similar or slightly better performance was observed for ERA5 in comparison to ERA5-L in estimating RH, T_{air} and R_s; whereas the u_{10} and ET_0 performances were more consistent by ERA5 and ERA5-L, respectively. From a climate point of view, R_s, RH, u_{10} and ET_0 estimates resulted in higher and lower performance under Csa and Bks climate conditions, respectively, by both reanalysis datasets; conversely, a reverse pattern was obtained for T_{air} estimates provided by ERA5, being more accurate under Bsk. Intermediate performance was observed instead under Cfa climate zones.

Furthermore, being precipitation data fundamental for determining IWR, and being one of the most challenging variables to estimate, a specific focus on this variable was conducted. Specifically, the use of alternative data sources, including interpolation and ERA5-L reanalysis datasets, was evaluated for improving the spatially distributed precipitation estimates at the basin scale. Firstly, the performance of 6 interpolation methods (i.e. IDW, NeN, NN, RBF, OK, CoOK) was tested for the study area. The best interpolation estimates, obtained by applying NN at monthly level, RBF for winter and autumn seasons, and IDW for spring and summer seasons, were later used as reference grid products to compare the reanalysis precipitation dataset, for improving the accuracy of the spatially distributed precipitation estimates. In general, ERA-Land underestimated precipitation values, but when local observations were used to correct the reference grid products, the performance has significantly improved and the underestimates have become milder. Additionally, the spatial distribution of the estimation error associated with ERA5-L suggested a dependence on the variation in altitude

within each cell of ERA5-L.

On the basis of these results, the main findings of the Thesis are the following:

- ArcDualK_c is a reliable model that could be applied for improving precision irrigation and water resource management at farm scale even in a context of deficit irrigation strategies. Additionally, the combined use of this RS-based model with forecast meteorological data as alternative data source, allows to obtain ET_c estimates in advance, permitting the farmers to better plan the irrigation scheduling;
- The proposed approach based on the coupling of the unsupervised classification and OPTRAM represents a potential tool for irrigation purposes, being able to be used as an operational monitoring system by water management authorities for regular reporting of irrigated areas. It could allow the promotion of efficient water saving strategies, assisting EU member states for meeting their obligations under the WFD;
- ERA5 and ERA5-L climate reanalysis are promising datasets that could be used as alternative data sources at the district scale to estimate ET_0 and thus CWR for irrigation water management in different climate contexts, overcoming the limited availability of observed agrometeorological data in many areas;
- Interpolation methods and ERA5-L represent potential alternative data sources for the estimation of spatially distributed precipitation data at the basin scale, although specific adjustments are required to reduce site-specific uncertainties due to microclimatic conditions.

However, some limitations of the Thesis should be also considered, needing further investigations:

- Even if ArcDualK_c was already validated by the original authors, in the *Chapter 2* a comparison between the outputs of the model and measured values in terms of ET_c and K_c was omissed. Additionally, the model was run in standard conditions, without considering eventual crop water stress. Thus, an updating of the model with the introduction of the stress coefficient K_s for the application in non-standard conditions would increase its reliability;
- The results of the proposed approach for detecting the irrigated areas in the *Chapter 3* are not completely accurate. In this sense, the advanced studies already discussed in the Section 3.1 would provide additional relevance;
- A practical application of ERA5 datasets presented in the *Chapter 4* and *Chapter 5* for improving the irrigation management would be valuable.

A future work could be based on the integration of ArcDualK_c model with climate reanalysys for determining IWR at the district scale for those irrigated areas determined by applying the proposed method based on the use of OPTRAM. The validation of this approach could be done at farm scale considering several reference farms by comparing the outputs with the actual irrigation volumes supplied by the farmers. Later, the IWR obtained at district scale could be compared with the irrigation volumes provided by the Reclamation Consortium in order to evaluate the overall irrigation water management and eventually detect unauthorized water uses.

7 Other research and academic activities

7.1 Scientific contributions

7.1.1 Published articles

1. Vanella, D, Ramírez-Cuesta, J.M., **Longo-Minnolo, G.**, Longo, D., D'Emilio, A. Consoli, S. (2022). Identifying soil-plant interactions in a mixed-age orange orchard using electrical resistivity imaging. *Plant and Soil*, 1-17. https://doi.org/10.1007/s11104-022-05733-6
2. Ramírez-Cuesta, J. M., Consoli, S., Longo, D., **Longo-Minnolo, G.**, Intrigliolo, D. S., & Vanella, D. (2022). Influence of short-term surface temperature dynamics on tree orchards energy balance fluxes. *Precision Agriculture*, 1-19. https://doi.org/10.1007/s11119-022-09891-6
3. Vanella, D., Ferlito, F., Torrisi, B., Giuffrida, A., Pappalardo, S., Saitta, D., **Longo-Minnolo, G.**, & Consoli, S. (2021). Long-term monitoring of deficit irrigation regimes on citrus orchards in Sicily. *Journal of Agricultural Engineering*, *52*(4). https://doi.org/10.4081/jae.2021.1193
4. **Longo-Minnolo, G.**, Vanella, D., Consoli, S., Intrigliolo, D. S., & Ramírez-Cuesta, J. M. (2021). Combining Remote Sensing and Weather Forecast for Crop Evapotranspiration Estimation Under Different Irrigation Strategies. *Acta Horticulturae*, 1314, pp. 17–22. https://doi.org/10.17660/ActaHortic.2021.1314.3
5. Saitta, D., Consoli, S., Ferlito, F., Torrisi, B., Allegra, M., **Longo-Minnolo, G.**, Ramírez-Cuesta, J. M., & Vanella, D. (2021). Adaptation of citrus orchards to deficit irrigation strategies. *Agricultural Water Management*, *247*, 106734. https://doi.org/10.1016/j.agwat.2020.106734

6. Vanella, D., Ramírez-Cuesta, J. M., Sacco, A., **Longo-Minnolo, G.**, Cirelli, G. L., & Consoli, S. (2021). Electrical resistivity imaging for monitoring soil water motion patterns under different drip irrigation scenarios. *Irrigation Science*, *39*(1), 145-157. https://doi.org/10.1007/s00271-020-00699-8
7. Vanella, D., Intrigliolo, D. S., Consoli, S., **Longo-Minnolo, G.**, Lizzio, G., Dumitrache, R. C., Mateescu, E., Deelstra, J., & Ramírez-Cuesta, J. M. (2020). Comparing the use of past and forecast weather data for estimating reference evapotranspiration. *Agricultural and Forest Meteorology*, *295*, 108196. https://doi.org/10.1016/j.agrformet.2020.108196
8. Saitta, D., Vanella, D., Ramírez-Cuesta, J. M., **Longo-Minnolo, G.**, Ferlito, F., & Consoli, S. (2020). Comparison of orange orchard evapotranspiration by eddy covariance, sap flow, and FAO-56 methods under different irrigation strategies. *Journal of Irrigation and Drainage Engineering*, *146*(7), 05020002. https://doi.org/10.1061/(ASCE)IR.1943-4774.0001479

7.1.2 Conference proceedings

1. **Longo-Minnolo, G.**, Deissenberger, F., Consoli, S., Vanella, D., Ramírez-Cuesta, J.M., Vuolo, F. (2022). Optical remote sensing for supporting irrigation management under different climate conditions. BIOSYSTEMS ENGINEERING TOWARDS THE GREEN DEAL, AIIA International Conference, 19-22 September 2022, Palermo;
2. Pappalardo, S., Chiaradia, A. E., **Longo-Minnolo, G.**, Vanella, D., Consoli, S. (2022). Monitoring and predicting irrigation requirements of tree crops in Eastern Sicily as a tool for sustainability. BIOSYSTEMS ENGINEERING TOWARDS THE GREEN DEAL, AIIA International Conference, 19-22 September 2022, Palermo;

3. Vanella, D., **Longo-Minnolo, G.**, Castagna, A., Quarta, R., Ippolito, M., Comegna, A., Belfiore, O.R. (2022). Estimating reference evapotranspiration by ERA5 products under different irrigation districts. BIOSYSTEMS ENGINEERING TOWARDS THE GREEN DEAL, AIIA International Conference, 19-22 September 2022, Palermo;
4. Belfiore, O.R., Castagna, A., **Longo-Minnolo, G.**, Ippolito, M., Bavieri, A., Comegna, A. (2022). Monitoring of irrigation water use in Italy by using IRRISAT methodology: the INCIPIT project. BIOSYSTEMS ENGINEERING TOWARDS THE GREEN DEAL, AIIA International Conference, 19-22 September 2022, Palermo;
5. Vanella, D., **Longo-Minnolo, G.**, Ramírez-Cuesta, J.M., Longo, D., D'Emilio, A., Consoli, S. (2022). Characterizing soil-plant interactions under heterogeneous micro-irrigated citrus orchards. https://doi.org/10.5194/egusphere-egu22-9931, EGU General Assembly, 23-27 May 2022, Vienna;
6. **Longo-Minnolo, G.**, Consoli, S., Vanella, D., S., Ramírez-Cuesta, J. M. (2021). Evaluation of climate reanalysis as potential data source for estimating reference evapotranspiration at national scale. 2nd Joint Meeting of Agriculture-oriented PhD Programs, 11-15 October 2021, Giovinazzo;
7. **Longo-Minnolo, G.**, Vanella, D., Consoli, S., Pappalardo, S., Ramírez-Cuesta, J. M. (2021). Accuracy evaluation of alternative precipitation data sources at basin scale. AISSA#under40 Conference, 1-2 July 2021, Sassari;
8. **Longo-Minnolo, G.**, Consoli, S., Vanella, D., Ramírez-Cuesta, J. M. (2020). Remote sensing for supporting the sustainable irrigation management under semi-arid conditions. 2nd Joint Meeting of Agriculture-oriented PhD Programs,14-16 September 2020, Catania;

7.1.3 Books

1. Analisi del regime pluviometrico del bacino del Fiume Simeto. A cura di: Simona Consoli, Daniela Vanella, Giuseppe Longo Minnolo, Salvatore Barbagallo. QUADERNI CSEI Catania III serie vol. 20. ISSN 2038-5854. Catania, Ottobre 2021.

7.2 Visiting research stays

A six months' period abroad was spent at the Institute of Geomatics of the University of Natural Resources and Life Sciences, Vienna (Austria), from 25 October 2021 to 30 April 2022, under the supervision of Dr. Francesco Vuolo. During this period, activities finalized to develop and test a stand-alone optical RS method were carried out in order to detect the irrigated areas under different climate contexts. Specifically, a deeper study on the Optical Trapezoid Model (OPTRAM) was conducted. After an initial phase of bibliographic review and data collection, OPTRAM was applied for calculating the soil water content of a test site and tested by using sensors measurements. Later, the OPTRAM was used as a tool for detecting the irrigation events and mapping the irrigated areas. This study was carried out for two test sites: the Marchfeld region (Austria) within the irrigation season 2021 and the irrigation district "Quota 102.50" in Sicily (Italy), within the irrigation seasons 2019-20. The results obtained from this training period abroad were summarized into two scientific contributions:

- Longo-Minnolo, G., Deissenberger, F., Consoli, S., Vanella, D., Ramírez-Cuesta, J.M., Vuolo, F. (2022). Optical remote sensing for supporting irrigation management under different climate conditions. BIOSYSTEMS ENGINEERING TOWARDS THE GREEN DEAL, AIIA International Conference, 19-22 September 2022, Palermo;
- Longo-Minnolo, G., Consoli, S., Vanella, D., Ramírez-Cuesta, J. M., Greimeister-Pfeil, I., Neuwirth, M., & Vuolo, F. (2022). A stand-alone remote sensing approach based on the use of the Optical Trapezoid Model for detecting the irrigated areas. Under review on *Agricultural Water Management*.

7.3 Participation at research projects

1. INCIPIT - INtegrated Computer modelling and monitoring for Irrigation Planning in Italy (homepage: https://www.principit2017.it/). The objective of the project is to develop and test a methodological framework for supporting the control and planning of irrigation water uses at different spatial scales and under different conditions of hydraulic and meteorological data availability;
2. HANDYWATER - Handy tools for sustainable irrigation management in Mediterranean crops. The objective of the project is to apply sustainable water management methodologies (e.g. deficit irrigation strategies), for the main crops in the Mediterranean area. Moreover, soil conservation techniques will be evaluated for the improving of hydrological soil properties:
3. WATER4AGRIFOOD - *Miglioramento delle produzioni agroalimentari mediterranee in condizioni di carenza di risorse idriche.* The project aims to find innovative solutions for improving the water use efficiency in agriculture.

7.4 Scientific collaborations

1. Collaborator at the CSEI Catania, Centre for the Study of Applied Economics to Engineering, within the project entitled "H2Olivo - Gestione sostenibile di impianti di ulivo attraverso tecniche di irrigazione deficitaria e uso di acque reflue". The project aims to the sustainable management of olive orchards through deficit irrigation strategies and wastewater use.
2. Collaborator at the CRISAM, Research Center for the Sustainable Development of the Mediterranean Area, within the project entitled "Progetto DOPCILIETNA, sottomisura 16.1 PSR Sicilia 2014-2020". The collaboration concerns the research activity for the irrigation of cherry trees.

3. Collaborator at the CSEI Catania, Centre for the Study of Applied Economics to Engineering, within the assignment entitled "Richiesta della concessione di grande derivazione ad uso irriguo delle fluenze del fiume Simeto a Barca di Paternò". The collaboration concerns the hydrological and hydraulic analysis of the basin under study to catch water for agricultural irrigation purposes.
4. Collaborator at the CSEI Catania, Centre for the Study of Applied Economics to Engineering, within the assignment entitled "Servizio di monitoraggio pluviometrico ed analisi di eventi di massima intensità di precipitazione presso le aree di cantiere del raddoppio della linea ferroviaria Bicocca-Catenanuova". The collaboration concerns the precipitation data analysis and monitoring of the study area and the detection of extreme events.
5. Collaborator at the CSEI Catania, Centre for the Study of Applied Economics to Engineering, within the assignment entitled "Servizio di analisi delle immagini multispettrali e database geografico dell'uso del suolo con caratterizzazione delle superfici agricole nell'intorno della costruenda ferrovia in località Bicocca-Catenanuova". The collaboration concerns the analysis of satellite images for the environmental monitoring of the study area.

7.5 Institutional activities

7.5.1 Scientific committee

1. Member of the scientific committee of the 3rd Joint Meeting of Agriculture-oriented PhD Programs UniCT, UniFG, UniUd, 11-15 October 2021, Giovinazzo.
2. Member of the scientific committee of the 2022 IEEE International Workshop on Metrology for Agriculture and Forestry, 3-5 November, Perugia.

7.5.2 Peer review of scientific articles

1. Reviewer (2 reviews) for the Journal of Hydrology: Regional Studies.

7.5.3 Given seminars

1. Consoli, S., Vanella, D., **Longo-Minnolo G.**, (2022). "Il ruolo del telerilevamento per il monitoraggio e la salvaguardia dell'ambiente". Contribution within the seminar "Il valore dell'ambiente" organized by the CSEI Catania and the Department of Agricultural, Food and Environment Science (Di3A) of the University of Catania. 31 May 2022, Catania.
2. **Longo-Minnolo G.** (2022). "Classificazione automatica delle immagini satellitari". Seminar for the students of the bachelor degree course in "Land and landscape planning and protection" at the Department of Agricultural, Food and Environment Science (Di3A), University of Catania, Italy. 23 May 2022, Catania.
3. **Longo-Minnolo G.** (2022). "Introduzione al telerilevamento". Seminar for the students of the bachelor degree course in "Land and landscape planning and protection" at the Department of Agricultural, Food and Environment Science (Di3A), University of Catania, Italy. 11 May 2022, Catania.

4. **Longo-Minnolo G.**, Ramírez-Cuesta, J. M. (2021). "Il telerilevamento a supporto dell'agricoltura irrigua". Seminar organized by the CSEI Catania and the Department of Agricultural, Food and Environment Science (Di3A) of the University of Catania. 11 May 2021, Catania.

7.5.4 Educational activities

1. Teaching support in "Hydrology and Water Resources Management" and "Basin Hydrology", within the bachelor degree course in "Land and landscape planning and protection" at the Department of Agricultural, Food and Environment Science (Di3A), University of Catania, Italy. During the courses, practical lessons of Geographic Information Systems, online data sources, hydrological analysis, spatial interpolation of meteorological data and remote sensing were given.

7.5.5 Thesis tutoring

1. Bachelor's degree in "Land and landscape planning and protection" at the Department of Agricultural, Food and Environment Science (Di3A), University of Catania, Italy. "Metodi di analisi pluviometrica per il monitoraggio del territorio" (April 2021). Student: Biagio Musarra. Tutor: Prof. Simona Consoli. Co-Tutor: Dott. Giuseppe Longo Minnolo.
2. Bachelor's degree in "Agricultural Science and Technology" at the Department of Agricultural, Food and Environment Science (Di3A), University of Catania, Italy. "Prospettive sull'uso del telerilevamento e dei SIT per la gestione delle risorse idriche in agricoltura" (November 2020). Student: Gaetano Florio. Tutor: Prof. Simona Consoli. Co-Tutor: Dott. Giuseppe Longo Minnolo.

7.6 Attendance to courses

1. Advanced methods in Remote Sensing, organised by the Institute of Geomatics - University of Natural Resources and Life Sciences, Vienna, 17 January - 04 February 2022 (duration 75 hrs);
2. *Analisi statistica multivariata*, organised by the PhD course (University of Catania), 27 September - 1 October 2021 (duration 40 hrs);
3. Advanced English Course – Centro Linguistico d'Ateneo organised by the University of Catania, 16 February - 22 April 2021 (duration 40 hrs);
4. CAD, GIS and Participatory Mapping course, organised by the PhD course (University of Catania), 8-18 February 2021 (duration 45 hrs);
5. *Corso di Python*, organised by JobFormazione, 20 January - 15 March 2021 (duration 40 hrs);
6. A Guide to a Succesful PhD Thesis: Connecting Structure, Research Methods and Management, organised by the University of Catania, 29 June - 03 July 2020 (duration 35 hrs);
7. Introduction to optical remote sensing: basic concepts and applications, organised by the CSEI Catania and the University of Catania,17 April 2020 (duration 2 hrs);
8. Biometry and data analysis course, organised by the PhD course (University of Catania) 18-22 November 2019 (duration 40 hrs).

Supplementary material

Tab. S3.1. Sentinel-2 images used in the study for the two test sites. For each image, the type of Sentinel satellite (A or B), the daily rainfall value (mm) and the cumulated rainfall value (mm) in the previous 10 days are reported. The dry dates selected during the irrigation season for applying the OPTRAM are also indicated with X.

MACHFELD CROPLAND REGION - 2021																																		
Acquisition date	1-Feb	24-Feb	26-Feb	26-Mar	31-Mar	12-Apr	10-May	4-Jun	16-Jun	19-Jun	24-Jun	29-Jun	6-Jul	16-Jul	21-Jul	24-Jul	26-Jul	29-Jul	3-Aug	10-Aug	13-Aug	15-Aug	4-Sep	9-Sep	2-Oct	4-Oct	14-Oct	17-Oct	24-Oct	6-Nov	23-Nov				
Satellite	S2B	S2B	S2A	S2B	S2A	S2B	S2A	S2B	S2A	S2A	S2B	S2A	S2A	S2A	S2B	S2B	S2A	S2A	S2B	S2B	S2B	S2A	S2A	S2B	S2B	S2A	S2A	S2A	S2A	S2A	S2A				
Rainfall (mm)	0.30	0.00	2.68	0.00	0.00	6.60	0.00	0.00	0.00	0.00	1.33	0.00	0.00	2.23	0.00	14.25	0.00	0.00	0.00	1.13	0.00	0.00	0.00	0.00	0.00	0.00	0.00	0.00	0.00	0.00	0.00				
Cumulated rainfall (mm)	16.35	4.15	3.65	4.33	0.35	9.10	6.63	1.63	3.25	2.90	1.33	2.00	2.28	17.65	42.73	46.95	51.05	24.35	31.73	45.93	35.00	13.98	8.53	3.23	12.53	12.53	19.85	2.03	0.00	17.25	0.98				
Selected dry dates								X	X	X			X																						
IRRIGATION DISTRICT QUOTA 102,50 - 2019																																			
Acquisition date	8-Jan	18-Jan	20-Jan	25-Jan	7-Feb	19-Feb	22-Feb	4-Mar	6-Mar	9-Mar	16-Mar	19-Mar	24-Mar	26-Mar	31-Mar	18-Apr	20-Apr	30-Apr	5-May	8-May	10-May	7-Jun	9-Jun	14-Jun	19-Jun	2-Jul	4-Jul	7-Jul	9-Jul	12-Jul	14-Jul	17-Jul	19-Jul	22-Jul	
Satellite	S2A	S2A	S2B	S2A	S2A	S2B	S2B	S2B	S2A	S2A	S2A	S2A	S2B	S2A	S2B	S2A	S2B	S2B	S2A	S2A	S2B	S2A	S2B	S2A	S2B	S2B	S2A	S2A	S2B	S2B	S2A	S2A	S2B	S2B	
Rainfall (mm)	0.20	0.30	0.70	0.15	0.00	0.05	0.00	0.00	0.00	0.05	0.00	0.00	0.05	0.15	0.00	0.00	0.15	0.05	0.05	0.05	0.00	0.00	0.00	0.10	0.00	0.00	0.00	0.00	0.00	0.00	0.00	0.00	0.00	0.00	
Cumulated rainfall (mm)	4.40	9.10	8.35	11.15	59.65	7.75	7.50	6.80	1.95	0.55	2.40	2.45	0.70	0.85	4.55	10.85	11.00	2.00	1.20	1.10	0.90	3.65	3.65	0.15	0.20	0.00	0.00	0.00	0.00	0.05	0.05	19.90	19.90	19.85	
Selected dry dates																											X		X						
Acquisition date	24-Jul	27-Jul	29-Jul	1-Aug	3-Aug	6-Aug	8-Aug	11-Aug	13-Aug	16-Aug	18-Aug	26-Aug	28-Aug	31-Aug	15-Sep	17-Sep	25-Sep	30-Sep	2-Oct	5-Oct	17-Oct	20-Oct	30-Oct	4-Nov	29-Nov	1-Dec	14-Dec	16-Dec	24-Dec	26-Dec	31-Dec				
Satellite	S2A	S2A	S2B	S2B	S2A	S2A	S2B	S2B	S2A	S2A	S2B	S2A	S2B	S2B	S2A	S2B	S2A	S2B	S2A	S2A	S2B	S2B	S2B	S2A	S2B	S2A	S2A	S2B	S2A	S2B	S2A				
Rainfall (mm)	0.00	0.00	0.00	0.00	0.00	0.00	0.00	0.00	0.00	0.00	0.00	0.00	3.40	0.20	0.00	0.00	0.00	0.00	3.10	0.00	0.00	0.00	3.85	9.00	0.00	0.00	0.80	0.00	0.20	0.00	0.00				
Cumulated rainfall (mm)	19.85	0.00	0.00	0.00	0.00	0.00	0.00	0.00	0.00	0.00	0.00	0.00	3.40	3.60	40.20	40.15	11.20	0.15	3.10	5.80	38.25	5.05	85.75	73.70	37.05	36.90	10.35	5.90	2.90	2.90	5.15				
Selected dry dates			X		X		X		X		X																								
IRRIGATION DISTRICT QUOTA 102,50 - 2020																																			
Acquisition date	3-Jan	10-Jan	15-Jan	18-Jan	30-Jan	7-Feb	9-Feb	12-Feb	17-Feb	22-Feb	27-Feb	13-Mar	20-Mar	9-Apr	12-Apr	16-Apr	9-May	12-May	24-May	1-Jun	8-Jun	11-Jun	18-Jun	21-Jun	28-Jun	1-Jul	3-Jul	8-Jul	11-Jul	13-Jul	23-Jul	28-Jul	31-Jul	2-Aug	
Satellite	S2A	S2A	S2B	S2B	S2A	S2B	S2A	S2A	S2B	S2A	S2B	S2A	S2A	S2A	S2A	S2B	S2A	S2A	S2B	S2A	S2A	S2A	S2A	S2A	S2A	S2A	S2B	S2A	S2A	S2B	S2B	S2A	S2A	S2B	
Rainfall (mm)	0.00	0.00	0.00	0.00	0.00	0.00	0.00	0.00	0.00	0.00	0.00	0.00	0.00	0.05	0.00	0.00	0.00	0.00	0.00	0.05	0.20	0.00	0.00	0.00	0.00	0.00	0.00	0.00	0.00	0.45	0.00	0.00	0.00	0.00	
Cumulated rainfall (mm)	4.15	0.45	2.05	2.05	8.35	4.80	4.80	4.80	0.00	0.00	0.05	6.15	0.35	2.60	1.20	0.20	0.00	0.05	0.95	4.25	10.45	9.00	2.80	0.05	0.05	0.00	0.00	1.25	1.25	1.70	41.25	4.50	0.00	0.00	
Selected dry dates																									X		X							X	
Acquisition date	5-Aug	10-Aug	12-Aug	15-Aug	17-Aug	20-Aug	22-Aug	25-Aug	27-Aug	30-Aug	1-Sep	4-Sep	9-Sep	19-Sep	24-Sep	9-Oct	11-Oct	21-Oct	29-Oct	31-Oct	8-Nov	10-Nov	15-Nov	20-Nov	5-Dec	10-Dec	15-Dec	23-Dec							
Satellite	S2B	S2A	S2B	S2B	S2A	S2A	S2B	S2B	S2A	S2A	S2B	S2B	S2A	S2A	S2B	S2A	S2B	S2B	S2A	S2B	S2A	S2B	S2A	S2B	S2A	S2B	S2A	S2B							
Rainfall (mm)	0.00	0.00	0.05	0.00	0.00	0.00	0.00	0.00	0.00	0.00	0.00	0.00	0.00	0.00	0.00	0.00	0.00	0.05	0.00	0.00	0.00	0.00	0.00	0.05	0.00	0.35	0.00	0.05							
Cumulated rainfall (mm)	1.10	1.10	1.15	0.05	0.05	0.05	0.00	0.00	0.00	0.00	0.00	0.10	1.35	73.70	46.85	0.30	0.30	21.55	8.85	8.70	0.00	0.00	0.00	23.10	50.50	39.15	25.55	44.80							
Selected dry dates					X		X		X		X																								

Tab. S3.2. OPTRAM parameters (i_d, s_d, i_w, s_w) obtained for the potentially irrigated clusters at Marchfeld Cropland for the irrigation season 2021.

CLUSTER	Dry edge		Wet edge	
	i_d	s_d	i_w	s_w
4	0.00	1.79	2.20	3.79
8	0.00	1.79	2.50	3.16
9	0.00	1.58	1.00	5.79
12	0.10	1.47	0.20	8.21
13	0.00	1.58	1.50	5.79
14	0.15	1.73	-5.55	16.36
15	0.50	2.50	-14.50	27.50
16	0.50	2.50	-30.43	47.43
19	0.00	2.50	-6.33	18.33
20	3.70	2.50	-13.00	30.00

Tab. S3.3. OPTRAM parameters (i_d, s_d, i_w, s_w) obtained for the potentially irrigated clusters at the irrigation district Quota 102,50 for the irrigation seasons 2019-2020.

2019					2020				
CLUSTER	Dry edge		Wet edge		CLUSTER	Dry edge		Wet edge	
	i_d	s_d	i_w	s_w		i_d	s_d	i_w	s_w
6	0.40	0.40	1.90	4.10	**8**	0.30	0.70	2.80	3.90
10	0.30	1.10	1.80	1.20	**9**	0.30	0.70	2.20	1.80
13	0.40	1.10	1.70	1.70	**12**	0.30	1.00	1.60	2.00
14	0.30	1.20	1.40	2.10	**14**	0.30	1.00	1.70	2.00
15	0.30	1.20	2.00	2.00	**15**	0.30	1.00	1.70	2.80
16	0.30	1.40	1.50	3.80	**16**	0.30	1.00	2.20	2.20
17	0.20	1.40	1.00	4.00	**17**	0.40	0.90	0.70	4.70
18	0.20	1.40	1.20	4.00	**18**	0.50	0.90	0.70	5.00
19	0.30	1.40	0.50	4.30	**19**	0.50	0.90	0.70	5.00
20	0.40	1.40	0.50	5.10	**20**	0.40	1.30	0.40	5.80

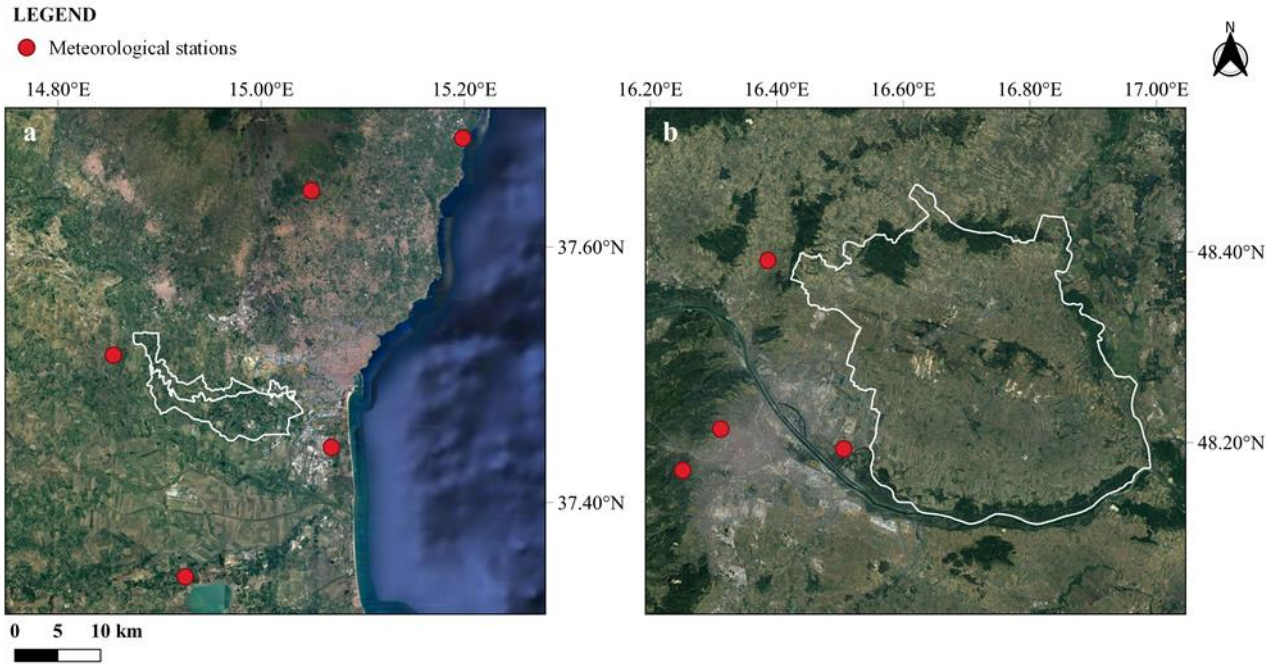

Fig. S3.1. Localization of the ground-based automatic meteorological stations used in the study for collecting rainfall data at the irrigation district Quota 102,50 (a) and at the Marchfeld Cropland region (b).

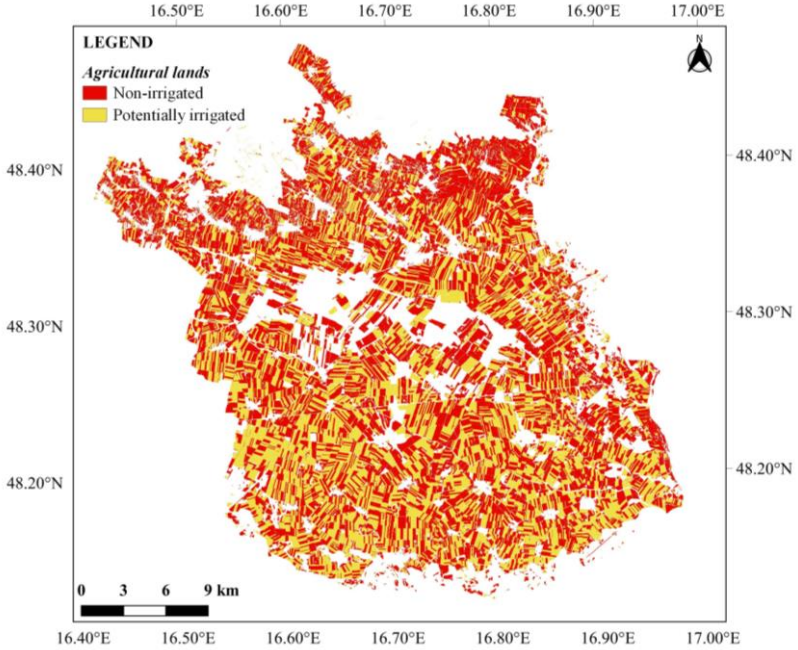

Fig. S3.2. Map of the potentially irrigated (yellow) and non-irrigated (red) areas obtained at the Marchfeld Cropland region during the irrigation seasons 2021

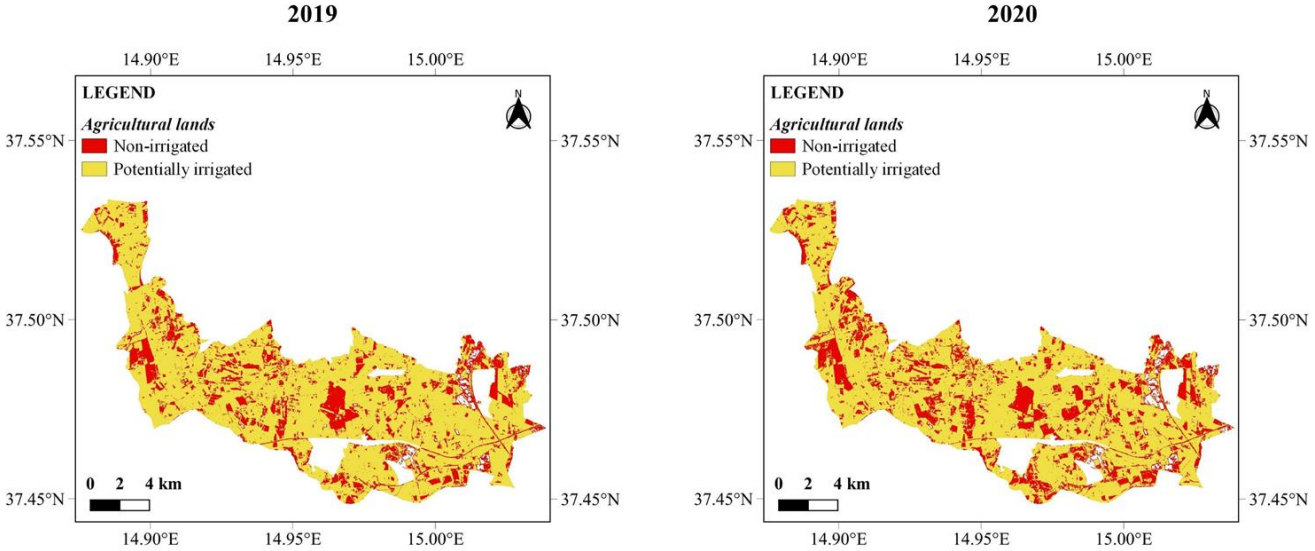

Fig. S3.3. Map of the potentially irrigated (yellow) and non-irrigated (red) areas obtained at the irrigation district Quota 102,50 during the irrigation seasons 2019-2020.

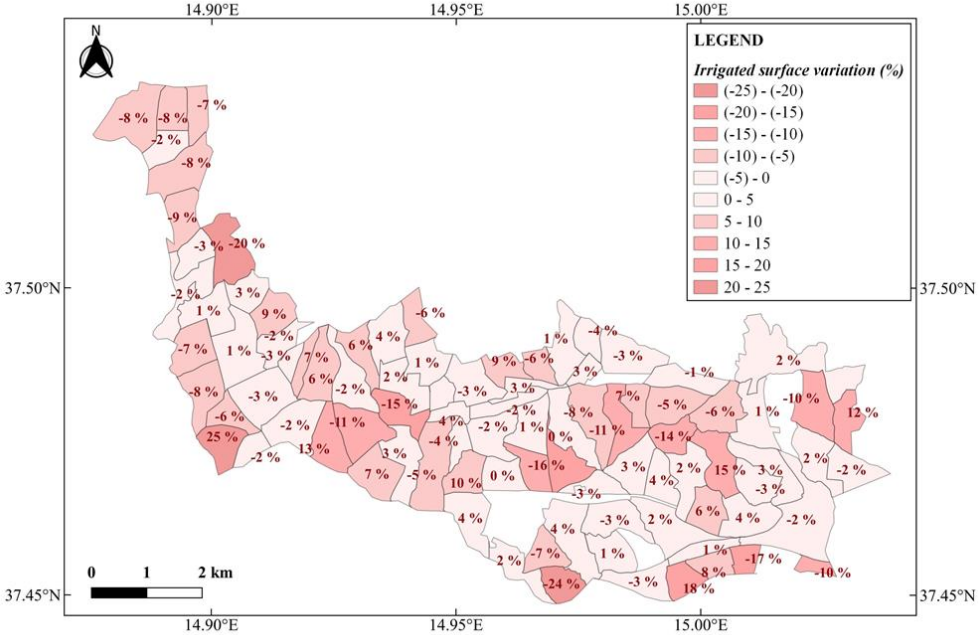

Fig. S3.4. Irrigated surface variation (%) between 2019 and 2020. The polygons represent the sub-districts at the irrigation district Quota 102,50.

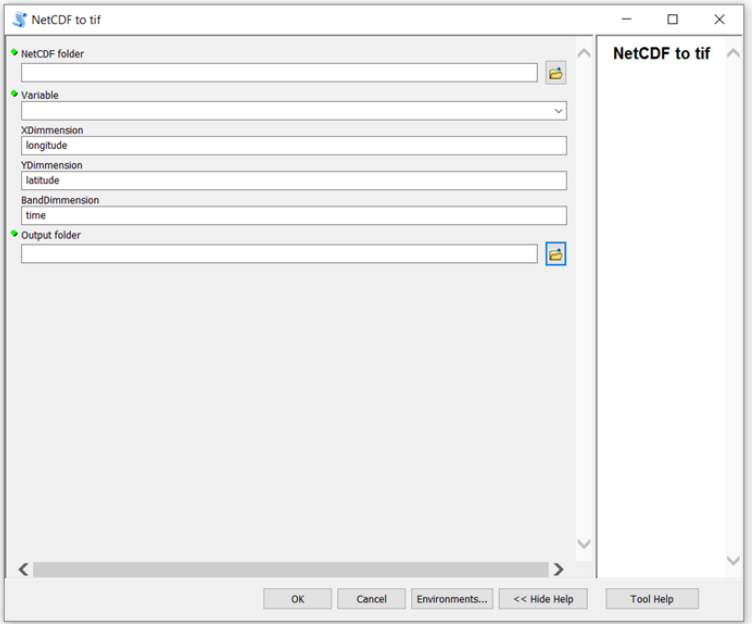

Fig. S4.1 User interface of the developed GIS-based toolbox used for converting the hourly reanalysis data from the source format (NetCDF) to a raster format (TIF). This toolbox uses 4 inputs and specifically the data input source folder, the desired variable to be converted and the raster extent, including the latitude a longitude coordinates.

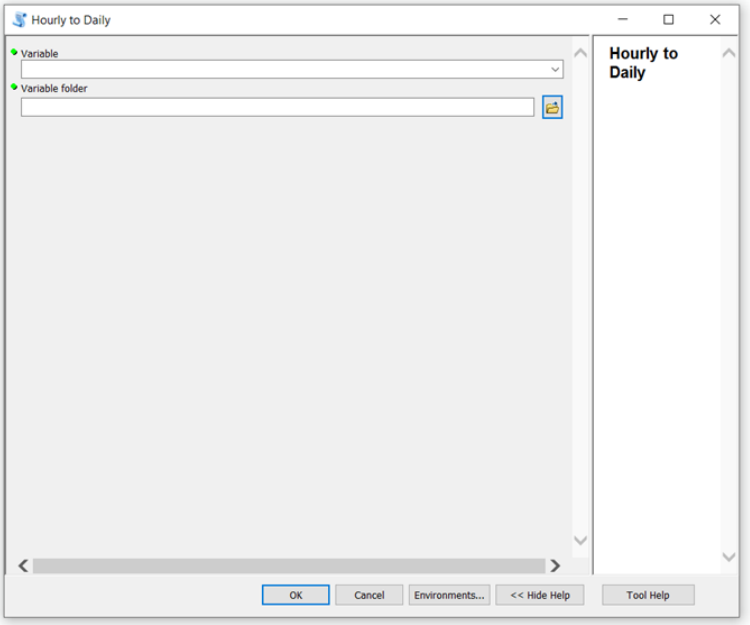

Fig. S4.2 User interface of the developed GIS-based toolbox used for aggregating the reanalysis data from hourly to daily time-step (e.g. for T_{air}, R_s, V10, U10).

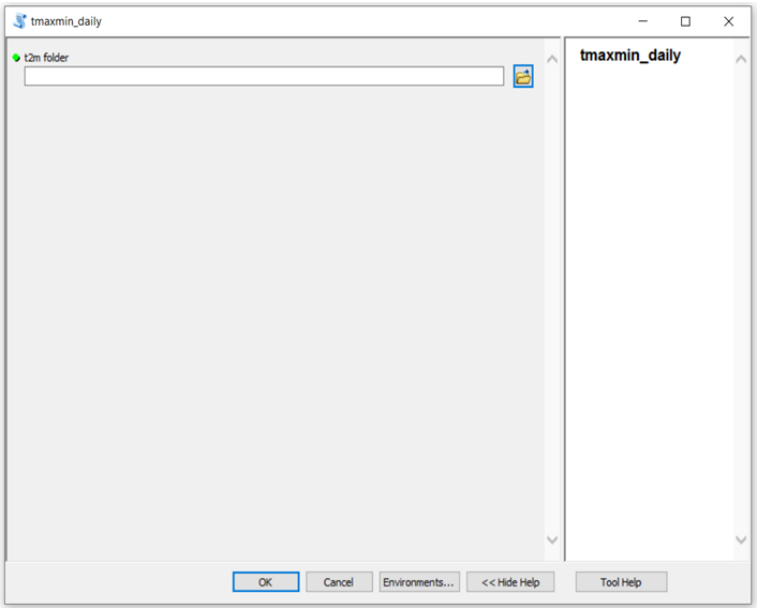

Fig. S4.3 User interface of the developed GIS-based toolbox used for determining daily maximum and minimum values for the interest variable (eg. for T_{air}), respectively.

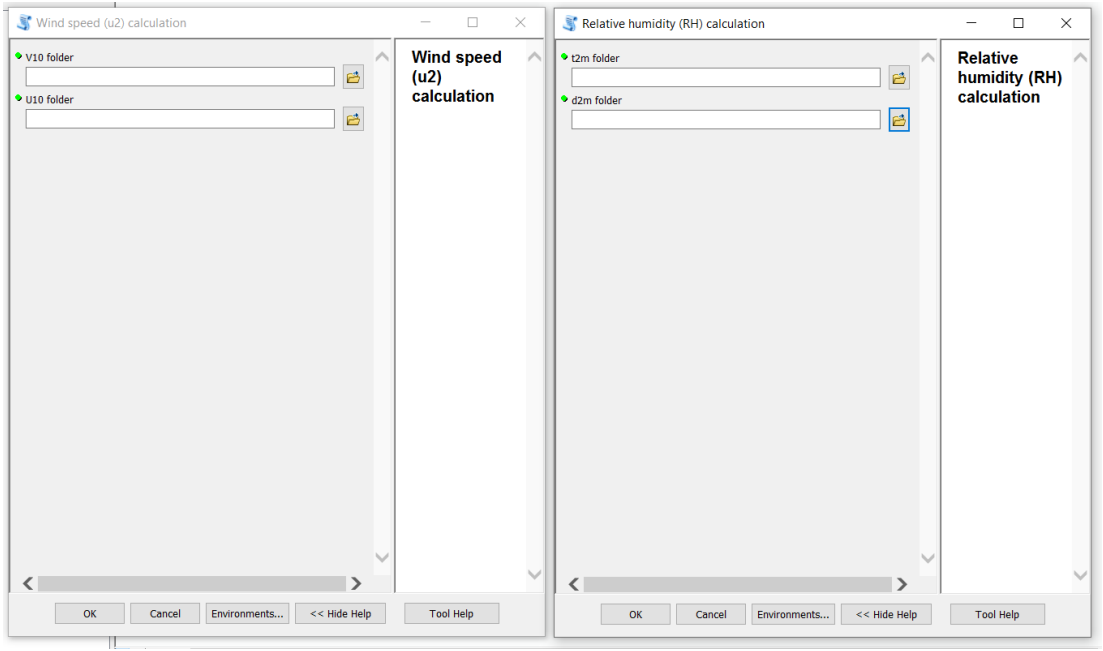

Fig. S4.4 User interface of developed the GIS-based toolboxes used for calculating: (on the left) the daily wind speed at 10 (u_{10}) and 2 m (u_2), using the V10 and U10 components from the reanalysis datasets; and (on the right) for estimating the daily relative humidity (RH) given in Eq. (1) – chapter 3.

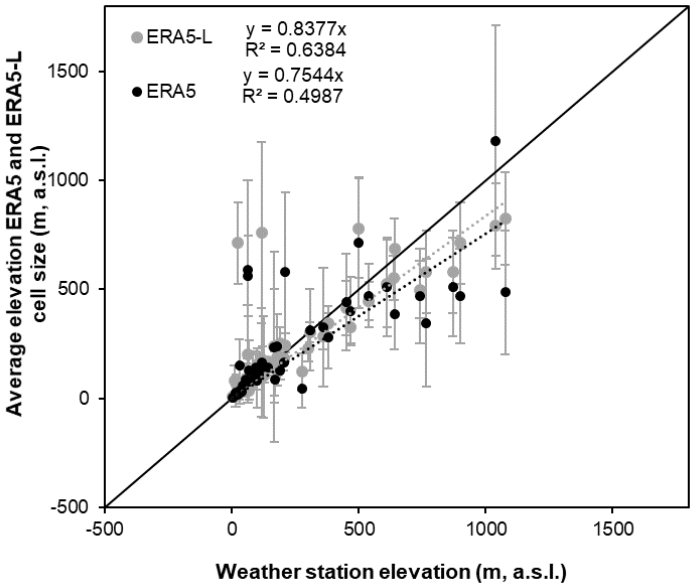

Fig S4.5. Scatterplots between the elevation (m, a.s.l.) of the weather station understudy and the average elevation (m, a.s.l.) observed ay the ERA5 and ERA5-L cell-size, respectively. The black line refers to the 1:1 line and the bars shows the standard deviation values.

Tab S5.1. Values of a and b parameters for the selected interpolation methods and temporal levels used in Eq. 1 to correct the bias of the selected interpolated precipitation dataset. IDW, NN, RBF refer to Inverse Distance Weighting, Natural Neighbour and Radial Basis Function methods, respectively.

Level	Interpolation method	a	b
Monthly	NN	6.93	0.74
Winter	RBF	12.83	0.74
Spring	IDW	4.51	0.80
Summer	IDW	5.33	0.72
Autumn	RBF	11.32	0.72

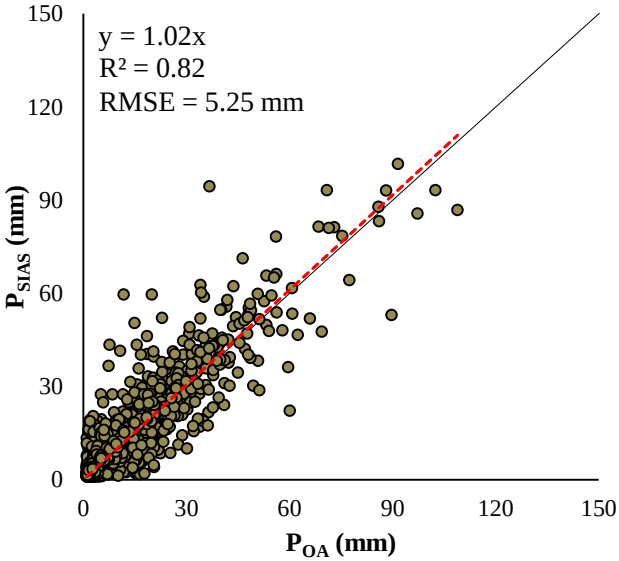

Fig. S5.1. Comparison of observed daily precipitation (mm) data from SIAS (P_{SIAS}) and OA (P_{OA}) networks for the reference period 2002-2019. The solid line is the 1:1 line, whereas the red dotted line is the trend line.

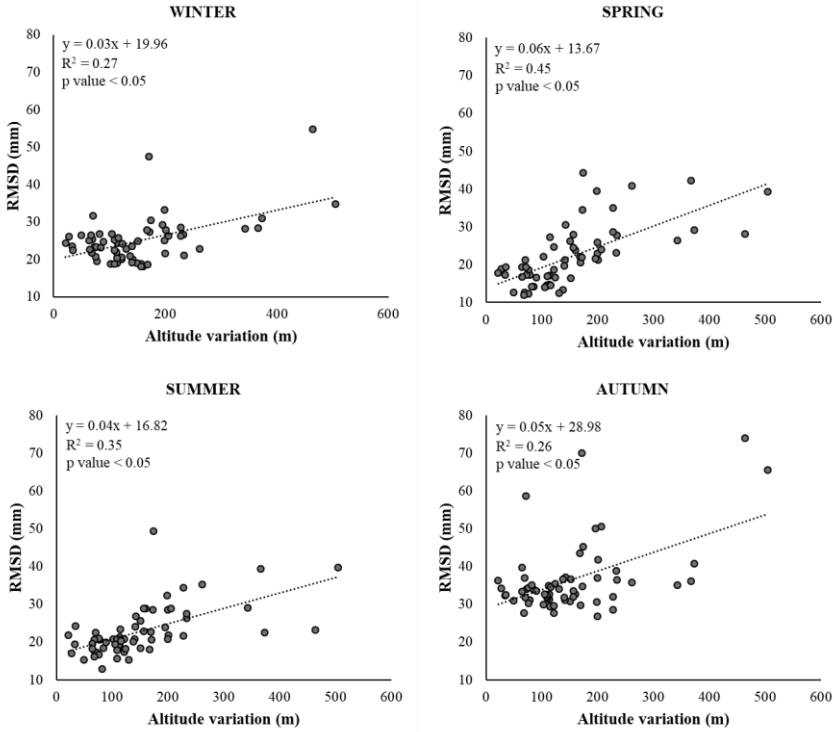

Fig. S5.2. Correlation between RSMD (mm) and altitude variation (m) within each ERA5-L cell, on a seasonal basis within the study area.